OULU 2015
C 518

ACTA
UNIVERSITATIS OULUENSIS

Laddu Keeth Saliya Jayasinghe

ANALYSIS ON MIMO RELAYING SCENARIOS IN WIRELESS COMMUNICATION SYSTEMS

UNIVERSITY OF OULU GRADUATE SCHOOL;
UNIVERSITY OF OULU,
FACULTY OF INFORMATION TECHNOLOGY AND ELECTRICAL ENGINEERING,
DEPARTMENT OF COMMUNICATIONS ENGINEERING;
CENTRE FOR WIRELESS COMMUNICATIONS

ACTA UNIVERSITATIS OULUENSIS
C Technica 518

LADDU KEETH SALIYA JAYASINGHE

ANALYSIS ON MIMO RELAYING SCENARIOS IN WIRELESS COMMUNICATION SYSTEMS

Academic dissertation to be presented, with the assent of the Doctoral Training Committee of Technology and Natural Sciences of the University of Oulu, for public defence in the OP auditorium (L10), Linnanmaa, on 12 February 2015, at 12 noon

UNIVERSITY OF OULU, OULU 2015

Copyright © 2015
Acta Univ. Oul. C 518, 2015

Supervised by
Professor Matti Latva-aho
Docent Nandana Rajatheva

Reviewed by
Professor Petar Popovski
Professor Krzyztof Wesolowski

Opponents
Professor Petar Popovski
Professor Olav Tirkkonen

ISBN 978-952-62-0738-4 (Paperback)
ISBN 978-952-62-0739-1 (PDF)

ISSN 0355-3213 (Printed)
ISSN 1796-2226 (Online)

Cover Design
Raimo Ahonen

JUVENES PRINT
TAMPERE 2015

Jayasinghe, Laddu Keeth Saliya, Analysis on MIMO relaying scenarios in wireless communication systems.
University of Oulu Graduate School; University of Oulu, Faculty of Information Technology and Electrical Engineering, Department of Communications Engineering; Centre for Wireless Communications
Acta Univ. Oul. C 518, 2015

Abstract

The thesis concentrates on evaluating and improving performances of various multiple-input multiple-output (MIMO) relaying scenarios that are particularly relevant to future wireless systems. A greater emphasis is placed on important practical situations, considering relay deployments, availability of channel state information (CSI), limitations of spectrum, and information secrecy.

Initially, the performance of a non-coherent amplify-and-forward (AF) MIMO relaying is analyzed when the relay is deployed with the relay-to-destination channel having a line-of-sight (LoS) path. The main attention is given to analyzing the performance of orthogonal space-time block coded based non-coherent AF MIMO system. Exact expressions of statistical parameters and performance metrics are derived considering the instantaneous signal-to-noise ratio (SNR) received at the destination. These performance metrics reveal that a strong LoS component in relay-destination channel always limits the performance promised by MIMO scattering environment when both nodes have multiple antennas.

The thesis also considers scenarios in MIMO two-way relaying (TWR) with physical layer network coding (PNC) mapping at the relay. PNC mapping becomes complex with multiple streams being combined at the relay node. Joint precoder-decoder schemes are considered to ease this, and various studies are carried out depending on the CSI. The zero-forcing criterion is used at the nodes when perfect CSI is available. For the imperfect CSI scenario, a robust joint precoder-decoder design is considered. The precoder and decoder matrices are obtained by solving optimization problems, which are formulated to maximize sum-rate and minimize weighted mean square error (WMSE) under transmit power constraints on the nodes.

Next, a precoder-decoder scheme for MIMO underlay device-to-device (D2D) communication system is investigated by considering two D2D modes; PNC based D2D and direct D2D. The joint design is based on minimizing mean square error (MSE) which is useful to mitigate interference, and to improve the performance of both D2D and cellular communications. Distributed and centralized algorithms are proposed considering bi-directional communication in both D2D and cellular communications. System performance is discussed with two transmit mode selection schemes as dynamic and static selection schemes. The results show that the PNC based D2D mode extends the coverage area of D2D communication.

Finally, secure beamforming schemes for the PNC based MIMO TWR systems are investigated when multiple eavesdroppers are attempting to intercept the user information. The CSI of the user-to-eavesdropper channels is imperfect at the users. The channel estimation errors are assumed with both ellipsoidal bound and Gaussian Markov uncertainty models. Robust optimization problems are formulated considering both scenarios to design beamforming vectors at the users and relay. Numerical results suggest that the proposed algorithms converge fast and provide higher security.

Keywords: cooperative relay, device-to-device communication, multiple-input multiple-output, physical layer network coding, physical layer security

Jayasinghe, Laddu Keeth Saliya, Moniantennitoistintekniikoiden analysointi langattomissa tietoliikennejärjestelmissä.

Oulun yliopiston tutkijakoulu; Oulun yliopisto, Tieto- ja sähkötekniikan tiedekunta, Tietoliikennetekniikan osasto; Centre for Wireless Communications

Acta Univ. Oul. C 518, 2015

Tiivistelmä

Tässä väitöskirjassa keskitytään arvioimaan ja parantamaan suorituskykyä useissa moniantennitoistinjärjestelmissä, jotka ovat ajankohtaisia tulevaisuuden langattomissa verkoissa. Erityisesti työssä analysoidaan tärkeitä käytännön tilanteita, sisältäen toistimien sijoittamisen, kanavatiedon saatavuuden, rajoitetun taajuuskaistan ja tiedon salauksen.

Aluksi epäkoherentin, vahvistavan ja jatkolähettävän moniantennitoistimen suorituskykyä analysoidaan tilanteessa, jossa toistin on sijoitettu siten, että kohteeseen on suora yhteys. Suorituskyvyn arvioinnin pääkohteena on ortogonaalinen tila-aika-tason lohkokoodattu epäkoherentti vahvistava ja jatkolähettävä moniantennitoistin. Työssä johdetaan tarkat lausekkeet tilastollisille parametreille ja suorituskykymittareille ottaen huomioon hetkellinen signaalikohinasuhde vastaanottimessa. Nämä suorituskykymittarit ilmaisevat, että toistimen ja kohteen välillä oleva vahva suoran yhteyden komponentti rajoittaa sitä suorituskykyä, jota moniantennijärjestelmän hajontaympäristö ennustaa.

Työssä tutkitaan myös kahdensuuntaisia moniantennitoistimia, jotka käyttävät fyysisen kerroksen verkkokoodausta. Koodauksesta tulee monimutkaista, kun monia datavirtoja yhdistetään toistimessa. Tämän helpottamiseksi käytetään yhdistettyä esikoodaus-dekoodausmenetelmää, jota tutkitaan erilaisten kanavatietojen tapauksissa. Täydellisen kanavatiedon tapauksessa käytetään nollaanpakotuskriteeriä. Epätäydellisen kanavatiedon tapauksessa käytetään robustia yhdistettyä esikoodaus-dekoodausmenetelmää. Esikoodaus- ja dekoodausmatriisit saadaan ratkaisemalla optimointiongelmat. Nämä ongelmat on muodostettu maksimoimaan summadatanopeus, ja minimoimaan painotettu keskineliövirhe, kun optimointirajoitteina ovat solmujen lähetystehot.

Seuraavaksi esikoodaus-dekoodausmenetelmää tutkitaan moniantennijärjestelmässä, jossa käytetään kahdentyyppistä laitteesta-laitteeseen (D2D) kommunikaatiomenetelmää: fyysisen kerroksen verkkokoodaukseen pohjautuvaa D2D- ja suoraa D2D-kommunikaatiota. Yhteissuunnittelu perustuu keskineliövirheen minimointiin, joka on hyödyllistä, kun halutaan vähentää häiriötä ja parantaa molempien verkkojen suorituskykyä. Työssä ehdotetaan hajautettuja ja keskitettyjä algoritmeja tilanteessa, jossa käytetään kaksisuuntaista kommunikaatiota molemmissa verkoissa. Järjestelmän suorituskykyä arvioidaan, kun käytetään kahta eri lähetystilan valintaa, dynaamista ja staattista. Tulokset osoittavat, että fyysisen kerroksen verkkokoodaukseen pohjautuva D2D kasvattaa D2D-kommunikaatiojärjestelmän kantamaa.

Lopuksi, turvallisia keilanmuodostustekniikoita arvioidaan fyysisen kerroksen verkkokoodaukseen pohjautuvassa kahdensuuntaisessa moniantennitoistinjärjestelmässä, kun useat salakuuntelijat yritävät siepata käyttäjätiedon. Käyttäjillä on epäideaalinen kanavatieto heidän ja salakuuntelijoiden välisten linkkien kanavista. Kanavatiedon estimointivirheitä arvioidaan ellipsoidisella ja Gauss-Markov-epävarmuusmallilla. Robustit optimointiongelmat, joissa suunnitellaan keilanmuodostusvektorit käyttäjän ja toistimen välille, muodostetaan molemmille malleille. Numeeriset tulokset osoittavat, että ehdotetut algoritmit konvergoituvat nopeasti ja tarjoavat korkeamman turvallisuuden.

Asiasanat: fyysisen kerroksen turvallisuus, fyysisen kerroksen verkkokoodaus, laitteesta-laitteeseen kommunikaatio, moniantennijärjestelmä, yhteistoiminnallinen toistin

To my family

Preface

This doctoral thesis contains the results of research undertaken at the Centre for Wireless Communications (CWC) and the Department of Communications Engineering, University of Oulu, Finland, during the years 2010-2014. During these years, I have acquired enormous personal and scientific benefits from all my superiors, colleagues, and fellow students who have supported me in my work towards this thesis. For this, I would like to kindly thank them.

First of all, I am grateful to my supervisor Professor Matti Latva-aho for giving me the opportunity to pursue doctoral studies in the Radio Access Technologies (RAT) group at the CWC. Since the very beginning, he gave me the freedom and encouragement to explore whatever scientific challenges I found interesting. The continual support, encouragement, and guidance from him over the years has been invaluable, and I wish to thank him for that.

I am deeply grateful to my advisor Adjunct Professor Premanandana Rajatheva for his meticulous guidance and support during my doctoral studies. Without his comments, advice, patience, inspiration and encouragement, I would not have come this far. I wish to thank the reviewers of the thesis, Professor Petar Popovski from the Aalborg University, Denmark, and Professor Krzysztof Wesolowski from the Poznan University of Technology, Poland, for having the patience to read my thesis and to provide constructive comments. Special thank to Dr. Chathuranga Weeraddana from the KTH Royal Institute of Technology, Sweden and Dr. Prathapasinghe Dharmawansa from the Stanford University, US, for the productive discussions and comments required to resolve several uncertainties encountered during my research. I have also had the pleasure to guide the M.Sc. thesis and to work as co-author for my younger brother Praneeth Jayasinghe, and I wish to thank him for that. I am also grateful to Petri Luoto and Markus Leinonen for Finnish translation of the thesis abstract, and Simon Scott for proofreading the manuscript.

My gratitude goes to Dr. Harri Posti and Dr. Ari Pouttu, the director of the CWC during my doctoral studies, for providing a dynamic and inspiring working environment.

During the years with the CWC, I have had the privilege to contribute

to multiple CWC projects such as METIS (Mobile and Wireless Communications Enablers for the Twenty-Twenty (2020) Information Society), EARTH (Energy Aware Radio and Network Technologies), LOCON (Local Connectivity and Cross-Layer Design for Future Broadband Mobile Systems), CRUCIAL (Solutions for Capacity Crunch in Wireless Access with Flexible Architectures), and 5Gto10G (5G radio access solutions to 10 GHz and beyond frequency bands) projects. I would like to thank the managers of these projects, Dr. Pekka Pirinen, Dr. Jouko Leinonen, Dr. Anna Pantelidou, and Adjunct Professor Premanandana Rajatheva. The projects were funded by European Commission, Finnish Funding Agency for Technology and Innovation (Tekes), Nokia Networks, Elektrobit, Renesas Mobile Europe, and many other industrial partners. I would like to acknowledge them. I was also fortunate to receive personal research grants for doctoral studies from the following Finnish foundations: HPY:n Tutkimussäätiö Foundation, Nokia Foundation, Tauno Tonningin Säätiö, and Riitta and Jorma J. Takanen Foundation.

During my doctoral studies, I have had the pleasure to be surrounded by cheerful colleagues of mine at the CWC including (in alphabetical order) Amin Ghazanfari, Dr. Animesh Yadav, Ayotunde Laiyemo, Bidushi Barua, Dr. Antti Tölli, Dr. Carlos Lima, Dr. Chathuranga Weeraddana, Dr. Fatih Bayramoglu, Ganesh Venkatraman, Harri Pennanen, Hamidreza Bagheri, Helal Chowdhury, Hirley Alves, Inosha Sugathapala, Kalle Lähetkangas, Dr. Kaveh Ghaboosi, Dr. Li Wei, Madhusanka Liyanage, Manosha Kapuruhamy, Dr. Marian Codreanu, Markus Leinonen, Dr. Mehdi Bennis, Mohammed ElBamby, Pawani Porambage, Dr. Pedro Nardelli, Petri Luoto, Dr. Pradeep Kumar, Prasanth Karunakaran, Qiang Xue, Ratheesh Kumar, Satya Joshi, Simon Scott, Sumudu Samarakoon, Suneth Namal, Tachporn Sanguanpuak, Uditha Lakmal, amongst all others. I very much enjoyed our daily exchange of ideas and thoughts, and the fun moments together. I am also very grateful to the administrative staff from the CWC, more specifically Antero Kangas, Elina Komminaho, Hanna Saarela, Jari Sillanpää, Kirsi Ojutkangas and many other.

During my stay in Oulu, I had the privilege to make some very good family friends, including Adjunct Professor Rajatheva & family, Chathuranga, Manosha, Namal, Satya, Sumudu, Ganesh, Sandun, Tharanga, Buddhika, Uditha, Upul, Madhusanka, Dilani, Vinudi, Inosha, Vidharsha, Kanchana, Chamari, Senehas, Somnas, Dimuthu, Dilru, Pawani, Ayswarya, Aditya, Sujeetha, Bidushi, and Ni-

vanthi. I give a special thank you to all my friends from Sri Lanka for their support and encouragement during these years.

I want to express my unreserved gratitude to my loving father Sarath Jayasinghe and my loving mother Shanthi de Zoysa for their love, kindness and support throughout my life. The sacrifices you have done during my life are priceless. I would like to thank my loving brothers and sisters Madhusha, Bhagya, Praneeth, Pradeesha and family members Prabhath, Lakshika, Sadhuneth for their love, joy and help during my life. I am also grateful to my loving grandparents Rathnasiri/ Rathnawathi, and parents-in-law Upali/ Leela for their love and blessings. To my sweet boy, Sahas Anuththara, thank you for the happiness you brought into my life and for reminding me the important things in life. Last, but not least, I thank my wife, Nirmalee Bhagya, for always being by my side, loving, supporting, and believing in me.

Oulu, Decemeber 31, 2014 Keeth Saliya Jayasinghe

Symbols and abbreviations

Symbols and functions

a	Relay gain constant in the AF MIMO system
b	Relay power control constant in the AF MIMO system
d	Normalized distance between the node 1 and relay in the TWR system
d_{ij}	Normalized distance between i and j
d_v	Diversity order
D_i	ith device in the D2D communication
diag$(\cdot)$	Diagonal matrix, if $\mathbf{A} = \text{diag}(a_1, .., a_n)$, then $\mathbf{A}$ is a diagonal matrix with entries $a_1, .., a_n$ in the diagonal.
$\mathbf{e}_b$	Error vector at the BS
$\mathbf{e}_i$	Error vector at the i node/ device
$\mathbf{e}_m$	Error vector at the MS
$\mathbf{e}_r$	Error vector at the relay
E_k	kth eavesdropper
$\mathbf{E}_i$	Estimation error of $\mathbf{H}_i$ in the TWR system
$\mathbf{E}_{ik}$	Estimation error of U_i-to-E_k channel ($\mathbf{H}_{ik}$) in the secure TWR system
$\mathbf{F}_b$	Precoder matrix at the BS
$\mathbf{F}_i$	Precoder matrix at the ith node/device; $i = 1, 2$
$\mathbf{F}_m$	Precoder matrix at the MS
$\mathbf{F}_r$	Precoder matrix at the relay
$f(\cdot)$	Probability density function
$F(\cdot)$	Cumulative distribution function
${}_0F_1(\cdot;\cdot)$	Generalized hypergeometric function
${}_1F_1(\cdot;\cdot;\cdot)$	Confluent hypergeometric function
G_a	Array gain
$\mathbf{G}$	Constant gain matrix at the relay in the AF MIMO system/ Decoder matrix at the relay in the TWR system
$\mathbf{G}_b$	Decoder matrix at the at the BS

$\mathbf{G}_i$	Decoder matrix at the ith node/device
$\mathbf{G}_m$	Decoder matrix at the at the MS
$\mathbf{G}_r$	Decoder matrix at the at the RS
$\mathbf{H}_1$	Source-to-relay channel in the AF MIMO system / Node 1-to-relay channel in the TWR system
$\mathbf{H}_2$	Relay-destination channel in the AF MIMO system / Node 2-to-relay channel in the TWR system
$\mathbf{H}_{\mathrm{Sn}}$	Source-to-relay n channel in the multi-relay AF MIMO system
$\mathbf{H}_{\mathrm{nD}}$	Relay n-to-destination channel in the multi-relay AF MIMO system
$\mathbf{H}_{bi}$	Relay-to-node i channel with antenna correlation during BC stage of TWR system
$\mathbf{H}_{mi}$	Node i-to-relay channel with antenna correlation during MA stage of TWR system
$\mathbf{H}_{xy}$	MIMO channel between x and y in the D2D communication and secure TWR systems. x, y represent first letter of the name of node. e.g. BS-to-MS channel is $\mathbf{H}_{bm}$
$\bar{\mathbf{H}}$	Estimated channel of $\mathbf{H}$
$\overline{\mathbf{H}}_2$	Specular (LoS) component of $\mathbf{H}_2$
$\widetilde{\mathbf{H}}_2$	Scattered component of $\mathbf{H}_2$
$\overline{\mathbf{H}}_{\mathrm{nD}}$	LoS component of $\mathbf{H}_{\mathrm{nD}}$
$\widetilde{\mathbf{H}}_{\mathrm{nD}}$	Scattered component of $\mathbf{H}_{\mathrm{nD}}$
$\mathrm{I_b}$	Interference threshold for D2D communication
$\mathrm{I_d}$	Interference threshold for BS-MS communication
$\mathrm{I_{th}}$	Interference threshold for general communication
K	Rician factor
$\mathbf{K}$	Conditional covariance matrix over $\mathbf{H}_2$
$K_n(\cdot)$	Modified Bessel function of the second kind and of order n
m_{ik}	Unmodulated kth message at the ith node
m_{rk}	Unmodulated kth message at the relay node
$M_\gamma(\cdot)$	Moment generating function of γ
n_{r_k}	kth element of $\mathbf{n}_r$
N	Number of i.i.d. symbols in OSTBC encoding/ Number of relay nodes in multi-relay AF MIMO system/ Number of antennas at nodes in the TWR system

N_D	Number of antennas at the destination in the AF MIMO system
N_i	Number of antennas of ith node
N_k	Number of antennas at the kth eavesdropper
N_r	Number of antennas at the relay
N_R	Number of antennas at the relay in the AF MIMO system
N_S	Number of antennas at the source in the AF MIMO system
N_T	Number of symbol periods used to send a OSTBC code word
n^*_{opt}	Optimal relay node
n^*_{sub}	Sub-optimal relay node
$\mathbf{n}_b$	Noise vector at the BS
$\mathbf{n}_D$	Noise vector at the destination in the optimal beamforming based AF MIMO system
$\mathbf{n}_{ek}$	Noise vector at kth eavesdropper
$\mathbf{n}_i$	Noise vector at the ith node/device/user during BC stage of the TWR system
$\mathbf{n}_k$	Noise vector at the relay during kth symbol period in the OSTBC based AF MIMO system
$\mathbf{n}_m$	Noise vector at the MS
$\mathbf{n}_r$	Noise vector at the relay during MA stage of the TWR system
$\mathbf{N}_i$	Noise matrix at the ith node
p	Maximum number of antennas at the relay and destination in the AF MIMO system, i.e., $\max(N_R, N_D) = p$
P_E	Bit error rate for BPSK in the AF MIMO system
p_{ik}	kth diagonal element of $\mathbf{P}_i$
p_{rk}	kth diagonal element of $\mathbf{P}_r$
$\mathrm{P}_{\max}$	Maximum transmit power
P_{r}	Transmit power of training sequence at the relay
P_{T}	Total transmit power constraint
P_{X}	Transmit power constraint at the X, where X denote the name of the node. e.g. Transmit power constraint at the BS is P_{B}
$\mathbf{P}_i$	Power matrix at the ith node in the ZF based TWR system
$\mathbf{P}_r$	Power matrix at the relay node in the ZF based TWR system
$P_{\text{out}}(\cdot)$	Outage probability
q	Minimum number of antennas at the relay and destination in the AF MIMO system, i.e., $\min(N_R, N_D) = q$

r	Received signal at the destination in the optimal beamforming based AF MIMO system
R	Code rate of OSTBC transmission, i.e., number of symbols/number of symbol periods used
R_n	Number of antennas at nth relay node
R_{sum}	Sum-Rate of the TWR system
R_{ij}^k	Rate from ith node to jth node for the kth stream.
$\bar{R}_{ij}^k$	Rate from ith node to jth node for the kth stream when PNC mapped symbol is transmitted
$\mathbf{r}_k$	Received signal at the destination during kth symbol period in the OSTBC based AF MIMO system
$\mathbf{R}_i$	Antenna correlation matrix of the ith node
$\mathbf{R}_r$	Antenna correlation matrix of the relay node
s_i	ith OSTBC symbol at the source in the AF MIMO system / transmitted symbol at ith user in the secure TWR
s_{ik}	kth element of $\mathbf{s}_i$
s_{rk}	kth element of $\mathbf{s}_r$
$\mathbf{s}_b$	Transmit symbol vector at the BS
$\mathbf{s}_i$	Transmitted symbol vector at the ith node/ device
$\mathbf{s}_r$	PNC mapped symbol vector at the relay
U_i	User i
$U(\cdot;\cdot;\cdot)$	Confluent hypergeometric function of the second kind
$\mathbf{v}_{\max}$	Eigenvector associated with $\xi_{\max}$ in the optimal beamforming based AF MIMO system
$\mathbf{v}_i$	Receive beamforming vector at user i in the secure TWR system
$\mathbf{v}_r$	Transmit beamforming vector at the relay in the secure TWR system
$\mathbf{w}_{ek}$	Receive beamforming vector at the kth eavesdropper
$\mathbf{w}_i$	Transmit beamforming vector at U_i in the secure TWR system
$\mathbf{w}_k$	Noise vector at the destination during the kth symbol period in the OSTBC based AF MIMO system
$\mathbf{w}_r$	Receive beamforming vector at the destination in the optimal beamforming based AF MIMO system / Receive beamforming vector at the relay in the secure TWR system
$\mathbf{w}_t$	Transmit beamforming vector at the source in optimal beamform-

	ing based AF MIMO system
$\mathbf{W}$	Weight matrix in the TWR system
x	Transmitted symbol by the source in the optimal beamforming based AF MIMO system
$\mathbf{x}_k$	kth column of X in the OSTBC based AF MIMO system
$\mathbf{X}$	Row orthogonal matrix in the OSTBC based AF MIMO system / A unitary matrix in the MIMO TWR system
$\mathbf{X}_t$	Transmitted training sequence at the relay to estimate channels
y_{ek}	Post processed signal at E_k in MA stage
y_i	Post-processed signal at the ith user
y_r	Post-processed signal at the relay in the secure TWR system
y_{r_k}	kth element of $\mathbf{y}_r$
$\hat{y}_{ek}$	Post-processed signal at the kth eavesdropper in BC stage
$\mathbf{y}$	Received signal vector
$\mathbf{y}_b$	Post processed signal at the BS
$\mathbf{y}_i$	Post processed signal vector at the ith node/device
$\mathbf{y}_m$	Post processed signal at the MS
$\mathbf{y}_k$	Received signal at the relay during kth symbol period in the OSTBC based AF MIMO system
$\mathbf{y}_r$	Post-processed signal vector at the relay during in the TWR system
$\mathbf{Y}_i$	Received signal matrix at ith node
α	Path loss exponent
β_i	Complex path amplitude of the ith component
β_{ik}	Parameter which controls the amount of uncertainty in U_i-to-E_k channel
β_{rk}	Parameter which controls the amount of uncertainty in relay-to-E_k channel
γ	Instantaneous SNR at the destination in the AF MIMO system
γ_k	Instantaneous SNR of kth symbol in the AF MIMO system / SNR threshold for kth eavesdropper
γ_{th}	SNR threshold
γ_n	Received SNR at the destination through nth relay node in the multi-relay AF MIMO system
$\bar{\gamma}$	Average transmit SNR in the AF MIMO system

$\Gamma(\cdot)$	Gamma function
ϵ	Small positive constant, i.e., ϵ ($<< 1$)
ε_{ik}	Error bound associated with $\mathbf{E}_{ik}$ in the ellipsoidal uncertainty model
η	Weight of the LoS component $\overline{\mathbf{H}}_2$
$\theta_{r,i}$	Angle of arrival for ith dominant path
$\theta_{t,i}$	Angle of departure for ith dominant path
λ_0	Lagrange multiplier associated with total transmit power constraint
λ_i	Eigenvalues of $\frac{\eta^2}{\sigma^2}\overline{\mathbf{H}}_2\overline{\mathbf{H}}_2{}^H$ in the OSTBC based AF MIMO system
λ_{ik}	Lagrange multiplier associated with inequalities; λ_{ik} associated with p_{ik}
σ	Weight of the scattering component $\widetilde{\mathbf{H}}_2$ in the AF MIMO system
σ^2	Variance of the noise at a receiver in the TWR system
σ_i^2	Variance of the elements of $\mathbf{E}_i$/ Variance of the elements of $\mathbf{n}_i$ in the D2D system and secure TWR system
$\sigma_{N_i}^2$	Variance of the elements of $\mathbf{N}_i$
σ_x^2	Variance of the elements of $\mathbf{n}_x$ in the D2D system, where $x = b, m, r, 1, 2$
ξ_i	Eigenvalues of $\frac{\eta^2}{\sigma^2}\overline{\mathbf{H}}_2\overline{\mathbf{H}}_2{}^H$ in the optimal beamforming based AF MIMO system
$\xi_{\max}$	Maximum eigenvalue of $\frac{\eta^2}{\sigma^2}\overline{\mathbf{H}}_2\overline{\mathbf{H}}_2{}^H$ in the optimal beamforming based AF MIMO system
ρ	Total transmit power across all N_S antennas in the AF MIMO system / Normalized average transmit power of PNC mapped symbol at the relay
ρ_R	Correlation coefficient parameter in matrix $\mathbf{R}_r$
ρ_{Si}	Correlation coefficient parameter in matrix $\mathbf{R}_i$

Mathematical Operators

$\mathbf{0}$	Vector of only zeros; size of the vector is implicit
$\mathbf{0}_{N\times M}$	$N \times M$ matrix of only zeros
$\mathbf{I}_N$	$N \times N$ identity matrix
$\mathbf{1}$	Vector with all elements equal to 1; size of the vector is implicit

$\lvert x \rvert$	Absolute value of the complex number x
$(x)^+$	Positive part of scalar x, i.e., $\max(0, x)$
$\lfloor x \rfloor$	Largest integer less than or equal to x
$\lvert\lvert \mathbf{x} \rvert\rvert_2$	ℓ_2-norm of complex vector $\mathbf{x}$
$x \in \mathcal{S}$	x is a member of set $\mathcal{S}$
$(x)_l$	Pochhammer symbol which is given by $(x)_l = \frac{\Gamma(x+l)}{\Gamma(x)}$
$\mathbf{X}^H$	Hermitian of matrix $\mathbf{X}$
$\mathbf{X}^*$	Conjugate of matrix $\mathbf{X}$
$\mathbf{X}^T$	Transpose of matrix $\mathbf{X}$
$\mathbf{X}^{-1}$	Inverse of matrix $\mathbf{X}$
$\mathbf{X}^\dagger$	Pseudo-inverse of matrix $\mathbf{X}$
$\mathbf{X} \otimes \mathbf{Y}$	Kronecker product of two matrices $\mathbf{X}$ and $\mathbf{Y}$
$\mathrm{vec}(\mathbf{X})$	The vector obtained by stacking the columns of $\mathbf{X}$
$(\mathbf{X})_{i,j}$	Element at the ith row and the jth column of matrix $\mathbf{X}$
$\lvert\lvert \mathbf{X} \rvert\rvert_F$	Frobenius norm of $\mathbf{X}$
$\mathrm{Tr}(\mathbf{X})$	Trace of matrix $\mathbf{X}$
$\det(\mathbf{X})$	Determinant of matrix $\mathbf{X}$
$\mathbb{C}$	Set of complex numbers
$\mathbb{C}^n$	Set of complex n-vectors
$\mathbb{C}^{m \times n}$	Set of complex $m \times n$ matrices
$\mathcal{CN}(x, y)$	Circularly symmetric complex Gaussian random variable with mean x and variance y
$\mathcal{CN}(\mathbf{x}, \mathbf{Y})$	Circularly symmetric complex Gaussian vector distribution with mean $\mathbf{x}$ and covariance matrix $\mathbf{Y}$
$\sim$	Distributed according to
$\succeq$	Denote generalized inequality: between vectors, it represents componentwise inequality; between symmetric matrices, it represents matrix inequality. $\mathbf{X} \succeq 0$ denote the $\mathbf{X}$ is positive semidefinite.
$\mathcal{L}^{-1}$	Inverse Laplace transformation
$\mathcal{E}\{\cdot\}$	Expectation
$\Re(z)$	Real part of z
$\log_2(\cdot)$	Logarithm in base 2
$\ln(\cdot)$	Natural logarithm
$\max(\cdot)$	Maximum
$\min(\cdot)$	Minimum

$\Pr(\cdot)$	Probability of the event
$x \oplus y$	XOR operation of x and y

Acronyms

3GPP	Third Generation Partnership Project
ABER	Average bit error rate
AF	Amplify-and-forward
AMSE	Average MSE
AoF	Amount of fading
BER	Bit error rate
BC	Broadcasting
BPSK	Binary phase shift keying
BS	Base station
CCI	Co-channel interference
CSI	Channel state information
c.d.f.	Cumulative distribution function
D2D	Device-to-device
GMU	Gaussian Markov uncertainty
i.i.d.	independent and identically distributed
KKT	Karush-Kuhn-Tucker
LMI	Linear matrix inequality
LoS	Line of sight
LTE	Long Term Evolution
M2M	Machine-to-machine
MA	Multiple access
MIMO	Multiple input multiple output
MISO	Multiple-input-single-output
ML	Maximum likelihood
MMSE	Minimum mean square error
MRC	Maximum ratio combining
MS	Mobile station
MSE	Mean square error
m.g.f.	Moment generating function
non-i.i.d.	independent and non-identically distributed

OSTBC	Orthogonal space time block coding
PNC	Physical layer network coding
PNCF	Finite-set PNC
PNCI	Infinite-set PNC
p.d.f.	Probability density function
QCQP	Quadratic constrained quadratic programming
QMP	Quadrature matrix programming
QPSK	Quadrature phase shift keying
QoS	Quality of service
RS	Relay station
SER	Symbol error rate
SINR	Signal-to-interference-plus-noise ratio
SIMO	Single-input-multiple-output
SISO	Single-input-single-output
SNR	Signal to noise ratio
SVD	Singular value decomposition
TDD	Time division duplex
TNC	Traditional network coding
TWR	Two way relaying
WMSE	Weighted MSE
ZF	Zero forcing

Contents

1 Introduction

Numerous modern technological applications are now substantially reliant on wireless communication systems which will soon become a commodity similar to the electricity. The application scenarios require various advances in wireless systems such as higher data rates, larger coverage areas, more reliable communication, smaller latency, and less complex designs with lower power and processing requirements. In particular for mobile technology, it is predicted that the number of mobile devices will exceed the world population over the next few years [1]. This is already one of the primary contributors of global wireless traffic growth. Traffic will further increase as future mobile devices will possess more sophisticated features compared to early generation devices. These challenges are tackled, e.g. by reducing cell size, which allows reusing the limited frequency spectrum in a more efficient manner. The ultimate goal of this is to bring the wireless devices as close as possible to infrastructure.

Interestingly, multiple-input multiple-output (MIMO) relaying [2–4] has also been identified as a candidate for meeting such challenges. MIMO systems provide higher spectral efficiency and improve the reliability of the communication [5]. Thus, they have distinct advantages over the single-input single-output (SISO)[6] case and provide higher spectral efficiency even in the presence of multipath fading channels [7, 8]. Cooperative relaying on the other hand provides broader coverage and reliable data transmission [9–14]. Furthermore, the relaying of information through several hops reduces the need to use large power at the transmitter, which in turn produces a lower level of interference to other nodes. Recently, relay has been considered in the standardization process in Long Term Evolution-Advanced (LTE-A) by the Third Generation Partnership Project (3GPP) for LTE and IEEE 802.16m by the IEEE for WiMAX [15–17]. Both these relay standards used only fundamental relaying functionalities. We see that the MIMO relaying can be valuable in future standardization process as it provides gains of both MIMO and relaying techniques. However, despite the importance of MIMO relaying, detailed investigations on such cases still remain limited.

This dissertation seeks to analyze different scenarios of MIMO relaying that

are particularly relevant to next generation wireless systems. For example, consideration of relay deployment procedures, availability of channel state information (CSI) at nodes, spectrum reusing techniques, and improving information secrecy still require detailed research. Prior to an in-depth discussion of MIMO relaying scenarios, it is important to review previous studies to gain more insight on various techniques associated with those.

1.1 Literature review

The relevant state of the art which is associated with the scope of the thesis is presented in this section. The *MIMO dual-hop relaying* schemes are described in Section 1.1.1, where the related work on relaying protocols and fading scenarios are discussed. In Section 1.1.2, *two-way relaying* (TWR) schemes literature is presented. The *device-to-device* (D2D) communication work is summarized in Section 1.1.3. Finally, the *physical layer security* related studies are presented in Section 1.1.4. These provide background for the detailed analysis considered in chapter 2-5.

1.1.1 MIMO dual-hop relaying

During the last decade, several relaying protocols have been proposed in the literature. Among them, MIMO relaying is mainly based on relaying protocols such as amplify-and-forward (AF) and decode-and-forward (DF). In the AF protocol, the relay node forwards an amplified version of the received signal to the destination node, and provides significant gains while using less complex processing. On the other hand, the DF protocol based relay node decodes the received signal, re-encodes and modulates, and forwards to the destination. Several researchers have shown that the AF protocol can be implemented in practice [18–20]. In [19], Murphy et. al. implemented an AF relaying system and compared it to direct transmission. The performance evaluation showed a clear advantage of using AF relays, revealing a significant bit error rate (BER) improvement under realistic wireless conditions. Both the AF and DF systems were investigated by Zetterberg et. al. in [20], and compared in terms of implementation loss and the complexity. They show that the AF protocol is less complex and has lower implementation loss (i.e., performance is very similar to the theoretical studies).

These findings further support the idea that an AF relaying protocol requires less complicated processing.

Previous studies on AF MIMO relaying largely assume that the instantaneous CSI is available at the relay terminals [21–24]. An extra signal processing requirement at the relay node is the most significant drawback of this technique. This is contradictory to the objective of using AF MIMO relaying as a less complex relaying protocol. The authors in [25–34] discuss systems with an alternative approach, which employ a fixed gain at the relay. This technique is often referred to as *non-coherent* or *fixed-gain* AF relaying.

A number of papers have analyzed the asymptotic network capacity and fundamental information-theoretic performance limits of non-coherent AF MIMO relaying, such as [25–28]. Most of these studies were carried out using the tools of asymptotic random-matrix theory. In [25], Bölcskei et. al. discussed both coherent and non-coherent AF MIMO systems to investigate the asymptotic capacity in large relay networks. Another study on a large scale multi-level AF relay network has been carried out in [26]. A more realistic scenario of AF relaying with multi-user interference was discussed in [27], and the authors found expressions for ergodic capacity and derived some bounds. Recent studies in [35–41] have investigated the analytical performance of AF MIMO dual-hop systems with the use of finite-dimensional random matrix theory. Jin et. al. [35], analytically characterized the ergodic capacity of non-coherent AF MIMO dual-hop systems. Other studies were mainly based on the techniques such as *orthogonal space-time block coding* (OSTBC) and *optimal beamforming*.

OSTBC used in MIMO provides the same diversity order as maximal-ratio receiver combining (MRC) as analyzed in the references [42–44]. In the context of OSTBC based MIMO relaying, the authors in [37] considered the diversity order of the system. They considered both source-destination and relayed links. In the absence of a direct link between source and destination, OSTBC MIMO relaying in dual-hop setting was investigated to improve end-to-end link performance through spatial diversity gain in the references [36, 45, 46]. Specifically, Dharmawansa et. al. in [36] discussed analytical performance measures with non-coherent AF MIMO relaying in Rayleigh fading channels.

Performance analysis of AF MIMO beamforming systems was carried out in [38–40]. Beamforming at nodes allows the channel fading effects to be mitigated by exploiting CSI. The authors in [38] studied such a system with antenna corre-

lation in terms of outage probability and symbol error rates (SER). AF MIMO beamforming over Nakagami-m fading channels was analyzed in [39]. Furthermore, the authors in [40] considered the outage probability of such AF MIMO dual-hop system with optimal beamforming. Most of these studies assumed the availability of CSI at the source and relay node. Also, these were carried out using a single antenna at the relay node. A non-coherent AF MIMO dual-hop system with optimal beamforming was discussed in [41], where the beamforming vectors were computed at the destination, and transmit beamforming vector was sent back to the transmitter via a feedback link. Optimal single stream beamforming vectors were obtained to maximize the received signal-to-noise ratio (SNR) at the destination.

The majority of aforementioned investigations were limited to Rayleigh fading scenarios, and which is usually not practical in actual relay deployments. In a more realistic relay environment, it is more appropriate to consider a situation where the relay is selected such that the relay to the destination channel has a line of sight (LoS) path [47, 48]. In these cases, symmetric channels are not available for the dual-hop relaying. This in turn makes the second hop channel likely to experience *Rician fading* due to the dominant LoS component. Even though the Rician fading channel is one of the relevant and general fading conditions in wireless systems, most of the research have been carried out over Rayleigh fading. Thus those result in only a limited evaluation of the wireless system conditions. To circumvent the analytical complexity associated with Rician fading, the Nakagami approximation has been widely used in the literature, however, it does not yield good accuracy at the tails of the probability density function (p.d.f.) as shown in [49, 50]. In particular, the error events and outages mainly occur during deep fades and these have a strong relation with the tail of the p.d.f.. Therefore, it is necessary to develop exact expressions to understand the interplay among system parameters. Some analytical performance results were derived in [47] over this particular Rayleigh-Rician channels with non-coherent AF with each node having a single antenna. Several studies on Rayleigh-Rician channel with non-coherent AF MIMO relaying have been considered in the author's contributions [51–56].

1.1.2 Two-way relaying

Relaying schemes have a disadvantage of capacity loss due to half-duplex transmission. As an example, the dual-hop traditional relay schemes consume four time slots for bi-directional communication. Many studies focused on this weakness, and new methods were proposed to overcome the problem [57–60]. In [57], Munoz et. al. considered a system where the base station (BS) transmits to K relays during K time slots, and the relays in turn transmit to users during the $K+1$th slot. This is a reduction of $K-1$ time slots compared to traditional relaying. The uplink communication on this system was analyzed in [58]. Larsson et. al. in [59] considered bi-directional communication of two users with network coding, where two users transmit to a relay over orthogonal channels and the relay computes XOR of transmitted messages. The next slot was used to transmit the XOR message. With time division duplexing (TDD), this requires three time slots to complete bi-directional communication. The authors in [60, 61] proposed a TWR scheme which required only two time slots to exchange the information between two nodes as opposed to four in a traditional relaying scheme. In the TWR systems, the first time slot is referred to as the multiple access (MA) stage, where both source nodes transmit to the relay at the same time. The second time slot is referred to as the broadcasting (BC) stage, where the relay broadcasts the linearly combined message.

Physical layer network coding

A more attractive TWR scheme, *physical layer network coding* (PNC), was introduced independently by Zhang et. al. in [62] and Popovski and Yomo in [63]. This was proposed as a method that uses interference to benefit the users, and it was found that PNC resulted in rate improvements of wireless relay systems [63]. Both [62, 63] consider PNC TWR schemes with two timeslots, where source nodes transmit symbols during the MA stage, and the relay maps the received signal to the XOR of the transmitted data. During the BC stage, the modulated symbol of the XOR data is transmitted to the source nodes. The source node carries out XOR operation to recover the desired information. Many other research studies on PNC were based on [62, 63], where PNC mapping was discussed without being limited only to XOR mapping [64–70]. Zhang et. al. in

[64] classified the PNC mapping into two categories, finite-set PNC (PNCF) and infinite-set PNC (PNCI). Nazer and Gastpar in [65] investigated a nested lattice codes based TWR scheme and referred to it as the compute-and-forward scheme. In [66], Nam et. al. showed that with the use of lattice codes, the TWR scheme can achieve rates near cut-set bounds of the TWR channel. Many other studies on PNC with channel coding, synchronization, modulation schemes, and information theoretic framework were summarized in the references [71, 72].

The PNC based MIMO TWR systems were considered in some recent research works [73–79]. Eventhough having multiple antennas at nodes provides higher spectral efficiency, MIMO PNC mapping becomes complex with the number of multiple streams combined at the relay node. Some studies have been carried out on MIMO PNC, and they have suggested possible methods of PNC mapping at the relay. A pre-equalizer before transmission was proposed in [73] to facilitate the XOR operations at the relay. In [74, 75], the authors adopted zero-forcing (ZF) criteria to simplify the PNC at the relay by treating streams independently. Koike-Akino [76] investigated various precoding schemes with availability of CSI at the source nodes. He used maximum likelihood (ML) estimation at the relay to estimate transmitted symbol vectors. Furthermore, other studies in the references [77–79] also suggested that precoder schemes were necessary to reduce the complexity of the PNC mapping at the relay node. In [80], the author of the thesis studied a power allocation scheme with ZF precoders/decoders at source nodes to reduce the complexity of PNC operation and maximize the sum-rate of the system. Further a *joint precoder-decoder* scheme was proposed for PNC based MIMO system in [81], where the the authors optimized precoding and decoding matrices to have independent streams at the relay node. Yang et. al. [77] studied an eigen-direction alignment precoding scheme for PNC based MIMO TWR, where the authors optimized power matrices by maximizing weighted sum-rate. Many other schemes have also focused on simplifying PNC mapping by using precoders at the transmitter sides [78, 79].

Joint precoder-decoder design

The joint precoder-decoder design was first used in point-to-point MIMO systems [82, 83] as an effective way to utilize CSI to improve performance. In particular, this can be used to reduce inter-data-stream interference by having

signal processing capability at both transmitters and receiver. Previous studies the joint precoder-decoder design in MIMO relaying often assumed AF relaying [84–89], and the authors achieved higher capacities and decoding performance. The focus was mainly on minimizing mean square error (MSE) and maximizing the sum-rate. Guan and Luo in [84] considered an AF MIMO system with a precoder at the relay and a decoder at the destination, where they minimized MSE to find optimal solutions. A MIMO TWR system was analyzed in [87]. Furthermore, in [86], Xu and Hua considered a similar AF MIMO TWR system to maximize the sum-rate. In the context of PNC based MIMO TWR, the authors' of the thesis considered joint precoder-decoder designs to minimize MSE at the relay and source nodes [81, 90, 91].

In most of these MIMO TWR related studies, CSI was assumed to be known perfectly at all nodes [85–87]. However, in general, channel estimation has errors, and affects system performance significantly. Several studies were carried out by considering various models of imperfect CSI, and their impact on the performance of wireless systems. The authors in [88, 92] used a training sequence to estimate the channel. In [88, 93, 94], robust joint designs for AF MIMO relaying were discussed because the CSI estimation process was not perfect. For MIMO TWR, the authors in [89] studied the impact of imperfect CSI on the system performance. Their work was limited to a single antenna with expressions for BER of binary phase shift keying (BPSK) scheme. Another imperfect CSI model was discussed in [95–97] for a scenario where the channel parameters were estimated at the receiver and fed to the transmitter and relay node. This can cause feedback delays, and the main concern is the difference between the actual CSI and the outdated CSI.

1.1.3 Device-to-device communication

The ongoing 3GPP LTE specification [98] has identified D2D communication as a potential technique to improve spectral efficiency, enhance end-user experience and improve energy efficiency. This can be directly applied to short-range communication scenarios. With the higher number of mobile devices that we expect in the future, there is a strong possibility they will be located nearby and hence engage in communication with each other. In the context of machine-to-machine communication (M2M), machines are normally associated with a large number

of autonomous devices. These devices also require direct communication without human intervention. The authors in [99, 100] considered spectrum reuse within a cell for D2D communication. In particular, Doppler et. al. [100] considered D2D communication as an underlay to an LTE-advanced cellular network. They illustrated a mechanism to control interference from D2D communication to the cellular network. This is a spectrally efficient method of communication similar to the cognitive radio related studies in [101–103].

Many other references [104–111] also considered D2D communication in an underlay situation. Most of the previous studies on D2D considered direct D2D mode and discussed the advantages over the cellular communication mode [100, 104, 105, 107, 108]. In [100, 104], the authors showed that the direct D2D mode can be used to obtain higher bit rates, lower latency, and reduced power consumption. These gains can be realized as in [106], where the authors formulated a joint mode selection, scheduling, and power control task as an optimization problem assuming the availability of a central entity. They also proposed a distributed sub-optimal joint mode selection and resource allocation scheme. In [107], Zulhasnine et. al. formulated a resource allocation problem for D2D communications as a mixed integer non-linear programming in the LTE architecture. The authors in [108] also discussed resource allocation schemes to optimize throughput over shared resources. An underlay D2D system with network coding was proposed in [105], and the authors employed network coding to achieve high diversity order. There, the devices used orthogonal channels for transmission. Furthermore, a performance analysis of a D2D system was carried out in [109] and the results suggested that D2D performance was dependent on the mode selection algorithms and the distance between devices. Direct D2D communication in a LTE-advanced cellular networks was discussed in [110]. Device discovery based on distributed approach was investigated in [111]. Further studies on D2D communication are listed in the reference [112].

When D2D communication coexists with the cellular network, the D2D transmit powers need to be constrained to allow reliable cellular communication. Therefore, the D2D communication is only possible, when the devices are located near each other. However, a relay placed in between D2D pair can extend the coverage area with less transmit power. This facilitates longer distance communication through D2D mode. Such studies of D2D with MIMO relaying are limited in the literature. The authors' contributions in [113, 114] focused on

underlay MIMO relaying based D2D communication scenario.

1.1.4 Physical layer security

The fundamental concept of physical layer security is to use the physical layer characteristics to provide secure communication by preventing the eavesdroppers intercepting the information. This idea was first introduced by Wyner [115] in the mid 70's, where he introduced the wire-tap channel, and showed that legitimate users exchanged perfectly secure information at a non-zero rate in the presence of an eavesdropper. The maximum achievable perfectly secure message rate was referred to as secrecy capacity. In general, the user channel condition should be better than user-eavesdropper channel to have non-zero secrecy rate. Some recent research studies were carried out to enable this by proposing multiple antennas or generating artificial noise [116–118] at the users, so that the received signal at the eavesdropper was not decodable. Cooperative relays to assist legitimate users were also proposed to improve the secrecy rates. The authors in [119–121] considered various cooperative relay networks in unsecure environments. In [119], AF relaying was used. Many other relaying protocols were considered in [120], where different scenarios were investigated to maximize the achievable secrecy rate subject to a transmit power constraint, and minimize the total transmit power subject to a secrecy rate constraint. Moreover, the authors in [121] studied bi-directional communication options with eavesdroppers and proposed a secrecy transmission protocol.

The optimization techniques were also used to further enhance physical layer security. The authors in [122] considered multiple users communicating with a common receiver in the presence of an eavesdropper. They provided an optimal transmit power allocation policy to maximize the secrecy sum-rate. Quality-of-service (QoS) oriented optimal secure beamforming schemes were considered in [123] for one-way transmission. Many studies were based on the knowledge of the eavesdropper's information at the transmitter side. In particular, the CSI of an eavesdropper's channel should be available at the legitimate users to provide secrecy of the transmission. Since the legitimate users do not receive any feedback from eavesdropping nodes, in many situations the CSI available at the legitimate users is imperfect. Recent studies [124–129] focused on this issue, and robust transmission schemes were proposed in such imperfect CSI

scenarios. Secrecy-rate maximization in the presence of multiple eavesdroppers with imperfect CSI was considered in [124]. Sabrian et. al. [125] proposed robust beamforming schemes for multiple-input single-output (MISO) channels. Mukherjee and Lee [126] formulated a MIMO beamforming scheme with imperfect CSI at the transmitter. They minimized signal-to-interference-plus-noise ratio (SINR) at the eavesdropper considering a SINR target at the destination node. In the context of MIMO relaying, robust beamforming designs to provide physical layer security were studied in [127–129]. The focus of Wang et. al. in [127] was beamforming at the relay to maximize the secrecy rate. The author in this thesis in [128, 129] focused on PNC at the relay node. Since both users transmit during the MA stage, a given eavesdropper experiences interference. Additionally, the relay transmits mapped XOR symbol during the BC stage, which is an encrypted symbol to the eavesdropper unless it already knows one symbol. This provides added security for the TWR scheme.

1.2 Aims, contributions and outline of the thesis

The aim of this thesis is to investigate certain MIMO relaying scenarios, which are important in various applications of future wireless communication systems. Specifically, a greater emphasis is placed on those that are shown in Fig.1.1. The tools of random matrix theory and optimization theory are applied to analyze and enhance the performance of these cases.

First, the thesis focuses on a scenario where source-destination communication is assisted by a relay node, which has a LoS path to the destination. As explained in Section 1.1.1, practical relay deployments have dual-hop asymmetric fading scenarios in the MIMO relaying. Next, the thesis considers TWR to support the cell edge users who are experiencing low performance. User-to-user communication or user-to-base station communication can be facilitated by MIMO TWR communication. The PNC based MIMO TWR is used since that provides higher spectral efficiency. In particular, joint precoder-decoder schemes are proposed depending on the availability of perfect or imperfect CSI. As shown in Fig.1.1, the thesis also considers a relaying scheme to assist underlay D2D communication, where D2D TWR communication coexists with cellular communication. Finally, physical layer security of TWR communication is considered in the thesis. The TWR communication is established with the use of a

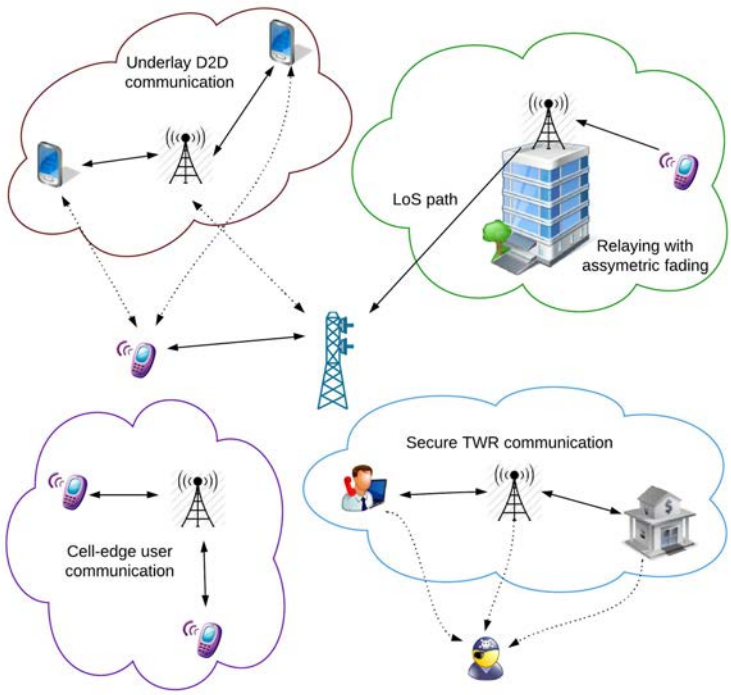

Fig 1.1. Various relaying scenarios for wireless systems

trusted relay in the presence of eavesdroppers. In the following, the outline of this thesis, is provided giving the main contributions contained in each chapter.

Chapter 2, the results of which have been documented in [51–56], presents a detailed analysis on non-coherent AF dual-hop MIMO relaying over asymmetric fading channels. The source-to-relay and relay-to-destination channels are considered to undergo Rayleigh and Rician fading, respectively. The analysis in the Chapter 2 is mainly focused on the OSTBC based AF MIMO relaying scenario. Due to the mathematical complexity associated with the Rician fading, it is very rarely discussed in the literature. Finite-dimensional random matrix theory is used to derive statistical parameters and performance metrics of instantaneous SNR at the destination. Several cases of Rician fading are considered depending on the rank of the LoS component of the Rician channel. Later in the chapter, the important results of optimal single stream beamforming based non-coherent

AF MIMO relaying and other AF MIMO relaying scenarios are summarized.

Chapter 3, the results of which have been presented in [80, 81, 90, 91, 130], proposes linear precoder-decoder schemes for PNC based MIMO TWR systems. The PNC mapping is complicated when multiple streams are combined at the relay node. This is simplified by a joint precoder-decoder design, which is also useful to enhance the overall performance of the system. Initially, the chapter considers a scenario where perfect CSI is available at the source nodes, and ZF criteria is utilized during both MA and BC stages. An optimal power allocation scheme is proposed using the Karush-Kuhn-Tucker (KKT) conditions. Next, a robust precoder-decoder design is proposed when CSI is imperfect at the source nodes. The design is based on minimizing the weighted mean square error (WMSE) of received signals. Both MA and BC stages are considered in the design. The WMSE based optimization problems become non-convex, and algorithms are presented to solve them optimally.

Chapter 4, the results of which have been documented in [113, 114], investigates joint precoder-decoder schemes for MIMO D2D communication underlaying cellular communication. First, a new D2D mode is introduced by adopting PNC based MIMO TWR. Joint precoder-decoder schemes based on minimizing MSE are investigated separately for bi-directional communication by adopting distributed and centralized approaches. Available transmit powers at the nodes are considered to be limited, and interference thresholds limits are used to minimize interference to other transmissions. In the distributed approach, the precoder-decoder scheme is proposed based on greedy optimization. In the centralized method, the joint design is formulated as a multicriterion optimization problem. Next, a joint precoder-decoder design is considered for the direct D2D communication. A similar distributed framework is used as in the PNC based D2D mode to solve the non-convex optimization problems. For a given distributed problem, the closed form expressions are derived for precoder-decoder matrices. Moreover, two mode selection schemes are proposed to select the best D2D mode. The selection schemes are numerically investigated to examine the possible coverage extensions by using the PNC based D2D communication.

Chapter 5, the results of which have been detailed in [128, 129], presents a secure beamforming design to prevent eavesdropping in MIMO TWR communication. The users communicate via trusted relay node which performs PNC, and multiple eavesdroppers are trying to intercept the user's information. At

users and relay, the CSI of the user-to-eavesdropper and relay-to-eavesdropper channels is imperfect. Optimization problems are formulated to minimize MSE, and adopt SNR threshold policy to prevent possible eavesdropping. First, an ellipsoidal channel uncertainty model is considered for the user-to-eavesdropper channel, and robust beamforming solution is obtained with an iterative method. Next, the Gaussian Markov uncertainty (GMU) model is assumed for user-to-eavesdropper and relay-to-eavesdropper channels. Robust optimization problems are formulated and solved for both MA and BC stages. Algorithms are proposed at each stage to analyze the performance of the TWR communication and the SNR distribution at a given eavesdropper.

Chapter 6, concludes the thesis and provides some possible future directions based on this work.

1.3 The author's contribution to the publications

The thesis is based, in parts, on five journal papers [51, 53, 90, 113, 128], and ten conference papers [52, 54–56, 80, 81, 91, 114, 129, 130]. All journal papers [51, 53, 90, 113, 128] have been already published. The conference papers [52, 54–56, 80, 81, 91, 114, 130] have been published, and [129] was submitted recently.

The author of this thesis had the main responsibility in conceiving the original ideas, derivation of the equations, developing the simulation software, generating the numerical results, and writing of the papers [51, 52, 80, 81, 90, 91, 113, 114, 128–130]. Other authors provided comments, criticism, and support during the process. For [53–56], the author of the thesis provided the ideas, comments, supported analysis, and the writing of the papers .

In addition to the papers above, the author has submitted one journal paper [131] that is not included in this thesis.

2 Analysis on dual-hop AF MIMO relaying over Rayleigh-Rician fading channels

This chapter investigates the scenarios of non-coherent AF MIMO relaying when the source-relay and relay-destination channels undergo Rayleigh and Rician fading respectively. This kind of asymmetric fading can be expected in the downlink of cellular communication when users are served by a relay node. Especially, when the relay is placed to assist indoor users, the base station-relay channel can be Rayleigh fading whereas relay-user channel undergoes Rician fading due to the dominant LoS path.

The main attention of this chapter is given to the scenario where space-time coding is used for a non-coherent AF dual-hop MIMO relaying. In particular, we employ OSTBC with a view to utilize simple (scalar) ML decoding at the destination [43, 132]. A pre-whitening filter is used at the destination to whiten the colored noise so that standard OSTBC decoding techniques can be applied, and it makes the statistical characterization of the instantaneous SNR more challenging. This issue is addressed with the tools of finite-dimensional random matrix theory. We first quantify the statistical measures of the SNR by deriving an exact expression for the moment generating function (m.g.f.). Different cases are considered for Rician channel depending on the rank of the LoS component. We obtain the first and second moments of the SNR. The exact expression for the probability density function (p.d.f.) and cumulative distribution function (c.d.f.) of the SNR are also derived for a specific antenna configuration. Having equipped with these statistical measures, the performance of the system is investigated by deriving analytical expressions for the BER of BPSK, outage probability and the amount of fading (AoF). In addition, we analyze the high SNR behavior by deriving diversity order and array gain of the system.

Later in this chapter, we summarize the findings in other scenarios of non-coherent AF MIMO relaying over Rayleigh-Rician environment. In particular, important results are presented on optimal beamforming based AF MIMO relaying, and relay selection schemes on OSTBC based AF MIMO relaying. For all these scenarios, statistical characterization of the instantaneous SNR and performance of the system are investigated by deriving analytical expressions.

2.1 System and channel models

We consider an AF MIMO dual-hop system with N_S source antennas, N_R relay antennas and N_D destination antennas as shown in Fig.2.1. System is half-duplex where the communication occurs from source to relay and relay to destination in two separate time slots. The source transmits to the relay during first time slot and the relay amplifies the received signal subject to a long-term power constraint and re-transmits to the destination in the second time slot. Moreover, we assume that there is no direct communication link between the source and destination.

Source-relay channel $\mathbf{H}_1 \in \mathbb{C}^{N_R \times N_S}$ is assumed to undergo Rayleigh fading and relay-destination channel $\mathbf{H}_2 \in \mathbb{C}^{N_D \times N_R}$ is subject to Rician fading. Entries of $\mathbf{H}_1$ are assumed to be $\sim \mathcal{CN}(0,1)$. We adopt the general non-coherent relaying assumption [26, 27] where the destination has perfect CSI knowledge, while both source and relay have no knowledge. In particular, CSI knowledge of $\mathbf{H}_2$ and $\mathbf{H}_2\mathbf{H}_1$ is sufficient at the destination. Furthermore, all terminals are assumed to be perfectly synchronized. $\mathbf{H}_2$ can be modeled with a specular component (LoS) $\overline{\mathbf{H}}_2$ and variable component (scattered) $\widetilde{\mathbf{H}}_2$ as

$$\mathbf{H}_2 = \eta\overline{\mathbf{H}}_2 + \sigma\widetilde{\mathbf{H}}_2, \tag{2.1}$$

where $\overline{\mathbf{H}}_2$ is an arbitrary rank matrix that consists of complex elements having unit magnitude, entries of $\widetilde{\mathbf{H}}_2$ are assumed to be $\sim \mathcal{CN}(0,1)$. Since mean of the $\widetilde{\mathbf{H}}_2$ is zero, we have

$$\mathcal{E}\{\mathbf{H}_2\} = \eta\overline{\mathbf{H}}_2, \tag{2.2}$$

We consider both η, σ to satisfy the following equation in our discussion.

$$\eta^2 + \sigma^2 = 1. \tag{2.3}$$

Since the transmitter employs OSTBC encoding, N i.i.d. symbols $s_1, s_2, .., s_N$ are mapped to a row orthogonal matrix $\mathbf{X} \in \mathbb{C}^{N_S \times N_T}$, where entries of $\mathbf{X}$ obtained by linear combinations of $s_1, s_2, .., s_N$ and their conjugates. These entries follow the exact construction method on the specific OSTBC used in [133]. Moreover, N_T is the number of symbol periods used to send a code word. Therefore, the code rate is $R = N/N_T$. Let $\mathbf{x}_k$ be the transmitted signal during the kth symbol period (i.e., the kth column of $\mathbf{X}$).

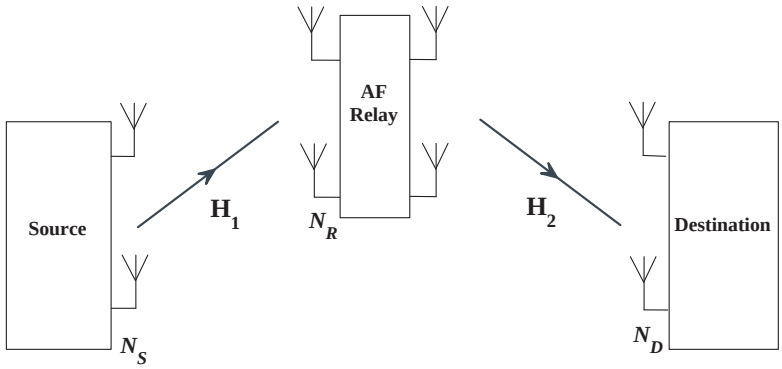

Fig 2.1. AF MIMO dual-hop system with N_S source antennas, N_R relay antennas and N_D destination antennas. Source-relay undergoes Rayleigh fading and relay-destination undergoes Rician fading, [51] © 2013, IEEE.

Here, we take $\mathbf{X} = (\mathbf{x}_1, ..., \mathbf{x}_{N_T})$ where $\mathbf{x}_i \in \mathbb{C}^{N_S \times 1}$ and ρ as the total transmit power across all N_S source antennas, i.e.,

$$\mathcal{E}\{\|\mathbf{x}_k\|^2\} = \rho. \tag{2.4}$$

During the kth symbol period, we have the received signal at the relay as

$$\mathbf{y}_k = \mathbf{H}_1\mathbf{x}_k + \mathbf{n}_k, \quad k = 1, 2, .., N_T \ , \tag{2.5}$$

where $\mathbf{n}_k \sim \mathcal{CN}(0, \mathbf{I}_{N_R})$ is the noise vector at the relay and noise has a unit variance. Due to the non-coherent AF relay assumption, the received signal at the relay is amplified by a constant gain matrix $\mathbf{G} = a\mathbf{I}_{N_R}$, where

$$a = \sqrt{\frac{b}{N_R(1+\rho)}}, \tag{2.6}$$

and b is a positive real number. Parameter a needs to satisfy the total power constraint,

$$\mathcal{E}\{\|\mathbf{G}\mathbf{y}_k\|^2\} \leq b. \tag{2.7}$$

After the amplification at the relay the received signal at the destination, $\mathbf{r}_k$ is given by

$$\mathbf{r}_k = a\mathbf{H}_2\mathbf{y}_k + \mathbf{w}_k, \quad k = 1, 2, .., N_T \ , \tag{2.8}$$

where $\mathbf{w}_k \sim \mathcal{CN}(0, \mathbf{I}_{N_D})$ is the noise vector at the destination and noise has a unit variance. Therefore, the end-to-end relationship for the overall system is

$$\mathbf{r}_k = a\mathbf{H}_2\mathbf{H}_1\mathbf{x}_k + a\mathbf{H}_2\mathbf{n}_k + \mathbf{w}_k, \quad k = 1, 2, .., N_T \ . \tag{2.9}$$

This full transmission equation is equivalent to a standard point-to-point MIMO system with channel matrix $a\mathbf{H}_2\mathbf{H}_1$ and colored Gaussian noise with conditional covariance matrix given by

$$\mathcal{E}\left\{(a\mathbf{H}_2\mathbf{n}_k + \mathbf{w}_k)(a\mathbf{H}_2\mathbf{n}_k + \mathbf{w}_k)^H|\mathbf{H}_2\right\} = \mathbf{K}, \tag{2.10}$$

where

$$\mathbf{K} = a^2\mathbf{H}_2\mathbf{H}_2^H + \mathbf{I}_{N_D} \ . \tag{2.11}$$

Before decoding is possible, we apply the noise whitening filter to $\mathbf{r}_k$ to yield

$$\widetilde{\mathbf{r}}_k = \mathbf{K}^{-1/2}\mathbf{r}_k = \widetilde{\mathbf{H}}\mathbf{x}_k + \widetilde{\mathbf{n}}_k, \tag{2.12}$$

where $\widetilde{\mathbf{H}} = a\mathbf{K}^{-1/2}\mathbf{H}_2\mathbf{H}_1$ and $\widetilde{\mathbf{n}}_k = \mathbf{K}^{-1/2}(a\mathbf{H}_2\mathbf{n}_k + \mathbf{w}_k)$. Now, the generalized end-to-end transmission equation for the codeword $\mathbf{X}$ can be written as

$$\widetilde{\mathbf{R}} = \widetilde{\mathbf{H}}\mathbf{X} + \widetilde{\mathbf{N}}, \tag{2.13}$$

where $\widetilde{\mathbf{R}} = (\widetilde{\mathbf{r}}_1, ..., \widetilde{\mathbf{r}}_{N_T})$ and $\widetilde{\mathbf{N}} \sim \mathcal{CN}(0, \mathbf{I}_{N_D} \otimes \mathbf{I}_{N_T})$. After linear OSTBC processing , the resultant SISO streams can be derived from (2.13) as [36], [132]

$$\tilde{s}_l = ||\widetilde{\mathbf{H}}||_F^2 s_l + \eta_l \ , \ l = 1, 2, \ldots, N, \tag{2.14}$$

where $\eta_l \sim \mathcal{CN}\left(0, ||\widetilde{\mathbf{H}}||_F^2\right)$. Following [132], we can obtain the instantaneous SNR γ_k as

$$\begin{aligned} \gamma_k &= ||\widetilde{\mathbf{H}}||_F^2 \mathcal{E}\left\{|s_k|^2\right\} \\ &= \alpha\overline{\gamma}a^2\mathrm{Tr}(\mathbf{H}_1^H\mathbf{H}_2^H\mathbf{K}^{-1}\mathbf{H}_2\mathbf{H}_1) \end{aligned} \tag{2.15}$$

where $\alpha = 1/RN_S$ and $\overline{\gamma}$ is the average transmit SNR which equal to ρ due to unit noise variance. Since γ_k is independent of k, we can simply denote the instantaneous SNR as γ.

To gain more insight into the system performance, we need to analyze the statistical properties of the SNR in (2.15). This problem will now be discussed with the use of finite-dimensional random matrix theory. For the sake of convenience we use the following notations: $p = \max(N_D, N_R)$, $q = \min(N_D, N_R)$, $t = p - q + 1$, $\mu_i = p + 1 - i$, $\nu_i = p - q + i - 2$ and $\nu_{ij} = p - q + i + j + 1$.

2.2 Statistics of the SNR

In what follows we derive some statistical parameters of the SNR γ. These are useful to study the system performance in terms of BER, AoF and outage probability. The statistical parameters are obtained for different cases of relay-destination channels. We start with the case rleay-destination channel undergoes independent non-identical Rician fading, where the entries of mean are non-identical. This is referred to as non-i.i.d. Rician. This simplifies and provides a pathway to the proofs for all other cases of the Rician distribution by considering correlated Rician (low rank), independent identical Rician fading, where mean is identical (i.i.d. Rician) and Rayleigh fading.

All these Rician fading scenarios can be anticipated in next-generation wireless communication systems as they are expected to employ a wider frequency spectrum. For instance, wavelength will be smaller for higher frequencies, and the antennas of transmitter/receiver are all spatially separated enough to have uncorrelated specular path gains. This provides independent non-identical entries for LoS component and i.i.d. entries for scattering component. Such a scenario is discussed under non-i.i.d. Rician. All other cases can also be expected based on the frequency band and antenna spacing.

2.2.1 Moment generating function of the SNR

Non-I.I.D. Rician

Here we consider the relay-destination channel with non-i.i.d. Rician fading, and derive the m.g.f. of the SNR γ.

Theorem 2.1. *The m.g.f. of the SNR γ is given by*

$$M_\gamma(s) = \frac{e^{-\mathrm{Tr}(\mathbf{\Lambda})}}{\Gamma(t)^q \ \det(\mathbf{V})} \ \det(\mathbf{I}(s)) \tag{2.16}$$

where $\mathbf{I}(s)$ is a $q \times q$ matrix with $(i,j)^{th}$ element given by

$$\begin{aligned}(\mathbf{I}(s))_{i,j} = &\sum_{k=0}^{N_S} \sum_{l=0}^{\infty} \frac{\binom{N_S}{k} a^{2k} \sigma^{2k} \lambda_j^l \ \Gamma(\mu_i + k + l)}{(t)_l \ l! \ (a^2\sigma^2(1+\alpha\overline{\gamma}s))^{\mu_i+k+l}} \\ &\times U\left(\mu_i+k+l; \mu_i+k+l+1-N_S; \frac{1/a^2\sigma^2}{1+\alpha\overline{\gamma}s}\right),\end{aligned} \tag{2.17}$$

where $0 < \lambda_1 < \lambda_2 < .. < \lambda_q < \infty$ *are non-zero ordered eigenvalues of* $\frac{\eta^2}{\sigma^2}\overline{\mathbf{H}}_2\overline{\mathbf{H}}_2{}^H$, $\mathbf{V}$ *is a* $q \times q$ *Vandermonde matrix whose determinant is given by* $\det(\mathbf{V}) = \det(\lambda_i^{q-j}) = \prod_{l<k}^{q}(\lambda_l - \lambda_k)$, $\mathbf{\Lambda} = \mathrm{diag}(\lambda_1, \lambda_2, ..., \lambda_q)$, $\Gamma(.)$ *is the gamma function,* $U(\cdot;\cdot;\cdot)$ *is the confluent hypergeometric function of the second kind and* $(t)_l$ *is the Pochhammer symbol which is given by* $(t)_l = \frac{\Gamma(t+l)}{\Gamma(t)}$.

Proof. See Appendix 1. □

Even though (2.17) consists of an infinite summation, it converges rapidly and sufficiently accurate results can be obtained for the m.g.f. by truncating at a sufficient depth. Our numerical observations show less than ten terms are sufficient to obtain accurate values. It can be easily seen that the m.g.f. has a direct dependence on the eigenvalues of $\frac{\eta^2}{\sigma^2}\overline{\mathbf{H}}_2\overline{\mathbf{H}}_2{}^H$, but not the mean value of the second hop channel. We use this expression to derive moments of the SNR, p.d.f. of the SNR and BER expressions in following sections.

Correlated Rician

Here we have the relay-destination channel with correlated Rician fading and derive the m.g.f. of the SNR γ.

Corollary 2.1. *The m.g.f. of the SNR* γ *is given by*

$$M_\gamma(s)_{cor} = \frac{\mathcal{K}^{-1} e^{-\mathrm{Tr}(\mathbf{\Lambda}_m)} \ \det(\mathbf{I}_{cor}(s))}{\Gamma(t)^m (\lambda_{q+1-m}\lambda_{q+2-m}...\lambda_q)^{q-m}} \tag{2.18}$$

where

$$\mathcal{K} = \prod_{z=1}^{q-m}\prod_{r=m}^{q-1}\Gamma(p-q+z)\Gamma(q-r) \ \det(\mathbf{V}_m), \tag{2.19}$$

and $\mathbf{I}_{cor}(s)$ *is a* $q \times q$ *matrix with* $(i,j)^{th}$ *element given by*

$$\{\mathbf{I}_{cor}(s)\}_{i,j} = \begin{cases} \sum_{k=0}^{N_S} \frac{\binom{N_S}{k}\ \Gamma(\nu_{ij}+k)}{(a\sigma)^{2\nu_{ij}}(1+\alpha\overline{\gamma}s)^{\nu_{ij}+k}} \\ \times U\left(\nu_{ij}+k; \nu_{ij}+1+k-N_S; \frac{1}{a^2\sigma^2(1+\alpha\overline{\gamma}s)}\right) \\ \qquad\qquad\qquad\qquad for \ \ 1 \le j \le q-m \\ \sum_{k=0}^{N_S}\sum_{l=0}^{\infty} \frac{\binom{N_S}{k} a^{2k}\sigma^{2k}\lambda_j^l \ \Gamma(\nu_i+k+l)}{(t)_l \ l! \ (a^2\sigma^2(1+\alpha\overline{\gamma}s))^{\nu_i+k+l}} \\ \times U\left(\nu_i+k+l; \nu_i+k+l+1-N_S; \frac{1}{a^2\sigma^2(1+\alpha\overline{\gamma}s)}\right) \\ \qquad\qquad\qquad\qquad for \ \ q-m < j \le q, \end{cases}$$

where $0 < \lambda_{q-m+1} < \lambda_{q-m+2} < .. < \lambda_q < \infty$ *are non-zero ordered eigenvalues of* $\frac{\eta^2}{\sigma^2}\overline{\mathbf{H}}_2\overline{\mathbf{H}}_2{}^H$, $\mathbf{V}_m$ *is a* $m \times m$ *Vandermonde matrix whose determinant is given by* $\det(\mathbf{V}_m) = \prod_{l<k}^{q}(\lambda_k - \lambda_l)$, *and* $\mathbf{\Lambda}_m = \mathrm{diag}(\lambda_{q-m+1}, \lambda_{q-m+2}, ..., \lambda_q)$.

Proof. See Appendix 2. □

Similar to the previous scenario, m.g.f. is not directly dependent on the LoS component. It depends on the m non-zero eigenvalues of $\frac{\eta^2}{\sigma^2}\overline{\mathbf{H}}_2\overline{\mathbf{H}}_2{}^H$. The derived result is used to find the impact of the LoS rank on the error performance in a later section.

I.I.D Rician

As another case we derive the m.g.f. of the SNR when the relay-destination channel undergoes i.i.d. Rician fading. Clearly, when the channel is i.i.d Rician $\frac{\eta^2}{\sigma^2}\overline{\mathbf{H}}_2\overline{\mathbf{H}}_2{}^H$ has only one eigenvalue given by $pq\eta^2/\sigma^2$.

Corollary 2.2. *The m.g.f. of the SNR* γ *in the i.i.d. Rician scenario is given by*

$$M_\gamma(s)_{iid} = \frac{e^{-\lambda_q}}{\Gamma(t)\lambda_q^{q-1}} \frac{\det(\mathbf{I}_{iid}(s))}{\prod_{m=1}^{q-1}\Gamma(q-m)\Gamma(p-m)}, \tag{2.20}$$

where λ_q *is the non-zero eigenvalue,* $\mathbf{I}_{iid}(s)$ *is a* $q \times q$ *matrix with entries are given by*

$$\{\mathbf{I}_{iid}(s)\}_{i,j} = \begin{cases} \sum_{k=0}^{N_S} \frac{\binom{N_S}{k}\ \Gamma(\nu_{ij}+k)}{(a\sigma)^{2\nu_{ij}}\,(1+\alpha\overline{\gamma}s)^{\nu_{ij}+k}} \\ \times U\left(\nu_{ij}+k; \nu_{ij}+1+k-N_S; \frac{1}{a^2\sigma^2(1+\alpha\overline{\gamma}s)}\right) \\ \qquad\qquad\qquad\qquad\qquad\qquad for\ \ 1 \le j \le q-1 \\ \sum_{k=0}^{N_S}\sum_{l=0}^{\infty} \frac{\binom{N_S}{k} a^{2k}\sigma^{2k}\lambda_j^l\ \Gamma(\nu_i+k+l)}{(t)_l\ \ l!\ \ (a^2\sigma^2(1+\alpha\overline{\gamma}s))^{\nu_i+k+l}} \\ \times U\left(\nu_i+k+l; \nu_i+k+l+1-N_S; \frac{1}{a^2\sigma^2(1+\alpha\overline{\gamma}s)}\right) \\ \qquad\qquad\qquad\qquad\qquad\qquad for\ \ j = q. \end{cases}$$

Proof. See Appendix 2. □

Rayleigh

When $\overline{\mathbf{H}}_2 = 0$ (i.e., Rayleigh fading), all eigenvalues become zero.

Corollary 2.3. *The m.g.f. of the SNR γ in the Rayleigh faded case is given by*

$$M_{\gamma}(s)_{R} = \frac{\det(\mathbf{I}_R(s))}{\prod_{m=1}^{q}\Gamma(q-m+1)\Gamma(p-m+1)}, \tag{2.21}$$

where $\mathbf{I}_R(s)$ is a $q \times q$ Hankel matrix with (i,j)th element given by

$$(\mathbf{I}_R(s))_{i,j} = \sum_{k=0}^{N_S}\binom{N_S}{k}\frac{\Gamma(\nu_{ij}+k)U\left(\nu_{ij}+k;\nu_{ij}+1+k-N_S;\frac{1}{a^2\sigma^2(1+\alpha\overline{\gamma}s)}\right)}{(a\sigma)^{2\nu_{ij}}(1+\alpha\overline{\gamma}s)^{\nu_{ij}+k}}.$$

Proof. Similar to the proof in Appendix 2. This can be obtained by taking the limit of $M_{\gamma}(s)_{\text{iid}}$ as $\lambda_q \to 0$. □

To discuss other statistical parameters in this section, we consider the non-i.i.d. Rician fading in the relay-destination channel. A similar procedure is valid for the correlated Rician, i.i.d. Rician and Rayleigh scenarios.

2.2.2 Moments of the SNR

Here we derive new expressions for the first and second moment of the SNR γ, which will be employed to quantify the AoF in the following section.

Theorem 2.2. *The first moment of the SNR γ is given by*

$$m_1 = \frac{N_S a^2\sigma^2\overline{\gamma}\alpha\ e^{-\mathrm{Tr}(\mathbf{\Lambda})}}{(\Gamma(t))^q\ \det(\mathbf{V})}\ \sum_{k=1}^{q}\det(\mathbf{I}(k)), \tag{2.22}$$

where $\mathbf{I}(k)$ is a $q \times q$ matrix and its $(i,j)^{th}$ element is given by

$$(\mathbf{I}(k))_{i,j} = \begin{cases} \sum_{l=0}^{\infty}\frac{\lambda_k^l\ \Gamma(p+l-i+2)U\left(p+l-i+2;p+l-i+2;\frac{1}{a^2\sigma^2}\right)}{(t)_l\ l!\ (a^2\sigma^2)^{p+l-i+2}} & \text{for } j=k \\ \Gamma(p-i+1)\,{}_1F_1(p-i+1;t;\lambda_j) & \text{for } j\neq k, \end{cases}$$

where ${}_1F_1(\cdot;\cdot;\cdot)$ denoting the confluent hypergeometric function [134]. This can be proved by taking the first derivative of the m.g.f. given in the (2.16).

Proof. See Appendix 3. □

Theorem 2.3. *The second moment of the SNR γ is given by*

$$m_2 = \frac{e^{-\mathrm{Tr}(\mathbf{\Lambda})}}{(\Gamma(t))^q\ \det(\mathbf{V})}\ \sum_{k=1}^{q}\sum_{l=1}^{q}\det(\mathbf{I}(k,l)) \tag{2.23}$$

where $\mathbf{I}(k,l)$ *is a* $q \times q$ *matrix with* k*th and* l*th columns are subjected to the differentiation and its* (i,j)*th element given as*

$$(\mathbf{I}(k,l))_{i,j} = \begin{cases} N_S(N_S+1)(\alpha\overline{\gamma}a^2\sigma^2)^2 \\ \times\sum_{l=0}^{\infty} \frac{\lambda_k^l \ \Gamma(p+l-i+3)U(p+l-i+3;p+l-i+2;\frac{1}{a^2\sigma^2})}{(t)_l \ l! \ (a^2\sigma^2)^{p+l-i+3}} & \text{for } \ j=l=k \\ N_S(\alpha\overline{\gamma}a^2\sigma^2) \\ \times\sum_{l=0}^{\infty} \frac{\lambda_k^l \ \Gamma(p+l-i+2)U(p+l-i+2;p+l-i+2;\frac{1}{a^2\sigma^2})}{(t)_l \ l! \ (a^2\sigma^2)^{p+l-i+2}} & \text{for } \ j=k \text{ or } j=l; k\neq l \\ \Gamma(p-i+1)_1F_1(p-i+1;t;\lambda_j) & \text{for } \ j\neq k \text{ and } j\neq l \end{cases}$$

Proof. By differentiating m.g.f. with respect to s twice, we obtain the above expression for the second moment. □

2.2.3 Exact probability distribution of the SNR

The distributions of instantaneous SNR are also useful to find the effect of the asymmetric fading. The analytical expressions of p.d.f. and c.d.f. are provided in this section.

Probability density function

The exact probability distribution of the SNR γ is considered for $q = 1$. Deriving a solution for the general case is mathematically hard. This solution can be used to evaluate the effect of the Rician factor on the SNR γ.

Theorem 2.4. *The p.d.f. of the SNR* γ *is given for the case* $\min(N_R, N_D) = 1$ *by*

$$\begin{aligned} f_\gamma(\gamma) =& \frac{2\gamma^{N_S-1}e^{\left(\frac{-\gamma}{\alpha\overline{\gamma}}\right)}e^{-\lambda}}{\Gamma(N_S)\Gamma(p)(\alpha\overline{\gamma}\sigma^2a^2)^{N_S}} \sum_{j=0}^{N_S}\sum_{l=0}^{\infty} \frac{\binom{N_S}{j}a^{2j}\sigma^{2j}\lambda^l}{(p)_l\Gamma(l+1)} \\ & \times \left(\frac{\gamma}{a^2\sigma^2\alpha\overline{\gamma}}\right)^{r/2} K_r\left(2\sqrt{\frac{\gamma}{a^2\sigma^2\alpha\overline{\gamma}}}\right), \end{aligned} \tag{2.24}$$

where $r = p+l+j-N_S$ *and* $K_n(z)$ *is the modified Bessel function of the second kind and of order* n.

Proof. See Appendix 4. □

The expression in (2.24) has an infinite summation, but it converges rapidly, and we can obtain sufficiently accurate results for the p.d.f. by truncating this summation. Fig.2.2 compares the probability distribution variation with different Rician factors ($K = \frac{\eta^2}{\sigma^2}$) for the Alamouti OSTBC with code rate $R = 1$. Both analytical and simulated curves are obtained for $K = -10, 0, 10$ dB with the antenna configuration of (2, 5, 1). Simulation curves are obtained by using Monte Carlo method with 10^6 random channel realizations. In particular, the entries of $\mathbf{H}_1, \widetilde{\mathbf{H}}_2$ are generated as circular symmetric Gaussian variables with unit variance. LoS part is generated according to [135] with full rank, where entries are non identical complex elements with unit magnitude. In particular, the LoS component is generated by,

$$\overline{\mathbf{H}}_2 = \sum_{i=1}^{m} \beta_i \mathbf{a}(\theta_{r,i})\mathbf{a}(\theta_{t,i})^T, \tag{2.25}$$

where $\mathbf{a}(\theta_{r,i})$ is the array response vector and $\mathbf{a}(\theta_{t,i})$ is the array steering vector for ith dominant path, $\theta_{r,i}$ and $\theta_{t,i}$ denote the angle of arrival and the angle of departure, respectively. β_i is the complex amplitude of the ith path. The rank of the matrix depends on the number of dominant paths and for full rank $m = q$. We also consider the average SNR to be $\bar{\gamma} = 10$ dB, and $b = 1$. As expected, both analytical and simulated curves are matched with reasonable accuracy. When the Rician factor K increases, the SNR distribution move towards the higher range.

Cumulative distributive function

Here, we consider $q = 1$ to derive the c.d.f.. Similar to the p.d.f. derivation, the m.g.f. of the SNR γ and the eigenvalue distribution of $\frac{1}{\sigma^2}\mathbf{H}_2\mathbf{H}_2^H$ are used to derive the c.d.f..

Theorem 2.5. *The c.d.f. of the SNR γ is given for the case* $\min(N_R, N_D) = 1$

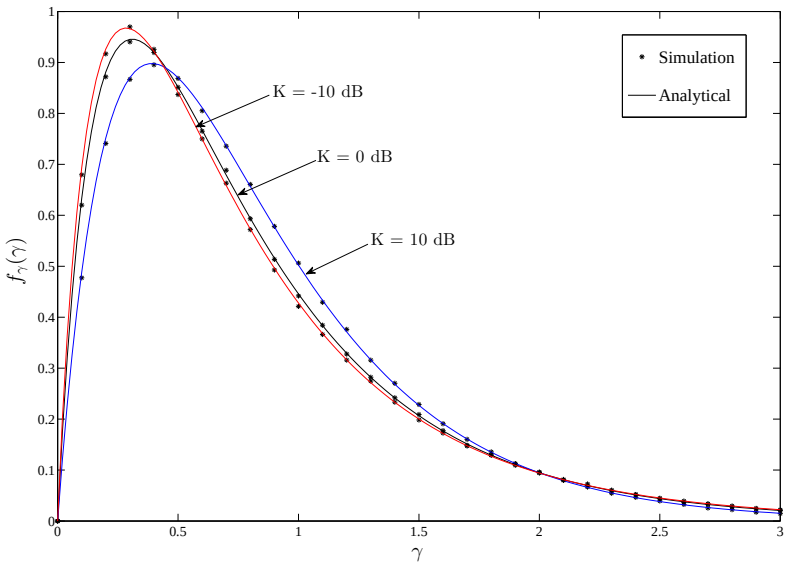

Fig 2.2. p.d.f. of γ for the antenna configuration (2,5,1). Results are shown for different values of the Rician factor $\left(K = \frac{\eta^2}{\sigma^2}\right)$. Alamouti OSTBC is used with $\overline{\gamma} =$ 10 dB with $b = 1$, [51] © 2013, IEEE.

by

$$F(\gamma) = 1 - \frac{2e^{-\left(\lambda + \frac{\gamma}{\alpha\overline{\gamma}}\right)}}{\Gamma(p)} \sum_{k=0}^{N_S-1} \sum_{i=0}^{k} \sum_{l=0}^{\infty} \frac{\binom{k}{i} \gamma^k \lambda^l \left(\sqrt{\frac{\gamma}{a^2\sigma^2\alpha\overline{\gamma}}}\right)^{p+l-i}}{k!\alpha^k \overline{\gamma}^k a^{2i} \sigma^{2i} (p)_l \Gamma(l+1)} \times K_{p+l-i}\left(2\sqrt{\frac{\gamma}{a^2\sigma^2\alpha\overline{\gamma}}}\right). \quad (2.26)$$

Proof. See Appendix 4. □

Next, Theorem 2.5 is used to plot the analytical c.d.f. curve in Fig.2.3, where figure shows the variation of the c.d.f. with different Rician factor K. Here, the results are shown for the same simulation parameters as in the p.d.f. case. Similar variations can be seen as in the Fig.2.2.

Many other statistical properties can also be derived for the instantaneous SNR of Rayleigh-Rician channels. The statistical properties that we obtain here are used to derive the system performance in terms of BER, diversity order, array gain, AoF and outage probability.

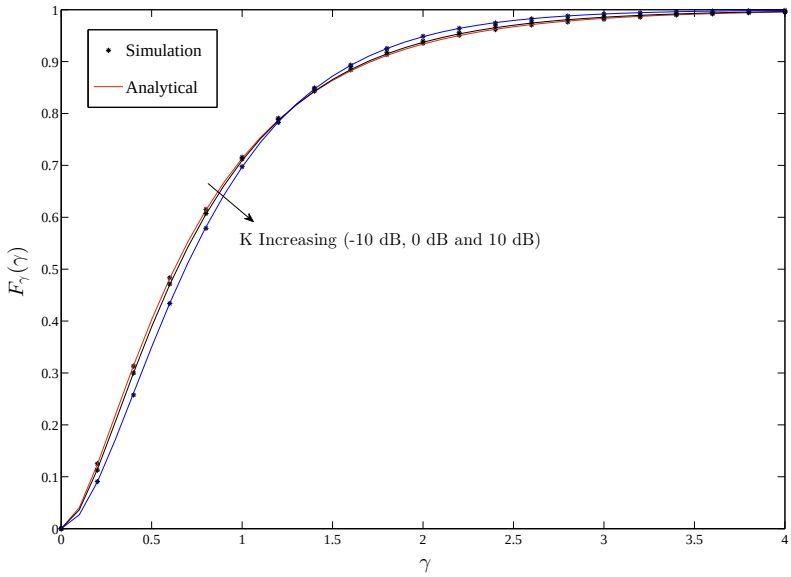

Fig 2.3. c.d.f. of γ for the antenna configuration (2,5,1) for non-i.i.d Rician Fading. Results are shown for the Alamouti OSTBC and $\overline{\gamma} = 10$ dB with $b = 1$, [51] © 2013, IEEE.

2.3 Performance analysis

In this section, we investigate some useful parameters which are widely used to measure wireless system performances.

2.3.1 BER of BPSK

BER is key performance metric to evaluate performance of a wireless system, which can be obtained using the m.g.f. considering different modulation schemes [136, Eq. 9.361]. BER P_E for BPSK scheme is given as,

$$P_E = \frac{1}{\pi} \int_0^{\frac{\pi}{2}} M_\gamma \left(\frac{1}{\sin^2\theta} \right) \, d\theta \; . \tag{2.27}$$

The m.g.f. expressions in (2.16)-(2.21) can be used find the behavior of BER with different antenna configurations and Rician factors. The integral seems intractable for a general antenna configuration. Therefore, we consider the case where the number of antennas in relay or destination equals to one, i.e., $q = 1$.

Then we use the m.g.f. expression in (1.0.10)(Appendix 1) to simplify (2.27) as,

$$P_E = \frac{c}{\pi}\int_0^{\frac{\pi}{2}}\int_0^{\infty} \frac{y^{p-1}e^{-y}(1+a^2\sigma^2 y)^{N_S}\ {}_0F_1(t;y\lambda)}{(1+a^2(1+\frac{\alpha\overline{\gamma}}{\sin^2\theta})\sigma^2 y)^{N_S}}\ dy\ d\theta\ , \tag{2.28}$$

where

$$c = \frac{e^{-\mathrm{Tr}(\mathbf{\Lambda})}}{(\Gamma(t))^q}\ , \tag{2.29}$$

and ${}_0F_1(\cdot;\cdot)$ is the generalized hypergeometric function defined in [134]. Now, we interchange the order of integration, and simplify the inner integral as

$$\begin{aligned}\int_0^{\frac{\pi}{2}} \frac{(1+a^2\sigma^2 y)^{N_S}}{(1+a^2\sigma^2 y+\frac{a^2\alpha\overline{\gamma}}{\sin^2\theta}\sigma^2 y)^{N_S}}\ d\theta =& \frac{\pi}{2} - \sum_{k=0}^{N_S-1}\frac{\frac{\pi}{2}\binom{2k}{k}}{4^k} \\ &\times \frac{\sqrt{a^2\alpha\overline{\gamma}\sigma^2 y}(1+a^2\sigma^2 y)^k}{(1+a^2(1+\alpha\overline{\gamma})\sigma^2 y)^{k+\frac{1}{2}}},\end{aligned} \tag{2.30}$$

which in turn gives the BER as

$$P_E = \frac{1}{2} - \frac{c}{2}\sum_{k=0}^{N_S-1}\binom{2k}{k}\int_0^{\infty} y^{p-1}\ e^{-y}\ {}_0F_1(p;y\lambda)\frac{\sqrt{a^2\alpha\overline{\gamma}\sigma^2 y}(1+a^2\sigma^2 y)^k}{4^k(1+a^2(1+\alpha\overline{\gamma})\sigma^2 y)^{k+\frac{1}{2}}}\ dy. \tag{2.31}$$

After some algebraic manipulations we have the closed form of BER as

$$\begin{aligned}P_E =& \frac{1}{2} - \frac{c}{2}\sum_{k=0}^{N_S-1}\sum_{i=0}^{k}\sum_{l=0}^{\infty}\frac{\binom{2k}{k}\binom{k}{i}\lambda^l\Gamma(p+l+i+\frac{1}{2})\sqrt{\alpha\overline{\gamma}}}{4^k(1+\alpha\overline{\gamma})^{(p+l+i+\frac{1}{2})}(a^2\sigma^2)^{p+l}(p)_l} \\ &\times \frac{U\left(p+l+i+\frac{1}{2};p+l+i-k;\frac{1}{a^2\sigma^2(1+\alpha\overline{\gamma})}\right)}{\Gamma(l+1)}.\end{aligned} \tag{2.32}$$

This expression is used to obtain analytical BER curve for $q = 1$, whereas (2.27) is used for other antenna configurations with the integral evaluated numerically using softwares such as Matlab or Mathematica for all parameters of our interest.

Fig.2.4 shows the analytical and simulation curves for three different antenna configurations with non-i.i.d. Rician fading in relay-destination channel. The results are obtained using Alamouti OSTBC technique. Channels are generated in a similar manner to the previous cases, and LoS part is generated according to [135] with full rank. Now b is selected as average transmit SNR $\bar{\gamma}$. Simulation and analytical curves are seen to match perfectly. As can be seen from the graph, the Rician factor has a constructive effect on the BER under the antenna

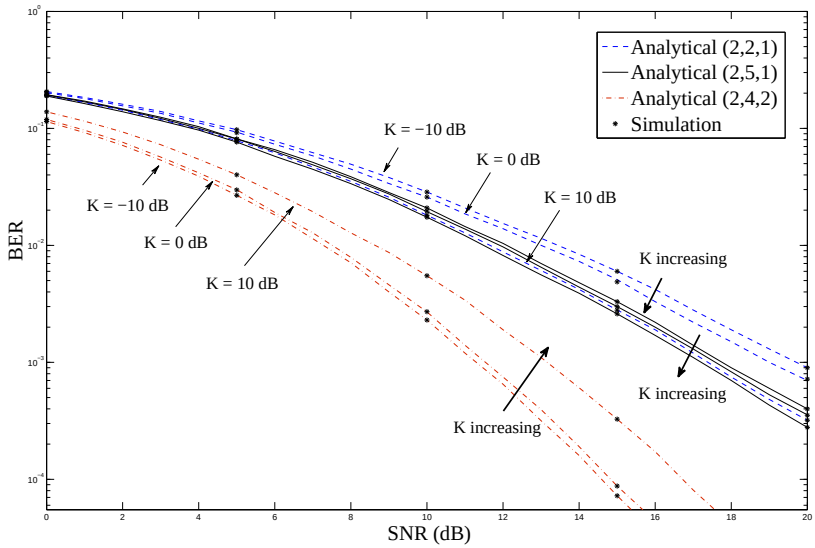

Fig 2.4. BER for BPSK versus average SNR $\overline{\gamma}$ in non-i.i.d Rician fading. Results are shown for different antenna configurations (N_S, N_R, N_D) and different values of the Rician factor $\left(K = \frac{v^2}{\sigma^2}\right)$. Alamouti OSTBC is used with $b = \overline{\gamma}$, [51] © 2013, IEEE.

configuration with $q = 1$. A careful inspection of the BER graphs reveals that the effect of Rician factor is not homogeneous on different antenna configurations. Clearly the performance improves with the increase of K for any configuration with $q = 1$. Also, a better performance can be obtained by increasing p and q for a given Rician factor K. On the contrary, the performance degrades with the increase of K for a fixed channel gain and a specific antenna configuration other than $q = 1$.

This can be explained intuitively as follows. $q = 1$ simply means that the relay-destination channel is either multiple-input single-output (MISO) or single-input multiple-output (SIMO) channel. There, having a good LoS path component improves the system performance. That is the reason for better performance of BER for $q = 1$. When $q \neq 1$, the relay destination channel is a pure MIMO channel. When the Rician factor increases (LoS components dominate over the scattering component) the benefit of the scattering environment reduces. Therefore, this weaker scattering component causes the performance degradation. Such an observation has been made by the authors in [137] related to point-to-point MIMO Rician channels.

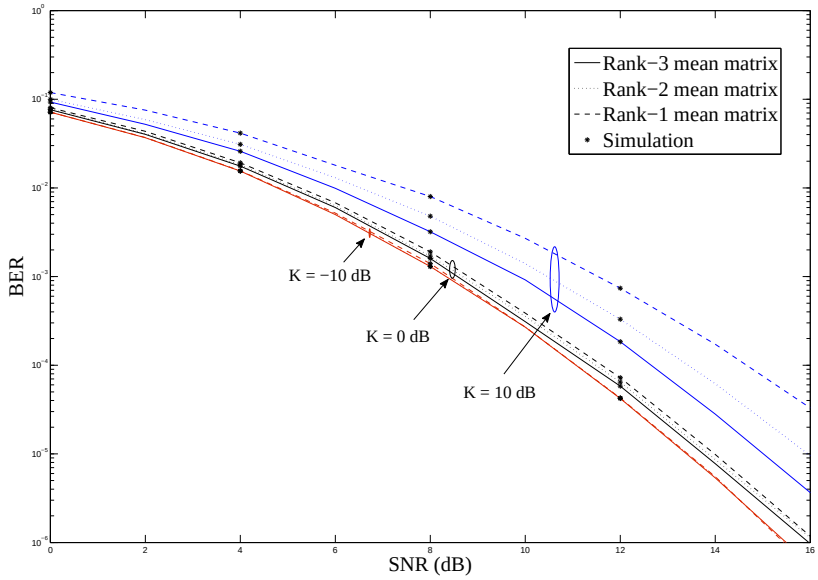

Fig 2.5. BER for BPSK versus average SNR $\overline{\gamma}$ in non-i.i.d Rician fading. Results are shown for different rank mean matrices for antenna configuration $(2, 5, 3)$ and different values of the Rician factor $\left(K = \frac{\eta^2}{\sigma^2}\right)$. Alamouti OSTBC is used with $b = \overline{\gamma}$, [51] © 2013, IEEE.

In the cases where LoS components are correlated, the rank of the mean is less than q. In such scenarios, $\frac{\eta^2}{\sigma^2}\overline{\mathbf{H}}_2\overline{\mathbf{H}}_2{}^H$ has m number of eigenvalues and the analytical expression for m.g.f. is given in (2.18). The Fig.2.5 shows analytical and simulation curves for BER with different rank mean matrices. We consider Alamouti OSTBC with similar simulation parameters used to obtain Fig.2.4. The LoS component is generated using (2.25). The rank of the LoS component is changed with the number of dominant paths in the relay-destination link. We analyzed the system by varying the mean matrix and evaluated average BER.

For all combinations, the simulated and analytical curves match with greater accuracy. The BER in Rician fading with no correlation (rank equal to q), behaves according to the previous explanation for Fig.2.4. The BER performance degraded with the rank of the LoS component. i.e., when the Rician factor is fixed, a higher rank mean matrix provides better performance than the lower rank LoS component scenarios. However, when the LoS component is weak (rician factor is small), we have almost similar error performance for all ranks. This is intuitively clear, since LoS component has less impact compared to scattering

component in such scenarios (eg. $K = -10$ dB).

2.3.2 High SNR analysis

To gain further understanding, we now consider the BER at high SNR. Here, diversity order and array gain are two main parameters which give an understanding about the behavior of the performance in high SNR region. Two different methods can be identified to discuss the high SNR scenario, which are increasing source transmit power $\rho(=\overline{\gamma})$ and increasing relay gain constant b. However, there is a finite limit for the SNR with both these methods. This was studied in [36] and they proposed an alternative "high SNR" scenario. The relay gain constant b is scaled according to the transmit power ρ. Now, $b = \beta\rho$ where β is a fixed constant. We can write (2.15) as $\gamma = \overline{\gamma}\alpha\tilde{a}^2\mathrm{Tr}(\mathbf{H}_1^H\mathbf{H}_2^H\tilde{\mathbf{K}}^{-1}\mathbf{H}_2\mathbf{H}_1)$, where $\tilde{a}^2 = \beta/N_R$ and $\tilde{\mathbf{K}} = \tilde{a}^2\mathbf{H}_2\mathbf{H}_2^H + \mathbf{I}_{N_D}$. This we write as $\gamma = \overline{\gamma}y$ and find asymptotic expansion of the m.g.f. of y. When $s \to \infty$, the following approximation of m.g.f. is used to find constant c_i and diversity order d_v [138],

$$M_y(s) \approx \frac{c_i}{s^{d_v}} \quad . \tag{2.33}$$

Array gain G_a is given by

$$G_a = \frac{c_i\ \Gamma(d_v + \frac{1}{2})}{2\sqrt{\pi}\Gamma(d_v + 1)}. \tag{2.34}$$

Here, a general solution on the diversity order and array gain is difficult. Therefore, we focus on deriving diversity order and array gain for the following antenna configurations.

Theorem 2.6. *The diversity order and array gain of the system for $q = 1$ are given by*

$$d_v = \begin{cases} N_S & for \quad p > N_S \\ p & for \quad p < N_S \end{cases}, \tag{2.35}$$

$$G_a = \begin{cases} \frac{c_1\Gamma(Ns+1/2)}{2\sqrt{\pi}\ \Gamma(Ns+1)} & for \quad p > N_S \\ \\ \frac{e^{-\lambda}\Gamma(N_S-p)\Gamma(p+1/2)}{2\sqrt{\pi}p(\tilde{a}\sigma)^{2p}\alpha^p\ \Gamma(N_S)\Gamma(p+1)} & for \quad p < N_S \end{cases}, \tag{2.36}$$

where

$$c_1 = \frac{e^{-\lambda}}{\Gamma(p)}\sum_{k=0}^{N_S}\sum_{l=0}^{\infty}\frac{\binom{N_S}{k}(\tilde{a}\sigma)^{2(k-N_S)}\lambda^l\Gamma(p+l+k-N_S)}{(p)_l l!\alpha^{N_S}}. \tag{2.37}$$

The diversity order and array gain of the system for $q = 2$ are given by

$$d_v = \begin{cases} 2p & for \quad p < N_S - 1 \\ 2N_S - 1 & for \quad p = N_S \\ 2N_S & for \quad p > N_S + 1 \end{cases}, \tag{2.38}$$

$$G_a = \begin{cases} \frac{c_2\Gamma(2p+\frac{1}{2})}{2\sqrt{\pi}\Gamma(2p+1)} & for \quad p < N_S - 1 \\ \frac{c_3\Gamma(2N_S-\frac{1}{2})}{2\sqrt{\pi}\Gamma(2N_S)} & for \quad p = N_S \\ \frac{c_4\Gamma(2N_S+\frac{1}{2})}{2\sqrt{\pi}\Gamma(2N_S+1)} & for \quad p > N_S + 1 \end{cases}, \tag{2.39}$$

where

$$c_2 = \frac{e^{-(\lambda_1+\lambda_2)}}{\Gamma(p-1)^2\tilde{a}^{2p}\sigma^{2p}\alpha^{2p}}\Big(\Gamma(p+1)\Gamma(p-1)\Gamma(N_S-p+1)\Gamma(N_S-p-1) - \Gamma(p)^2\Gamma(N_S-p)^2\Big), \tag{2.40}$$

$$c_3 = \frac{e^{-(\lambda_1+\lambda_2)}}{\Gamma(p-1)^2(\lambda_2-\lambda_1)}\sum_{k=0}^{N_S}\sum_{l=0}^{\infty}\binom{N_S}{k}\frac{{a_1}^{2k}\sigma^{2k}\Gamma(p-1)}{(p-1)_l\ l!\ \Gamma(N_S)} \times \frac{\Gamma(p+k+l-N_S)(\lambda_2^l-\lambda_1^l)}{(\tilde{a}^2\sigma^2\alpha)^{2N_S-1}}, \tag{2.41}$$

and

$$c_4 = \frac{e^{-(\lambda_1+\lambda_2)}}{\Gamma(p-1)^2(\lambda_2-\lambda_1)}\sum_{k=0}^{N_S}\sum_{m=0}^{N_S}\sum_{l=0}^{\infty}\sum_{n=0}^{\infty}\frac{\binom{N_S}{k}\binom{N_S}{m}(\tilde{a}\sigma)^{2(k+m)}}{(p-1)_l(p-1)_n} \times \frac{\Gamma(p+m+n-N_S-1)\Gamma(p+k+l-N_S)(\lambda_2^l\lambda_1^n-\lambda_1^l\lambda_2^n)}{l!\ n!\ (\tilde{a}^2\sigma^2\alpha)^{2N_S}}. \tag{2.42}$$

Proof. See Appendix 5. □

A few array gain expressions have infinite summations. However, truncated series gives accurate results. Fig.2.6 shows the asymptotic analysis on BER with Rician factor for different antenna configurations. Average BER for BPSK for asymptotic scenario is approximated with $P_E = G_a/\overline{\gamma}^{d_v}$. Similar simulation parameters are used as in Fig.2.4. BER curves in Fig.2.6 verify the accuracy of the high SNR analysis. Rician factor has a similar effect as can be seen in Fig.2.4.

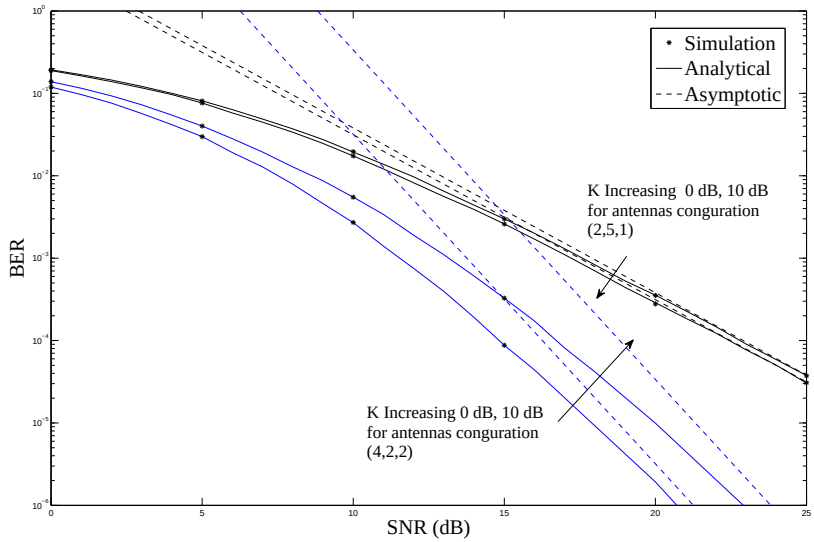

Fig 2.6. Asymptotic analysis on BER versus SNR γ in non-i.i.d Rician fading. Results are shown for different antenna configurations (N_S, N_R, N_D) and different values of the Rician factor $\left(K = \frac{\eta^2}{\sigma^2}\right)$. Alamouti OSTBC is used with $b = \overline{\gamma}$, [51] © 2013, IEEE.

2.3.3 Amount of fading

The AoF is another important performance parameter which measures the severity of the fading channel [139]. Following [136, 139, 140], we can write the AoF as

$$\text{AoF} = \frac{m_2 - m_1^2}{m_1^2}. \tag{2.43}$$

The non-i.i.d Rician fading scenario is considered to discuss the AoF with Rician factor K. The first and second moments of the SNR γ derived in Theorem 2.2 and Theorem 2.3 are used to evaluate AoF. Fig.2.7 illustrates the AoF versus b for different antenna configurations and Rician factors. Here also the results are obtained using Alamouti OSTBC techniques with code rate $R = 1$ and assuming parameters as in earlier sub-section. Both the simulation and analytical curves seem to match accurately with each other.

The AoF graph also confirms that the effect of Rician factor is not homogeneous on different antenna configurations. A similar effect for antenna configuration with $q = 1$ and $q \neq 1$ can be observed. Also, a better performance can be

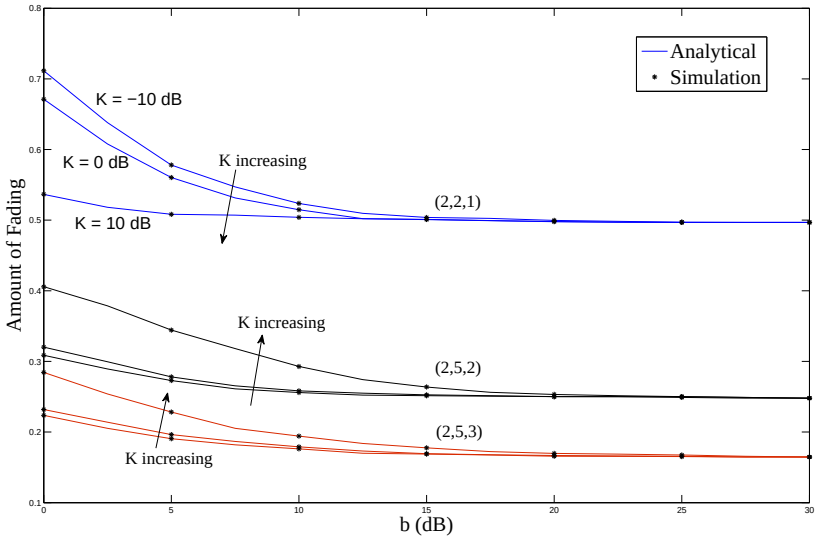

Fig 2.7. AoF versus average b for different antenna configurations (N_S, N_R, N_D) **and different values of the Rician factor** $\left(K = \frac{\eta^2}{\sigma^2}\right)$**. Alamouti OSTBC is used with** $\overline{\gamma} = 10$ **dB, [51] © 2013, IEEE.**

obtained by increasing p and q for a given Rician factor K.

We can also observe an asymptotic floor of AoF as the relay gain b becomes large. This can be explained as follows. As $b \to \infty$ then $a^2 \to \infty$, we can write $M_{\gamma|\mathbf{\Phi}}(s) = 1/\left(1 + \alpha\overline{\gamma}s\right)^{N_S q}$, the Laplace inversion of which gives $f_\gamma(\gamma) = \gamma^{N_S q - 1} e^{-\gamma/\alpha\overline{\gamma}} / \Gamma(N_S q)(\alpha\overline{\gamma})^{N_S q}$. As such, the moments of γ become functions of $N_S q$ only. Therefore, being a function of the moments, AoF becomes also a function of $N_S q$, which produces the AoF floors in the graph.

2.3.4 Outage probability

Outage probability is an important parameter which is widely used to evaluate the performance of wireless systems. That is given by

$$P_{\text{out}}(\gamma_{\text{th}}) = \Pr(\gamma \leq \gamma_{\text{th}}) = F(\gamma_{\text{th}}). \tag{2.44}$$

where γ_{th} is the SNR threshold value. The outage probability of the system is obtained by applying c.d.f. (2.26) into (2.44). Fig.2.8 shows the effect of the Rician factor on the outage probability. Two different antenna configurations are used with the Alamouti OSTBC system. We also consider the average SNR

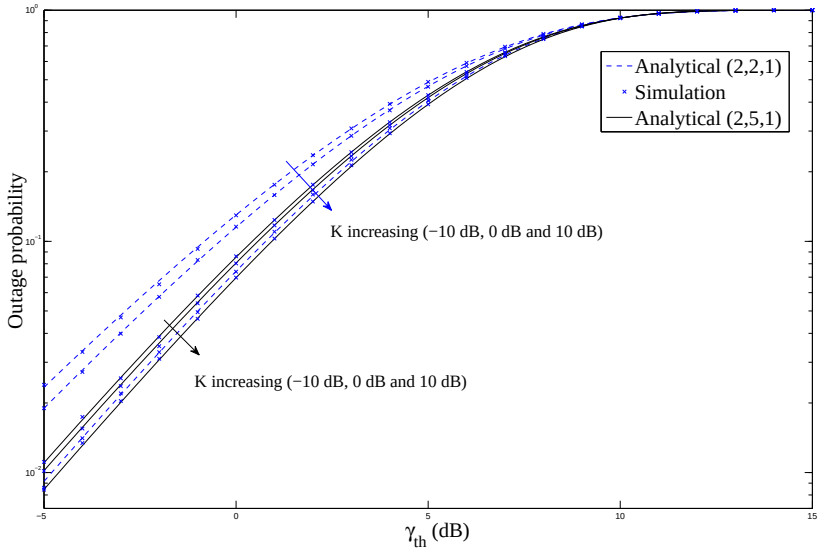

Fig 2.8. Illustration on the effect of the Rician factor K on the outage probability for different antenna configurations (N_S, N_R, N_D). Alamouti OSTBC has been used with $\overline{\gamma} = 10$ dB and $b = 1$, [51] © 2013, IEEE.

$\bar{\gamma} = 10$ dB, and $b = 1$. The outage probability increases with the SNR threshold γ_{th}. For both antenna configurations, where $q = 1$, the outage probability decreases with the Rician factor. This is in parallel with the earlier observations.

Next, we investigate performance of optimal single stream beamforming AF MIMO relaying for Rayleigh-Rician channels. This can be used to obtain further understanding on Rayleigh-Rician scenarios.

2.4 Optimal single stream beamforming

In this section, we summarize the study on optimal single stream beamforming based non-coherent AF MIMO relaying over Rayleigh-Rician fading environment. The beamforming vectors are designed to maximize the instantaneous SNR at the destination. The CSI at the destination is used to find these optimal beamforming vectors, and transmit beamforming vector is sent back to the source prior data transmission. The tools of finite-dimensional random matrix theory are used to analyze the performance of the system with different Rician fading scenarios. New statistical results of the instantaneous SNR at the destination

are derived in terms of the c.d.f., p.d.f., and moments. Then, we use these statistical expressions to derive equations for outage probability, SER and ergodic capacity. Diversity orders are derived for simplified scenarios in the high SNR analysis. These performance metrics are used to evaluate the performance of the AF MIMO system with different antenna configurations, Rician factors, and different Rician fading scenarios. Additionally, the saturation loss at the relay is quantified in terms of the outage probability. Finally, the system is compared with the OSTBC based AF MIMO system. Here, we present only the system model and some important results. A detailed analysis can be find in [53].

2.4.1 System model

A similar system model as in Fig.2.1 is considered with beamforming vectors at the source and destination. The source node transmits beamformed version of modulated symbol $x \in \mathbb{C}$ after being beamformed by a transmit beamforming vector $\mathbf{w}_{\mathrm{t}} \in \mathbb{C}^{N_{\mathrm{S}}}$, where $\mathcal{E}\{|x|^2\} = \rho$, and $||\mathbf{w}_{\mathrm{t}}||^2 = 1$. The destination detects the signal after using a receive beamforming vector $\mathbf{w}_{\mathrm{r}} \in \mathbb{C}^{N_{\mathrm{D}}}$, where $||\mathbf{w}_{\mathrm{r}}||^2 = 1$. The received signal r at the destination is given as

$$r = \sqrt{a}\mathbf{w}_{\mathrm{r}}^H \mathbf{H}_2 \mathbf{H}_1 \mathbf{w}_{\mathrm{t}} x + \sqrt{a}\mathbf{w}_{\mathrm{r}}^H \mathbf{H}_2 \mathbf{n}_R + \mathbf{w}_{\mathrm{r}}^H \mathbf{n}_D, \tag{2.45}$$

where $\mathbf{n}_D \sim \mathcal{CN}(0, \mathbf{I}_{N_{\mathrm{D}}})$ is noise vector at the destination. The instantaneous SNR at the destination is given by

$$\gamma = \frac{a\rho \mathbf{w}_{\mathrm{r}}^H \mathbf{H}_2 \mathbf{H}_1 \mathbf{w}_{\mathrm{t}} \mathbf{w}_{\mathrm{t}}^H \mathbf{H}_1^H \mathbf{H}_2^H \mathbf{w}_{\mathrm{r}}}{\mathbf{w}_{\mathrm{r}}^H (a\mathbf{H}_2 \mathbf{H}_2^H + \mathbf{I}_{N_{\mathrm{D}}}) \mathbf{w}_{\mathrm{r}}}. \tag{2.46}$$

Here, the SNR γ can be maximized by optimal beamforming design. As in the Section 2.1, we assume CSI of $\mathbf{H}_2$ and $\mathbf{H}_2\mathbf{H}_1$ is available at the destination, while both source and relay have no knowledge. The destination computes the optimal beamforming vectors $\mathbf{w}_{\mathrm{t}}$ and $\mathbf{w}_{\mathrm{r}}$. Then, the optimal transmit beamforming vector is sent back to the transmitter via a dedicated feedback link [41]. The optimal receive beamforming vector $\mathbf{w}_{\mathrm{r}}$ that maximize the SNR is given by

$$\mathbf{w}_{\mathrm{r}} = (a\mathbf{H}_2 \mathbf{H}_2^H + \mathbf{I}_{N_{\mathrm{D}}})^{-1} \mathbf{H}_2 \mathbf{H}_1 \mathbf{w}_{\mathrm{t}}. \tag{2.47}$$

Then, substituting (2.47) into (2.46) gives

$$\gamma = a\rho \mathbf{w}_{\mathrm{t}}^H \mathbf{H}_1^H \mathbf{H}_2^H (a\mathbf{H}_2 \mathbf{H}_2^H + \mathbf{I}_{N_{\mathrm{D}}})^{-1} \mathbf{H}_2 \mathbf{H}_1 \mathbf{w}_{\mathrm{t}}. \tag{2.48}$$

Next, we consider eigenvalues of $\mathbf{H}_1^H\mathbf{H}_2^H(a\mathbf{H}_2\mathbf{H}_2^H+\mathbf{I}_{N_\mathrm{D}})^{-1}\mathbf{H}_2\mathbf{H}_1$ as $\xi_1,\xi_2,..,\xi_{N_S}$. The maximum eigenvalue is denoted as $\xi_{\max}$, which is given by

$$\xi_{\max}=\max(\xi_1,\xi_2,..,\xi_{N_\mathrm{S}}). \tag{2.49}$$

The eigenvector associated with $\xi_{\max}$ is $\mathbf{v}_{\max}\in\mathbb{C}^{N_\mathrm{S}}$. Therefore,

$$\mathbf{H}_1^H\mathbf{H}_2^H(a\mathbf{H}_2\mathbf{H}_2^H+\mathbf{I}_{N_\mathrm{D}})^{-1}\mathbf{H}_2\mathbf{H}_1\mathbf{v}_{\max}=\xi_{\max}\mathbf{v}_{\max}. \tag{2.50}$$

It is evident that $\mathbf{w}_\mathrm{t}=\mathbf{v}_{\max}$ provides the maximum instantaneous SNR γ in (2.48), and γ is simplified into

$$\gamma=a\rho\xi_{\max}. \tag{2.51}$$

The statistical propoerties and performance metrics of the SNR is derived based on the properties of $\xi_{\max}$.

2.4.2 Comparison to OSTBC based AF relaying

Fig.2.9 shows average BER versus average transmit SNR $\bar{\gamma}$ (equals to ρ due to unit noise variance) for BPSK modulation considering OSTBC and optimal beamforming schemes. The OSTBC based AF MIMO system uses Alamouti OSTBC with code rate one to make a fair comparison. Similar simulation parameters are assumed as in the previous cases with $b=\bar{\gamma}$. The average BER performance is considered with different Rician factors for antenna configurations (2,4,2). The average BER performance is better in low Rician factors. This is similar to the behavior we observed in OSTBC based AF MIMO relaying. For all Rician factors, the optimal single stream beamforming based MIMO dual-hop system performs better than OSTBC based AF MIMO system.

2.5 Relay selection over asymmetric fading channels

This section, the results of which are presented in [55], summarizes the analysis of OSTBC based AF MIMO system, where the source-destination communication is now assisted by multiple AF relays. All relays are deployed to have LoS path to the destination. The system model is illustrated in Fig.2.10, where all relays (N) perform non-coherent AF relaying. The relay node n $(=1,..N)$ has R_n antennas.

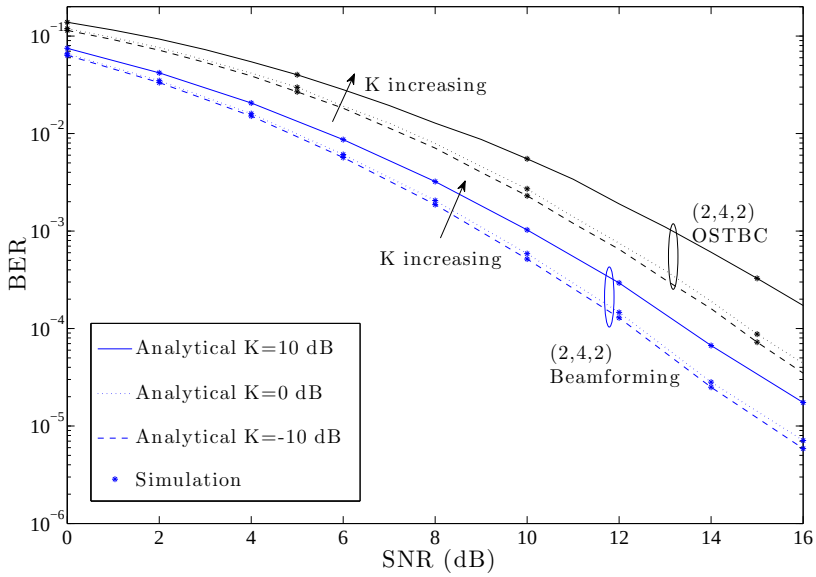

Fig 2.9. Difference between OSTBC and beamforming based AF MIMO system. Alamouti OSTBC, BPSK modulation and $b = \bar{\gamma}$ is used with antenna configuration (2,4,2), [53] © 2014, IEEE.

General non-coherent AF relaying assumption is made as in the previous scenarios. The source-relay channels are assumed to undergo Rayleigh fading and relay-destination channels are subject to Rician fading. The channel matrices between the source-to-nth relay and nth relay-to-destination are denoted as $\mathbf{H}_{\mathrm{S}n} \in \mathbb{C}^{R_n \times N_{\mathrm{S}}}$ and $\mathbf{H}_{n\mathrm{D}} \in \mathbb{C}^{N_{\mathrm{D}} \times R_n}$, respectively. Entries of $\mathbf{H}_{\mathrm{S}n}$ are assumed to be $\sim \mathcal{CN}(0,1)$. We model $\mathbf{H}_{n\mathrm{D}}$ with a specular component (LoS) $\overline{\mathbf{H}}_{n\mathrm{D}}$ and variable component (scattered) $\widetilde{\mathbf{H}}_{n\mathrm{D}}$ as $\mathbf{H}_{n\mathrm{D}} = \eta_n \overline{\mathbf{H}}_{n\mathrm{D}} + \sigma_n \widetilde{\mathbf{H}}_{n\mathrm{D}}$, where $\eta_n^2 + \sigma_n^2 = 1$. $\overline{\mathbf{H}}_{n\mathrm{D}}$ consists of complex elements having unit magnitude, entries of $\widetilde{\mathbf{H}}_{n\mathrm{D}}$ are assumed to be $\sim \mathcal{CN}(0,1)$.

Following the same procedure as in (2.4)-to-(2.15), we can obtain the instantaneous SNR at the destination through the n th relay as

$$\gamma_n = \alpha \overline{\gamma} a_n^2 \mathrm{Tr}\left(\mathbf{H}_{\mathrm{S}n}^H \mathbf{H}_{n\mathrm{D}}^H (a_n^2 \mathbf{H}_{n\mathrm{D}} \mathbf{H}_{n\mathrm{D}}^H + \mathbf{I}_{N_{\mathrm{D}}})^{-1} \mathbf{H}_{n\mathrm{D}} \mathbf{H}_{\mathrm{S}n}\right), \tag{2.52}$$

where relay gain $a_n = \sqrt{\frac{b_n}{R_n(1+\rho)}}$ and b_n is a positive real value which depends on the long term average transmit power at the relay. We investigate two relay selection schemes at the destination.

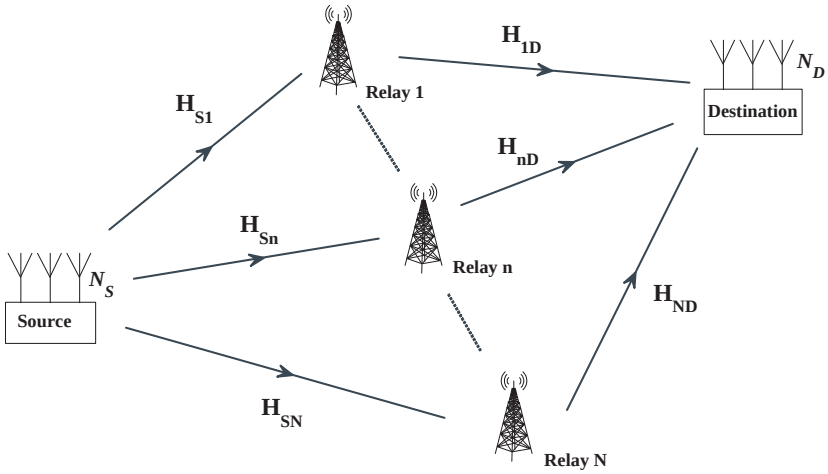

Fig 2.10. AF MIMO dual-hop system with N relays. Source-relay undergoes Rayleigh fading and relay- destination undergoes Rician fading, [55] © 2014, IEEE.

Optimal relay selection scheme

The selection method is following a SNR policy in the sense that the selected relay achieves the maximum instantaneous SNR. i.e,

$$n^*_{\text{opt}} = \arg \max_{n\in\{1,\ldots,N\}} \gamma_n. \tag{2.53}$$

Sub-optimal relay selection scheme

The relay node, which has maximum $\text{Tr}(\mathbf{H}_{n\text{D}}\mathbf{H}^H_{n\text{D}})$ is selected in this method, i.e.,

$$n^*_{\text{sub}} = \arg \max_{n\in\{1,\ldots,N\}} \text{Tr}(\mathbf{H}_{n\text{D}}\mathbf{H}^H_{n\text{D}}). \tag{2.54}$$

This selection method is easy to be implemented with partial CSI knowledge. For both schemes, analytical expressions of the c.d.f. and p.d.f. are derived using Theorem 2.4 and 2.5.

The average BER for BPSK with average SNR is investigated in Fig.2.11 to observe the impact of aforementioned relay selection schemes. Simulation curves are obtained by generating entries of $\mathbf{H}_{\text{S}n}, \widetilde{\mathbf{H}}_{n\text{D}}$ as circular symmetric Gaussian variables with unit variance. LoS components are generated according to [135], where entries are non-identical complex elements with a unit magnitude.

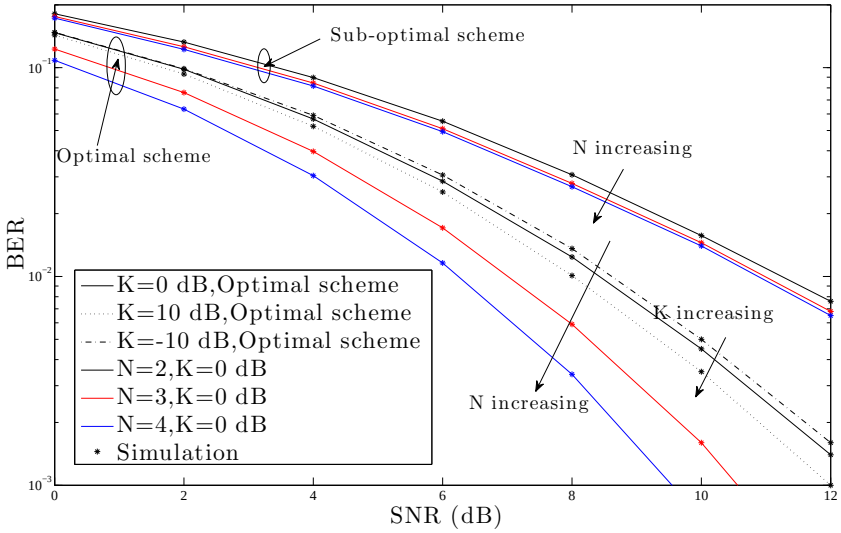

Fig 2.11. BER for BPSK vs average SNR $\bar{\gamma}$. Curves are obtained for the different Rician factors and relay pool sizes N with antenna configuration (2,4,1). Alamouti coding is used with $\bar{\gamma} = 10$ dB, and $b_n = 1$, [55] © 2014, IEEE.

We consider the Alamouti coding, average SNR $\bar{\gamma} = 10$ dB, and relay gain parameter $b_n = 1$ for all relays. The BER for the optimal relay selection scheme is considered for three Rician factors with $N = 2$ for antenna configuration (2, 4, 1), where the performance improves with the Rician factor. Moreover, the BER performance with respect to the relay pool size N is obtained for Rician factor $K = 0$ dB. When N increases, there is a significant performance improvement in the optimal relay selection scheme. Therefore, we can use a higher number of relay nodes to assist source to destination communication and take advantage of diversity gain.

2.6 Summary and discussion

In this chapter, we have studied several scenarios of non-coherent AF MIMO relaying over asymmetric fading channels. In particular, the source-relay and relay-destination channels were assumed to undergo Rayleigh fading and Rician fading, respectively. Depending on the rank of the LoS component of Rician channel, we discussed different Rician fading scenarios such as non-i.i.d. Rician,

correlated Rician, i.i.d. Rician and Rayleigh fading. The finite-dimensional random matrix theory was used to derive the statistical properties of the instantaneous SNR at the destination.

Main attention on this chapter was given to OSTBC based non-coherent AF MIMO relaying. We derived closed form expressions for the m.g.f., first and second moments, p.d.f., and c.d.f. of the instantaneous SNR at the destination. Additionally, we obtained m.g.f. for correlated Rician, i.i.d. Rician, and verified the m.g.f. expression for Rayleigh fading scenario. These results were used subsequently to analyze system performance with BER, AoF, and outage probability. Exact expressions for diversity order and array gain were derived for certain antenna configurations. We investigated the effect of the Rician factor, rank of the LoS component and the antenna configuration on the system performance. The analysis revealed that for a fixed channel gain, the system performance was improved with the increase of Rician factor for any configuration with $\min(N_R, N_D) = 1$. The $\min(N_R, N_D) = 1$ simply meant that the relay-destination channel is either MISO or SIMO channel. There, having a good LoS path component improved the system performance. However, the system performance was degraded with the increase of Rician factor for a fixed channel gain and a specific antenna configuration other than $\min(N_R, N_D) = 1$, which was MIMO channel of the relay-destination link. For a fixed channel gain, when the Rician factor increased, i.e., the LoS components dominated over the scattering component, the benefit of the scattering environment reduced. This weaker scattering component caused the performance degradation.

Next, we summarized the study on an optimal single stream beamforming for a non-coherent AF MIMO relay system. The optimal transmit and receive beamforming vectors were designed to maximize the instantaneous SNR at the destination. As with the OSTBC, the numerical analysis verified that the higher Rician factor in relay-destination channel enhanced the system performance for $\min(N_R, N_D) = 1$, whereas the performance decreased with Rician factor for MIMO cases. Additionally, results revealed that the average BER performance of the optimal beamforming was superior to the OSTBC based AF MIMO system.

We considered possible relay selection schemes for non-coherent AF MIMO OSTBC system with multiple relays. All relay-destination channels were assumed to undergo Rician fading. Two relay selection schemes were considered depending on the availability of the CSI at the destination. The maximum SNR

based relay selection scheme (optimal scheme) improved the performance significantly with the size of the relay pool. The relay selection based on the best relay-destination channel (sub-optimal) always provided a lower performance compared to the optimal method. All these studies verified that the in a fixed channel gain, the Rician fading only benefited SIMO or MISO cases of relay-destination channel.

3 Precoder-decoder design schemes for PNC based MIMO two-way relaying system

In this chapter, we consider linear precoder-decoder schemes for physical layer network coding (PNC) based MIMO two-way relaying (TWR) system. When nodes transmit multiple streams, the PNC mapping becomes complex at the relay node. This problem can be minimized by adopting precoding and decoding techniques at the nodes. The precoder-decoder schemes are further useful to enhance the overall performance of the system. Depending on the availability of CSI at the nodes, we investigate two precoder-decoder design schemes for PNC based MIMO TWR systems.

First, we consider the perfect CSI to be available at the nodes, and the zero-forcing (ZF) criterion is used at both MA and BC stages of TWR. An optimal resource allocation problem is considered in order to maximize the sum-rate of the TWR under a total power constraint. The optimal power allocation scheme is derived by using the Karush-Kuhn-Tucker (KKT) conditions.

Next, we propose robust precoder-decoder design when the CSI is imperfect at the nodes. The design is based on minimizing the weighted mean square error (WMSE) of received signals. A channel estimation method is proposed for TWR systems using already known orthogonal sequence transmission techniques. Errors in the estimation are illustrated, and utilized in the joint precoder-decoder design problems. Both MA and BC stages are considered in the design. The WMSE based optimization problems become non-convex, and we present methods of solving those by suitable reformulation. Different scenarios are investigated to find the impact of the estimation error, antenna correlation, weighting parameters, relay location, and the number of antennas. Performance differences are highlighted comparing joint precoder-decoder design with other possibilities.

3.1 Zero-forcing precoding/decoding scheme

Here, we assume the perfect CSI is available at the nodes, therefore, the ZF precoders/decoders can be used at the nodes.

3.1.1 System model

We consider the basic TWR system model as illustrated in the Fig.3.1. Node 1 and node 2 transmit data between themselves with the assistance of a relay node. During the MA stage, both nodes 1 and 2 transmit their corresponding signals to the relay as shown in the Fig.3.1(a). The relay receives both signals at the same time and performs PNC as in [62] to estimate the XOR of the two transmitted symbol vectors. During the BC stage, the relay broadcasts the PNC mapped signal as shown in the Fig.3.1(b). Both nodes (1 and 2) estimate the broadcasted symbol, and reconstruct the desired symbol using XOR operation. We assume all nodes have same number of antennas N and the relay is located at a normalized distance d from the node 1. Node-to-relay channels undergo Rayleigh fading with $\mathbf{H}_1 \in \mathbb{C}^{N\times N}$ and $\mathbf{H}_2 \in \mathbb{C}^{N\times N}$. Entries of $\mathbf{H}_1$ are assumed to be $\sim \frac{1}{d^\alpha}\ \mathcal{CN}(0,1)$ and entries of $\mathbf{H}_2$ are assumed to be $\sim \frac{1}{(1-d)^\alpha}\ \mathcal{CN}(0,1)$, where α is the path loss exponent.

Multiple access stage

Precoding matrices are selected as pseudo-inverse of the channel matrices. Those are given by $\mathbf{H}_1^\dagger = \mathbf{H}_1^H(\mathbf{H}_1\mathbf{H}_1^H)^{-1}$ and $\mathbf{H}_2^\dagger = \mathbf{H}_2^H(\mathbf{H}_2\mathbf{H}_2^H)^{-1}$. Modulated symbol vectors are fed into the node 1 and 2, each given as, $\mathbf{s}_1 = \begin{pmatrix} s_{11} & s_{12} & ... & s_{1N}\end{pmatrix}^T$ and $\mathbf{s}_2 = \begin{pmatrix} s_{21} & s_{22} & ... & s_{2N}\end{pmatrix}^T$, where $s_{ik} \in \mathbb{C}$ $(i \in \{1,2\}, k \in \{1,2..,N\})$. The powers of the transmitting signals should be less than the maximum available power. Therefore, the powers associated with the symbols are represented separately by $\mathbf{P}_i = \text{diag}(\sqrt{p_{i1}}, \sqrt{p_{i2}}, ..., \sqrt{p_{iN}})$. Moreover, throughout this section, the term m_{ik} is used as the respective unmodulated information of s_{ik}. During the MA stage, the received signal vector $\mathbf{y}_r$ at the relay is given by

$$\mathbf{y}_r = \mathbf{P}_1\mathbf{s}_1 + \mathbf{P}_2\mathbf{s}_2 + \mathbf{n}_r, \tag{3.1}$$

where $\mathbf{n}_r \sim \mathcal{CN}(0, \sigma^2\mathbf{I}_N)$.

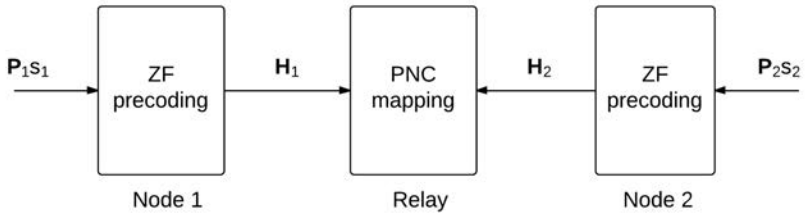

(a)

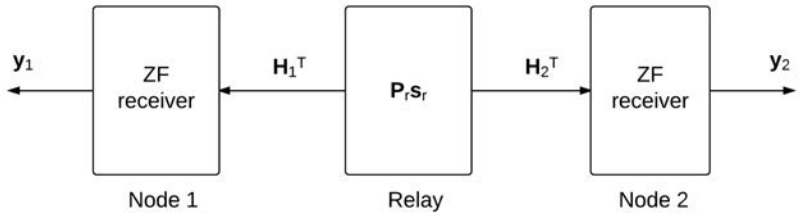

(b)

Fig 3.1. PNC based two-way relaying : (a) Multiple access stage; (b) Broadcasting stage.

Physical layer network coding at the relay

It is evident from (3.1) that the relay receives independent streams at each antenna. The received signal at the kth antenna of the relay y_{r_k} is given by

$$y_{r_k} = \sqrt{p_{1k}} s_{1k} + \sqrt{p_{2k}} s_{2k} + n_{r_k}, \quad k = 1, .., N. \tag{3.2}$$

There is no interference from other streams, and this leads us to consider multi-stream PNC mapping as N number of independent PNC operations. Therefore, the relay estimates $m_{rk} = m_{1k} \oplus m_{2k}$ from the received signal y_{r_k} $(\forall k)$. ML detection can be used to estimate m_{rk}. There, we follow general definitions of PNC mapping as given in [62]. After the PNC mapping, the modulated symbol of m_{rk}, denoted by s_{rk}, is broadcast during the next time slot.

Broadcast (BC) stage

During the second time slot, relay broadcasts PNC mapped signal vector $\mathbf{s}_r$ after being subjected to power levels $\mathbf{P}_r = \text{diag}(\sqrt{p_{r1}}, \sqrt{p_{r2}}, ..., \sqrt{p_{rN}})$. As shown in the Fig.3.1(b), we consider ZF receivers at the node 1 and 2. The receiver side signal processing ensures that channel effect is no longer with the received signal, though the noise variance is not the same any longer. The received signals at nodes are given by

$$\begin{aligned} \mathbf{y}_1 &= \mathbf{P}_r \mathbf{s}_r + ((\mathbf{H}_1^T)^H \mathbf{H}_1^T)^{-1} (\mathbf{H}_1^T)^H \mathbf{n}_1 \\ \mathbf{y}_2 &= \mathbf{P}_r \mathbf{s}_r + ((\mathbf{H}_2^T)^H \mathbf{H}_2^T)^{-1} (\mathbf{H}_2^T)^H \mathbf{n}_2 \end{aligned}, \tag{3.3}$$

where $\mathbf{n}_1 \sim \mathcal{CN}(0, \sigma^2 \mathbf{I}_N)$ and $\mathbf{n}_2 \sim \mathcal{CN}(0, \sigma^2 \mathbf{I}_N)$. The received signal $\mathbf{y}_1$ at the node 1 is used to obtain $\mathbf{s}_r$, which then mapped to unmodulated information $\mathbf{m}_r = \begin{pmatrix} m_{r1} & m_{r2} & ... & m_{rN} \end{pmatrix}^T$. Now, the XOR operation $m_{rk} \oplus m_{1k}$ is used to obtain m_{2k} $(\forall k)$. A similar procedure is applied at the node 2. This completes the two-way communication with two time slots.

3.1.2 Power allocation

Here, the optimal $\mathbf{P}_1$, $\mathbf{P}_2$ and $\mathbf{P}_r$ are obtained to maximize the sum-rate of the MIMO TWR system. The total transmit power at all nodes is considered to be limited. For a given symbol stream, the weakest link of the transmission path decides the achievable rate. Therefore, the rate in each direction and each stream is defined by the minimum rate of the path. By considering all these facts the sum-rate R_{sum} of the TWR system is given by

$$R_{\text{sum}} = \sum_{k=1}^{N} \left(\frac{1}{2} \min \left(R_{1r}^k, \bar{R}_{r2}^k \right) + \frac{1}{2} \min \left(R_{2r}^k, \bar{R}_{r1}^k \right) \right), \tag{3.4}$$

where R_{ij}^k refers to the rate from ith node to jth node for the kth stream, $\bar{R}_{ij}^k$ refers to the rate from ith node to jth node for the kth stream when PNC-mapped symbol is transmitted. There is a factor 1/2 due to the two channel uses, required for the relaying. The achievable rates for the kth stream are

obtained as

$$R_{1r}^{k} = \log_2\left(1 + \frac{p_{1k}}{\sigma^2}\right) \tag{3.5}$$

$$R_{2r}^{k} = \log_2\left(1 + \frac{p_{2k}}{\sigma^2}\right) \tag{3.6}$$

$$\bar{R}_{r2}^{k} = \log_2\left(1 + \frac{p_{rk}}{[\mathbf{H}_2\mathbf{H}_2{}^H]_{kk}^{-1}\sigma^2}\right) \tag{3.7}$$

$$\bar{R}_{r1}^{k} = \log_2\left(1 + \frac{p_{rk}}{[\mathbf{H}_1\mathbf{H}_1{}^H]_{kk}^{-1}\sigma^2}\right). \tag{3.8}$$

During BC stage, the achievable rates (3.7) and (3.8) are obtained with the Shannon capacity equation by substituting relevant receiver SNR at each node. To the best of our knowledge, the exact rates for data streams during the MA stage of the PNC based TWR system have various expressions in the literature. In [141], the authors showed that it can reach to $\log_2(\frac{1}{2} + \mathrm{SNR})$. Some argue that it can reach up to individual upper bound rates of the MA channel. In this analysis, we assume the individual upper bound rates as the achievable rates of the PNC based relaying, which are obtained as (3.5) and (3.6).

The PNC operation combines both receive symbols into one symbol, which ultimately contains both information. If the relay cannot transmit all received data, higher rates in the first time slot are useless. Therefore, the relationship among four rates in kth sub-stream can be written in the form of following inequalities.

$$R_{1r}^{k} \leq \bar{R}_{r2}^{k}, \tag{3.9}$$

$$R_{2r}^{k} \leq \bar{R}_{r1}^{k}. \tag{3.10}$$

With these observations, we formulate the following optimization problem to maximize the sum-rate of the two-way transmissions under the total transmit power constraint $\mathrm{P_T}$.

$$\begin{aligned} &\text{maximize} \quad \sum_{k=1}^{N} \log_2\left(1 + \frac{p_{1k}}{\sigma^2}\right) + \sum_{k=1}^{N} \log_2\left(1 + \frac{p_{2k}}{\sigma^2}\right) \\ &\text{sub. to} \begin{cases} \log_2\left(1 + \frac{p_{1k}}{\sigma^2}\right) \leq \log_2\left(1 + \frac{p_{rk}}{[\mathbf{H}_2\mathbf{H}_2{}^H]_{kk}^{-1}\sigma^2}\right) & k = 1, ..N \\ \log_2\left(1 + \frac{p_{2k}}{\sigma^2}\right) \leq \log_2\left(1 + \frac{p_{rk}}{[\mathbf{H}_1\mathbf{H}_1{}^H]_{kk}^{-1}\sigma^2}\right) & k = 1, ..N \\ \mathrm{Tr}\left(\mathbf{H}_1^{\dagger}\mathbf{P}_1(\mathbf{H}_1^{\dagger}\mathbf{P}_1)^H + \mathbf{H}_2^{\dagger}\mathbf{P}_2(\mathbf{H}_2^{\dagger}\mathbf{P}_2)^H + \mathbf{P}_r\mathbf{P}_r^H\right) \leq \mathrm{P_T}. \end{cases} \end{aligned} \tag{3.11}$$

The total transmit power constraint can be simplified into following form

$$\sum_{k=1}^{N}[\mathbf{H}_1\mathbf{H}_1{}^H]_{kk}^{-1}p_{1k}+\sum_{k=1}^{N}[\mathbf{H}_2\mathbf{H}_2{}^H]_{kk}^{-1}p_{2k}+\sum_{k=1}^{N}p_{rk}\leq \mathrm{P_T}. \tag{3.12}$$

Furthermore, the rate constraints can be reformulated into a linear form without loss of generality. Then this power allocation problem becomes a convex optimization problem, and well-known optimization techniques can be used to solve it. Lagrangian for the problem is given as

$$\begin{aligned}\Lambda = &-\sum_{k=1}^{N}\log_2\Big(1+\frac{p_{1k}}{\sigma^2}\Big)-\sum_{k=1}^{N}\log\Big(1+\frac{p_{2k}}{\sigma^2}\Big)+\sum_{k=1}^{N}\lambda_{1k}\big([\mathbf{H}_2\mathbf{H}_2{}^H]_{kk}^{-1}p_{1k}\\ &-p_{rk}\big)+\sum_{k=1}^{N}\lambda_{2k}\Big([\mathbf{H}_1\mathbf{H}_1{}^H]_{kk}^{-1}p_{2k}-p_{rk}\Big)+\lambda_0\Big(\sum_{k=1}^{N}\big([\mathbf{H}_1\mathbf{H}_1{}^H]_{kk}^{-1}p_{1k}\\ &+[\mathbf{H}_2\mathbf{H}_2{}^H]_{kk}^{-1}p_{2k}+p_{rk}\big)-\mathrm{P_T}\Big),\end{aligned} \tag{3.13}$$

where the λ_{1k} is the Lagrange multiplier associated with the kth inequality constraint, λ_{2k} is the Lagrange multiplier associated with the $(N+k)$th inequality constraint, and λ_0 is the Lagrange multiplier associated with the $(2N+1)$th inequality constraint. KKT conditions [142] are used to find optimum solutions.

$$\frac{\partial\Lambda}{\partial p_{1k}^*}=\frac{-1}{\sigma^2+p_{1k}^*}+\lambda_{1k}^*[\mathbf{H}_2\mathbf{H}_2{}^H]_{kk}^{-1}+\lambda_0^*[\mathbf{H}_1\mathbf{H}_1{}^H]_{kk}^{-1}=0 \quad ,\forall k \tag{3.14}$$

$$\frac{\partial\Lambda}{\partial p_{2k}^*}=\frac{-1}{\sigma^2+p_{2k}^*}+\lambda_{2k}^*[\mathbf{H}_1\mathbf{H}_1{}^H]_{kk}^{-1}+\lambda_0^*[\mathbf{H}_2\mathbf{H}_2{}^H]_{kk}^{-1}=0 \quad ,\forall k \tag{3.15}$$

$$\frac{\partial\Lambda}{\partial p_{rk}^*}=-\lambda_{1k}^*-\lambda_{2k}^*+\lambda_0^*=0 \quad ,\forall k \tag{3.16}$$

$$\lambda_{1k}^*\Big([\mathbf{H}_2\mathbf{H}_2{}^H]_{kk}^{-1}p_{1k}^*-p_{rk}^*\Big)=0 \quad ,\forall k \tag{3.17}$$

$$\lambda_{2k}^*\Big([\mathbf{H}_1\mathbf{H}_1{}^H]_{kk}^{-1}p_{2k}^*-p_{rk}^*\Big)=0 \quad ,\forall k \tag{3.18}$$

$$\lambda_0^*\Big(\sum_{k=1}^{N}\Big([\mathbf{H}_1\mathbf{H}_1{}^H]_{kk}^{-1}p_{1k}^*+[\mathbf{H}_2\mathbf{H}_2{}^H]_{kk}^{-1}p_{2k}^*+p_{rk}^*\Big)-\mathrm{P_T}\Big)=0 \quad . \tag{3.19}$$

In (3.19), λ_0^* should be strictly positive to utilize all the power $\mathrm{P_T}$. There are three possible scenarios for λ_{1k}^* and λ_{2k}^*. Obtained optimal solutions are given below with each scenario.

1. When $\lambda_{1k}^* > 0$ and $\lambda_{2k}^* = 0$ ($[\mathbf{H}_2\mathbf{H}_2{}^H]_{kk}^{-1} > [\mathbf{H}_1\mathbf{H}_1{}^H]_{kk}^{-1}$)

$$\begin{aligned} p_{1k}^* &= \left(\frac{1}{([\mathbf{H}_2\mathbf{H}_2{}^H]_{kk}^{-1} + [\mathbf{H}_1\mathbf{H}_1{}^H]_{kk}^{-1})\lambda_0^*} - \sigma^2 \right)^+ \\ p_{2k}^* &= \left(\frac{1}{[\mathbf{H}_2\mathbf{H}_2{}^H]_{kk}^{-1}\lambda_0^*} - \sigma^2 \right)^+ \\ p_{rk}^* &= \left(\frac{[\mathbf{H}_2\mathbf{H}_2{}^H]_{kk}^{-1}}{([\mathbf{H}_2\mathbf{H}_2{}^H]_{kk}^{-1} + [\mathbf{H}_1\mathbf{H}_1{}^H]_{kk}^{-1})\lambda_0^*} - [\mathbf{H}_2\mathbf{H}_2{}^H]_{kk}^{-1}\sigma^2 \right)^+ . \end{aligned} \tag{3.20}$$

2. When $\lambda_{1k}^* = 0$ and $\lambda_{2k}^* > 0$ ($[\mathbf{H}_2\mathbf{H}_2{}^H]_{kk}^{-1} < [\mathbf{H}_1\mathbf{H}_1{}^H]_{kk}^{-1}$)

$$\begin{aligned} p_{1k}^* &= \left(\frac{1}{[\mathbf{H}_1\mathbf{H}_1{}^H]_{kk}^{-1}\lambda_0^*} - \sigma^2 \right)^+ \\ p_{2k}^* &= \left(\frac{1}{([\mathbf{H}_2\mathbf{H}_2{}^H]_{kk}^{-1} + [\mathbf{H}_1\mathbf{H}_1{}^H]_{kk}^{-1})\lambda_0^*} - \sigma^2 \right)^+ \\ p_{rk}^* &= \left(\frac{[\mathbf{H}_1\mathbf{H}_1{}^H]_{kk}^{-1}}{([\mathbf{H}_2\mathbf{H}_2{}^H]_{kk}^{-1} + [\mathbf{H}_1\mathbf{H}_1{}^H]_{kk}^{-1})\lambda_0^*} - [\mathbf{H}_1\mathbf{H}_1{}^H]_{kk}^{-1}\sigma^2 \right)^+ . \end{aligned} \tag{3.21}$$

3. When $\lambda_{1k}^* > 0$ and $\lambda_{2k}^* > 0$ ($[\mathbf{H}_2\mathbf{H}_2{}^H]_{kk}^{-1} = [\mathbf{H}_1\mathbf{H}_1{}^H]_{kk}^{-1}$)

$$\begin{aligned} p_{1k}^* &= \left(\frac{2}{3[\mathbf{H}_2\mathbf{H}_2{}^H]_{kk}^{-1}\lambda_0^*} - \sigma^2 \right)^+ \\ p_{2k}^* &= \left(\frac{2}{3[\mathbf{H}_2\mathbf{H}_2{}^H]_{kk}^{-1}\lambda_0^*} - \sigma^2 \right)^+ \\ p_{rk}^* &= \left(\frac{2}{3\lambda_0^*} - [\mathbf{H}_2\mathbf{H}_2{}^H]_{kk}^{-1}\sigma^2 \right)^+ . \end{aligned} \tag{3.22}$$

where $(x)^+ = \max(0, x)$. Considering all N streams, we find the solutions for power variables as in (3.20)-(3.22). Next, (3.19) is used to evaluate λ_0^*. This provides the optimal power allocations to maximize the sum-rate of PNC based MIMO TWR system.

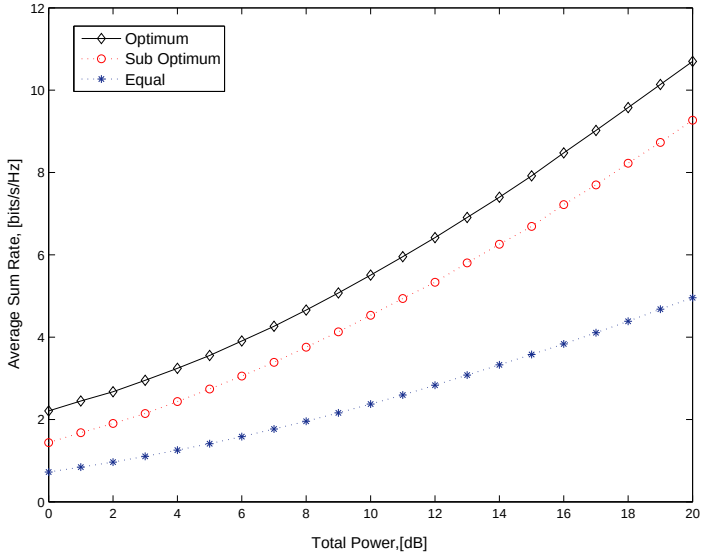

Fig 3.2. Sum-rate of the TWR system versus total transmit power $\mathrm{P_T}/\sigma^2$. Optimal scheme is compared with two other possible schemes. $N = 2$ and $d = 0.5$, [80] © 2012, IEEE.

3.1.3 Numerical results

In this section, we numerically analyze the proposed power allocation scheme to get an insight of the sum-rate in PNC based MIMO TWR system. Basic TWR system is considered where the relay is located at a normalized distance d from the node 1. The channels $\mathbf{H}_1$ and $\mathbf{H}_2$ are generated using exponential path loss model, i.e. $\sim \frac{1}{d^2}\,\mathcal{CN}(0,1)$ and $\sim \frac{1}{(1-d)^2}\,\mathcal{CN}(0,1)$, respectively. At the relay node, independent ML estimations are used for all the streams to estimate XORs of transmitted messages. The modulated symbol vector is broadcast during the next time slot.

Since the primary goal of this section is to evaluate the proposed power allocation scheme, two other power allocation methods are considered to compare the performance. The first method is a sub-optimal power allocation method where the powers are obtained by considering $R_{1r}^k = \bar{R}_{r2}^k$ and $R_{2r}^k = \bar{R}_{r1}^k$. The power is not wasted on this method as the rates matched each other. The second method is equal power allocation strategy, where all the power variables use the same value. Fig.3.2 shows the behaviour of the average sum-rate with the total

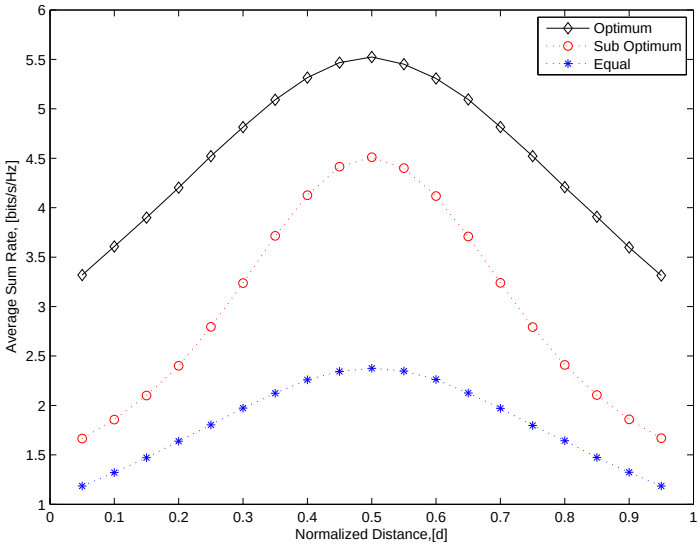

Fig 3.3. Sum-rate of the system versus normalized distance d. Optimal scheme compared with two other possible schemes. $N = 2$ and $\mathrm{P_T}/\sigma^2 = 10$ dB, [80] © 2012, IEEE.

power $\mathrm{P_T}$. Each node consists of two antennas and the normalized distance to the node 1 to relay is $d = 0.5$. As clearly visible in the figure, the sum-rate for optimum power allocation scheme provides a better performance than the other two schemes.

In the next numerical example, we change the location of the relay. The total power is fixed as $\mathrm{P_T}/\sigma^2 = 10$ dB, and all nodes equipped with two antennas. Fig.3.3 illustrates the variation of the average sum-rate with d. Three power allocation schemes are used as in the previous example. A clear advantage with the proposed optimal power allocation scheme is visible in Fig.3.3. The maximum sum-rate is highest when the relay is located at the center of both node 1 and 2.

3.2 Joint precoder-decoder design

In this section, we propose a joint precoder-decoder design for PNC based MIMO TWR system. The design is considered with imperfect CSI and antenna corre-

lations at the nodes.

3.2.1 System model

The same MIMO TWR system model is assumed as in the earlier section. Now, Fig.3.4 illustrates the MA and BC stages of TWR communication. During the MA stage, the nodes 1 and 2 transmit $\mathbf{s}_1$ and $\mathbf{s}_2$ after precoded by $\mathbf{F}_1 \in \mathbb{C}^{N\times N}$ and $\mathbf{F}_2 \in \mathbb{C}^{N\times N}$. The relay receives both signals at the same time and uses the decoder $\mathbf{G} \in \mathbb{C}^{N\times N}$ prior performing any PNC operation. During BC stage, the relay retransmits PNC mapped symbol vector $\mathbf{s}_r$ after being subjected to a precoder $\mathbf{F}_r \in \mathbb{C}^{N\times N}$. Both nodes 1 and 2 use decoders $\mathbf{G}_1 \in \mathbb{C}^{N\times N}$ and $\mathbf{G}_2 \in \mathbb{C}^{N\times N}$ and each reconstructs the required symbol with the help of their own information. All nodes dynamically adjust their precoders and decoders matrices with the channel information.

Moreover, we consider $\mathbf{R}_i \in \mathbb{C}^{N\times N}$ as the antenna correlation matrix of the ith node ($i = 1, 2$), and $\mathbf{R}_r \in \mathbb{C}^{N\times N}$ is the antenna correlation matrix at the relay node. These matrices are assumed to be symmetric. We denote $\mathbf{H}_{m1} = \mathbf{R}_r^{\frac{1}{2}}\mathbf{H}_1\mathbf{R}_1^{\frac{1}{2}}$ and $\mathbf{H}_{m2} = \mathbf{R}_r^{\frac{1}{2}}\mathbf{H}_2\mathbf{R}_2^{\frac{1}{2}}$ to be the channel matrices from node 1-to-relay and node 2-to-relay. The reverse channels are denoted as $\mathbf{H}_{b1} = \mathbf{R}_1^{\frac{1}{2}}\mathbf{H}_1^T\mathbf{R}_r^{\frac{1}{2}}$ and $\mathbf{H}_{b2} = \mathbf{R}_2^{\frac{1}{2}}\mathbf{H}_2^T\mathbf{R}_r^{\frac{1}{2}}$. Antenna correlations are also assumed to be known at the nodes. During the MA stage, the post-processed received signal vector $\mathbf{y}_r \in \mathbb{C}^{N\times 1}$ at the relay is given by

$$\mathbf{y}_r = \mathbf{G}\mathbf{H}_{m1}\mathbf{F}_1\mathbf{s}_1 + \mathbf{G}\mathbf{H}_{m2}\mathbf{F}_2\mathbf{s}_2 + \mathbf{G}\mathbf{n}_r, \tag{3.23}$$

where notations are similar to the previous section.

Physical layer network coding at the relay

The post-processed signal $\mathbf{y}_r$ can be used to obtain the estimate corresponding to the sum of modulated signals $(\mathbf{s}_1 + \mathbf{s}_2)$, which leads to N number of spatial streams. The kth entry of the post-processed signal $\mathbf{y}_r$ can be used to obtain the estimate corresponding to $s_{1k} + s_{2k}$. This scheme reduces the complexity of the MIMO PNC mapping [68]. We denote the PNC mapping of $s_{1k} + s_{2k}$ as $s_{rk} \in \mathbb{C}$ $(k = 1, .., N)$. During the next time slot, $\mathbf{s}_r = (s_{r1}\ s_{r2}...s_{rN})^T$ is broadcast to other nodes.

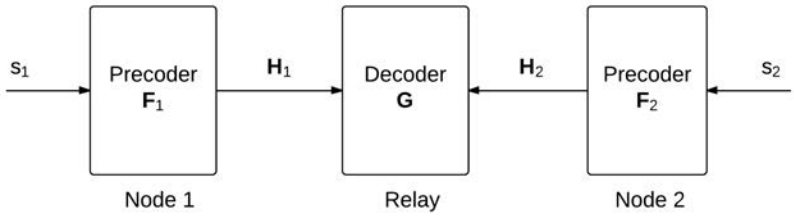

(a)

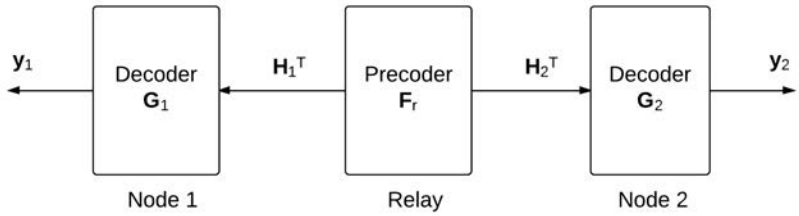

(b)

Fig 3.4. PNC based two-way relaying : (a) Multiple access stage; (b) Broadcasting stage.

For each stream, two categories of PNC mapping are possible at the relay. In the first method, the estimate corresponding to $s_{1k}+s_{2k}$ $(k = 1, .., N)$ is mapped to XOR of two transmitted unmodulated information [62]. This is possible for simple modulation schemes like BPSK and quadrature phase shift keying (QPSK). Then, the modulated version of the XOR is broadcast during the next time slot. Each node estimates the $\mathbf{s}_r$, and uses that to find the desired symbol which is transmitted by other node. The second method is appropriate for many modulation schemes, where the estimate corresponding to $\mathbf{s}_1 + \mathbf{s}_2$ is broadcast during the BC stage [64, 72]. Here, we present generalized discussion that is valid for both schemes. More importantly, the accuracy of the PNC mapping is dependent on the estimate of the sum of two symbols. This, therefore, requires minimizing the MSE between received signal and sum of transmitted signals. Thus, it is evident that an optimum joint precoder-decoder design is needed to

have an accurate estimation process.

The received signal $\mathbf{y}_1 \in \mathbb{C}^{N\times 1}$ at the node 1 during the BC stage is given by

$$\mathbf{y}_1 = \mathbf{G}_1\mathbf{H}_{b1}\mathbf{F}_r\mathbf{s}_r + \mathbf{G}_1\mathbf{n}_1, \tag{3.24}$$

Similarly, the received signal vector $\mathbf{y}_2 \in \mathbb{C}^{N\times 1}$ at the node 2 is given by

$$\mathbf{y}_2 = \mathbf{G}_2\mathbf{H}_{b2}\mathbf{F}_r\mathbf{s}_r + \mathbf{G}_2\mathbf{n}_2, \tag{3.25}$$

The precoder-decoder matrices during the BC stage can be obtained via similar MSE approach.

The CSI of $\mathbf{H}_1$ and $\mathbf{H}_2$ are required at the nodes to find these precoders and the decoder. The following sub-section describes the channel estimation procedure at nodes 1 and 2 to accomplish this.

Channel estimation

Prior to data transmission, the relay node transmits an orthogonal training sequence [92, 143] to estimate channels. We assume the channel coherence interval is high enough to transmit such training sequence to estimate the channels. The relay broadcasts $\mathbf{X}_t$ training sequence, where $\mathbf{X}_t$ is an $N \times N$ matrix. The received signal at the node 1 is given by

$$\mathbf{Y}_1 = \mathbf{H}_{b1}\mathbf{X}_t + \mathbf{N}_1, \tag{3.26}$$

where $\mathbf{N}_1$ is an $N \times N$ matrix with entries $\sim \mathcal{CN}(0, \sigma^2_{N_1})$. As commonly used in orthogonal sequence channel estimation [92], we use $\mathbf{X}_t = \mathbf{R}_r^{-\frac{1}{2}}\mathbf{X}$, where $\mathbf{X}$ is a unitary $N \times N$ matrix with multiplication factor $\sqrt{\mathrm{P_r}/\mathrm{Tr}(\mathbf{R}_r^{-1})}$ with the relay transmit power $\mathrm{P_r}$. The node 1 pre-multiplies the received signal matrix by $\mathbf{R}_1^{-\frac{1}{2}}$ and post multiplies it by $\mathbf{X}^{-1}$. Therefore, the received channel matrix $\widetilde{\mathbf{H}}_1^T$ is given by

$$\widetilde{\mathbf{H}}_1^T = \mathbf{R}_1^{-\frac{1}{2}}\mathbf{R}_1^{\frac{1}{2}}\mathbf{H}_1^T\mathbf{R}_r^{\frac{1}{2}}\mathbf{R}_r^{-\frac{1}{2}}\mathbf{X}\mathbf{X}^{-1} + \mathbf{R}_1^{-\frac{1}{2}}\mathbf{N}_1\mathbf{X}^{-1} = \mathbf{H}_1^T + \mathbf{R}_1^{-\frac{1}{2}}\widetilde{\mathbf{N}}_1, \tag{3.27}$$

where $\widetilde{\mathbf{N}}_1$ is an $N\times N$ matrix with entries $\sim \mathcal{CN}(0, \sigma_1^2)$ and $\sigma_1^2 = \sigma^2_{N_1}\,\mathrm{Tr}(\mathbf{R}_r^{-1})/\mathrm{P_r}$. The minimum MSE (MMSE) criterion is used to obtain the channel estimate from $\widetilde{\mathbf{H}}_1^T$. The MMSE estimate is

$$\bar{\mathbf{H}}_1^T = \mathcal{E}\{\mathbf{H}_1^T|\widetilde{\mathbf{H}}_1^T\} = \left[\mathbf{I}_N + \sigma_1^2\mathbf{R}_1^{-1}\right]^{-1}\widetilde{\mathbf{H}}_1^T. \tag{3.28}$$

The estimation error can be obtained [94] as $\mathbf{R}_1^{-\frac{1}{2}}\left[\mathbf{I}_N+\sigma_1^2\mathbf{R}_1^{-1}\right]^{-\frac{1}{2}}\mathbf{E}_1$, where $\mathbf{E}_1$ is an $N\times N$ matrix with entries $\sim\mathcal{CN}(0,\sigma_1^2)$. Therefore, the channel matrix now consists of MMSE estimate and the estimation error part as

$$\mathbf{H}_1^T=\bar{\mathbf{H}}_1^T+\mathbf{R}_1^{-\frac{1}{2}}\left[\mathbf{I}_N+\sigma_1^2\mathbf{R}_1^{-1}\right]^{-\frac{1}{2}}\mathbf{E}_1. \tag{3.29}$$

A similar result is valid for the estimation of $\mathbf{H}_2^T$ and it is given by $\mathbf{H}_2^T=\bar{\mathbf{H}}_2^T+\mathbf{R}_2^{-\frac{1}{2}}\left[\mathbf{I}_N+\sigma_2^2\mathbf{R}_2^{-1}\right]^{-\frac{1}{2}}\mathbf{E}_2$, where $\mathbf{E}_2$ is an $N\times N$ matrix with entries $\sim\mathcal{CN}(0,\sigma_2^2)$ and $\sigma_2^2=\sigma_{N_2}^2\mathrm{Tr}(\mathbf{R}_r^{-1})/\mathrm{P_r}$.

Since we assume the channel reciprocity, using (3.28) and (3.29) we can write the node i-to-relay channels $\mathbf{H}_{mi}$ as

$$\mathbf{H}_{mi}=\mathbf{R}_r^{\frac{1}{2}}\mathbf{H}_i\mathbf{R}_i^{\frac{1}{2}}=\mathbf{R}_r^{\frac{1}{2}}\bar{\mathbf{H}}_i\mathbf{R}_i^{\frac{1}{2}}+\mathbf{R}_r^{\frac{1}{2}}\mathbf{E}_i^T\left[\mathbf{I}_N+\sigma_i^2\mathbf{R}_i^{-1}\right]^{-\frac{T}{2}}\mathbf{R}_i^{-\frac{T}{2}}\mathbf{R}_i^{\frac{1}{2}}\qquad i=1,2. \tag{3.30}$$

Correlation matrices are assumed as symmetric, and for simplicity, we denote $\bar{\mathbf{H}}_{mi}=\mathbf{R}_r^{\frac{1}{2}}\bar{\mathbf{H}}_i\mathbf{R}_i^{\frac{1}{2}}$ and $\mathbf{E}_{mi}=\mathbf{R}_r^{\frac{1}{2}}\mathbf{E}_i^T\left[\mathbf{I}_N+\sigma_i^2\mathbf{R}_i^{-1}\right]^{-\frac{T}{2}}$, where these represent each channel matrix with a mean part and an estimation error part. We use these estimated channels to design precoders and decoders.

3.2.2 Problem formulation

As the MA and BC stages of TWR are different from each other, the analysis is considered separately for both stages. For each stage, the total power considered to be limited. Therefore, $\mathrm{P_T}$ is considered as the maximum transmit power available in each stage. A similar problem formulation and solving procedure is valid for individual power constraints of nodes.

Multiple access stage

In this stage, both nodes 1 and 2 transmit to the relay, and the transmitted powers of the nodes should satisfy the following constraint

$$\mathrm{Tr}(\mathbf{F}_1\mathbf{F}_1^H)+\mathrm{Tr}(\mathbf{F}_2\mathbf{F}_2^H)\leq\mathrm{P_T}, \tag{3.31}$$

where $\mathcal{E}\{\mathbf{s}_i\mathbf{s}_i^H\}=\mathbf{I}_N$ $(i=1,2)$. The received signal (3.23) during the MA stage is used to estimate $\mathbf{s}_1+\mathbf{s}_2$. Therefore, the estimation error vector $\mathbf{e}_r$ at the relay node can be defined as

$$\mathbf{e}_r=\mathbf{G}\mathbf{H}_{m1}\mathbf{F}_1\mathbf{s}_1+\mathbf{G}\mathbf{H}_{m2}\mathbf{F}_2\mathbf{s}_2+\mathbf{G}\mathbf{n}_r-\mathbf{s}_1-\mathbf{s}_2. \tag{3.32}$$

Data streams may need different quality of service (QoS). This is facilitated by introducing weights for different streams. A diagonal $N \times N$ positive definite weight matrix $\mathbf{W}$ is used for that purpose. Then, the WMSE at the relay node can be expressed as

$$\text{WMSE}_m = \mathcal{E}_{\mathbf{x},\mathbf{n}}\{\|\mathbf{W}^{1/2}\mathbf{e}_r\|^2\} = \text{Tr}(\mathbf{W}\mathcal{E}_{\mathbf{x},\mathbf{n}}\{\mathbf{e}_r\mathbf{e}_r^H\}), \tag{3.33}$$

where $\mathcal{E}_{\mathbf{s},\mathbf{n}}\{\mathbf{e}_r\mathbf{e}_r^H\}$ is given by

$$\begin{aligned}\mathcal{E}_{\mathbf{s},\mathbf{n}}\{\mathbf{e}_r\mathbf{e}_r^H\} =&(\mathbf{G}\mathbf{H}_{m1}\mathbf{F}_1 - \mathbf{I}_N)(\mathbf{G}\mathbf{H}_{m1}\mathbf{F}_1 - \mathbf{I}_N)^H + \sigma^2\mathbf{G}\mathbf{G}^H \\ &+ (\mathbf{G}\mathbf{H}_{m2}\mathbf{F}_2 - \mathbf{I}_N)(\mathbf{G}\mathbf{H}_{m2}\mathbf{F}_2 - \mathbf{I}_N)^H.\end{aligned} \tag{3.34}$$

We use $\mathcal{E}_{\mathbf{s},\mathbf{n}}\{\mathbf{s}_i\mathbf{s}_i^H\} = \mathbf{I}_N$ $(i = 1, 2)$, $\mathcal{E}_{\mathbf{s},\mathbf{n}}\{\mathbf{s}_1\mathbf{s}_2^H\} = \mathbf{0}_{N\times N}$, $\mathcal{E}_{\mathbf{s},\mathbf{n}}\{\mathbf{s}_i\mathbf{n}_r^H\} = \mathbf{0}_{N\times N}$ $(i = 1, 2)$, and $\mathcal{E}_{\mathbf{s},\mathbf{n}}\{\mathbf{n}_r\mathbf{n}_r^H\} = \sigma^2\mathbf{I}_N$ to obtain (3.34).

The performance of the TWR system and accuracy of the PNC mapping can be improved by minimizing the WMSE_m subject to the total power constraint. Then the solutions of the optimum precoders and decoder can be used at the nodes. However, for given channel instances of $\mathbf{H}_{m1}$ and $\mathbf{H}_{m2}$, the estimation error becomes a random variable. The error has a Gaussian distribution, and we focus on the expected value of the WMSE_m, given as,

$$\begin{aligned}\mathcal{E}_{\mathbf{E}}\{\text{WMSE}_m\} = \mathcal{E}_{\mathbf{E}}\Big\{\text{Tr}\big(&\mathbf{W}(\mathbf{G}\mathbf{H}_{m1}\mathbf{F}_1 - \mathbf{I}_N)(\mathbf{G}\mathbf{H}_{m1}\mathbf{F}_1 - \mathbf{I}_N)^H + \sigma^2\mathbf{W}\mathbf{G}\mathbf{G}^H \\ &+ \mathbf{W}(\mathbf{G}\mathbf{H}_{m2}\mathbf{F}_2 - \mathbf{I}_N)(\mathbf{G}\mathbf{H}_{m2}\mathbf{F}_2 - \mathbf{I}_N)^H\big)\Big\}.\end{aligned} \tag{3.35}$$

Channel estimates in (3.30) consist of the MMSE estimate and the error part as $\mathbf{H}_{mi} = \bar{\mathbf{H}}_{mi} + \mathbf{E}_{mi}$ for $i = 1, 2$. Therefore, expanding (3.35) into

$$\begin{aligned}\mathcal{E}_{\mathbf{E}}\{\text{WMSE}_m\} = \sum_{i=1}^{2}\mathcal{E}_{\mathbf{E}}\Big\{\text{Tr}\Big(&\mathbf{W}\mathbf{G}\bar{\mathbf{H}}_{mi}\mathbf{F}_i\mathbf{F}_i^H\bar{\mathbf{H}}_{mi}^H\mathbf{G}^H + \mathbf{W}\mathbf{G}\mathbf{E}_{mi}\mathbf{F}_i\mathbf{F}_i^H\bar{\mathbf{H}}_{mi}^H\mathbf{G}^H \\ &+ \mathbf{W}\mathbf{G}\bar{\mathbf{H}}_{mi}\mathbf{F}_i\mathbf{F}_i^H\mathbf{E}_{mi}^H\mathbf{G}^H + \mathbf{W}\mathbf{G}\mathbf{E}_{mi}\mathbf{F}_i\mathbf{F}_i^H\mathbf{E}_{mi}^H\mathbf{G}^H \\ &- \mathbf{W}\mathbf{G}\bar{\mathbf{H}}_{mi}\mathbf{F}_i - \mathbf{W}\mathbf{F}_i^H\bar{\mathbf{H}}_{mi}^H\mathbf{G}^H - \mathbf{W}\mathbf{G}\mathbf{E}_{mi}\mathbf{F}_i - \mathbf{W}\mathbf{F}_i^H\mathbf{E}_{mi}^H\mathbf{G}^H\Big)\Big\} \\ &+ \text{Tr}(2\mathbf{W} + \sigma^2\mathbf{W}\mathbf{G}\mathbf{G}^H).\end{aligned} \tag{3.36}$$

Since $\mathcal{E}_{\mathbf{E}}\{\mathbf{E}_{mi}\} = \mathbf{0}_{N\times N}$, (3.36) reduces to

$$\mathcal{E}_{\mathbf{E}}\{\mathrm{WMSE}_m\} = \sum_{i=1}^{2}\Big(\mathrm{Tr}(\mathbf{WG}\bar{\mathbf{H}}_{mi}\mathbf{F}_i\mathbf{F}_i^H\bar{\mathbf{H}}_{mi}^H\mathbf{G}^H - \mathbf{WG}\bar{\mathbf{H}}_{mi}\mathbf{F}_i - \mathbf{W}\mathbf{F}_i^H\bar{\mathbf{H}}_{mi}^H\mathbf{G}^H) + \mathcal{E}_{\mathbf{E}}\{\mathrm{Tr}(\mathbf{WGE}_{mi}\mathbf{F}_i\mathbf{F}_i^H\mathbf{E}_{mi}^H\mathbf{G}^H)\}\Big) + \mathrm{Tr}(2\mathbf{W} + \sigma^2\mathbf{WGG}^H). \tag{3.37}$$

Moreover, we can expand the following term as

$$\begin{aligned}
&\mathcal{E}_{\mathbf{E}}\{\mathrm{Tr}(\mathbf{WGE}_{mi}\mathbf{F}_i\mathbf{F}_i^H\mathbf{E}_{mi}^H\mathbf{G}^H)\}\\
&= \mathcal{E}_{\mathbf{E}}\{\mathrm{Tr}(\mathbf{WGR}_r^{\frac{1}{2}}\mathbf{E}_i^T\left[\mathbf{I}_N + \sigma_i^2\mathbf{R}_i^{-1}\right]^{-\frac{T}{2}}\mathbf{F}_i\mathbf{F}_i^H\left[\mathbf{I}_N + \sigma_i^2\mathbf{R}_i^{-1}\right]^{-\frac{T}{2}}\mathbf{E}_i^*\mathbf{R}_r^{\frac{1}{2}}\mathbf{G}^H)\}\\
&= \mathcal{E}_{\mathbf{E}}\{\mathrm{Tr}(\mathbf{R}_r^{\frac{1}{2}}\mathbf{G}^H\mathbf{WGR}_r^{\frac{1}{2}}\mathbf{E}_i^T\left[\mathbf{I}_N + \sigma_i^2\mathbf{R}_i^{-1}\right]^{-\frac{T}{2}}\mathbf{F}_i\mathbf{F}_i^H\left[\mathbf{I}_N + \sigma_i^2\mathbf{R}_i^{-1}\right]^{-\frac{T}{2}}\mathbf{E}_i^*)\}\\
&= \mathcal{E}_{\mathbf{E}}\{\mathrm{Tr}(\mathbf{P}_i\mathbf{E}_i^T\mathbf{Q}_i\mathbf{E}_i^*)\},
\end{aligned} \tag{3.38}$$

where $\mathbf{Q}_i = \left(\mathbf{I}_N + \sigma_i^2\mathbf{R}_i^{-1}\right)^{-\frac{1}{2}}\mathbf{F}_i\mathbf{F}_i^H\left(\mathbf{I}_N + \sigma_i^2\mathbf{R}_i^{-1}\right)^{-\frac{1}{2}}$ and $\mathbf{P}_i = \mathbf{R}_r^{\frac{1}{2}}\mathbf{G}^H\mathbf{WGR}_r^{\frac{1}{2}}$. Next, the relationship between trace and vectors is used to simplify (3.38) into

$$\begin{aligned}
\mathcal{E}_{\mathbf{E}}\{\mathrm{Tr}(\mathbf{P}_i\mathbf{E}_i^T\mathbf{Q}_i\mathbf{E}_i^*)\} &= \mathcal{E}_{\mathbf{E}}\{\mathrm{vec}(\mathbf{E}_i^*)\mathrm{vec}(\mathbf{P}_i\mathbf{E}_i^T\mathbf{Q}_i)\}\\
&= \mathcal{E}_{\mathbf{E}}\{\mathrm{vec}(\mathbf{E}_i^*)(\mathbf{Q}_i\otimes\mathbf{P}_i)\mathrm{vec}(\mathbf{E}_i^T)\}\\
&= \mathrm{Tr}((\mathbf{Q}_i\otimes\mathbf{P}_i)\mathcal{E}_{\mathbf{E}}\{\mathrm{vec}(\mathbf{E}_i^T)\mathrm{vec}(\mathbf{E}_i^*)\}).
\end{aligned} \tag{3.39}$$

We know $\mathcal{E}\{\mathrm{vec}(\mathbf{E}_i^T)\mathrm{vec}(\mathbf{E}_i^*)\} = \sigma_i^2\mathbf{I}_{N^2}$, and by using $\mathrm{Tr}((\mathbf{Q}_i\otimes\mathbf{P}_i)) = \mathrm{Tr}(\mathbf{Q}_i)\mathrm{Tr}(\mathbf{P}_i)$ the following expression can be obtained for (3.37).

$$\mathcal{E}_{\mathbf{E}}\{\mathrm{WMSE}_m\} = \sum_{i=1}^{2}\Big(\mathrm{Tr}(\mathbf{WG}\bar{\mathbf{H}}_{mi}\mathbf{F}_i\mathbf{F}_i^H\bar{\mathbf{H}}_{mi}^H\mathbf{G}^H - \mathbf{WG}\bar{\mathbf{H}}_{mi}\mathbf{F}_i - \mathbf{W}\mathbf{F}_i^H\bar{\mathbf{H}}_{mi}^H\mathbf{G}^H) + \sigma_i^2\mathrm{Tr}(\mathbf{Q}_i)\mathrm{Tr}(\mathbf{P}_i)\Big) + \mathrm{Tr}(2\mathbf{W} + \sigma^2\mathbf{WGG}^H). \tag{3.40}$$

The optimization problem can be formulated as below to find robust precoder-decoder matrices

$$\begin{aligned}
\mathcal{A}: \quad &\min_{\mathbf{F}_1,\mathbf{F}_2,\mathbf{G}} \quad \mathcal{E}_{\mathbf{E}}\{\mathrm{WMSE}_m\}\\
&\text{subject to} \quad \mathrm{Tr}(\mathbf{F}_1\mathbf{F}_1^H) + \mathrm{Tr}(\mathbf{F}_2\mathbf{F}_2^H) \le \mathrm{P_T}.
\end{aligned} \tag{3.41}$$

This is a non-convex optimization problem. In Section 3.2.3, we propose an algorithm to solve this optimally.

Broadcasting stage

The PNC mapped symbol $\mathbf{s}_r$ is broadcast during this stage. Similar to the MA stage, the joint design is considered to minimize the WMSE of received signals at nodes. The transmit power at the relay node should satisfy the following constraint

$$\mathrm{Tr}(\mathbf{F}_r\mathbf{F}_r^H) \leq \mathrm{P_T}/\rho. \tag{3.42}$$

where we assume $\mathcal{E}_{\mathbf{s}}\{\mathbf{s}_r\mathbf{s}_r^H\} = \rho\mathbf{I}_N$ with $(\rho \geq 1)$ is the normalized average power compared to the average power of symbol s_{ik}. The ρ depends on the modulation alphabet of the PNC mapped signal. For BPSK and QPSK schemes $\rho = 1$, where the PNC mapped symbol can be transmitted with the same modulation. The estimation error vector at ith node is given as

$$\mathbf{e}_i = \mathbf{G}_i\mathbf{H}_{bi}\mathbf{F}_r\mathbf{s}_r + \mathbf{G}_i\mathbf{n}_i - \mathbf{s}_r. \tag{3.43}$$

A similar method as in the MA stage is used to provide QoS for different streams. Then, the WMSE at node i can be evaluated as,

$$\mathrm{WMSE}_i = \rho\mathbf{W}(\mathbf{G}_i\mathbf{H}_{bi}\mathbf{F}_r - \mathbf{I}_N)(\mathbf{G}_i\mathbf{H}_{bi}\mathbf{F}_r - \mathbf{I}_N)^H + \sigma^2\mathbf{W}\mathbf{G}_i\mathbf{G}_i^H. \quad i = 1, 2 \tag{3.44}$$

The channel $\mathbf{H}_{bi}$ has random error component. Therefore, the expected value of the WMSE_i is considered to find optimum precoder-decoder matrices. The expected value of the WMSE_i can be obtained as

$$\begin{aligned}\mathcal{E}_{\mathbf{E}}\{\mathrm{WMSE}_i\} =& \rho\mathrm{Tr}\big(\mathbf{W}\mathbf{G}_i\bar{\mathbf{H}}_{mi}^T\mathbf{F}_r\mathbf{F}_r^H\bar{\mathbf{H}}_{mi}^*\mathbf{G}_i^H - \mathbf{W}\mathbf{G}_i\bar{\mathbf{H}}_{mi}^T\mathbf{F}_r - \mathbf{W}\mathbf{F}_r^H\bar{\mathbf{H}}_{mi}^*\mathbf{G}_i^H \\ &+ \mathbf{W}\big) + \rho\sigma_i^2\mathrm{Tr}(\mathbf{L}_i)\mathrm{Tr}(\mathbf{K}) + \mathrm{Tr}(\sigma^2\mathbf{W}\mathbf{G}_i\mathbf{G}_i^H) \qquad i = 1, 2,\end{aligned} \tag{3.45}$$

where $\mathbf{L}_i = (\mathbf{I}_N + \sigma_i^2\mathbf{R}_i^{-1})^{-\frac{1}{2}}\mathbf{G}_i^H\mathbf{W}\mathbf{G}_i^H(\mathbf{I}_N + \sigma_i^2\mathbf{R}_i^{-1})^{-\frac{1}{2}}$, and $\mathbf{K} = \mathbf{R}_r^{\frac{1}{2}}\mathbf{F}_r\mathbf{F}_r^H\mathbf{R}_r^{\frac{1}{2}}$.

Both $\mathcal{E}_{\mathbf{E}}\{\mathrm{WMSE}_1\}$ and $\mathcal{E}_{\mathbf{E}}\{\mathrm{WMSE}_2\}$ should be minimized during the BC stage. Here, we consider sum-WMSE, and the problem is formulated as

$$\begin{aligned}\mathcal{B}: \quad &\min_{\mathbf{F}_r, \mathbf{G}_1, \mathbf{G}_2} \quad \frac{1}{2}\mathcal{E}_{\mathbf{E}}\{\mathrm{WMSE}_1\} + \frac{1}{2}\mathcal{E}_{\mathbf{E}}\{\mathrm{WMSE}_2\} \\ &\text{subject to} \quad \mathrm{Tr}(\mathbf{F}_r\mathbf{F}_r^H) \leq \mathrm{P_T}/\rho.\end{aligned} \tag{3.46}$$

The problem $\mathcal{B}$ is non-convex, and solutions are proposed in the next section.

3.2.3 Optimum joint designs

Here, we propose algorithms to solve the non-convex optimization problems $\mathcal{A}$ and $\mathcal{B}$. Specially, it can be proved that both problems have global minima, and we can achieve those using our proposed algorithms. The proof is given in Appendix 6.

Optimum precoder-decoder design for MA stage

Here, an algorithm is proposed to solve problem $\mathcal{A}$ by dividing the problem into two sub-problems. Two different sets of variables can be identified to form sub-problems, where the precoders can be categorized into one set of variables and the decoder into the other. With these observations, we proceed with the following method. First, the precoders $\mathbf{F}_1$ and $\mathbf{F}_2$ are considered to be fixed. We find $\mathbf{G}$ to minimize expected value of WMSE_m. Next, the decoder $\mathbf{G}$ is considered to be fixed and $\mathbf{F}_1$ and $\mathbf{F}_2$ are variables. These are identified as the two sub-problems of the original problem. The sub-problems are solved iteratively until $\mathbf{G}$, $\mathbf{F}_1$ and $\mathbf{F}_2$ converge to fixed matrices.

Sub-problem $\mathcal{A}1$

The $\mathbf{F}_1$ and $\mathbf{F}_2$ are fixed, and the problem reduced to the following form,

$$\mathcal{A}1: \quad \min_{\mathbf{G}} \quad \mathcal{E}_{\mathbf{E}}\{\mathrm{WMSE}_m\}. \tag{3.47}$$

The power constraint is independent of $\mathbf{G}$. We take derivative of the objective function and make that equal to zero. The solution for $\mathbf{G}$ is the optimum during that iteration and is given as a function of $\mathbf{F}_1$, $\mathbf{F}_2$ and other parameters.

$$\frac{\partial\ \mathcal{E}_{\mathbf{E}}\{\mathrm{WMSE}_m\}}{\partial \mathbf{G}^*} = 0, \tag{3.48}$$

$$\begin{aligned}\mathbf{G} = (\mathbf{F}_1^H \bar{\mathbf{H}}_{m1}^H + \mathbf{F}_2^H \bar{\mathbf{H}}_{m2}^H)(\bar{\mathbf{H}}_{m1}\mathbf{F}_1\mathbf{F}_1^H\bar{\mathbf{H}}_{m1}^H + \bar{\mathbf{H}}_{m2}\mathbf{F}_2\mathbf{F}_2^H\bar{\mathbf{H}}_{m2}^H \\ + \sigma_1^2\mathrm{Tr}(\mathbf{Q}_1)\mathbf{R}_r + \sigma_2^2\mathrm{Tr}(\mathbf{Q}_2)\mathbf{R}_r + \sigma^2\mathbf{I}_N)^{-1}.\end{aligned} \tag{3.49}$$

Complex valued matrix function differentiation as in [144] is used to obtain the result.

Sub-problem $\mathcal{A}2$

Now, $\mathbf{G}$ is fixed in the problem $\mathcal{A}$. Then, the modified optimization problem can be reformulated as

$$\begin{aligned}\min_{\mathbf{F}_1,\mathbf{F}_2} \quad & \sum_{i=1}^{2}\Big(\mathrm{Tr}(\mathbf{W}\mathbf{G}\bar{\mathbf{H}}_{mi}\mathbf{F}_i\mathbf{F}_i^H\bar{\mathbf{H}}_{mi}^H\mathbf{G}^H - \mathbf{W}\mathbf{G}\bar{\mathbf{H}}_{mi}\mathbf{F}_i - \mathbf{W}\mathbf{F}_i^H\bar{\mathbf{H}}_{mi}^H\mathbf{G}^H) \\ & + \sigma_i^2\mathrm{Tr}(\mathbf{Q}_i)\mathrm{Tr}(\mathbf{P}_i)\Big) + \mathrm{Tr}(2\mathbf{W} + \sigma^2\mathbf{W}\mathbf{G}\mathbf{G}^H) \\ \text{s. t.} \quad & \mathrm{Tr}(\mathbf{F}_1\mathbf{F}_1^H) + \mathrm{Tr}(\mathbf{F}_2\mathbf{F}_2^H) \leq \mathrm{P_T}.\end{aligned} \tag{3.50}$$

A variable transformation is considered before solving this problem. Define new matrix variables $\mathbf{F} \in \mathbb{C}^{2N\times 2N}$ as $\mathbf{F} = [\mathbf{F}_1 \quad \mathbf{0}_{N\times N}\ ;\ \mathbf{0}_{N\times N} \quad \mathbf{F}_2]$. We also define the following matrices $\mathbf{A}$ and $\mathbf{C}$ to simplify the other parameters, where $\mathbf{A} = [\mathbf{W}^{\frac{1}{2}}\mathbf{G}\bar{\mathbf{H}}_{m1} \quad \mathbf{0}_{N\times N}\ ;\ \mathbf{0}_{N\times N} \quad \mathbf{W}^{\frac{1}{2}}\mathbf{G}\bar{\mathbf{H}}_{m2}]$, and

$$\mathbf{C} = \begin{bmatrix} \sqrt{\sigma_1^2\mathrm{Tr}(\mathbf{P}_1)}\left(\mathbf{I}_N + \sigma_1^2\mathbf{R}_1^{-1}\right)^{-\frac{1}{2}} & \mathbf{0}_{N\times N} \\ \mathbf{0}_{N\times N} & \sqrt{\sigma_2^2\mathrm{Tr}(\mathbf{P}_2)}\left(\mathbf{I}_N + \sigma_2^2\mathbf{R}_2^{-1}\right)^{-\frac{1}{2}} \end{bmatrix}. \tag{3.51}$$

Then the reformulated optimization problem is given as

$$\begin{aligned}\min_{\mathbf{F}} \quad & \mathrm{Tr}\big(\mathbf{F}^H(\mathbf{A}^H\mathbf{A} + \mathbf{C}^H\mathbf{C})\mathbf{F}\big) - 2\Re(\mathrm{Tr}(\mathbf{W}^{\frac{1}{2}}\mathbf{A}\mathbf{F})) + \mathrm{Tr}(2\mathbf{W} + \sigma^2\mathbf{W}\mathbf{G}\mathbf{G}^H) \\ \text{s.t.} \quad & \mathrm{Tr}(\mathbf{F}\mathbf{F}^H) \leq \mathrm{P_T}\end{aligned} \tag{3.52}$$

where $\mathbf{A}^H\mathbf{A}$ is a positive semi-definite matrix. This is convex and is known as the quadrature matrix programming (QMP) problem. We transpose this into quadratic constrained quadratic programming (QCQP) problem which is given by

$$\begin{aligned}\mathcal{A}2: \quad \min_{\mathbf{z}} \quad & \mathrm{vec}(\mathbf{F})^*(\mathbf{I}_{2N}\otimes(\mathbf{A}^H\mathbf{A} + \mathbf{C}^H\mathbf{C}))\mathrm{vec}(\mathbf{F}) \\ & - 2\Re\big(\mathrm{vec}(((\mathbf{W}^{\frac{1}{2}}\otimes\mathbf{I}_N)\mathbf{A})^H)^*\mathrm{vec}(\mathbf{F})\big) + c_m \\ \text{s.t.} \quad & \mathrm{vec}(\mathbf{F})^*(\mathbf{I}_{2N}\otimes\mathbf{I}_{2N})\mathrm{vec}(\mathbf{F}) \leq \mathrm{P_T},\end{aligned} \tag{3.53}$$

where $\mathbf{z} = \mathrm{vec}(\mathbf{F})$ and $c_m = \mathrm{Tr}(2\mathbf{W} + \sigma^2\mathbf{W}\mathbf{G}\mathbf{G}^H)$. This can be easily solved with QCQP solvers, which ultimately gives optimum matrices of $\mathbf{F}_1$ and $\mathbf{F}_2$ in that iteration. In the numerical analysis, we use interior point method to solve this sub-problem.

Algorithm 3.1 Joint design for MA stage

Information about N, $\bar{\mathbf{H}}_i$, $\mathbf{R}_i$, $\mathbf{R}_r$, $\mathrm{P_r}$, $\mathrm{P_T}$, $\sigma^2_{N_i}$, and σ^2 $(i = 1, 2)$ is available.

1: **initialize** : Precoders $\mathbf{F}_i = \sqrt{(\mathrm{P_T}/2N)}\mathbf{I}_N$ $(i = 1, 2)$.

2: **repeat**

3: Fix $\mathbf{F}_1$ and $\mathbf{F}_2$ obtained from step 4 (Or step 1 at initial point). Find optimum $\mathbf{G}$ from (3.49).

4: Fix $\mathbf{G}$ obtained from step 3. Solve problem $\mathcal{A}2$ to find optimum $\mathbf{F}$. Then, obtain $\mathbf{F}_1$ and $\mathbf{F}_2$.

5: **until** $|\mathrm{WMSE}_m^{k+1} - \mathrm{WMSE}_m^k| \leq \epsilon$, where k denotes the iteration number, and ϵ $(<< 1)$ is a positive constant.

6: Update precoders and decoder at all nodes.

To solve original problem $\mathcal{A}$, we start by fixing $\mathbf{F}_1$ and $\mathbf{F}_2$ giving initial values. The sub-problems $\mathcal{A}1$ and $\mathcal{A}2$ are iteratively solved until the objective gives fixed value. The final algorithm is given as Algorithm 3.1.

The proposed algorithm converges rapidly with a small number of iterations. Initialization point does not have any effect on the final convergence point. According to the Appendix 6, this always reaches the global optimum.

Optimum precoder decoder design for BC stage

During the BC stage, the joint precoder-decoder matrices are obtained by solving problem $\mathcal{B}$. Similar to the MA stage, an iterative algorithm is used to find the optimum solution. First, we consider fixed $\mathbf{F}_r$ matrix, and find $\mathbf{G}_1$ and $\mathbf{G}_2$. Next, $\mathbf{G}_1$ and $\mathbf{G}_2$ are fixed to find $\mathbf{F}_r$. These can be identified as two sub-problems of the original problem $\mathcal{B}$.

Sub-problem $\mathcal{B}1$

When $\mathbf{F}_r$ is fixed, and the problem $\mathcal{B}$ reduces to

$$\mathcal{B}1: \quad \min_{\mathbf{G}_1,\mathbf{G}_2} \quad \frac{1}{2}\mathcal{E}_{\mathbf{E}}\{\mathrm{WMSE}_1\} + \frac{1}{2}\mathcal{E}_{\mathbf{E}}\{\mathrm{WMSE}_2\}, \tag{3.54}$$

the power constraint is independent of $\mathbf{G}_1$ and $\mathbf{G}_2$. Therefore, we take the first derivative of the objective function over $\mathbf{G}_1$ and $\mathbf{G}_2$, and make those equal to

zero. Optimal $\mathbf{G}_i$ $(i = 1, 2)$ is given as

$$\mathbf{G}_i = \rho \mathbf{F}_r^H \bar{\mathbf{H}}_{mi}^* \Big(\rho \bar{\mathbf{H}}_{mi}^T \mathbf{F}_r \mathbf{F}_r^H \bar{\mathbf{H}}_{mi}^* + \rho \sigma_i^2 \mathrm{Tr}(\mathbf{K}) \big(\mathbf{I}_N + \sigma_i^2 \mathbf{R}_i^{-1} \big)^{-1} + \sigma^2 \mathbf{I}_N \Big)^{-1}. \tag{3.55}$$

Sub-problem $\mathcal{B}2$

When the decoders $\mathbf{G}_1$ and $\mathbf{G}_2$ are fixed, the problem $\mathcal{B}$ becomes

$$\begin{aligned} \min_{\mathbf{F}_r} \quad & \sum_{i=1}^{2} \frac{\rho}{2} \Big(\mathrm{Tr}(\mathbf{W}\mathbf{G}_i \bar{\mathbf{H}}_{mi}^T \mathbf{F}_r \mathbf{F}_r^H \bar{\mathbf{H}}_{mi}^* \mathbf{G}_i^H - \mathbf{W}\mathbf{G}_i \bar{\mathbf{H}}_{mi}^T \mathbf{F}_r - \mathbf{W}\mathbf{F}_r^H \bar{\mathbf{H}}_{mi}^* \mathbf{G}_i^H) \\ & + \sigma_i^2 \mathrm{Tr}(\mathbf{L}_i)\mathrm{Tr}(\mathbf{K}) \Big) + \frac{1}{2} \mathrm{Tr}(2\rho \mathbf{W} + \sigma^2 \mathbf{W}\mathbf{G}_1 \mathbf{G}_2^H + \sigma^2 \mathbf{W}\mathbf{G}_2 \mathbf{G}_2^H) \\ \text{s. t.} \quad & \mathrm{Tr}(\mathbf{F}_r \mathbf{F}_r^H) \leq \mathrm{P_T}/\rho \ . \end{aligned} \tag{3.56}$$

This problem can also transform into QCQP, which is given by

$$\begin{aligned} \mathcal{B}2: \qquad \min_{\mathbf{z}} \quad & \frac{\rho}{2} \mathrm{vec}(\mathbf{F}_r)^* \Big(\sum_{i=1}^{2} \mathbf{I}_N \otimes (\mathbf{A}_i^H \mathbf{A}_i + \mathbf{C}_i^H \mathbf{C}_i) \Big) \mathrm{vec}(\mathbf{F}_r) \\ & - \rho \Re(\mathrm{vec}(\mathbf{B}^H)^* \mathrm{vec}(\mathbf{F}_r)) + c_b \\ \text{s. t.} \quad & \mathrm{vec}(\mathbf{F}_r)^* (\mathbf{I}_N \otimes \mathbf{I}_N) \mathrm{vec}(\mathbf{F}_r) \leq \mathrm{P_T}/\rho, \end{aligned} \tag{3.57}$$

where $\mathbf{z} = \mathrm{vec}(\mathbf{F}_r)$, $\mathbf{A}_i = \mathbf{W}^{\frac{1}{2}} \mathbf{G}_i \bar{\mathbf{H}}_{mi}^T$, $\mathbf{C}_i = \sqrt{\sigma_i^2 \mathrm{Tr}(\mathbf{L}_i)} \mathbf{R}_r^{\frac{1}{2}}$, $\mathbf{B} = \mathbf{W}\mathbf{G}_1 \bar{\mathbf{H}}_{m1}^T + \mathbf{W}\mathbf{G}_2 \bar{\mathbf{H}}_{m2}^T$, and $c_b = \mathrm{Tr}(\rho \mathbf{W} + \frac{1}{2}\sigma^2 \mathbf{W}\mathbf{G}_1 \mathbf{G}_1^H + \frac{1}{2}\sigma^2 \mathbf{W}\mathbf{G}_2 \mathbf{G}_2^H)$. This is a convex problem, and can be solved with any QCQP solver. We use interior point method to solve this in our numerical analysis. Finally, the problem $\mathcal{B}$ can be solved with Algorithm 3.2.

The proposed algorithm converges with a small number of iterations, and initial point does not have any effect on the final solution. As we explain in Appendix 6, this reaches the global optimum.

We assume the proposed algorithms are used at the node 1 and 2. This requires exchanging estimated CSI between two nodes. Furthermore, once the algorithms are converged, the relay precoder $\mathbf{F}_r$, and decoder $\mathbf{G}$ are sent to the relay node.

Algorithm 3.2 Joint design for BC stage

Information about N, $\bar{\mathbf{H}}_i$, $\mathbf{R}_i$, $\mathbf{R}_r$, $\mathrm{P_r}$, $\mathrm{P_T}$, ρ, $\sigma^2_{N_i}$, and σ^2 $(i = 1, 2)$ is available.

1: **initialize** : Precoder $\mathbf{F}_r = \sqrt{(\mathrm{P_T}/\rho N)}\mathbf{I}_N$.
2: **repeat**
3: Fix $\mathbf{F}_r$ obtained from step 4 (Or step 1 at initial point). Find optimum $\mathbf{G}_1$ and $\mathbf{G}_2$ from (3.55).
4: Fix $\mathbf{G}_1$ and $\mathbf{G}_2$ obtained from step 3. Solve problem $\mathcal{B}2$ to find optimum $\mathbf{F}_r$.
5: **until** $|\mathrm{WMSE}_1^{k+1} + \mathrm{WMSE}_2^{k+1} - \mathrm{WMSE}_1^{k} - \mathrm{WMSE}_2^{k}| \leq \epsilon$.
6: Update precoder and decoders at all nodes.

3.2.4 Numerical results

In this section, we provide numerical examples using the proposed algorithms to illustrate the effects of channel estimation error, correlation coefficients, relay location, and weight parameters on the error probability. For our Monte Carlo simulations, the node-to-relay channels are generated using exponential path loss model, where entries of $\mathbf{H}_1$ are $\sim \frac{1}{d^2}\ \mathcal{CN}(0, 1)$ and entries of $\mathbf{H}_2$ are taken to be $\sim \frac{1}{(2-d)^2}\ \mathcal{CN}(0, 1)$, with 2 is the path loss exponent and d is the normalized distance. The distance between any node to mid-point of two nodes is considered as the reference distance. The antenna correlation matrix at the node 1 is defined by $(\mathbf{R}_1)_{ij} = \rho_{S1}^{|i-j|}$ $(i, j \in 1, .., N)$, where ρ_{S1} is the correlation coefficient. A similar definition is used for $\mathbf{R}_2$ and $\mathbf{R}_r$ with correlation coefficients ρ_{S2} and ρ_R, respectively. For a given channel realization, the noise matrices $\mathbf{N}_1$ and $\mathbf{N}_2$ are generated with entries $\sim \mathcal{CN}(0, \sigma^2)$. Here, the variance of the noise is considered equal at all nodes, i.e., $\sigma^2_{N_i} = \sigma^2$ for $i = 1, 2$. The MMSE estimates $\bar{\mathbf{H}}_1$ and $\bar{\mathbf{H}}_2$ are obtained according to (3.27) -(3.28). The estimation error part $\mathbf{E}_{mi}$ $(i = 1, 2)$ of channel estimation is considered as in (3.30), and the error variance σ_i^2 is used to quantify the contribution of the error. In particular, the error variance σ_i^2 is obtained by $\sigma_i^2 = \sigma^2 \mathrm{Tr}(\mathbf{R}_r^{-1})/\mathrm{P_r}$, where $\mathrm{P_r}$ is changed to vary σ_i^2.

Algorithm 3.1 and 3.2 are used to find precoder and decoder matrices at the MA and BC stages for each channel realization. We consider the nodes transmit BPSK symbols with average transmit SNR γ. The relay node performs independent ML estimations for all the streams to estimate the sum of transmitted

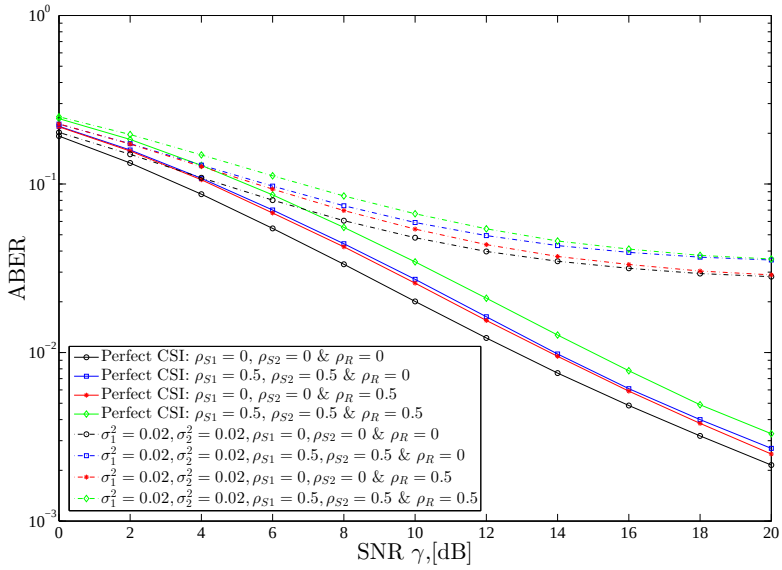

Fig 3.5. Average BER variation with SNR (γ) for different antenna correlations and estimation error variances. $N = 2$, $\mathrm{P_T}/\sigma^2 = 8\gamma$

symbols, and broadcasts the estimated summation during the next slot. Therefore, the average normalized power ρ of the broadcast symbol equals to two. Many of the following examples are performed for 10000 channel realizations.

Fig.3.5 shows the average BER (ABER) performance with the transmit SNR (γ) of a modulated symbol. The ABER is obtained by using average error rates at both nodes after a complete cycle. The weighting matrix is considered as $\mathbf{W} = \frac{1}{N}\mathbf{I}_N$, the relay is located at mid-point ($d = 1$), number of antennas $N = 2$, convergence constant $\epsilon = 0.0001$, and total transmit power $\mathrm{P_T}$ is selected such that $\mathrm{P_T}/\sigma^2 = 8\gamma$. We consider both perfect and imperfect channel estimation scenarios with different antenna correlation coefficients. As seen in Fig.3.5, joint precoder-decoder design with the perfect channel knowledge performs better than the rest. The performance degrades when the estimation error increases. This figure also shows the antenna correlation effect on the ABER. It is clear that when all nodes have some amount of correlation, the performance is degraded, whereas a significant difference is visible in the perfect estimation.

Next, we consider two other design schemes to compare the benefits of the proposed scheme. The scheme A considers signal processing only at the nodes 1

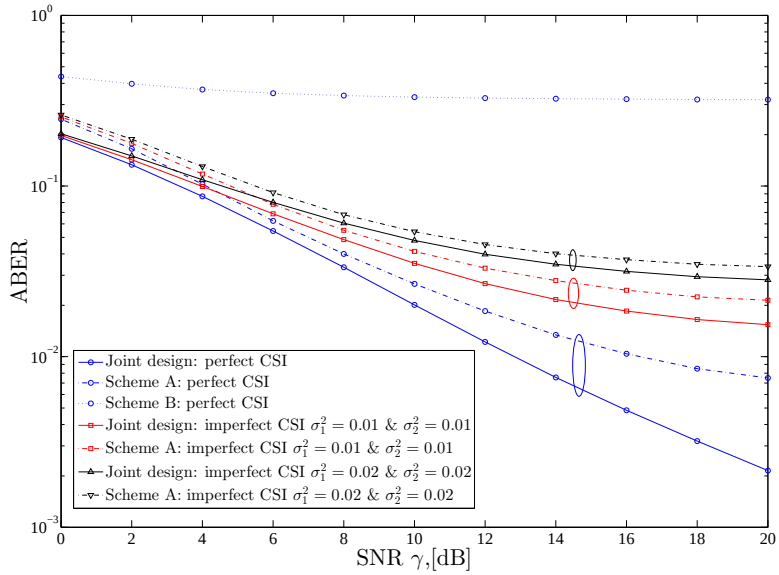

Fig 3.6. Average BER variation with SNR (γ) for three different design schemes. $N = 2$**,** $\mathrm{P_T}/\sigma^2 = 8\gamma$**.**

and 2 during both MA and BC stages. During the MA stage, optimum precoder design is utilized to minimize WMSE at the nodes. Here, decoder is not taken into account. Similarly, at the BC stage, the decoder design is employed to minimize WMSE, where a precoder at the relay is not considered. The scheme B is the opposite of the previous scheme. During the MA stage, a decoder at the relay node is used. During BC stage, a precoder at the relay is considered. These two schemes are useful to find the benefits of the proposed joint design. Fig.3.6 shows the ABER variation of these three schemes with the transmit SNR. We consider $\mathbf{W} = \frac{1}{N}\mathbf{I}_N$, $N = 2$, $\epsilon = 0.0001$, $\mathrm{P_T}/\sigma^2 = 8\gamma$ and $d = 1$. Fig.3.6 shows that the joint design scheme performs better than the rest. In the low SNR region, the scheme A gives a small variation in ABER performance, whereas when SNR increases the joint design has a significant performance improvement. When the error variance is high, the difference between the joint design and scheme A is small.

In Fig.3.7, we consider the ABER variation with normalized distance d. The BER of the bi-directional transmissions and the average BER are considered with $N = 2$, $\epsilon = 0.0001$, $\gamma = 15$ dB and $\mathrm{P_T}/\sigma^2 = 8\gamma$. It can be seen that the

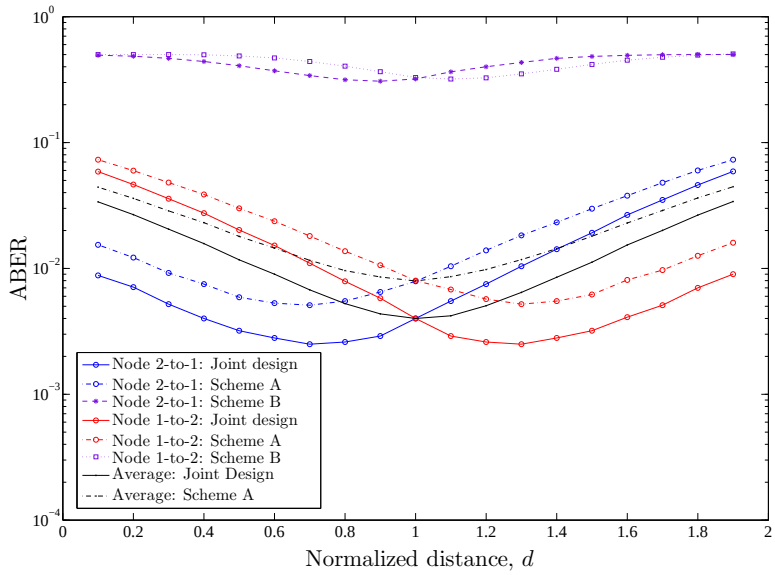

Fig 3.7. Average BER variation with normalized distance (d) for three different design schemes. $N = 2$**,** $\gamma = 15$ **dB and** $\mathrm{P_T}/\sigma^2 = 8\gamma$

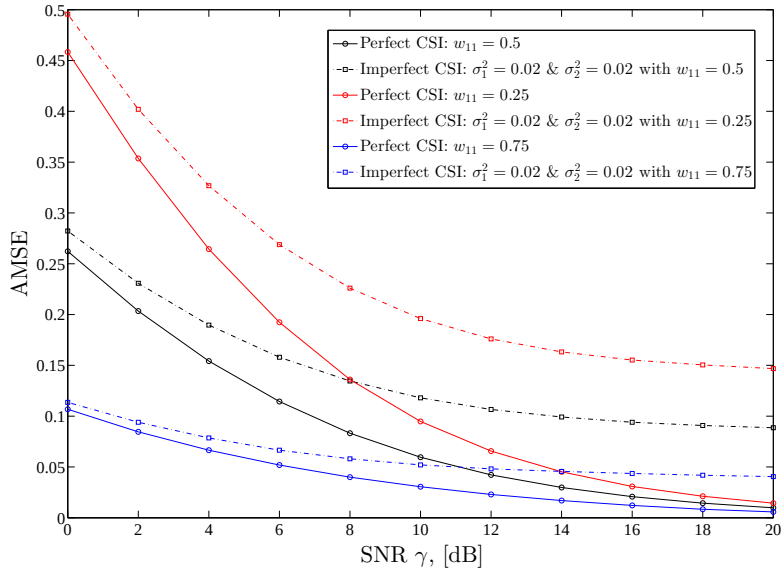

Fig 3.8. Average MSE variation with SNR (γ) for different weight parameters in the multiple access stage. $N = 2$**,** $\mathrm{P_T}/\sigma^2 = 8\gamma$

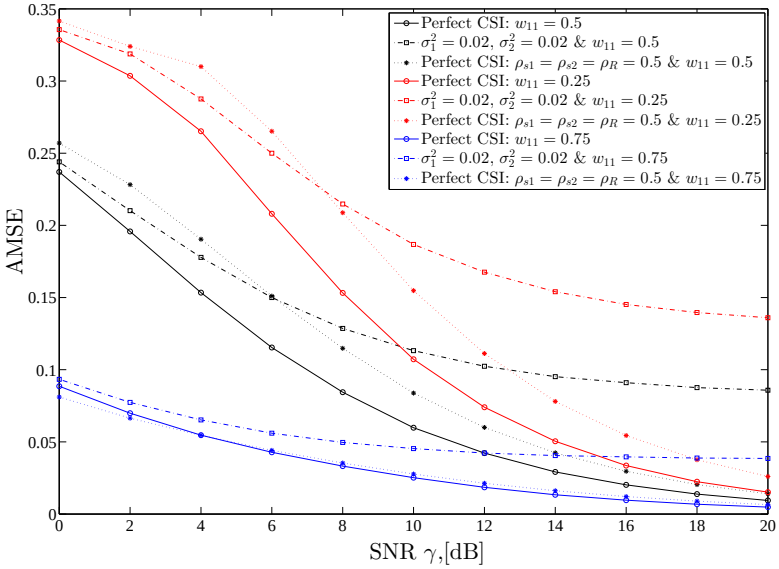

Fig 3.9. Average MSE variation for node 1 with SNR (γ) for different weight parameters in broadcasting stage. $N = 2$**,** $\mathrm{P_T}/\sigma^2 = 8\gamma$**.**

joint design performs better the rest for all relay locations.

Fig.3.8 shows the average MSE (AMSE) of the first data stream received at the relay (during MA stage). Same simulation parameters are used as in the Fig.3.6. The data stream is considered with three possible weights 0.25, 0.50, and 0.75. The AMSE reduces with the transmit SNR for each scenario. More importantly, when the weight parameter is high, the AMSE is lower. This is therefore suitable to provide specific QoS requirements for multiple streams. Fig.3.9 shows a similar numerical analysis for the BC stage. The received signal at the node 2 is used to find AMSE. Here, we assume antenna correlation at nodes, and it can be seen that the correlation has a less impact on the performance compared to channel estimation errors.

Fig.3.10 shows the average number of iterations required for the convergence of the Algorithms 3.1 and 3.2. We use $\mathbf{W} = \frac{1}{N}\mathbf{I}_N$, $\gamma = 4$ dB, $\sigma_1^2 = \sigma_2^2 = 0.02$, $\rho_{S1} = \rho_{S2} = \rho_R = 0.5$, $\epsilon = 0.0001$ and $\mathrm{P_T}/\sigma^2 = 4N\gamma$. When the system has a higher number of antennas, more iterations are needed for Algorithms 3.1. These are realistic numbers, which can be used in practice with large MIMO systems. Algorithms 3.2 converges with a fewer number of iterations and variation with

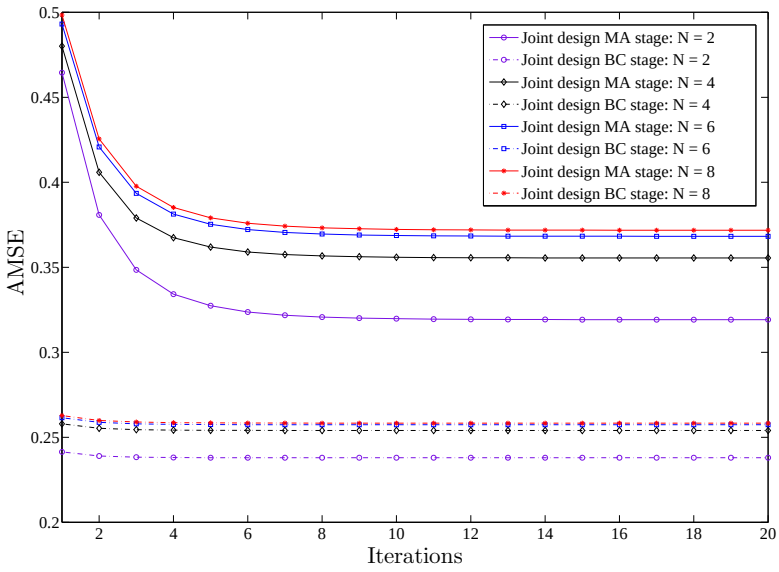

Fig 3.10. Average number of iteration to converge with number of antenna. $\gamma = 4$ **dB and** $\mathrm{P_T}/\sigma^2 = 4N\gamma$**.**

the initial point is extremely low.

3.3 Summary and discussion

In this chapter, we considered precoder-decoder schemes for MIMO TWR system when the PNC mapping is used at the relay node. When the full CSI was available at the nodes, TWR system used ZF criterion at the nodes. ZF precoders were used at the nodes during the MA stage while ZF receivers were used during the BC stage. Multi-stream PNC mapping was simplified by adopting such set-up, and the relay used PNC mapping at independent streams. Next, the performance of the TWR system was enhanced by considering optimal resource allocation scheme, where we maximized the sum-rate of the TWR under a total power constraint. The optimum power allocation scheme was derived using KKT conditions. Numerical examples were carried out to illustrate the achievable sum-rate variation with the total power. The proposed power allocation scheme provided better sum-rate than the sub-optimal and the equal power allocation strategies. Average sum-rate variation versus normalized distance suggested that

the relay should be half-way between the two nodes.

Next, we proposed generalized design for MIMO TWR system by considering imperfect CSI at the nodes. Specifically, a robust joint precoder-decoder design scheme was investigated for the PNC based MIMO TWR system. The proposed design was based on minimizing WMSE, which can be used to facilitate simple PNC mapping, provide QoS for multiple streams, and to enhance the performance of the TWR system. An orthogonal training sequence based channel estimation process was considered to quantify the mean and error components of the CSI, which were used to evaluate WMSEs. During the MA stage, the relay estimated sum of two transmitted symbols, then the WMSE_m was assessed considering that. During the BC stage, the WMSEs at both nodes were considered together. The joint design problems became non-convex, and we divided those into sub-problems and solved them iteratively. Numerical results were presented by considering the BER performance, MSE with different weight matrices, relay location and the number of antennas.

The study showed that the joint precoder-decoder design performed better than the other schemes. The weight matrix can be used to provide QoS requirements of multiple data streams in MIMO TWR. The mid-point was seen to be the best location for the relay node to assist two-way communication. The proposed algorithms converged in a fewer iterations, and the number of iterations increased slowly with the number of antennas. Overall, these findings can be useful to have less complex PNC mapping, improve the error performance, and to mitigate the half-duplex issue of cooperative relays.

4 Linear precoder-decoder design for MIMO device-to-device communication

This chapter investigates joint precoder-decoder schemes for MIMO D2D communication underlaying cellular communication. The designs are proposed by considering two modes of D2D communication. Both modes coexist with the cellular communication in the same frequency spectrum. Therefore, in a given scenario, multiple flows (D2D and BS-mobile station (MS) communications) are considered to improve the system performance.

First, we consider PNC based MIMO D2D communication mode. Joint precoder-decoder schemes are investigated separately for bi-directional communication. There are two stages in D2D communication, which are MA and BC. In BS-MS communication, two stages are downlink and uplink. For a given stage, the precoder-decoder scheme is proposed based on distributed and centralized approaches. Optimization problems are formulated to minimize MSE of both D2D and BS-MS communications. Available powers at nodes are considered to be limited, and interference thresholds are used to minimize the interference to the other link. In the distributed approach, the precoder-decoder problem is formulated based on greedy optimization approach. Distributed algorithms are proposed to solve the optimization problems as they are non-convex. In the centralized approach, the problem is formulated as a multicriterion optimization problem. The objective function is scalarized, and an iterative method is proposed to find Pareto optimal solutions.

Next, we focus on MIMO direct D2D communication mode, where joint precoder-decoder design is considered to enhance the performance, and mitigate the interference. A similar approach is used to formulate greedy optimization problems to minimize MSE of both D2D and BS-MS communications. A distributed framework is applied to solve these optimization problems. For a given distributed problem, we find closed form expressions for precoder-decoder matrices. A detailed numerical analysis is carried out to explore the advantages of the proposed designs, where convergence of proposed algorithms, effect of the interference and power constraints, inter-cell interference and various other comparisons are discussed. Moreover, two mode selection schemes are proposed

to select the D2D mode. The selection schemes are numerically investigated to examine the possible coverage extensions by using the PNC based D2D communication.

4.1 System Model

TWR based MIMO underlay D2D communication is considered, where a relay station (RS) assists D2D communication as illustrated in Fig.4.1. The RS performs PNC, and we refer this to as the PNC based D2D communication. Both D2D and BS-MS communications operate in the same frequency band. The TDD mode is assumed where two time slots are required to facilitate bi-directional communication. The proposed PNC based D2D mode is discussed along with the existing D2D communication mode [104] (direct D2D communication) which is shown in the Fig.4.2, where D2D pair communicates without the RS. Both D2D modes are improved by employing precoders and decoders at transmitter and receiver sides. Later in the chapter, we use D2D mode selection scheme to gain benefits of both D2D modes. Since the PNC based D2D requires the RS to facilitate D2D communication, the discussion on the precoder-decoder designs is divided into two sections.

The bi-directional communications of the PNC based D2D and BS-MS communications are shown as in Fig.4.1(a) and Fig.4.1(b). Fig.4.1(a) illustrates the first time slot, where D2D communication is in the MA stage. Both D_1 and D_2 transmit to the RS while the MS is in downlink. Fig.4.1(b) shows the second time slot, where D2D communication is in the BC stage with the RS transmitting the PNC mapped signal to devices. During this phase, the MS is in uplink. Both D2D and BS-MS communications are interfering with each other as shown in dotted lines. We assume that the MS is located much further from D2D pair than the BS. Then, downlink/uplink transmissions are aligned with MA/BC stages of D2D communication to minimize the overall interference. The opposite case, uplink/downlink align with MA/BC stages, have a similar analysis. Additionally, we assume all nodes to be equipped with N antennas, and each channel is frequency-flat and quasi-static. Perfect synchronization is assumed at the RS.

Fig.4.2 shows the bi-directional direct D2D communication mode for the same system set-up. During the first time slot, the D_1 transmits to the D_2, and

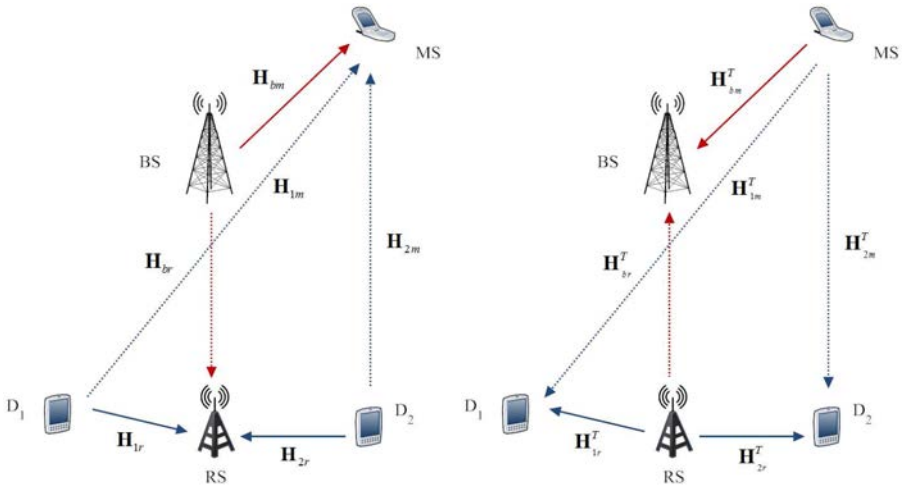

Fig 4.1. PNC based Underlay D2D Communication: (a) First time slot; (b) Second time slot, [113] © 2014, IEEE.

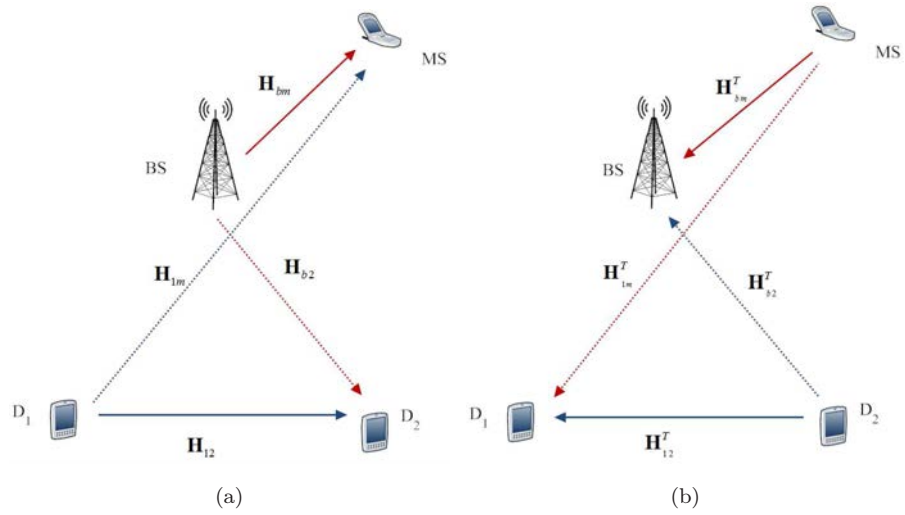

Fig 4.2. Underlay Direct D2D Communication. (a). First time slot; (b). Second time slot, [113] © 2014, IEEE.

the BS transmits to the MS. During the second time slot, D_2 transmits to the D_1, and MS transmits to the BS. Further details on the direct D2D mode is provided in the Section 4.3.

4.1.1 First time slot

During the first time slot, D_1 and D_2 transmit symbols to the RS. The D_1 transmits $\mathbf{s}_1 = (s_{11}\ s_{12}...s_{1N})^T \in \mathbb{C}^N$ after precoding by $\mathbf{F}_1 \in \mathbb{C}^{N\times N}$. Similarly, the D_2 transmits $\mathbf{s}_2 = (s_{21}\ s_{22}...s_{2N})^T \in \mathbb{C}^N$ after precoding by $\mathbf{F}_2 \in \mathbb{C}^{N\times N}$. The BS-to-MS communication also takes place during this time slot, where the BS transmits $\mathbf{s}_b \in \mathbb{C}^N$ after precoding by $\mathbf{F}_b \in \mathbb{C}^{N\times N}$ to the MS.

At the RS, an equalizer $\mathbf{G}_r \in \mathbb{C}^{N\times N}$ is employed to estimate the summation of two symbols $(\mathbf{s}_1 + \mathbf{s}_2)$. The post-processed signal $\mathbf{y}_r \in \mathbb{C}^N$ is given by

$$\mathbf{y}_r = \mathbf{G}_r\mathbf{H}_{1r}\mathbf{F}_1\mathbf{s}_1 + \mathbf{G}_r\mathbf{H}_{2r}\mathbf{F}_2\mathbf{s}_2 + \mathbf{G}_r\mathbf{H}_{br}\mathbf{F}_b\mathbf{s}_b + \mathbf{G}_r\mathbf{n}_r, \tag{4.1}$$

where $\mathbf{H}_{ir} \in \mathbb{C}^{N\times N}$ $(i = 1, 2)$ and $\mathbf{H}_{br} \in \mathbb{C}^{N\times N}$ are MIMO channel matrices from D_i-to-RS, and BS-to-RS, respectively, and $\mathbf{n}_r$ is the additive Gaussian noise vector at the RS with zero-mean and covariance matrix $\mathcal{E}\{\mathbf{n}_r\mathbf{n}_r^H\} = \sigma_r^2\mathbf{I}_N$. Concurrently, the MS estimates $\mathbf{s}_b$ after using equalizer $\mathbf{G}_m \in \mathbb{C}^{N\times N}$. The post-processed signal $\mathbf{y}_m \in \mathbb{C}^N$ is given by

$$\mathbf{y}_m = \mathbf{G}_m\mathbf{H}_{bm}\mathbf{F}_b\mathbf{s}_b + \mathbf{G}_m\mathbf{H}_{1m}\mathbf{F}_1\mathbf{s}_1 + \mathbf{G}_m\mathbf{H}_{2m}\mathbf{F}_2\mathbf{s}_2 + \mathbf{G}_m\mathbf{n}_m, \tag{4.2}$$

where $\mathbf{H}_{im} \in \mathbb{C}^{N\times N}$ $(i = 1, 2)$ and $\mathbf{H}_{bm} \in \mathbb{C}^{N\times N}$ are MIMO channel matrices from D_i-to-MS, and BS-to-MS, respectively, and $\mathbf{n}_m$ is an additive Gaussian noise vector at the MS with zero-mean and covariance matrix $\mathcal{E}\{\mathbf{n}_m\mathbf{n}_m^H\} = \sigma_m^2\mathbf{I}_N$. The post-processed signals (4.1) and (4.2) consist of desired signal, interference and noise components.

Physical layer network coding at the RS

The similar PNC mapping scheme is used as in the Chapter 3.2.1, where the post-processed signal $\mathbf{y}_r$ is used to obtain the estimate corresponding to the sum of modulated signals $(\mathbf{s}_1 + \mathbf{s}_2)$, which leads to N number of spatial streams. The PNC mapping of $s_{1k} + s_{2k}$ is denoted as $s_{rk} \in \mathbb{C}$ $(k = 1, .., N)$. During the next time slot, $\mathbf{s}_r = (s_{r1}\ s_{r2}...s_{rN})^T$ is broadcast to other nodes.

4.1.2 Second time slot

During this time slot, the RS broadcasts $\mathbf{s}_r$ after precoding by $\mathbf{F}_r \in \mathbb{C}^{N\times N}$. The MS transmits $\mathbf{s}_m \in \mathbb{C}^N$ after precoding by $\mathbf{F}_m \in \mathbb{C}^{N\times N}$. The D_i $(i = 1, 2)$

estimates $\mathbf{s}_r$ using decoder $\mathbf{G}_i \in \mathbb{C}^{N\times N}$. The post-processed signal $\mathbf{y}_i \in \mathbb{C}^N$ is given by

$$\mathbf{y}_i = \mathbf{G}_i\mathbf{H}_{ir}^T\mathbf{F}_r\mathbf{s}_r + \mathbf{G}_i\mathbf{H}_{im}^T\mathbf{F}_m\mathbf{s}_m + \mathbf{G}_i\mathbf{n}_i \qquad i = 1, 2, \tag{4.3}$$

where $\mathbf{n}_i$ is an additive Gaussian noise vector at the D_i with zero-mean and covariance matrix $\mathcal{E}\{\mathbf{n}_i\mathbf{n}_i^H\} = \sigma_i^2\mathbf{I}_N$. The post-processed signal at the BS after using equalizer $\mathbf{G}_b \in \mathbb{C}^{N\times N}$ is given by

$$\mathbf{y}_b = \mathbf{G}_b\mathbf{H}_{bm}^T\mathbf{F}_m\mathbf{s}_m + \mathbf{G}_b\mathbf{H}_{br}^T\mathbf{F}_r\mathbf{s}_r + \mathbf{G}_b\mathbf{n}_b, \tag{4.4}$$

where $\mathbf{n}_b$ is an additive Gaussian noise vector at BS with zero-mean and covariance matrix $\mathcal{E}\{\mathbf{n}_b\mathbf{n}_b^H\} = \sigma_b^2\mathbf{I}_N$. In the following sections, we consider unitary covariance matrix for the transmitted modulated signals $\mathbf{s}_i$, $\mathbf{s}_m$, and $\mathbf{s}_b$. The covariance matrix for the PNC mapped signal $\mathbf{s}_r$ is assumed as $\mathcal{E}\{\mathbf{s}_r\mathbf{s}_r^H\} = \rho\mathbf{I}_N$, and ρ (≥ 1) represent the normalized average power of the symbol s_{rk}.

4.2 Precoder-decoder design for PNC based D2D mode

Here, joint precoder-decoder designs are considered separately for distributed and centralized approaches. The main attention is given to the distributed approach, which is a more realistic to find the precoder-decoder matrices. The centralized approach is used to examine the optimality of the solutions.

4.2.1 Distributed approach

Since the bi-directional communication of the D2D and BS-MS complete in two time slots, the joint designs are considered separately for both time slots. In each stage, minimizing MSE is employed as the design criterion.

First time slot

PNC mapping at the RS requires estimating $(\mathbf{s}_1 + \mathbf{s}_2)$. Thus, the error vector at the RS is given by

$$\mathbf{e}_r = \mathbf{G}_r\mathbf{H}_{1r}\mathbf{F}_1\mathbf{s}_1 + \mathbf{G}_r\mathbf{H}_{2r}\mathbf{F}_2\mathbf{s}_2 + \mathbf{G}_r\mathbf{H}_{br}\mathbf{F}_b\mathbf{s}_b + \mathbf{G}_r\mathbf{n}_r - (\mathbf{s}_1 + \mathbf{s}_2). \tag{4.5}$$

We express MSE at the RS as

$$\text{MSE}_r \quad = \quad \mathcal{E}_{\mathbf{s},\mathbf{n}}\{\|\mathbf{e}_r\|^2\} = \mathcal{E}_{\mathbf{s},\mathbf{n}}\{\text{Tr}(\mathbf{e}_r\mathbf{e}_r^H)\} = \text{Tr}(\mathcal{E}_{\mathbf{s},\mathbf{n}}\{\mathbf{e}_r\mathbf{e}_r^H\}), \tag{4.6}$$

where $\mathcal{E}_{\mathbf{s},\mathbf{n}}\{\mathbf{e}_r\mathbf{e}_r^H\}$ is given by

$$\begin{aligned}\mathcal{E}_{\mathbf{s},\mathbf{n}}\{\mathbf{e}_r\mathbf{e}_r^H\} &= (\mathbf{G}_r\mathbf{H}_{1r}\mathbf{F}_1 - \mathbf{I}_N)(\mathbf{G}_r\mathbf{H}_{1r}\mathbf{F}_1 - \mathbf{I}_N)^H + \sigma_r^2\mathbf{G}_r\mathbf{G}_r^H \\ &\quad + (\mathbf{G}_r\mathbf{H}_{2r}\mathbf{F}_2 - \mathbf{I}_N)(\mathbf{G}_r\mathbf{H}_{2r}\mathbf{F}_2 - \mathbf{I}_N)^H + (\mathbf{G}_r\mathbf{H}_{br}\mathbf{F}_b)(\mathbf{G}_r\mathbf{H}_{br}\mathbf{F}_b)^H,\end{aligned} \tag{4.7}$$

where statistical properties $\mathcal{E}_{\mathbf{s},\mathbf{n}}\{\mathbf{s}_i\mathbf{s}_i^H\} = \mathbf{I}_N$, $\mathcal{E}_{\mathbf{s},\mathbf{n}}\{\mathbf{s}_b\mathbf{s}_b^H\} = \mathbf{I}_N$, $\mathcal{E}_{\mathbf{s},\mathbf{n}}\{\mathbf{s}_i\mathbf{s}_b^H\} = \mathbf{0}_{N\times N}$, $\mathcal{E}_{\mathbf{s},\mathbf{n}}\{\mathbf{s}_i\mathbf{n}_r^H\} = \mathbf{0}_{N\times N}$, $\mathcal{E}_{\mathbf{s},\mathbf{n}}\{\mathbf{s}_b\mathbf{n}_r^H\} = \mathbf{0}_{N\times N}$ and $\mathcal{E}_{\mathbf{s},\mathbf{n}}\{\mathbf{n}_r\mathbf{n}_r^H\} = \sigma_r^2\mathbf{I}_N$ with $i = 1, 2$ are used to obtain (4.7). MSE_r is a function of variables $\mathbf{F}_1$, $\mathbf{F}_2$, $\mathbf{F}_b$, and $\mathbf{G}_r$.

Since both D2D and BS-MS communications use the same spectrum, there should be a maximum level that nodes are allowed to interfere with each other. This is addressed by considering different interference threshold limits for D2D and BS-MS communications. The interference generated by the D2D communication to the BS-MS communication should not exceed an interference threshold I_d. The interference generated by the BS-MS communication to the D2D communication should not exceed an interference threshold I_b. It is fair to assume $\text{I}_\text{b} \geq \text{I}_\text{d}$ when the BS-MS communication is considered as the primary communication.

We consider transmit power constraints at the nodes. In general, the BS has a higher transmit power capability than the rest. The available battery power is certainly different at the MS, RS and devices. These nodes can also be subjected to uplink power control. We generalize all these cases by assuming different power constraints at the nodes. Therefore, the maximum transmit power at the BS, MS, RS and D_i are denoted as P_B, P_M, P_R and $\text{P}_{\text{D}_\text{i}}$, respectively. Minimizing MSE_r under these constraints is essential to mitigate interference, enhance the accuracy of PNC, and improve the error performance. The formulated optimization problem is given by

$$\begin{aligned}\mathcal{P}_1 : \quad & \min_{\mathbf{F}_1,\mathbf{F}_2,\mathbf{F}_b,\mathbf{G}_r} \quad \text{MSE}_r[\mathbf{F}_1, \mathbf{F}_2, \mathbf{F}_b, \mathbf{G}_r] \\ & \text{subject to} \quad \text{Tr}(\mathbf{F}_i\mathbf{F}_i^H) \leq \text{P}_{\text{D}_\text{i}} \qquad i = 1, 2 \\ & \qquad\qquad \text{Tr}\big(\mathbf{H}_{1m}\mathbf{F}_1\mathbf{F}_1^H\mathbf{H}_{1m}^H + \mathbf{H}_{2m}\mathbf{F}_2\mathbf{F}_2^H\mathbf{H}_{2m}^H\big) \leq \text{I}_\text{d}.\end{aligned} \tag{4.8}$$

Considering the BS-MS communication, the error vector at the MS can be obtained as

$$\mathbf{e}_m = \mathbf{G}_m\mathbf{H}_{bm}\mathbf{F}_b\mathbf{s}_b + \mathbf{G}_m\mathbf{H}_{1m}\mathbf{F}_1\mathbf{s}_1 + \mathbf{G}_m\mathbf{H}_{2m}\mathbf{F}_2\mathbf{s}_2 + \mathbf{G}_m\mathbf{n}_m - \mathbf{s}_b. \tag{4.9}$$

MSE at the MS is MSE_m, and this is expressed by

$$\mathrm{MSE}_m = \mathcal{E}_{\mathbf{s},\mathbf{n}}\{\|\mathbf{e}_m\|^2\} = \mathcal{E}_{\mathbf{s},\mathbf{n}}\{\mathrm{Tr}(\mathbf{e}_m\mathbf{e}_m^H)\} = \mathrm{Tr}(\mathcal{E}_{\mathbf{s},\mathbf{n}}\{\mathbf{e}_m\mathbf{e}_m^H\}), \tag{4.10}$$

where $\mathcal{E}_{\mathbf{s},\mathbf{n}}\{\mathbf{e}_m\mathbf{e}_m^H\}$ given by

$$\begin{aligned}\mathcal{E}_{\mathbf{s},\mathbf{n}}\{\mathbf{e}_m\mathbf{e}_m^H\} &= (\mathbf{G}_m\mathbf{H}_{bm}\mathbf{F}_b - \mathbf{I}_N)(\mathbf{G}_m\mathbf{H}_{bm}\mathbf{F}_b - \mathbf{I}_N)^H + \sigma_m^2\mathbf{G}_m\mathbf{G}_m^H \\ &\quad + (\mathbf{G}_m\mathbf{H}_{2m}\mathbf{F}_2)(\mathbf{G}_m\mathbf{H}_{2m}\mathbf{F}_2)^H + (\mathbf{G}_m\mathbf{H}_{1m}\mathbf{F}_1)(\mathbf{G}_m\mathbf{H}_{1m}\mathbf{F}_1)^H.\end{aligned} \tag{4.11}$$

We use $\mathcal{E}_{\mathbf{s},\mathbf{n}}\{\mathbf{s}_b\mathbf{n}_m^H\} = \mathbf{0}_{N\times N}$ and $\mathcal{E}_{\mathbf{s},\mathbf{n}}\{\mathbf{s}_i\mathbf{n}_m^H\} = \mathbf{0}_{N\times N}$ with $i = 1, 2$ to obtain (4.11). Similar to the D2D communication, minimizing MSE_m is carried out to improve the performance of the BS-MS communication. The problem formulation is given as

$$\begin{aligned}\mathcal{P}_2 : \quad & \min_{\mathbf{F}_b,\mathbf{F}_1,\mathbf{F}_2,\mathbf{G}_m} \quad \mathrm{MSE}_m[\mathbf{F}_b, \mathbf{F}_1, \mathbf{F}_2, \mathbf{G}_m] \\ & \text{subject to} \quad \mathrm{Tr}(\mathbf{F}_b\mathbf{F}_b^H) \le \mathrm{P_B} \\ & \qquad\qquad \mathrm{Tr}\big(\mathbf{H}_{br}\mathbf{F}_b\mathbf{F}_b^H\mathbf{H}_{br}^H\big) \le \mathrm{I_b}.\end{aligned} \tag{4.12}$$

Both BS-MS and D2D communications are minimizing their own MSE, and this is referred to as the greedy approach. The problems $\mathcal{P}_1$ and $\mathcal{P}_2$ are non-convex optimization problems. The precoder variables are common to both problems. The following observations enable us to solve both problems in a distributed manner.

- In the problem $\mathcal{P}_1$, precoders $\mathbf{F}_1$ and $\mathbf{F}_2$, and decoder $\mathbf{G}_r$ are directly associated with the D2D communication.
- In the problem $\mathcal{P}_2$, precoder $\mathbf{F}_b$ and decoder $\mathbf{G}_m$ are directly associated with the BS-MS communication.

For both problems, it is possible to obtain globally optimal solutions separately only with the directly associated variables. However, these are not globally optimal solutions of the original problems $\mathcal{P}_1$ and $\mathcal{P}_2$. These solutions can be

further improved by considering all variables in a timely manner. This provides an improved solution with all variables. The optimality of the final solution is illustrated in Section 4.4. The procedure to solve the problems $\mathcal{P}_1$ and $\mathcal{P}_2$ is outlined below.

Distributed design for D2D communication: Solving $\mathcal{P}_1$

The problem $\mathcal{P}_1$ is considered with fixed $\mathbf{F}_b$. Then, the modified $\mathcal{P}_1$ has variables $\mathbf{F}_1, \mathbf{F}_2$, and $\mathbf{G}_r$. This is a non-convex optimization problem, however, this is shown to have a global minimum. The proof follows similar steps as given in the Appendix 6. The modified $\mathcal{P}_1$ is solved by two sub-problems. First, we solve for $\mathbf{G}_r$ by fixing $\mathbf{F}_1$ and $\mathbf{F}_2$. Next, we solve for $\mathbf{F}_1$ and $\mathbf{F}_2$ by fixing $\mathbf{G}_r$.

Sub-problem I : After fixing $\mathbf{F}_1$ and $\mathbf{F}_2$ in the $\mathcal{P}_1$, we have the first sub-problem as

$$\min_{\mathbf{G}_r} \quad \mathrm{MSE}_r[\mathbf{G}_r]. \tag{4.13}$$

The objective function is minimized when the derivative with respect to $\mathbf{G}_r$ is zero, i.e.,

$$\begin{aligned}\mathbf{G}_r = (\mathbf{F}_1^H\mathbf{H}_{1r}^H + \mathbf{F}_2^H\mathbf{H}_{2r}^H)(\mathbf{H}_{1r}\mathbf{F}_1\mathbf{F}_1^H\mathbf{H}_{1r}^H + \mathbf{H}_{2r}\mathbf{F}_2\mathbf{F}_2^H\mathbf{H}_{2r}^H \\ +\mathbf{H}_{br}\mathbf{F}_b\mathbf{F}_b^H\mathbf{H}_{br}^H + \sigma_r^2\mathbf{I}_N)^{-1}.\end{aligned} \tag{4.14}$$

Sub-problem II : In the second sub-problem, decoder $\mathbf{G}_r$ is fixed, the $\mathcal{P}_1$ is solved with variables $\mathbf{F}_1$ and $\mathbf{F}_2$. Variable transformations are utilized to solve this sub-problem. A new matrix variable $\mathbf{F} \in \mathbb{C}^{2N\times 2N}$ is introduced as $\mathbf{F} = (\mathbf{F}_1 \;\; \mathbf{0}_{N\times N} \;;\; \mathbf{0}_{N\times N} \;\; \mathbf{F}_2)$. We also define matrices $\mathbf{A}_r \in \mathbb{C}^{2N\times 2N}$, $\mathbf{B}_r \in \mathbb{C}^{2N\times 2N}$, and $\mathbf{P}_i \in \mathbb{C}^{2N\times 2N}$ $(i = 1, 2)$ to simplify the other parameters, where $\mathbf{A}_r = (\mathbf{G}_r\mathbf{H}_{1r} \;\; \mathbf{0}_{N\times N} \;;\; \mathbf{0}_{N\times N} \;\; \mathbf{G}_r\mathbf{H}_{2r})$, $\mathbf{B}_r = (\mathbf{H}_{1m} \;\; \mathbf{0}_{N\times N} \;;\; \mathbf{0}_{N\times N} \;\; \mathbf{H}_{2m})$, $\mathbf{P}_1 = (\mathbf{I}_N \;\; \mathbf{0}_{N\times N} \;;\; \mathbf{0}_{N\times N} \;\; \mathbf{0}_{N\times N})$, and $\mathbf{P}_2 = (\mathbf{0}_{N\times N} \;\; \mathbf{0}_{N\times N} \;;\; \mathbf{0}_{N\times N} \;\; \mathbf{I}_N)$. Then the reformulated optimization problem $\mathcal{P}_1$ is given as

$$\begin{aligned} \min_{\mathbf{F}} \quad & \mathrm{Tr}(\mathbf{F}^H\mathbf{A}_r^H\mathbf{A}_r\mathbf{F}) - 2\Re(\mathrm{Tr}(\mathbf{A}_r\mathbf{F})) + c_r \\ \text{subject to} \quad & \mathrm{Tr}(\mathbf{F}^H\mathbf{P}_i^H\mathbf{P}_i\mathbf{F}) \le \mathrm{P_{D_i}} \qquad i = 1, 2 \\ & \mathrm{Tr}(\mathbf{F}^H\mathbf{B}_r^H\mathbf{B}_r\mathbf{F}) \le \mathrm{I_d}\ , \end{aligned} \tag{4.15}$$

where $c_r = \mathrm{Tr}(2\mathbf{I}_N + \mathbf{G}_r\mathbf{H}_{br}\mathbf{F}_b\mathbf{F}_b^H\mathbf{H}_{br}^H\mathbf{G}_r^H + \sigma_r^2\mathbf{G}_r\mathbf{G}_r^H)$. This is convex QMP,

and can be transformed into QCQP as

$$\begin{aligned} \min_{\mathrm{vec}(\mathbf{F})} \quad & \mathrm{vec}(\mathbf{F})^*(\mathbf{I}_{2N} \otimes (\mathbf{A}_r^H \mathbf{A}_r))\mathrm{vec}(\mathbf{F}) - 2\Re(\mathrm{vec}(\mathbf{A}_r^H)^*\mathrm{vec}(\mathbf{F})) + c_r \\ \text{subject to} \quad & \mathrm{vec}(\mathbf{F})^*(\mathbf{I}_{2N} \otimes (\mathbf{P}_i^H \mathbf{P}_i))\mathrm{vec}(\mathbf{F}) \leq \mathrm{P}_{\mathrm{D_i}} \qquad i = 1, 2 \\ & \mathrm{vec}(\mathbf{F})^*(\mathbf{I}_{2N} \otimes (\mathbf{B}_r^H \mathbf{B}_r))\mathrm{vec}(\mathbf{F}) \leq \mathrm{I_d} \ . \end{aligned} \tag{4.16}$$

This can be easily solved with QCQP solver [145, 146] to obtain optimal solution for $\mathbf{F}_1$ and $\mathbf{F}_2$. In the numerical analysis, we used the interior point method to solve this sub-problem. Both sub-problems are solved iteratively to get the global minimum of modified problem $\mathcal{P}_1$.

Distributed design for BS-MS communication: Solving $\mathcal{P}_2$

The precoder matrices $\mathbf{F}_1$ and $\mathbf{F}_2$ are considered to be fixed in the problem $\mathcal{P}_2$. Therefore, the modified problem $\mathcal{P}_2$ has variables $\mathbf{F}_b$ and $\mathbf{G}_m$. This also is a non-convex optimization problem, and has a global minimum. The proof follows similar steps to the proof given in the Appendix 6. The problem is divided into two sub-problems, and they are given as follows.

Sub-problem I : The optimal $\mathbf{G}_m$ is obtained by fixing $\mathbf{F}_b$. $\min_{\mathbf{G}_m} \mathrm{MSE}_m[\mathbf{G}_m]$ gives

$$\begin{aligned} \mathbf{G}_m = (\mathbf{F}_b^H \mathbf{H}_{bm}^H)(\mathbf{H}_{bm}\mathbf{F}_b\mathbf{F}_b^H\mathbf{H}_{bm}^H + \mathbf{H}_{1m}\mathbf{F}_1\mathbf{F}_1^H\mathbf{H}_{1m}^H \\ + \mathbf{H}_{2m}\mathbf{F}_2\mathbf{F}_2^H\mathbf{H}_{2m}^H + \sigma_m^2\mathbf{I}_N)^{-1}. \end{aligned} \tag{4.17}$$

Sub-problem II : $\mathbf{G}_m$ is fixed to obtain $\mathbf{F}_b$. Then the problem $\mathcal{P}_2$ reduces to

$$\begin{aligned} \min_{\mathbf{F}_b} \quad & \mathrm{Tr}\left(\mathbf{F}_b^H(\mathbf{G}_m\mathbf{H}_{bm})^H(\mathbf{G}_m\mathbf{H}_{bm})\mathbf{F}_b\right) - 2\Re(\mathrm{Tr}(\mathbf{G}_m\mathbf{H}_{bm}\mathbf{F}_b)) + c_m \\ \text{subject to} \quad & \mathrm{Tr}(\mathbf{F}_b^H\mathbf{F}_b) \leq \mathrm{P_B} \\ & \mathrm{Tr}(\mathbf{F}_b^H\mathbf{H}_{br}^H\mathbf{H}_{br}\mathbf{F}_b) \leq \mathrm{I_b}, \end{aligned} \tag{4.18}$$

where $c_m = \mathrm{Tr}\big(2\mathbf{I}_N + \mathbf{G}_m(\mathbf{H}_{1m}\mathbf{F}_1\mathbf{F}_1^H\mathbf{H}_{1m}^H + \mathbf{H}_{2m}\mathbf{F}_2\mathbf{F}_2^H\mathbf{H}_{2m}^H + \sigma_m^2\mathbf{I}_N)\mathbf{G}_m^H\big)$. This can be solved with convex optimization tools. Then, both sub-problems can be solved iteratively to reach the global minimum of the modified problem $\mathcal{P}_2$.

Both modified problems of $\mathcal{P}_1$ and $\mathcal{P}_2$ can be solved independently from one another. However, the following steps are required to improve the solutions.

– The D2D communication minimizes MSE_r by solving modfied problem $\mathcal{P}_1$. Updated $\mathbf{F}_b$ (precoder variable of modified $\mathcal{P}_2$) is required to further minimize the MSE_r.

– The BS-MS communication minimizes MSE_m by solving modified problem $\mathcal{P}_2$. Updated $\mathbf{F}_1$ and $\mathbf{F}_2$ (precoder variables of modified $\mathcal{P}_1$) are required to further minimize the MSE_m.

Therefore, the precoding matrices should be exchanged in a timely manner to improve the solutions. This further minimizes MSE_r and MSE_m, and converge. As mentioned previously, it is not guaranteed that these convergent points are global minima of the problems. However, this is sufficient to overcome the interferences and enhance the performance of the system. We now propose Algorithm 4.1 to find the precoders decoders during the first time slot based on above circumstances.

Algorithm 4.1 Joint design for PNC based D2D mode - First time slot

Channel state information is available. Information about N, K, $\mathrm{P_B}$, $\mathrm{P_{D_i}}$, $\mathrm{I_b}$, $\mathrm{I_d}$, σ_m^2 and σ_r^2 is available.

initialize : Precoders $\mathbf{F}_i = \sqrt{(\mathrm{P_{D_i}}/N)}\mathbf{I}_N$ $(i = 1, 2)$, and $\mathbf{F}_b = \sqrt{(\mathrm{P_B}/N)}\mathbf{I}_N$. Decoders $\mathbf{G}_r = \mathbf{I}_N$, and $\mathbf{G}_m = \mathbf{I}_N$.

repeat

  for $k = 1 : K$ **do** ▷ D2D

    Fix $\mathbf{F}_1$ and $\mathbf{F}_2$ obtained from step 5 (Or step 1 at $k = 1$). Find optimum $\mathbf{G}_r$ from (4.14).

    Fix $\mathbf{G}_r$ obtained from step 4. Solve problem (4.16) to find optimum $\mathbf{F}$. Then obtain $\mathbf{F}_1$ and $\mathbf{F}_2$.

  end for

  for $k = 1 : K$ **do** ▷ BS-MS

    Fix $\mathbf{F}_b$ obtained from step 9 (Or step 1 at $k = 1$). Find optimum $\mathbf{G}_m$ from (4.17).

    Fix $\mathbf{G}_m$ obtained from step 8. Solve problem (4.18) to find optimum $\mathbf{F}_b$.

  end for

  Update $\mathbf{F}_b$ in step 4. ▷ D2D

  Update $\mathbf{F}_1$ and $\mathbf{F}_2$ in step 8. ▷ BS-MS

until MSE_r and MSE_m converge.

Update precoders and decoders at all nodes.

Second time slot

During the second time slot, the RS broadcasts $\mathbf{s}_r$, and each device estimates that to recover desired transmitted symbol by the other device. Error vector at D_i is $\mathbf{e}_i = \mathbf{y}_i - \mathbf{s}_r$, and MSE at D_i is denoted as $\text{MSE}_{D_i} = \mathcal{E}_{\mathbf{s},\mathbf{n}}\{\|\mathbf{e}_i\|^2\}$. Proceeding in similar steps as in the previous cases, we can find MSE_{D_i} $(i = 1, 2)$ as

$$\begin{aligned}\text{MSE}_{D_i} = \text{Tr}\big(&\rho(\mathbf{G}_i\mathbf{H}_{ir}^T\mathbf{F}_r - \mathbf{I}_N)(\mathbf{G}_i\mathbf{H}_{ir}^T\mathbf{F}_r - \mathbf{I}_N)^H + \sigma_i^2\mathbf{G}_i\mathbf{G}_i^H \\ &+ (\mathbf{G}_i\mathbf{H}_{im}^T\mathbf{F}_m)(\mathbf{G}_i\mathbf{H}_{im}^T\mathbf{F}_m)^H\big).\end{aligned} \tag{4.19}$$

MSE_{D_1} is a function of variables $\mathbf{F}_r$, $\mathbf{G}_1$, and $\mathbf{F}_m$. MSE_{D_2} is a function of variables $\mathbf{F}_r$, $\mathbf{G}_2$, and $\mathbf{F}_m$. Both MSE_{D_1} and MSE_{D_2} are considered together in the optimization problem. The sum of MSE is considered as the objective function. The optimization problem is given by

$$\begin{aligned}\mathcal{Q}_1 : \quad &\min_{\mathbf{F}_r,\mathbf{F}_m,\mathbf{G}_1,\mathbf{G}_2} \ \frac{1}{2}\text{MSE}_{D_1}[\mathbf{F}_r,\mathbf{F}_m,\mathbf{G}_1] + \frac{1}{2}\text{MSE}_{D_2}[\mathbf{F}_r,\mathbf{F}_m,\mathbf{G}_2] \\ &\text{subject to} \quad \rho\text{Tr}(\mathbf{F}_r\mathbf{F}_r^H) \le \text{P}_\text{R} \\ &\qquad\qquad \rho\text{Tr}(\mathbf{H}_{br}^T\mathbf{F}_r\mathbf{F}_r^H\mathbf{H}_{br}^*) \le \text{I}_\text{d}.\end{aligned} \tag{4.20}$$

Similarly, the error vector at the BS can be found as $\mathbf{e}_b = \mathbf{y}_b - \mathbf{s}_m$. MSE at the BS is $\text{MSE}_b = \mathcal{E}_{\mathbf{s},\mathbf{n}}\{\|\mathbf{e}_b\|^2\}$, and this can be expanded as

$$\begin{aligned}\text{MSE}_b = \text{Tr}\big(&(\mathbf{G}_b\mathbf{H}_{bm}^T\mathbf{F}_m - \mathbf{I}_N)(\mathbf{G}_b\mathbf{H}_{bm}^T\mathbf{F}_m - \mathbf{I}_N)^H \\ &+ \rho(\mathbf{G}_b\mathbf{H}_{br}^T\mathbf{F}_r)(\mathbf{G}_b\mathbf{H}_{br}^T\mathbf{F}_r)^H + \sigma_b^2\mathbf{G}_b\mathbf{G}_b^H\big).\end{aligned} \tag{4.21}$$

The optimization problem to minimize MSE_b is given as

$$\begin{aligned}\mathcal{Q}_2 : \quad &\min_{\mathbf{F}_m,\mathbf{F}_r,\mathbf{G}_b} \quad \text{MSE}_b[\mathbf{F}_m,\mathbf{F}_r,\mathbf{G}_b] \\ &\text{subject to} \quad \text{Tr}(\mathbf{F}_m\mathbf{F}_m^H) \le \text{P}_\text{M} \\ &\qquad\qquad \text{Tr}(\mathbf{H}_{im}^T\mathbf{F}_m\mathbf{F}_m^H\mathbf{H}_{im}^*) \le \text{I}_\text{b} \quad i = 1, 2.\end{aligned} \tag{4.22}$$

As in the first time slot, we consider solving problems separately for D2D and BS-MS communications.

Distributed design for D2D communication: Solving $\mathcal{Q}_1$

Here, we solve $\mathcal{Q}_1$ by fixing $\mathbf{F}_m$. The modified problem $\mathcal{Q}_1$ is also a non-convex

optimization problem, which has a global minimum. The same iterative approach is used to solve this.

Sub-problem I : First, we fix $\mathbf{F}_r$ in the modified problem of (4.20), and the problem then reduces to,

$$\min_{\mathbf{G}_1,\mathbf{G}_2} \quad \frac{1}{2}\mathrm{MSE}_{D_1}[\mathbf{G}_1] + \frac{1}{2}\mathrm{MSE}_{D_2}[\mathbf{G}_2] \tag{4.23}$$

Objective function is minimized when the derivative with respect to $\mathbf{G}_i$ is zero, i.e.,

$$\mathbf{G}_i = (\rho\mathbf{F}_r^H\mathbf{H}_{ir}^*)(\rho\mathbf{H}_{ir}^T\mathbf{F}_r\mathbf{F}_r^H\mathbf{H}_{ir}^* + \mathbf{H}_{im}^T\mathbf{F}_m\mathbf{F}_m^H\mathbf{H}_{im}^* + \sigma_i^2\mathbf{I}_N)^{-1} \quad i = 1, 2. \tag{4.24}$$

Sub-problem II : Both $\mathbf{G}_1$ and $\mathbf{G}_2$ are fixed, (4.20) is reformulated into

$$\begin{aligned} \min_{\mathbf{F}_r} \quad & \frac{\rho}{2}\mathrm{Tr}\Big(\mathbf{F}_r^H\big(\mathbf{H}_{1r}^*\mathbf{G}_1^H\mathbf{G}_1\mathbf{H}_{1r}^T + \mathbf{H}_{2r}^*\mathbf{G}_2^H\mathbf{G}_2\mathbf{H}_{2r}^T\big)\mathbf{F}_r\Big) \\ & - \rho\Re\Big(\mathrm{Tr}\big((\mathbf{G}_1\mathbf{H}_{1r}^T + \mathbf{G}_2\mathbf{H}_{2r}^T)\mathbf{F}_r\big)\Big) + c_d \\ \text{subject to} \quad & \rho\mathrm{Tr}(\mathbf{F}_r^H\mathbf{H}_{br}^*\mathbf{H}_{br}^T\mathbf{F}_r) \le \mathrm{I_d} \\ & \rho\mathrm{Tr}(\mathbf{F}_r\mathbf{F}_r^H) \le \mathrm{P_R}, \end{aligned} \tag{4.25}$$

where $c_d = \frac{1}{2}\mathrm{Tr}\big((\mathbf{G}_1\mathbf{H}_{1m}^T\mathbf{F}_m)(\mathbf{G}_1\mathbf{H}_{1m}^T\mathbf{F}_m)^H + (\mathbf{G}_2\mathbf{H}_{2m}^T\mathbf{F}_m)(\mathbf{G}_2\mathbf{H}_{2m}^T\mathbf{F}_m)^H + \sigma_1^2\mathbf{G}_1\mathbf{G}_1^H + \sigma_2^2\mathbf{G}_2\mathbf{G}_2^H + 4\mathbf{I}_N\big)$. The problem (4.25) can be solved with QCQP method. Both (4.24) and (4.25) are solved iteratively to obtain optimal solutions for $\mathbf{F}_r$, $\mathbf{G}_1$ and $\mathbf{G}_2$.

Distributed design for BS-MS communication: Solving $\mathcal{Q}_2$

A similar method as solving $\mathcal{P}_2$ is used to solve $\mathcal{Q}_2$, where the solution for $\mathbf{G}_b$ is given by

$$\mathbf{G}_b = (\mathbf{F}_m^H\mathbf{H}_{bm}^*)(\mathbf{H}_{bm}^T\mathbf{F}_m\mathbf{F}_m^H\mathbf{H}_{bm}^* + \rho\mathbf{H}_{br}^T\mathbf{F}_r\mathbf{F}_r^H\mathbf{H}_{br}^* + \sigma_b^2\mathbf{I}_N)^{-1}, \tag{4.26}$$

and, $\mathbf{F}_m$ can be found by solving following optimization problem.

$$\begin{aligned} \min_{\mathbf{F}_m} \quad & \mathrm{Tr}\left(\mathbf{F}_m^H(\mathbf{G}_b\mathbf{H}_{bm}^T)^H(\mathbf{G}_b\mathbf{H}_{bm}^T)\mathbf{F}_m\right) - 2\Re(\mathrm{Tr}(\mathbf{G}_b\mathbf{H}_{bm}^T\mathbf{F}_m)) + c_b \\ \text{subject to} \quad & \mathrm{Tr}(\mathbf{F}_m^H\mathbf{H}_{im}^*\mathbf{H}_{im}^T\mathbf{F}_m) \le \mathrm{I_b} \qquad i = 1, 2 \\ & \mathrm{Tr}(\mathbf{F}_m^H\mathbf{F}_m) \le \mathrm{P_M}, \end{aligned} \tag{4.27}$$

Algorithm 4.2 Joint design for PNC based D2D mode - Second time slot

Channel state information is available. Information about N, K, $\mathrm{P_R}$, $\mathrm{P_M}$, $\mathrm{I_d}$, $\mathrm{I_b}$, σ_b^2, σ_1^2, and σ_2^2 is available.

1: **initialize** : Precoders $\mathbf{F}_r = \sqrt{(\mathrm{P_R}/N)}\mathbf{I}_N$, and $\mathbf{F}_m = \sqrt{(\mathrm{P_M}/N)}\mathbf{I}_N$.
Decoders $\mathbf{G}_b = \mathbf{I}_N$, $\mathbf{G}_i = \mathbf{I}_N$ $(i = 1, 2)$.

2: **repeat**

3: **for** $k = 1 : K$ **do** ▷ D2D

4: Fix $\mathbf{F}_r$ obtained from step 5 (Or step 1 at $k = 1$). Find optimum $\mathbf{G}_1$, and $\mathbf{G}_2$ from (4.24).

5: Fix $\mathbf{G}_1$ and $\mathbf{G}_2$ obtained from step 4. Solve problem (4.25) to find optimum $\mathbf{F}_r$.

6: **end for**

7: **for** $k = 1 : K$ **do** ▷ BS-MS

8: Fix $\mathbf{F}_m$ obtained from step 9 (Or step 1 at $k = 1$). Find optimum $\mathbf{G}_b$ from (4.26).

9: Fix $\mathbf{G}_b$ obtained from step 8. Solve problem (4.27) to find optimum $\mathbf{F}_m$.

10: **end for**

11: Update $\mathbf{F}_m$ in step 4. ▷ D2D

12: Update $\mathbf{F}_r$ in step 8. ▷ BS-MS

13: **until** MSE_{D_1}, MSE_{D_2} and MSE_b converge.

14: Update precoders and decoders at all nodes.

where $c_b = \mathrm{Tr}\left(\rho(\mathbf{G}_b\mathbf{H}_{br}^T\mathbf{F}_r)(\mathbf{G}_b\mathbf{H}_{br}^T\mathbf{F}_r)^H + \sigma_b^2\mathbf{G}_b\mathbf{G}_b^H + \mathbf{I}_N\right)$. We propose Algorithm 4.2 to find optimal precoder-decoder design during the second time slot.

The proposed algorithms converge with a finite number of iterations and exchanges, and we use these during the numerical analysis to discuss the system performance. Next, we investigate a possible distributed framework and design coordination mechanism to the proposed algorithms.

4.2.2 Distributed framework and design coordination

Channel Estimation

The distributed framework depends on how much CSI is allowed to be shared between different nodes. In the case of all CSI (including the cross channels. e.g. $\mathbf{H}_{1r}, \mathbf{H}_{2r}$) is collected at a central controller (e.g. BS), a centralized design is possible, where the computations are carried out at the central controller, and precoder-decoder information is forwarded to other nodes. However, there is a huge cost of overhead signalling in this scenario. The distributed approach can avoid the huge overheads in solving the problems.

Since we assume the channels are frequency flat and quasi-static, the coherence interval is long enough to estimate CSI, compute precoder-decoder matrices, and transmit data. In particular, the coherence interval is divided into three parts. The first part is dedicated to transmit training sequences, where nodes can estimate CSI. The second part is dedicated to computation, where nodes run the distributed algorithms and exchange information. The third part is the actual data transmission.

During the first part of coherence interval, all nodes transmit training sequences [92, 143] so that other nodes can estimate their connected channels. All nodes are divided into two groups referring to D2D and BS-MS communications. The RS acts as the main measurement point of the D2D group. The BS is the main measurement point of the BS-MS group. After the completion of transmitting training sequences, the RS has CSI knowledge of $\mathbf{H}_{1r}$, $\mathbf{H}_{2r}$, $\mathbf{H}_{br}$. The BS has CSI knowledge of $\mathbf{H}_{br}$ and $\mathbf{H}_{bm}$. The MS, D_1, D_2 have CSI knowledge of $\mathbf{H}_{1m}$ and $\mathbf{H}_{2m}$. The BS, RS acquire that information prior any further computations. $\mathbf{H}_{bm}$ is not required to nodes in the D2D group. Similarly, $\mathbf{H}_{1r}$, $\mathbf{H}_{2r}$ are not required to cellular group. Therefore, local CSI is sufficient to run Algorithm 4.1 and 4.2 at the RS and BS.

Design coordination

The coordination between BS and RS after K local iterations further minimize the MSE. This can be done with the same channel or a different channel. In particular, the information about $\mathbf{F}_1\mathbf{F}_1^H$, $\mathbf{F}_2\mathbf{F}_2^H$, and $\mathbf{F}_r\mathbf{F}_r^H$ are required at the

BS. Since all are hermitian matrices, upper triangular or lower triangular part of these matrices are sufficient to exchange during the cooperation. Similarly, the RS required information about $\mathbf{F}_b\mathbf{F}_b^H$ and $\mathbf{F}_m\mathbf{F}_m^H$. After certain number of iterations (or upon the convergence of MSE), the RS update relevant precoder and decoder matrices to devices, while BS update them to MS. With highly sophisticated processing capabilities available at the modern devices, we believe these computations will not be that complex.

When channels have smaller coherence interval, the algorithms can be stopped after few iterations, exchanging information between BS and MS might also not possible. We consider such incidents in the Section 4.4.

4.2.3 Centralized approach

In this subsection, we formulate the centralized optimization problem when all CSI is available at a central unit. This central unit computes the precoder and decoder matrices, and updates prior to the data transmission. As mentioned in the earlier subsection, this method requires higher signalling overhead. However, the centralized design is useful to compare the performance difference with the distributed approach. In the following, we consider the precoder-decoder design for the first time slot. A similar approach can be used for the second timeslot, hence omitted.

In the distributed approach, the problems $\mathcal{P}_1$ and $\mathcal{P}_2$ minimize MSE_r and MSE_m with respective constraints. However, the optimal precoder and decoder matrices can be obtained only when the two problems are considered in a single problem. Thus, joint design problem converts to a multicriterion optimization problem, where multiple objectives are present in the problem. This is given as

$$
\begin{aligned}
\mathcal{C}: \quad & \min_{\mathbf{F}_1,\mathbf{F}_2,\mathbf{F}_b,\mathbf{G}_r,\mathbf{G}_m} && (\mathrm{MSE}_r, \mathrm{MSE}_m) \\
& \text{subject to} && \mathrm{Tr}(\mathbf{F}_b\mathbf{F}_b^H) \le \mathrm{P_B}, \quad \mathrm{Tr}(\mathbf{F}_i\mathbf{F}_i^H) \le \mathrm{P_{D_i}} \quad \text{for} \;\; i = 1, 2, \\
& && \mathrm{Tr}\big(\mathbf{H}_{1m}\mathbf{F}_1\mathbf{F}_1^H\mathbf{H}_{1m}^H + \mathbf{H}_{2m}\mathbf{F}_2\mathbf{F}_2^H\mathbf{H}_{2m}^H\big) \le \mathrm{I_d}, \quad (4.28) \\
& && \mathrm{Tr}\big(\mathbf{H}_{br}\mathbf{F}_b\mathbf{F}_b^H\mathbf{H}_{br}^H\big) \le \mathrm{I_b}.
\end{aligned}
$$

Here, the objectives are non-competing over decoder variables, i.e., there are no compromises to be made among MSE_r and MSE_m. However, the precoder variables are common between objectives, therefore, the problem $\mathcal{C}$ does not have

a single solution that simultaneously optimizes each objective. For such cases, there exists a number of Pareto optimal solutions. We adopt the scalarization of the objective, which is regarded as a standard method for finding Pareto optimal points [142, p.178, Sec. 4.7.4]. For scalarization, we consider $\lambda \in [0,1]$ as the weight associated with MSE_r and $1-\lambda$ as the weight associated with MSE_m. Then the objective of problem $\mathcal{C}$ becomes $\lambda \mathrm{MSE}_r + (1-\lambda)\mathrm{MSE}_m$.

The set of Pareto optimal points of the problem $\mathcal{C}$ can be obtained by solving scalarized problem for different λ values. This gives the optimal trade-off curve for MSE_r and MSE_m. The scalarized problem is non-convex, and we utilize iterative method to solve it. Similar to Appendix 6, iterative method converges to a Pareto optimal point for a given λ. First, the precoder variables are fixed, and decoders are evaluated by differentiating in terms of $\mathbf{G}_r$ and $\mathbf{G}_m$, where the solutions are given as (4.14) and (4.17) respectively. Next, $\mathbf{G}_r$ and $\mathbf{G}_m$ are fixed, and the problem is solved with the precoder variables. The problem can be reformulated as

$$\begin{aligned} \min_{\tilde{\mathbf{F}}} \quad & \mathrm{Tr}(\tilde{\mathbf{F}}^H(\tilde{\mathbf{A}}_1+\tilde{\mathbf{A}}_2)\tilde{\mathbf{F}}) - 2\Re(\mathrm{Tr}(\tilde{\mathbf{B}}\tilde{\mathbf{F}})) + \tilde{c} \\ \text{subject to} \quad & \mathrm{Tr}(\tilde{\mathbf{F}}^H\tilde{\mathbf{P}}_b\tilde{\mathbf{F}}) \le \mathrm{P_B}, \quad \mathrm{Tr}(\tilde{\mathbf{F}}^H\tilde{\mathbf{P}}_i\tilde{\mathbf{F}}) \le \mathrm{P_{D_i}} \quad \text{for} \;\; i=1,2, \\ & \mathrm{Tr}(\tilde{\mathbf{F}}^H\tilde{\mathbf{B}}_r\tilde{\mathbf{F}}) \le \mathrm{I_d}, \quad \mathrm{Tr}(\tilde{\mathbf{F}}^H\tilde{\mathbf{B}}_m\tilde{\mathbf{F}}) \le \mathrm{I_b}, \end{aligned} \tag{4.29}$$

where

$$\tilde{\mathbf{F}} = \begin{pmatrix} \mathbf{F}_1 & \mathbf{0}_{N\times N} & \mathbf{0}_{N\times N} \\ \mathbf{0}_{N\times N} & \mathbf{F}_2 & \mathbf{0}_{N\times N} \\ \mathbf{0}_{N\times N} & \mathbf{0}_{N\times N} & \mathbf{F}_b \end{pmatrix}, \tilde{\mathbf{B}} = \begin{pmatrix} \lambda\mathbf{G}_r\mathbf{H}_{1r} & \mathbf{0}_{N\times N} & \mathbf{0}_{N\times N} \\ \mathbf{0}_{N\times N} & \lambda\mathbf{G}_r\mathbf{H}_{2r} & \mathbf{0}_{N\times N} \\ \mathbf{0}_{N\times N} & \mathbf{0}_{N\times N} & (1-\lambda)\mathbf{G}_m\mathbf{H}_{bm} \end{pmatrix},$$

$$\tilde{\mathbf{A}}_1 = \begin{pmatrix} \lambda\mathbf{H}_{1r}^H\mathbf{G}_r^H\mathbf{G}_r\mathbf{H}_{1r} & \mathbf{0}_{N\times N} & \mathbf{0}_{N\times N} \\ \mathbf{0}_{N\times N} & \lambda\mathbf{H}_{2r}^H\mathbf{G}_r^H\mathbf{G}_r\mathbf{H}_{2r} & \mathbf{0}_{N\times N} \\ \mathbf{0}_{N\times N} & \mathbf{0}_{N\times N} & (1-\lambda)\mathbf{H}_{bm}^H\mathbf{G}_m^H\mathbf{G}_m\mathbf{H}_{bm} \end{pmatrix},$$

$$\tilde{\mathbf{A}}_2 = \begin{pmatrix} (1-\lambda)\mathbf{H}_{1m}^H\mathbf{G}_m^H\mathbf{G}_m\mathbf{H}_{1m} & \mathbf{0}_{N\times N} & \mathbf{0}_{N\times N} \\ \mathbf{0}_{N\times N} & (1-\lambda)\mathbf{H}_{2m}^H\mathbf{G}_m^H\mathbf{G}_m\mathbf{H}_{2m} & \mathbf{0}_{N\times N} \\ \mathbf{0}_{N\times N} & \mathbf{0}_{N\times N} & \lambda\mathbf{H}_{br}^H\mathbf{G}_r^H\mathbf{G}_r\mathbf{H}_{br} \end{pmatrix},$$

$$\tilde{\mathbf{P}}_1 = (\mathbf{I}_N \quad \mathbf{0}_{N\times 2N} \;;\; \mathbf{0}_{2N\times 3N}), \; \tilde{\mathbf{P}}_2 = (\mathbf{0}_{N\times 3N} \;;\; \mathbf{0}_{N\times N} \quad \mathbf{I}_N \quad \mathbf{0}_{N\times N}; \mathbf{0}_{N\times 3N}),$$

$\tilde{\mathbf{P}}_b = (\mathbf{0}_{2N\times 3N}\ ;\ \mathbf{0}_{N\times 2N}\ \ \mathbf{I}_N)$,

$$\tilde{\mathbf{B}}_r = \begin{pmatrix} \mathbf{0}_{N\times N} & \mathbf{0}_{N\times N} & \mathbf{0}_{N\times N} \\ \mathbf{0}_{N\times N} & \mathbf{0}_{N\times N} & \mathbf{0}_{N\times N} \\ \mathbf{0}_{N\times N} & \mathbf{0}_{N\times N} & \mathbf{H}_{br}^H\mathbf{H}_{br} \end{pmatrix}, \tilde{\mathbf{B}}_m = \begin{pmatrix} \mathbf{H}_{1m}^H\mathbf{H}_{1m} & \mathbf{0}_{N\times N} & \mathbf{0}_{N\times N} \\ \mathbf{0}_{N\times N} & \mathbf{H}_{2m}^H\mathbf{H}_{2m} & \mathbf{0}_{N\times N} \\ \mathbf{0}_{N\times N} & \mathbf{0}_{N\times N} & \mathbf{0}_{N\times N} \end{pmatrix},$$

and $\tilde{c} = \mathrm{Tr}(2\lambda\mathbf{I}_N + (1-\lambda)\mathbf{I}_N + \sigma_r^2\lambda\mathbf{G}_r\mathbf{G}_r^H + \sigma_m^2(1-\lambda)\mathbf{G}_m\mathbf{G}_m^H)$. This is a convex problem and can be solved with convex optimization tools such as QCQP. For a given value of λ, iteratively solving (4.14),(4.17), and (4.29) gives Pareto optimal solution. λ is varied to attain the optimal trade-off curve.

In Section 4.4, we use the aforementioned method to find Pareto optimal points, and illustrate that the distributed algorithms also provide near Pareto optimal points.

4.3 Precoder-decoder design for direct D2D mode

The direct D2D communication can also improve by adoping joint precoder-decoder design. Here, a similar MSE procedure is used to find optimal precoder-decoder matrices. In order to keep the consistency of the discussion, the precoder and decoder variables at nodes use the same notation.

During the first time slot, the post-proceessed signals at the D_2 and MS are given by,

$$\mathbf{y}_2 = \mathbf{G}_2\mathbf{H}_{12}\mathbf{F}_1\mathbf{s}_1 + \mathbf{G}_2\mathbf{H}_{b2}\mathbf{F}_b\mathbf{s}_b + \mathbf{G}_2\mathbf{n}_2, \tag{4.30}$$

$$\mathbf{y}_m = \mathbf{G}_m\mathbf{H}_{bm}\mathbf{F}_b\mathbf{s}_b + \mathbf{G}_m\mathbf{H}_{1m}\mathbf{F}_1\mathbf{s}_1 + \mathbf{G}_m\mathbf{n}_m, \tag{4.31}$$

where $\mathbf{H}_{12} \in \mathbb{C}^{N\times N}$ is the MIMO channel from D_1-to-D_2. During the second time slot, the post-processed signals at the D_1 and BS are given by,

$$\mathbf{y}_1 = \mathbf{G}_1\mathbf{H}_{12}^T\mathbf{F}_2\mathbf{s}_2 + \mathbf{G}_1\mathbf{H}_{m1}\mathbf{F}_m\mathbf{s}_m + \mathbf{G}_1\mathbf{n}_1, \tag{4.32}$$

$$\mathbf{y}_b = \mathbf{G}_b\mathbf{H}_{bm}^T\mathbf{F}_m\mathbf{s}_m + \mathbf{G}_b\mathbf{H}_{2b}\mathbf{F}_2\mathbf{s}_2 + \mathbf{G}_b\mathbf{n}_b. \tag{4.33}$$

Next, we consider the first time slot of the communication to discuss the optimal design. The same procedure is applied in the second time slot.

4.3.1 First time slot

During the first time slot, the error vectors at D_2 and MS are given by,

$$\mathbf{e}_2 = \mathbf{G}_2\mathbf{H}_{12}\mathbf{F}_1\mathbf{s}_1 + \mathbf{G}_2\mathbf{H}_{b2}\mathbf{F}_b\mathbf{s}_b + \mathbf{G}_2\mathbf{n}_2 - \mathbf{s}_1, \tag{4.34}$$

$$\mathbf{e}_m = \mathbf{G}_m\mathbf{H}_{bm}\mathbf{F}_b\mathbf{s}_b + \mathbf{G}_m\mathbf{H}_{1m}\mathbf{F}_1\mathbf{s}_1 + \mathbf{G}_m\mathbf{n}_m - \mathbf{s}_b. \tag{4.35}$$

The MSE at D_2 and MS are denoted as $\mathrm{MSE}_2^{\mathrm{dir}}$ and $\mathrm{MSE}_m^{\mathrm{dir}}$, respectively. They are given by,

$$\begin{aligned}\mathrm{MSE}_2^{\mathrm{dir}} =& \mathrm{Tr}\big((\mathbf{G}_2\mathbf{H}_{12}\mathbf{F}_1 - \mathbf{I}_N)(\mathbf{G}_2\mathbf{H}_{12}\mathbf{F}_1 - \mathbf{I}_N)^H + \sigma_2^2\mathbf{G}_2\mathbf{G}_2^H \\ &+ (\mathbf{G}_2\mathbf{H}_{b2}\mathbf{F}_b)(\mathbf{G}_2\mathbf{H}_{b2}\mathbf{F}_b)^H\big), \end{aligned}\tag{4.36}$$

$$\begin{aligned}\mathrm{MSE}_m^{\mathrm{dir}} =& \mathrm{Tr}\big((\mathbf{G}_m\mathbf{H}_{bm}\mathbf{F}_b - \mathbf{I}_N)(\mathbf{G}_m\mathbf{H}_{bm}\mathbf{F}_b - \mathbf{I}_N)^H + \sigma_m^2\mathbf{G}_m\mathbf{G}_m^H \\ &+ (\mathbf{G}_m\mathbf{H}_{1m}\mathbf{F}_1)(\mathbf{G}_m\mathbf{H}_{1m}\mathbf{F}_1)^H\big). \end{aligned}\tag{4.37}$$

The greedy optimization approach based design is considered with the same constraints as in the previous section. Here, both problems are matched with each other. This can be generalized into a common format, and given as

$$\begin{aligned}\mathcal{P}: \quad & \min_{\mathbf{F},\mathbf{G},\mathbf{F}_I} \quad \mathrm{MSE}^{\mathrm{dir}}[\mathbf{F},\mathbf{G},\mathbf{F}_I] \\ & \text{subject to} \quad \mathrm{Tr}((\mathbf{H}_{og}\mathbf{F})(\mathbf{H}_{og}\mathbf{F})^H) \le \mathrm{I}_{\mathrm{th}} \\ & \qquad\qquad\quad \mathrm{Tr}(\mathbf{F}\mathbf{F}^H) \le \mathrm{P}_{\max}, \end{aligned}\tag{4.38}$$

where

$$\mathrm{MSE}^{\mathrm{dir}} = \mathrm{Tr}\Big((\mathbf{G}\mathbf{H}\mathbf{F} - \mathbf{I}_N)(\mathbf{G}\mathbf{H}\mathbf{F} - \mathbf{I}_N)^H + (\mathbf{G}\mathbf{H}_{ic}\mathbf{F}_I)(\mathbf{G}\mathbf{H}_{ic}\mathbf{F}_I)^H + \sigma^2\mathbf{G}\mathbf{G}^H\Big), \tag{4.39}$$

where $\mathbf{G}$ is the decoder at the receiver, $\mathbf{F}$ is the precoder at the transmitter, $\mathbf{H}$ is the channel between the transmitter and receiver, $\mathbf{F}_I$ is the precoder at the interfering transmitter, $\mathbf{H}_{ic}$ is the incoming channel from the interfering transmitter, $\mathbf{H}_{og}$ is the outgoing channel which is interfered by the original transmission, σ^2 is the noise variance at the receiver, I_{th} is the interference threshold level at the transmitter, and $\mathrm{P}_{\max}$ is the maximum transmit power. Following transformations give original optimization problems.

– Joint design for D2D communication: $\mathbf{F} = \mathbf{F}_1$, $\mathbf{F}_I = \mathbf{F}_b$, $\mathbf{G} = \mathbf{G}_2$, $\mathbf{H} = \mathbf{H}_{12}$, $\mathbf{H}_{og} = \mathbf{H}_{1m}$, $\mathbf{H}_{ic} = \mathbf{H}_{b2}$, $\sigma = \sigma_2$, $\mathrm{I}_{\mathrm{th}} = \mathrm{I}_{\mathrm{d}}$, and $\mathrm{P}_{\max} = \mathrm{P}_{\mathrm{D}_1}$.

– Joint design for BS-MS communication: $\mathbf{F} = \mathbf{F}_b$, $\mathbf{F}_I = \mathbf{F}_1$, $\mathbf{G} = \mathbf{G}_m$, $\mathbf{H} = \mathbf{H}_{bm}$, $\mathbf{H}_{og} = \mathbf{H}_{b2}$, $\mathbf{H}_{ic} = \mathbf{H}_{1m}$, $\sigma = \sigma_m$ $\mathrm{I_{th}} = \mathrm{I_b}$, and $\mathrm{P_{max}} = \mathrm{P_B}$.

When $\mathbf{F}_I$ is fixed, the problem $\mathcal{P}$ can be solved to find closed form solutions of globally optimal $\mathbf{F}$ and $\mathbf{G}$. The detailed procedure is given in the Appendix 7, where exact solutions are derived considering different cases of $\mathrm{P_{max}}$ and $\mathrm{I_{th}}$. The Algorithm 7.0.1 is proposed with these cases to find optimal $\mathbf{F}$ and $\mathbf{G}$.

The Algorithm 7.0.1 can be used separately at both D2D and BS-MS communications. This is a similar distributed approach as in the previous section. The Algorithm 4.3 summarizes the joint design in the first time slot.

Algorithm 4.3 Joint design for direct D2D mode - First time slot

Channel state information is available. Information about N, $\mathrm{P_B}$, $\mathrm{P_{D_1}}$, $\mathrm{I_b}$, $\mathrm{I_d}$, σ_m^2, and σ_2^2 is available.

1: **initialize** : Precoders $\mathbf{F}_1 = \sqrt{(\mathrm{P_{D_1}}/N)}\mathbf{I}_N$, and $\mathbf{F}_b = \sqrt{(\mathrm{P_B}/N)}\mathbf{I}_N$.
Decoders $\mathbf{G}_2 = \mathbf{I}_N$, $\mathbf{G}_m = \mathbf{I}_N$.

2: **repeat**

3: Fix $\mathbf{F}_b$ obtained from step 5 (Or step 1 at start). Use Algorithm 7.0.1 (under D2D variables) to find optimum $\mathbf{F}_1$, and $\mathbf{G}_2$.

4: Fix $\mathbf{F}_1$ obtained from step 6 (Or step 1 at start). Use Algorithm 7.0.1 (under BS-MS variables) to find optimum $\mathbf{F}_b$, and $\mathbf{G}_m$.

5: Update $\mathbf{F}_b$ in step 3. ▷ D2D

6: Update $\mathbf{F}_1$ in step 4. ▷ BS-MS

7: **until** $\mathrm{MSE}_2^{\mathrm{dir}}$ and $\mathrm{MSE}_m^{\mathrm{dir}}$ converge.

8: Update precoders and decoders at all nodes.

4.3.2 Second time slot

During the second time slot, both D_2-to-D_1 and MS-to-BS communications are considered together. The Algorithm 4.3 can be used with the channels replaced by their respective transposes to find optimal precoder-decoder matrices.

4.3.3 Distributed framework and design coordination

A similar distributed framework as in Section 4.2.2 can be used for direct D2D mode. Now, the D_1 acts as the main measurement point of the D2D group. The BS is the main measurement point in the BS-MS group. The D_1 requires CSI knowledge of $\mathbf{H}_{12}$, $\mathbf{H}_{1m}$, and $\mathbf{H}_{b2}$. The BS requires CSI knowledge of $\mathbf{H}_{bm}$, $\mathbf{H}_{1m}$, and $\mathbf{H}_{b2}$. As with the PNC based D2D, the BS and D_1 acquire that information prior any further computations. $\mathbf{H}_{bm}$ is not required at the D_1. Similarly, $\mathbf{H}_{12}$ is not required at the BS.

The coordination between BS and D_1 can further minimize the MSE, where the information about $\mathbf{F}_1\mathbf{F}_1^H$, and $\mathbf{F}_2\mathbf{F}_2^H$ are required at the BS. Similarly, the D_1 requires information about $\mathbf{F}_b\mathbf{F}_b^H$ and $\mathbf{F}_m\mathbf{F}_m^H$. Since Algorithm 4.3 does not possess sub-problems, it has very fast convergence.

4.4 Numerical results

In this section, several numerical examples are provided to illustrate the proposed D2D schemes. We consider a single cell with one underlay D2D pair as described in Section 4.4. Monte Carlo simulations are carried out to evaluate the BER and MSE performances of the proposed algorithms. The entries of $\mathbf{H}_{ij}$ are assumed to be $\sim \frac{1}{d_{ij}^2} c_{ij}$, where the first term represents the path loss factor and $c_{ij} \sim \mathcal{CN}(0,1)$ represents the Rayleigh small-scale fading. The d_{ij} is the normalized distance between ith and jth nodes. The shadow fading is not considered here. The power constraint of the devices, MS and RS is taken to be $\mathrm{P_D}$. All noise variables are considered to have the same variance (σ^2). The Table 4.1 provides the basic simulation parameters that are used in all the numerical examples, where we assume a normalized XY grid with $[-3,+3]$ for both axis. A user at the edge can experience received power between (-10 dB to 20 dB) depending on the $\mathrm{P_D}/\sigma^2$ (0 dB to 30 dB). The BS and RS are located at $(0,0)$ and $(0,-2)$, respectively. Additionally, the transmitted symbols are assumed to be equiprobable BPSK symbols. During the MA stage of PNC based D2D mode, the RS performs independent ML estimation for all received streams to estimate the sum of transmitted symbols $\mathbf{s}_1$ and $\mathbf{s}_2$. We adopt the same ML criterion to estimate desired symbols at all other nodes. Unless specifically mentioned, the distributed approach is used in the following numerical examples.

Table 4.1. Basic simulation parameters

Parameter	Value
Cell	Normalized XY grid $[-3, 3]$
Fixed nodes	BS $= (0, 0)$, RS $= (0, -2)$.
Normalized distance between nodes i and j	d_{ij}
Entries of $\mathbf{H}_{ij}$	$\frac{1}{d_{ij}^2}\mathcal{CN}(0, 1)$
N	2
K	5
ρ	2
Modulation	BPSK
$\mathrm{P_D}/\sigma^2$	$0\mathrm{dB} - 30\mathrm{dB}$
Edge SNR	$-10\mathrm{dB} - 20\mathrm{dB}$
$\mathrm{I_d}/\mathrm{P_D}$	$-20\mathrm{dB} - 0\mathrm{dB}$

First, we consider the MIMO PNC based underlay D2D system. Fig.4.3 shows the convergence of average MSE (AMSE) of each communication for both Algorithms 4.1 and 4.2. The MS and D_1 are fixed at $(1, 0)$ and $(-0.5, -2)$, respectively. The D_2 location is assumed to have a uniform distribution over the grid. Two cases are considered for $\mathrm{P_D}/\sigma^2 = 19$ dB and 16 dB with $\mathrm{P_B} = \mathrm{P_D}$, $\mathrm{I_d}/\sigma^2 = 7$ dB and $\mathrm{I_b} = \mathrm{I_d}$. The proposed algorithms converge fast, and, much lower AMSE values can be achieved with higher $\mathrm{P_D}$. The BS and RS exchange precoder information for every five ($K = 5$) iterations, and this improves the solution as we can observe a sudden drop of AMSE at those iterations. The AMSE at the RS has an exponential decay and converges with 25 iterations. All other AMSEs converge with 6 iterations. When the channel coherence interval is very short, the algorithms have to stop after a smaller number of iterations. Then, the joint design for D2D during the first time slot may not in the converged solution. However, Fig.4.3 shows an exponential decay, and the AMSE has significant improvement than a non-optimized scenario.

Fig. 4.4 illustrates the optimality of the converged MSE values of Algorithm 4.1. The scalarized problem $\mathcal{C}$ is solved for different $\lambda \in [0, 1]$ to obtain the optimal trade-off curve of MSE_r and MSE_m. These curves are plotted for three $\mathrm{P_D}/\sigma^2$ values. The MS, D_1, and D_2 are fixed at $(1, 0)$, $(-0.5, -2)$, and $(0.5, -2)$, respectively. Moreover, we consider $\mathrm{P_B} = \mathrm{P_D}$, $\mathrm{I_d}/\sigma^2 = 7$ dB and $\mathrm{I_b} = \mathrm{I_d}$. The

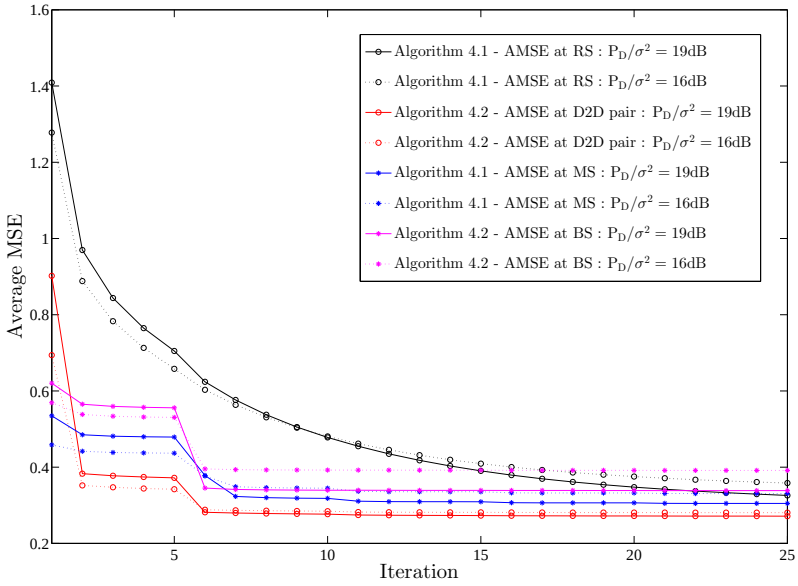

Fig 4.3. Algorithms for PNC based D2D communication for both time slots. Average number of iteration to converge MSE. MS $= (1, 0)$**, RS** $= (-0.5, -2)$**.** $\mathrm{P_B} = \mathrm{P_D}$**,** $\mathrm{I_d}/\sigma^2 = 7$ **dB, and** $\mathrm{I_b} = \mathrm{I_d}$**, [113] © 2014, IEEE.**

points on the trade-off curves represent Pareto optimal points of the problem $\mathcal{C}$. The circles represent MSE values obtained using Algorithm 4.1. The same algorithm without the cooperation between the RS and BS is considered to find the non-cooperative solution, where MSE values are represented by the squares. The proposed distributed scheme provides near Pareto optimal solutions. More importantly, this performance is achieved with less signalling overhead and CSI compared to the centralized approach. The non-cooperative scheme provides the lowest performance due to independent designs for D2D and BS-MS communications.

Fig.4.5(a) illustrates the average BER (ABER) of the PNC based D2D communication for different D_2 locations. The same simulation parameters are used as those of Fig.4.3 except for power constraint $\mathrm{P_D}/\sigma^2 = 16$ dB. PNC based D2D communication provides good BER performance for nearby locations to D_1 and RS. All other locations have higher BER, and are not suitable for D2D communication. The ABER of the BS-MS communication is shown in Fig.4.5(b). It is evident that the BS-MS communication does not have any problem with ABER

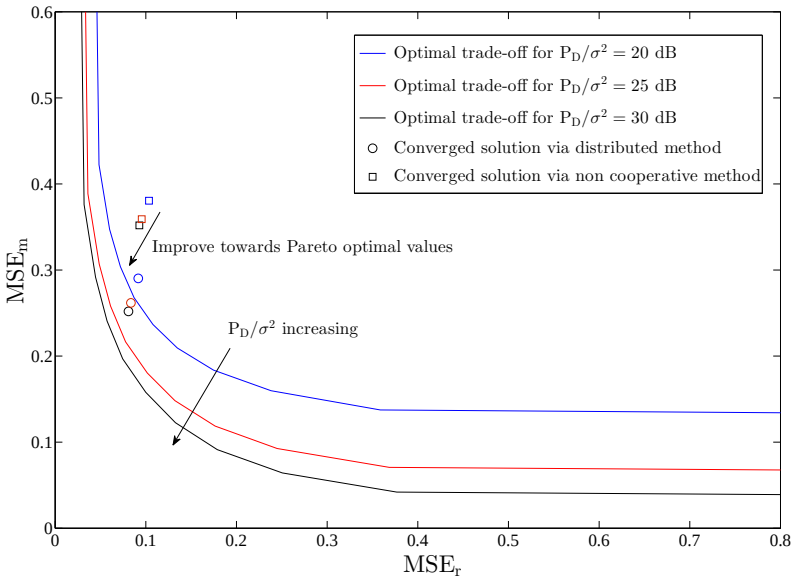

Fig 4.4. Optimal solutions via centralized and distributed approaches. MS $= (1, 0)$**,** $D_1 = (-0.5, -2)$**,** $D_2 = (0.5, -2)$**,** $P_B = P_D$**,** $I_d/\sigma^2 = 7$ **dB, and** $I_b = I_d$**, [113] © 2014, IEEE.**

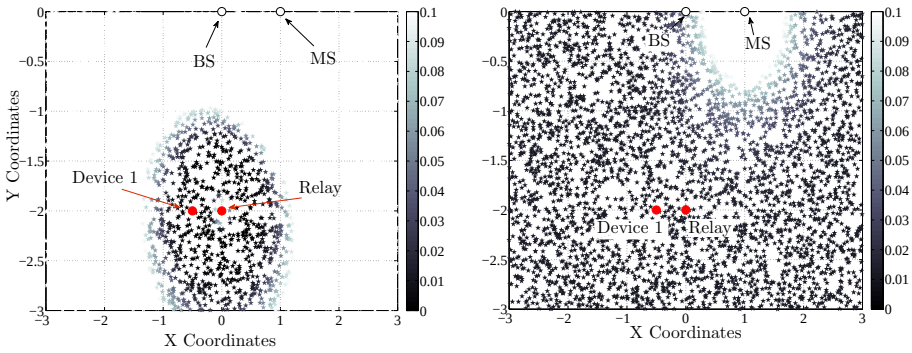

Fig 4.5. Average BER variation with the location of D2 for both D2D and BS-MS communications. (a). Average BER variation of PNC based D2D pair ; (b). Average BER variation of BS-MS pair. MS $= (1, 0)$**, RS** $= (-0.5, -2)$**.** $P_D/\sigma^2 = 16$ **dB,** $P_B = P_D$**,** $I_d/\sigma^2 = 7$ **dB, and** $I_b = I_d$**, [113] © 2014, IEEE.**

unless D_2 is located very near the MS or the BS.

The error performance versus $\mathrm{I_d/P_D}$ and $\mathrm{P_D}/\sigma^2$ are investigated in Fig.4.6 and Fig.4.7. There, we consider following scenarios to compare the system performance.

1. Scenario 1: The cooperation between the BS and RS to exchange precoder information is allowed. Both D2D and BS-MS communications are subjected to different interference threshold levels, where $\mathrm{I_b} = 2\mathrm{I_d}$.
2. Scenario 2: The cooperation between the BS and RS to exchange precoder information is allowed. The BS-MS communication is treated as the primary transmission. Therefore, the problem $\mathcal{P}_2$ is not subjected to an interference threshold level, where $\mathrm{I_b} = \infty$.
3. Scenario 3: No cooperation is considered between the BS and RS to exchange the precoder information. Algorithm 4.1 and 4.2 are stopped after 5 local iterations. Both D2D and BS-MS communications are subjected to different interference threshold levels. $\mathrm{I_b} = 2\mathrm{I_d}$.
4. Scenario 4: No cooperation between the BS and RS is allowed to exchange the precoder information. The BS-MS communication is treated as the primary transmission. $\mathrm{I_b} = \infty$.

Fig.4.6 shows the ABER versus $\mathrm{I_d/P_D}$ when the $\mathrm{P_D}/\sigma^2 = 20$ dB, and $\mathrm{P_B}/\sigma^2 = 25$ dB. Here, the MS, D_1, and D_2 are fixed at $(0.8, 0)$, $(-0.4, -2)$, and $(0.4, -2)$, respectively. The error performances of D2D communication and BS-MS communication are plotted separately for Scenario 1 and 2. The average error performance is illustrated considering all scenarios. When $\mathrm{I_d/P_D}$ is low, the BS-MS performance in Scenario 1 is poorer compared to Scenario 2. However, the D2D error shows an opposite outcome. More importantly, Scenario 1 provides a better average error performance of the system. This is intuitively clear, since the transmit powers of D2D pair in Scenario 2 are always limited due to $\mathrm{I_d}$ constraint while the transmit powers of BS-MS pair are not limited. This creates higher interference on the D2D communication, thus, performance degrades. The average errors of non-cooperative Scenario 3 and 4 give lower performances than the rest. In the high $\mathrm{I_d/P_D}$ region, the error performance reaches a floor as $\mathrm{P_D}/\sigma^2$ is limited.

In Fig.4.7, the ABER versus $\mathrm{P_D}/\sigma^2$ is considered when the $\mathrm{I_d/P_D}$ is fixed at -10 dB. Both D2D and BS-MS communications have good error performance

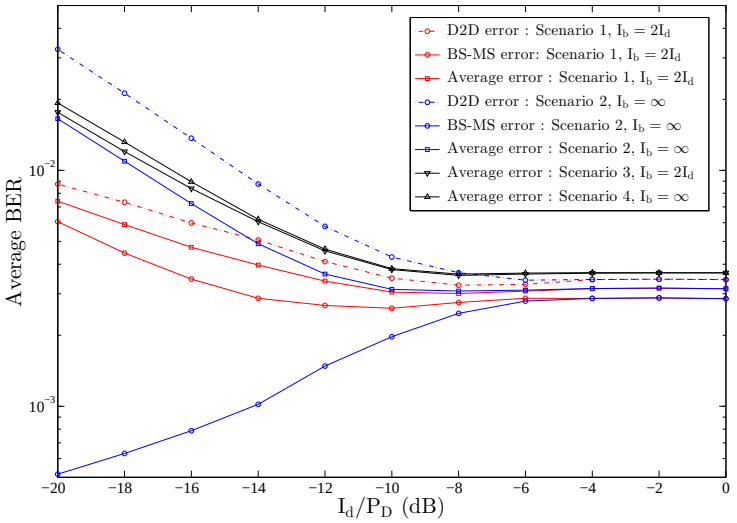

Fig 4.6. Average BER vs I_d/P_D for PNC based MIMO D2D communication. MS $= (0.8, 0)$, $D_1 = (-0.4, -2)$, and $D_2 = (0.4, -2)$. $P_D/\sigma^2 = 20$ dB, $P_B/\sigma^2 = 25$ dB, [113] © 2014, IEEE.

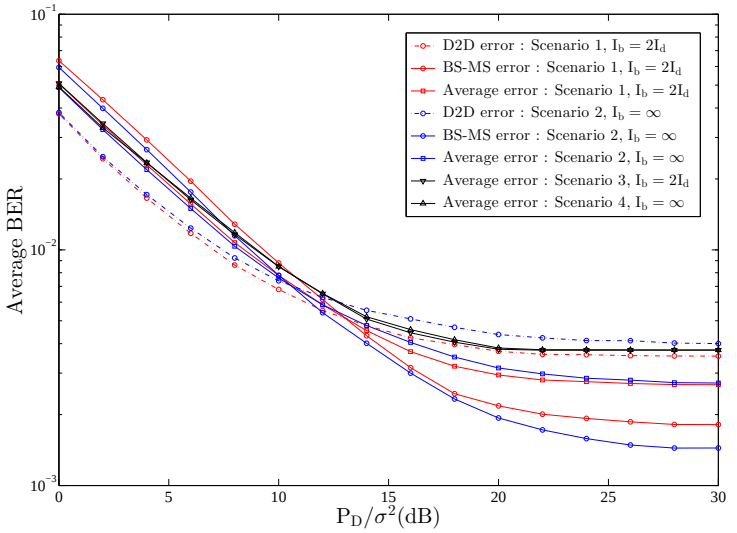

Fig 4.7. Average BER vs P_D/σ^2 for PNC based MIMO D2D communication. MS $= (0.8, 0)$, $D_1 = (-0.4, -2)$, and $D_2 = (0.4, -2)$. $I_d/P_D = -10$ dB, $P_B = 2P_D$, [113] © 2014, IEEE.

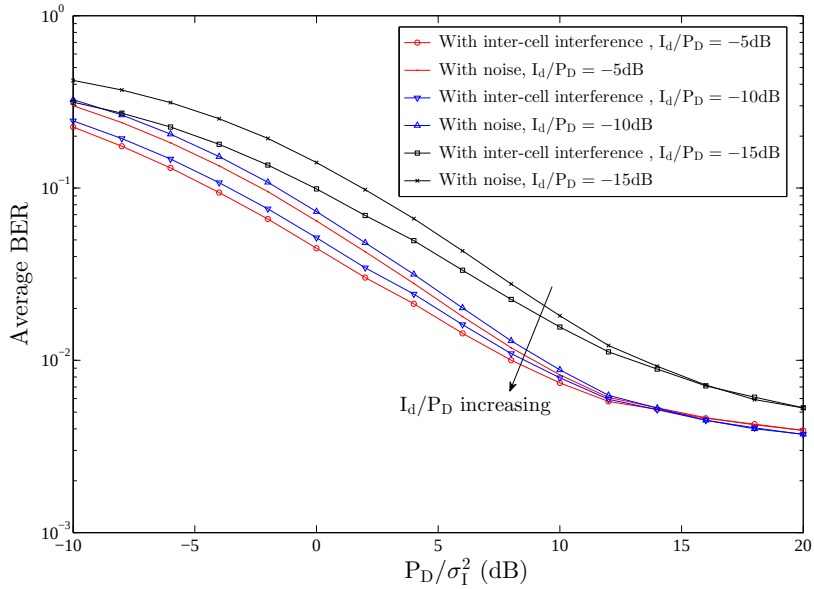

Fig 4.8. Average BER vs P_D/σ_I^2 for PNC based MIMO D2D communication under inter-cell interference. MS $= (0.8, 0)$, $D_1 = (-0.4, -2)$, and $D_2 = (0.4, -2)$. $P_D/\sigma^2 = 25$ dB, $P_B/\sigma^2 = 28$ dB, $I_d/P_D = -10$ dB, and $I_d = 2I_b$, [113] © 2014, IEEE.

with high P_D/σ^2. A similar behavior can be observed as in Fig.4.6 for Scenarios 1−4. For all the cases, the ABER is in the range of $(10^{-1}$– $10^{-3})$. This is due to the selection of the node locations, where normalized distance is relatively high for D2D communication. However, as in the Fig.4.5(a), the D2D communications at nearby distances provide better ABER than the selected node set-up in Fig.4.7. The selected node set-up helps us to compare different schemes with minimal round-off errors.

Next, the PNC based D2D communication system is investigated under inter-cell interference, where we consider interference coming from other cells. The interference is modeled as additive Gaussian interference vector $\mathbf{n}_I \in \mathbb{C}^N$ with zero-mean and covariance matrix $\mathcal{E}\{\mathbf{n}_I \mathbf{n}_I^H\} = \sigma_I^2 \mathbf{I}_N$. The proposed precoder-decoder schemes can be easily transformed to consider this extra interference. In Fig.4.8, the average error performance versus P_D/σ_I^2 is considered for three I_d/P_D levels (−15 dB, −10 dB and −5 dB). For a given I_d/P_D level, two scenarios are considered named as “with inter-cell interference" and “with noise". In the inter-cell interference scenario, we adopt interference in the precoder-decoder

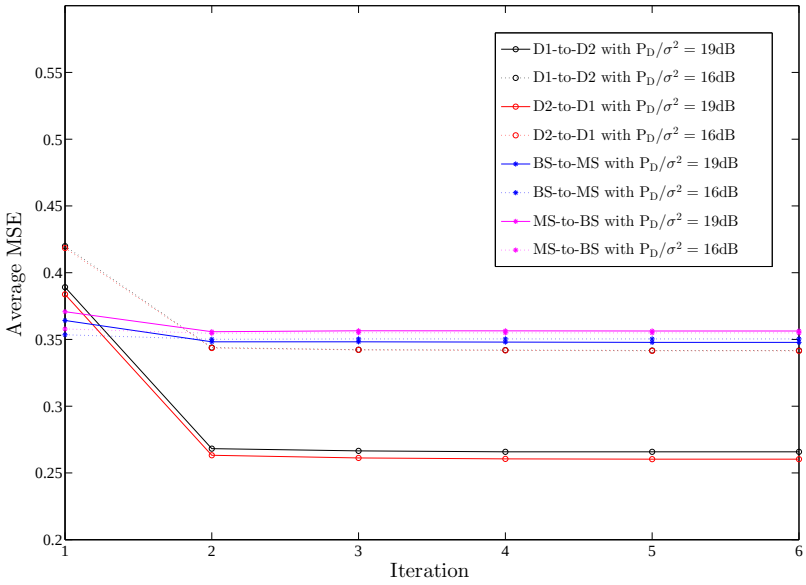

Fig 4.9. Convergence of direct D2D joint design (Algorithm 4.3). Average MSE versus number of iteration. MS $= (1, 0)$**,** $D_1 = (-0.5, -2)$**,** $\mathrm{P_B} = \mathrm{P_D}$**,** $\mathrm{I_d}/\sigma^2 = 7$ **dB and** $\mathrm{I_b} = \mathrm{I_d}$**, [113] © 2014, IEEE.**

designs, while in the other scenario the inter-cell interference is not taken into account. When inter-cell interference is higher, the performance difference between two scenarios is high. However, when the inter-cell interference is small, the two designs provide similar performances.

Next, we consider direct D2D communication. The Fig.4.9 shows the convergence of AMSE of each communication for Algorithm 4.3. Here also two cases are considered for $\mathrm{P_D}/\sigma^2 = 19$ dB and $\mathrm{P_D}/\sigma^2 = 16$ dB. We consider the MS and D_1 at $(1, 0)$ and $(-0.5, -2)$, $\mathrm{I_d}/\sigma^2 = 7$ dB, and $\mathrm{I_d} = \mathrm{I_b}$. The BS and RS exchange precoder details at each iteration ($K = 1$) and this improves the solution. It is evident that direct D2D requires a very small number of iterations to converge. This is due to the fact that at each iteration, the closed form expressions are used to find optimum precoder and decoder matrices.

The final solutions obtained via proposed algorithms can be used together to evaluate the best D2D mode for a given channel instance. In particular, when the total MSE (considering both D2D and BS-MS transmissions) of respective D2D modes is available at the D_1, the performance of D2D communication

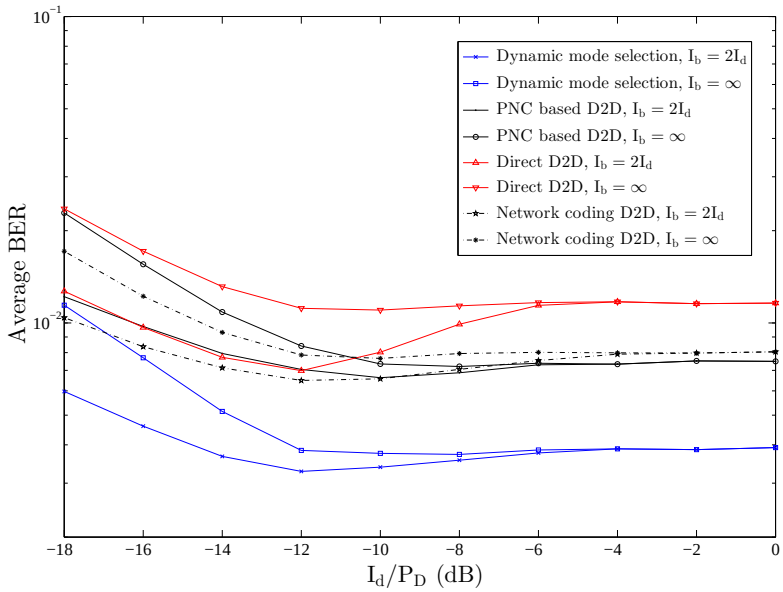

Fig 4.10. Average BER vs I_d/P_D for various D2D modes. MS $= (1, 0)$, $D_1 = (-0.5, -2)$, $D_2 = (0.5, -2)$, $P_B/\sigma^2 = 25$ dB, and $P_D/\sigma^2 = 20$ dB, [113] © 2014, IEEE.

can further improve. In such a situation, both D2D modes are available for selection. This can be referred to as the **dynamic mode** selection scheme, where D2D pair selects the transmitting mode which gives the minimum total MSE. Fig.4.10 shows the ABER versus I_d/P_D to illustrate the advantages of dynamic mode selection. In addition to the basic simulation parameters listed in Table I, we use MS $= (1, 0)$, $D_1 = (-0.5, -2)$, $D_2 = (0.5, -2)$, $P_B/\sigma^2 = 25$ dB, and $P_D/\sigma^2 = 20$ dB. A traditional network coding (TNC) based D2D communication is also considered in the analysis. This requires three time slots for bi-directional D2D communication. The proposed joint-precoder decoder schemes can be easily modified to obtain precoder-decoder scheme for this mode. The disadvantage is that TNC is not as spectrally efficient as PNC. Two separate cases are considered for interference threshold limits at the BS-MS communication as in the Fig.4.6 and 4.7. For this node configuration, the direct D2D communication has a worse ABER than the other modes. The PNC based D2D mode performs better than TNC based D2D at high I_d/P_D region. Also, consideration of I_b at the BS-MS pair improves the ABER for all scenarios. The dynamic mode selection provides

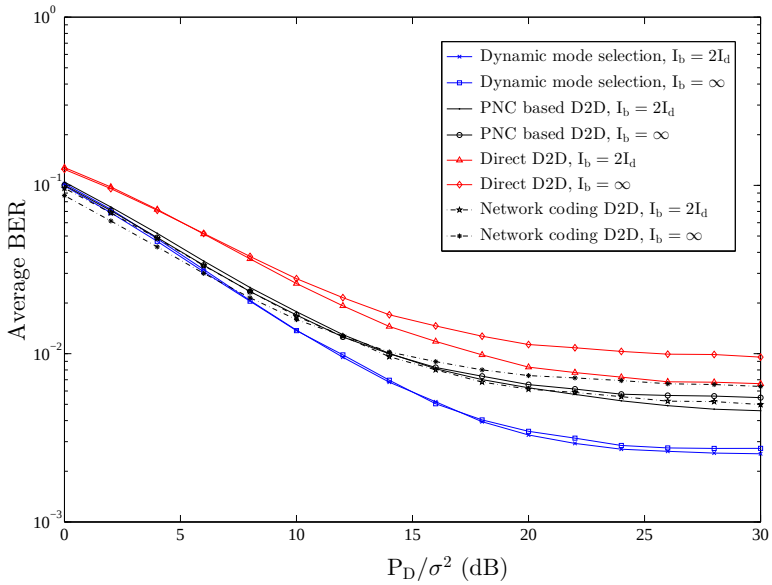

Fig 4.11. Average BER vs P_D/σ^2 for various D2D modes. MS $= (1, 0)$, $D_1 = (-0.5, -2)$, $D_2 = (0.5, -2)$, $P_B/P_D = 5$ dB, and $I_d/P_D = -10$ dB, [113] © 2014, IEEE.

better ABER than all other modes.

In Fig.4.11, the dynamic mode selection scheme is analyzed with P_D/σ^2 when $I_b/\sigma^2 = 10$ dB, $P_B/P_D = 5$ dB. Here, the ABER of all modes improve with P_D/σ^2, and the dynamic mode selection with $I_b = 2I_d$ gives better performance. Additionally, the PNC based D2D mode performs better than the rest for this node set-up.

Finally, we focus on the long-term average based mode selection (**static mode selection**) for D2D communication. Fig.4.12 shows the selected transmit mode of the D2D pair in a color map. This helps to understand the coverage enhancement resulted from the PNC based D2D mode. In particular, the D2D mode is selected depending on the long-term total AMSE. In Fig.4.12(a), we change the location of the D_2 while other nodes are fixed, where MS $= (1, 0)$, $D_1 = (-0.5, -2)$. Moreover, the location of the RS is changed in Fig.4.12(b) while D_2 is fixed at $(0.5, -2)$. Similar simulation parameters are used as in the earlier examples with $P_D/\sigma^2 = 20$ dB, $P_B = P_D$, $I_d/\sigma^2 = 7$ dB, and $I_b = I_b$. Only the nearby locations (with ABER < 0.01) are plotted in the XY grid. From

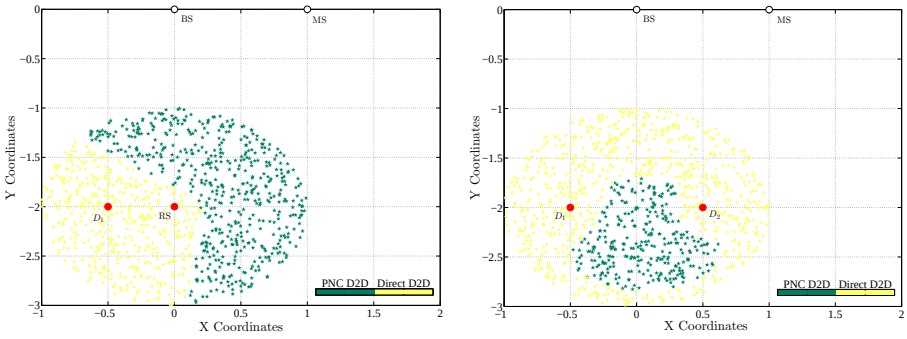

(a) (b)

Fig 4.12. Transmit modes for D2D pair with the location of D2 and RS. (a) Selection with the location of D_2 ; (b). Selection with the location of RS. MS $= (1, 0)$, $D_1 = (-0.5, -2)$, $\mathrm{P_D}/\sigma^2 = 20$ dB, $\mathrm{P_B} = \mathrm{P_D}$, $\mathrm{I_d}/\sigma^2 = 7$ dB, and $\mathrm{I_b} = \mathrm{I_b}$, [113] © 2014, IEEE.

Fig.4.12(a), it is evident that the both PNC based D2D and direct D2D modes are useful, and can be used to extend the D2D coverage area. According to Fig.4.12(b), when the RS near to the BS or MS, the direct D2D mode becomes the preferred method.

4.5 Summary and discussion

In this chapter, we considered joint precoder-decoder schemes for MIMO underlay D2D communication. Two transmit modes for D2D communications were considered as PNC based D2D, and direct D2D. Both D2D and BS-MS communications used the same spectrum band. Joint designs were employed to mitigate interference, improve the performance and simplify the PNC mapping. Minimizing MSE of received and desired signals in each communication link was used as the objective to design precoder-decoder matrices, and designs were considered separately for bi-directional communication. Additionally, the interference threshold and maximum transmit power limits were imposed in the problem formulations. For PNC based D2D communication mode, we proposed distributed and centralized approaches to find precoder and decoder matrices. In the distributed method, greedy optimization was used, and practical distributed framework was proposed to solve the optimization problems. A centralized approach was also addressed to obtain optimal precoder-decoder matrices. The

scalarization method was applied to find Pareto optimal points as the problem became a multicriterion optimization problem. Moreover, in the case of direct D2D communication mode, we obtained closed form solutions for distributed optimization problems, and proposed an algorithm based on those.

Analysis suggested that the algorithms converged fast enough to be used in wireless systems. They also provided near Pareto optimal solutions. The effects of interference threshold and maximum power were also investigated. In PNC based D2D mode, consideration of interference threshold limit at the BS-MS communication improved the D2D performance. However, D2D performance degraded when BS-MS communication was considered as the primary transmission, i.e., interference threshold limit was not included in problem P_1. Moreover, the analysis was easily reformulated to consider inter-cell interference. The direct D2D mode and TNC based D2D were also compared to the PNC based D2D. There, a dynamic mode selection scheme was proposed, and it performed better than other modes. More importantly, long-term average based analysis implied that the PNC based D2D helped to improve the coverage of the D2D communication.

5 Secure beamforming design for PNC based MIMO TWR

In this chapter, we study secure beamforming designs to prevent eavesdropping on the PNC based MIMO TWR communication. Multiple eavesdroppers are attempting to intercept the user information. Since PNC based TWR system performs XOR operation on the user information, a given eavesdropper must successfully decode at least one user message during the MA stage in order to decode the other message. Therefore, PNC based TWR have an added security feature which is not available with any other TWR scheme. As discussed in the earlier chapters, the accurate PNC operation requires minimizing MSE at the relay. The secrecy of the TWR is enhanced by employing beamforming at the nodes, which generate weak signals at eavesdroppers. Therefore, we consider optimization problems to minimize MSE, and adopt SNR threshold policy to prevent possible eavesdropping. However, the CSI of user-eavesdropper channels are imperfect at the user side. First, we use ellipsoidal channel uncertainty model, and a robust optimization problem is formulated and solved with an iterative method. Numerical results are carried out to investigate the convergence of the proposed algorithm and SINR distribution at a given eavesdropper. Next, the Gaussian Markov uncertainty (GMU) model is assumed for user-eavesdropper and relay-eavesdropper channels. Robust optimization problems are formulated and solved for both MA and BC stages. Algorithms are proposed at each stage to analyze the performance of the TWR system and the SINR distribution at a given eavesdropper.

5.1 System model

We consider two user nodes communicate in an unsecured environment using a trusted relay node as shown in the Fig.5.1. Multiple eavesdroppers attempt to intercept the information of the users. Bi-directional communication of the users are assumed with TDD and the relay performs PNC mapping. N_i, N_r and N_k are the number of antennas at the ith user (denoted U_i with $i = 1, 2$), relay and kth eavesdropper (denoted E_k with $k = 1, 2.., K$), respectively. We consider

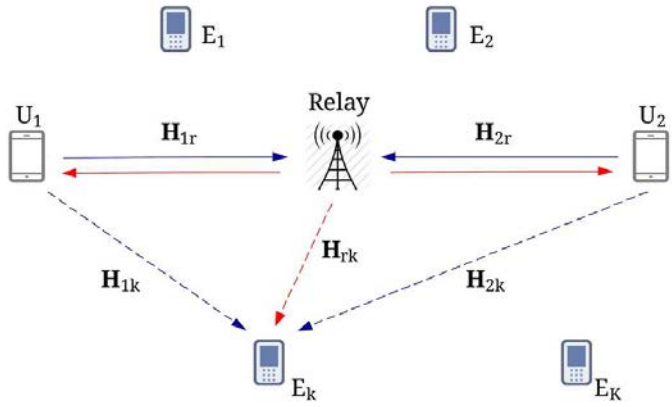

Fig 5.1. A relay assisted TWR communication in unsecured environment. Multiple eavesdroppers $(E_k \in \{1, .., K\})$ **attempt to decode communication.**

channels to be frequency-flat and quasi-static. Single stream transmissions are assumed with perfect synchronization at the relay node.

5.1.1 Multiple access stage

During the first time slot, both devices transmit their modulated information $s_i \in \mathbb{C}$ beamformed by $\mathbf{w}_i \in \mathbb{C}^{N_i \times 1}$ $(i = 1, 2)$. The relay node estimates the sum of two transmitted symbols after going through a receive beamforming vector $\mathbf{w}_r \in \mathbb{C}^{N_r \times 1}$. The post-processed signal at the relay node is given by,

$$y_r = \mathbf{w}_r^H \mathbf{H}_{1r} \mathbf{w}_1 s_1 + \mathbf{w}_r^H \mathbf{H}_{2r} \mathbf{w}_2 s_2 + \mathbf{w}_r^H \mathbf{n}_r, \tag{5.1}$$

where $\mathbf{H}_{ir} \in \mathbb{C}^{N_r \times N_i}$ $(i = 1, 2)$ is the channel between the U_i and relay with entries are assumed to be $\sim \mathcal{CN}(0, \sigma^2)$, $\mathbf{n}_r$ is an additive Gaussian noise vector at the relay with zero-mean and covariance matrix $\mathcal{E}\{\mathbf{n}_r \mathbf{n}_r^H\} = \sigma_r^2 \mathbf{I}_{N_r}$. The kth eavesdropper E_k uses receive beamforming vector $\mathbf{w}_{ek} \in \mathbb{C}^{N_k \times 1}$ during the first time slot. Therefore, the post-processed signal at the E_k is

$$y_{ek} = \mathbf{w}_{ek}^H \mathbf{H}_{1k} \mathbf{w}_1 s_1 + \mathbf{w}_{ek}^H \mathbf{H}_{2k} \mathbf{w}_2 s_2 + \mathbf{w}_{ek}^H \mathbf{n}_{ek}, \ k \in \{1, ., K\}, \tag{5.2}$$

where $\mathbf{H}_{ik} \in \mathbb{C}^{N_k \times N_i}$ is the channel between the U_i and E_k with entries assumed to be $\sim \mathcal{CN}(0, \sigma^2)$, and $\mathbf{n}_{ek}$ is an additive Gaussian noise vector at the E_k with

zero-mean and covariance matrix $\mathcal{E}\{\mathbf{n}_{ek}\mathbf{n}_{ek}^H\} = \sigma_{ek}^2\mathbf{I}_{N_k}$. We assume that the E_k does not have the knowledge about beamforming vectors of the TWR system, and hence blindly combines the received signal vector to decode each symbol separately. Therefore, the receiver beamforming vector at the E_k is assumed as $\mathbf{w}_{ek} = \frac{1}{\sqrt{N_k}}\mathbf{1}$. We also assume the user pair do not have the perfect CSI about the $\mathbf{H}_{1k}$ and $\mathbf{H}_{2k}$ $(\forall k)$.

5.1.2 Physical layer network coding

The post-processed signal y_r can be used to obtain the estimate corresponding to $s_1 + s_2$. As used in the previous chapters, two categories of PNC mapping are possible at the relay node. In this chapter we adopt the first method, where the estimation is mapped to XOR of two transmitted unmodulated information [62]. Then, the modulated version of the XOR (denoted by $s_r \in \mathbb{C}$) is broadcast during the second time slot. Each user estimates the s_r, and uses that to find the desired symbol which is transmitted by other user.

5.1.3 Broadcasting stage

During the second time slot, the relay broadcasts s_r beamformed by $\mathbf{v}_r \in \mathbb{C}^{N_r \times 1}$. The U_i estimates s_r after going through a receive beamforming vector $\mathbf{v}_i \in \mathbb{C}^{N_i \times 1}$ $(i = 1, 2)$. The post-processed signal at the U_i is given by,

$$y_i = \mathbf{v}_i^H \mathbf{H}_{ir}^T \mathbf{v}_r s_r + \mathbf{v}_i^H \mathbf{n}_i \quad i = 1, 2, \tag{5.3}$$

where $\mathbf{n}_i$ is an additive Gaussian noise vector at the U_i with zero-mean and covariance matrix $\mathcal{E}\{\mathbf{n}_i\mathbf{n}_i^H\} = \sigma_i^2\mathbf{I}_{N_i}$. The post-processed signal at the E_k is

$$\hat{y}_{ek} = \mathbf{w}_{ek}^H \mathbf{H}_{rk} \mathbf{v}_r s_r + \mathbf{w}_{ek}^H \mathbf{n}_{ek}, \quad k \in \{1, .., K\} \tag{5.4}$$

where $\mathbf{H}_{rk} \in \mathbb{C}^{N_k \times N_r}$ is the channel between the relay and the E_k with entries assumed to be $\sim \mathcal{CN}(0, \sigma^2)$. The CSI of the $\mathbf{H}_{rk}$ is imperfect at the relay node.

5.2 Problem formulation

The beamforming vectors are designed to provide secrecy of the TWR communication. The physical layer security during the MA stage is more important to

prevent eavesdropping, because at least one message from s_1 or s_2 is required to decode the s_r. However, the secrecy can be further improved by the beamforming design in the BC stage. Therefore, we consider both MA and BC stages in the beamforming design.

Problem formulation for MA stage

The proposed secure beamforming design is based on minimizing MSE at the relay. This is necessary to facilitate an accurate PNC operation at the relay node. The error at the relay is $e_r = y_r - (s_1 + s_2)$, and the MSE at the relay is $\mathrm{MSE}_r = \mathcal{E}_{s,\mathbf{n}}\{\|e_r\|^2\}$. This can be further expanded into

$$\mathrm{MSE}_r = \sum_{i=1}^{2}\big(\mathbf{w}_r^H\mathbf{H}_{ir}\mathbf{w}_i\mathbf{w}_i^H\mathbf{H}_{ir}^H\mathbf{w}_r - 2\Re(\mathbf{w}_r^H\mathbf{H}_{ir}\mathbf{w}_i)\big) + 2 + \sigma_r^2\mathbf{w}_r^H\mathbf{w}_r. \quad (5.5)$$

We assume statistical properties $\mathcal{E}_{s,\mathbf{n}}\{s_i s_i^*\} = 1$, $\mathcal{E}_{s,\mathbf{n}}\{s_1 s_2^*\} = 0$, $\mathcal{E}_{s,\mathbf{n}}\{s_i\mathbf{n}_r^H\} = \mathbf{0}$, and $\mathcal{E}_{s,\mathbf{n}}\{\mathbf{n}_r\mathbf{n}_r^H\} = \sigma_r^2\mathbf{I}_{N_r}$ with $i = 1, 2$ to obtain (5.5).

The transmit powers at the users are limited to $\mathrm{P}_{\max}$. The physical layer security of TWR is provided by limiting the received SNR at all eavesdroppers. An eavesdropper intends to decode one symbol during first time slot, and use that to decode the other symbol during the next time slot. In such cases, one symbol acts as an interference to the other one. Therefore, the received SINR of s_i $(i = 1, 2)$ at the E_k $(k \in \{1, .., K\})$ is given by,

$$\mathrm{SINR}_k^i = \frac{\mathbf{h}_{ik}^H\mathbf{w}_i\mathbf{w}_i^H\mathbf{h}_{ik}}{\mathbf{h}_{jk}^H\mathbf{w}_j\mathbf{w}_j^H\mathbf{h}_{jk} + \sigma_{ek}^2} \quad (i,j) \ \in \ \{i \neq j|1,2\}, \quad (5.6)$$

where $\mathbf{h}_{ik}^H = \frac{1}{\sqrt{N_k}}\mathbf{1}^T\mathbf{H}_{ik}$. Both SINR values at the E_k should be less than a certain threshold γ_k to prevent the eavesdropping. Considering all these, the following optimization problem is formulated to find transmit and receive beamforming vectors:

$$\begin{aligned} \min_{\mathbf{w}_1,\mathbf{w}_2,\mathbf{w}_r} \quad & \mathrm{MSE}_r & & \\ \text{subject to} \quad & \mathbf{w}_i^H\mathbf{w}_i \leq \mathrm{P}_{\max} & \forall\ i & \quad (5.7) \\ & \mathrm{SINR}_k^i \leq \gamma_k & \forall\ i\ \&\ \forall\ k. & \end{aligned}$$

Problem formulation for BC stage

During the BC stage, the security of the TWR can be further improved by employing beamforming vectors at the nodes. A similar method as in the MA stage is used to find the optimal beamforming vectors. Both users estimate s_r, and the MSE at the U_i (denoted by MSE_i) can be obtained as

$$\mathrm{MSE}_i = \rho \mathbf{v}_i^H \mathbf{H}_{ir}^T \mathbf{v}_r \mathbf{v}_r^H \mathbf{H}_{ir}^* \mathbf{v}_i - 2\rho \Re(\mathbf{v}_i^H \mathbf{H}_{ir}^T \mathbf{v}_r) + \sigma_i^2 \mathbf{v}_i^H \mathbf{v}_i + \rho \quad i = 1, 2, \quad (5.8)$$

where, $\mathcal{E}\{s_r s_r^*\} = \rho$, and ρ represent the average normalized power of symbol s_r. Both MSE_1 and MSE_2 are considered together by taking the sum-MSE as the objective function. The received SNR of s_r at the E_k is $\mathrm{SNR}_k = \rho \mathbf{h}_{rk}^H \mathbf{v}_r \mathbf{v}_r^H \mathbf{h}_{rk} / \sigma_{ek}^2$, where $\mathbf{h}_{rk}^H = \frac{1}{\sqrt{N_k}} \mathbf{1}^T \mathbf{H}_{rk}$. The received SNR should be less than a certain threshold $\hat{\gamma}_k$ to prevent intercepting s_r at the E_k. Then, the optimal transmit and receive beamforming vectors can be obtained solving the following optimization problem:

$$\begin{aligned} \min_{\mathbf{v}_r, \mathbf{v}_1, \mathbf{v}_2} \quad & 0.5\mathrm{MSE}_1 + 0.5\mathrm{MSE}_2 \\ \text{subject to} \quad & \mathbf{v}_r^H \mathbf{v}_r \leq \mathrm{P}_{\max}/\rho \\ & \mathrm{SNR}_k \leq \hat{\gamma}_k \quad \forall k. \end{aligned} \quad (5.9)$$

5.3 Robust beamforming under ellipsoidal uncertainty model

Here, we consider CSI of $\mathbf{H}_{ik}$ $(\forall k)$ is imperfect at the users, i.e., $\mathbf{H}_{ik} = \bar{\mathbf{H}}_{ik} + \mathbf{E}_{ik}$ $(i = 1, 2)$, where $\bar{\mathbf{H}}_{ik}$ is the estimated channel coefficients at the ith user, $\mathbf{E}_{ik}$ represents the channel uncertainty part. We rewrite this considering post-processing at the kth eavesdropper as $\mathbf{h}_{ik} = \bar{\mathbf{h}}_{ik} + \mathbf{e}_{ik}$, where $\bar{\mathbf{h}}_{ik}$ and $\mathbf{e}_{ik}$ are estimated component and error component, respectively. An ellipsoidal bound for the error component $\mathbf{e}_{ik}$ is assumed, which is given by $\|\mathbf{e}_{ik}\|_2 \leq \varepsilon_{ik}$ $(\forall i \ \& \ \forall k)$.

5.3.1 Beamforming for MA stage

Here, the optimization problem (5.7) is considered with channel uncertainty model. Now, the modified optimization problem can be obtained as in (5.10)-(5.12).

$$\min_{\mathbf{w}_1,\mathbf{w}_2,\mathbf{w}_r} \quad \sum_{i=1}^{2}\left(\mathbf{w}_r^H\mathbf{H}_{ir}\mathbf{w}_i\mathbf{w}_i^H\mathbf{H}_{ir}^H\mathbf{w}_r - 2\Re(\mathbf{w}_r^H\mathbf{H}_{ir}\mathbf{w}_i)\right) + \sigma_r^2\mathbf{w}_r^H\mathbf{w}_r + 2 \tag{5.10}$$

$$\text{sub. to} \quad \mathbf{w}_i^H\mathbf{w}_i \leq \mathrm{P}_{\max} \qquad i = 1,2 \tag{5.11}$$

$$\begin{aligned}&\mathbf{e}_{ik}^H\mathbf{w}_i\mathbf{w}_i^H\mathbf{e}_{ik} + 2\Re(\bar{\mathbf{h}}_{ik}^H\mathbf{w}_i\mathbf{w}_i^H\mathbf{e}_{ik}) + \bar{\mathbf{h}}_{ik}^H\mathbf{w}_i\mathbf{w}_i^H\bar{\mathbf{h}}_{ik} - \gamma_k\mathbf{e}_{jk}^H\mathbf{w}_j\mathbf{w}_j^H\mathbf{e}_{jk}\\ &- 2\gamma_k\Re(\bar{\mathbf{h}}_{jk}^H\mathbf{w}_j\mathbf{w}_j^H\mathbf{e}_{jk}) - \gamma_k\bar{\mathbf{h}}_{jk}^H\mathbf{w}_j\mathbf{w}_j^H\bar{\mathbf{h}}_{jk} - \gamma_k\sigma_{ek}^2 \leq 0,\ \mathbf{e}_{ik}^H\mathbf{e}_{ik} \leq \varepsilon_{ik}^2\\ &\&\ \mathbf{e}_{jk}^H\mathbf{e}_{jk} \leq \varepsilon_{jk}^2,\ \ (i,j)\ \in\ \{i \neq j|1,2\}\ \&\ \forall k.\end{aligned} \tag{5.12}$$

The problem is non-convex, and we solve it by dividing into following sub-problems:

Sub-problem I

Here, the transmit beamforming vectors $\mathbf{w}_1$ and $\mathbf{w}_2$ are considered fixed. The receiver beamforming vector $\mathbf{w}_r$ is only associated with the objective function. Therefore, taking the derivative with respect to $\mathbf{w}_r$ and equalling that to zero gives the optimal solution,

$$\mathbf{w}_r = \Big(\sum_{i=1}^{2}(\mathbf{H}_{ir}\mathbf{w}_i\mathbf{w}_i^H\mathbf{H}_{ir}^H) + \sigma_r^2\mathbf{I}_N\Big)^{-1}\Big(\sum_{i=1}^{2}\mathbf{H}_{ir}\mathbf{w}_i\Big). \tag{5.13}$$

When $\mathbf{w}_r$ is fixed, the problem still a non-convex problem. Some modifications in the SINR constraints are required to solve the problem for $\mathbf{w}_1$ and $\mathbf{w}_2$. Here, we reformulate the constraints (5.12) as

$$\mathbf{e}_k^H\mathbf{B}_{ik}\mathbf{e}_k + 2\Re(\mathbf{d}_{ik}^H\mathbf{e}_k) + c_{ik} \leq 0 \ \text{ with } \ \mathbf{e}_k^H\mathbf{e}_k \leq \varepsilon_k^2, \qquad i \in \{1,2\}\ \&\ k \in \{1,..,K\}, \tag{5.14}$$

where $\mathbf{e}_k = [\mathbf{e}_{1k};\mathbf{e}_{2k}] \in \mathbb{C}^{N_1+N_2}$,

$$\mathbf{B}_{1k} = \begin{bmatrix} \mathbf{w}_1\mathbf{w}_1^H & \mathbf{0}_{N_1\times N_2} \\ \mathbf{0}_{N_2\times N_1} & -\gamma_k\mathbf{w}_2\mathbf{w}_2^H \end{bmatrix}, \tag{5.15}$$

$$\mathbf{B}_{2k} = \begin{bmatrix} -\gamma_k\mathbf{w}_1\mathbf{w}_1^H & \mathbf{0}_{N_1\times N_2} \\ \mathbf{0}_{N_2\times N_1} & \mathbf{w}_2\mathbf{w}_2^H \end{bmatrix}, \tag{5.16}$$

$\mathbf{d}_{1k} = [\mathbf{w}_1\mathbf{w}_1^H\bar{\mathbf{h}}_{1k}; -\gamma_k\mathbf{w}_2\mathbf{w}_2^H\bar{\mathbf{h}}_{2k}]$, $\mathbf{d}_{2k} = [-\gamma_k\mathbf{w}_1\mathbf{w}_1^H\bar{\mathbf{h}}_{1k}; \mathbf{w}_2\mathbf{w}_2^H\bar{\mathbf{h}}_{2k}]$, and $c_{ik} = \bar{\mathbf{h}}_{ik}^H\mathbf{w}_i\mathbf{w}_i^H\bar{\mathbf{h}}_{ik} - \gamma_k\bar{\mathbf{h}}_{jk}^H\mathbf{w}_j\mathbf{w}_j^H\bar{\mathbf{h}}_{jk} - \sigma_{ek}^2\gamma_k$ for $(i,j)\ \in\ \{i \neq j|1,2\}$. More importantly, we introduce a new error bound $\mathbf{e}_k$ to satisfy both error bounds $\mathbf{e}_{1k}$ and

$\mathbf{e}_{2k}$ $(\forall k)$. ε_k^2 is selected to satisfy $\varepsilon_{1k}^2 + \varepsilon_{2k}^2 \leq \varepsilon_k^2$. The modified constraint in (5.14) can be reformulated into a linear matrix inequality (LMI) using the S-procedure as in [142, p.655, Ap. B.2], i.e.,

$$\begin{bmatrix} \theta_{ik}\mathbf{I}_{N_i} - \mathbf{B}_{ik} & -\mathbf{d}_{ik} \\ -\mathbf{d}_{ik}^H & -c_{ik} - \theta_{ik}\varepsilon_k^2 \end{bmatrix} \succeq 0, \qquad i \in \{1,2\} \;\&\; k \in \{1,..,K\}, \quad (5.17)$$

where $\theta_{ik} \geq 0$. This is useful to formulate other sub-problems and continue to solve the problem.

Sub-problem II

Here, we fix both $\mathbf{w}_2$ and $\mathbf{w}_r$ and solve for the $\mathbf{w}_1$. The problem is a quadratic optimization problem. The semidefinite program (SDP) relaxation [142, p.654, Ap. B.1] can be obtained as in (5.18)-(5.22), where $\mathbf{A}_i = \mathbf{H}_{ir}^H \mathbf{w}_r \mathbf{w}_r^H \mathbf{H}_{ir}$, $\mathbf{b}_i = \mathbf{w}_r \mathbf{H}_{ir}^H$ $(i = 1, 2)$. Now, the problem is convex, and we solve this with SDP solver.

$$\min_{\mathbf{W}_1, \mathbf{w}_1, \theta_{ik} \geq 0} \quad \mathrm{Tr}(\mathbf{A}_1\mathbf{W}_1) - 2\Re(\mathbf{b}_1^H\mathbf{w}_1) + \mathbf{w}_2^H\mathbf{A}_2\mathbf{w}_2 - 2\Re(\mathbf{b}_2^H\mathbf{w}_2) + \sigma_r^2\mathbf{w}_r^H\mathbf{w}_r + 2 \quad (5.18)$$

subject to,

$$\mathrm{Tr}(\mathbf{W}_1) - \mathrm{P}_{\max} \leq 0, \quad (5.19)$$

$$\begin{bmatrix} \mathbf{W}_1 & \mathbf{w}_1 \\ \mathbf{w}_1^H & 1 \end{bmatrix} \succeq 0, \quad (5.20)$$

$$\begin{bmatrix} \theta_{1k}\mathbf{I}_{N_1} - \mathbf{W}_1 & \mathbf{0}_{N_1\times N_2} & -\mathbf{W}_1\bar{\mathbf{h}}_{1k} \\ \mathbf{0}_{N_2\times N_1} & \theta_{1k}\mathbf{I}_{N_2} + \gamma_k\mathbf{w}_2\mathbf{w}_2^H & \gamma_k\mathbf{w}_2\mathbf{w}_2^H\bar{\mathbf{h}}_{2k} \\ -\bar{\mathbf{h}}_{1k}^H\mathbf{W}_1 & \gamma_k\bar{\mathbf{h}}_{2k}^H\mathbf{w}_2\mathbf{w}_2^H & \big(-\theta_{1k}\varepsilon_k^2 - \bar{\mathbf{h}}_{1k}^H\mathbf{W}_1\bar{\mathbf{h}}_{1k} \\ & & +\gamma_k\bar{\mathbf{h}}_{2k}^H\mathbf{w}_2\mathbf{w}_2^H\bar{\mathbf{h}}_{2k} + \sigma_{ek}^2\gamma_k\big) \end{bmatrix} \succeq 0 \quad \text{for} \;\; k \in \{1,..,K\}, \quad (5.21)$$

$$\begin{bmatrix} \theta_{2k}\mathbf{I}_{N_1} + \gamma_k\mathbf{W}_1 & \mathbf{0}_{N_1\times N_2} & \gamma_k\mathbf{W}_1\bar{\mathbf{h}}_{1k} \\ \mathbf{0}_{N_2\times N_1} & \theta_{2k}\mathbf{I}_{N_1} - \mathbf{w}_2\mathbf{w}_2^H & -\mathbf{w}_2\mathbf{w}_2^H\bar{\mathbf{h}}_{2k} \\ \gamma_k\bar{\mathbf{h}}_{1k}^H\mathbf{W}_1 & -\bar{\mathbf{h}}_{2k}^H\mathbf{w}_2\mathbf{w}_2^H & \big(-\theta_{2k}\varepsilon_k^2 + \gamma_k\bar{\mathbf{h}}_{1k}^H\mathbf{W}_1\bar{\mathbf{h}}_{1k} \\ & & -\bar{\mathbf{h}}_{2k}^H\mathbf{w}_2\mathbf{w}_2^H\bar{\mathbf{h}}_{2k} + \sigma_{ek}^2\gamma_k\big) \end{bmatrix} \succeq 0 \quad \text{for} \;\; k \in \{1,..,K\}, \quad (5.22)$$

In general, rank-one solution of $\mathbf{W}_1$ is required to find the optimal $\mathbf{w}_1$ of the original problem. In (5.18)-(5.22), we found that $\mathbf{W}_1 = \mathbf{w}_1\mathbf{w}_1^H$ is the optimal rank-one solution. This can happen in the case of variables are strictly feasible in the original problem [142, p.654, Ap. B.1].

Sub-problem III

We fix both $\mathbf{w}_1$ and $\mathbf{w}_r$, and solve for the $\mathbf{w}_2$. This is also a quadratic optimization problem. The SDP relaxation can be obtained similar to the sub-problem II. Replacing $\mathbf{W}_2$ with $\mathbf{w}_2\mathbf{w}_2^H$ and grouping coefficients accordingly provides the optimization problem as (5.23)-(5.27).

$$\min_{\mathbf{W}_2,\mathbf{w}_2,\vartheta_{ik}\geq 0} \quad \mathrm{Tr}(\mathbf{A}_2\mathbf{W}_2) - 2\Re(\mathbf{b}_2^H\mathbf{w}_2) + \mathbf{w}_1^H\mathbf{A}_1\mathbf{w}_1 - 2\Re(\mathbf{b}_1^H\mathbf{w}_1) + \sigma_r^2\mathbf{w}_r^H\mathbf{w}_r + 2 \tag{5.23}$$

subject to,

$$\mathrm{Tr}(\mathbf{W}_2) - \mathrm{P}_{\max} \leq 0, \tag{5.24}$$

$$\begin{bmatrix} \mathbf{W}_2 & \mathbf{w}_2 \\ \mathbf{w}_2^H & 1 \end{bmatrix} \succeq 0, \tag{5.25}$$

$$\begin{bmatrix} \vartheta_{1k}\mathbf{I}_{N_1} - \mathbf{w}_1\mathbf{w}_1^H & \mathbf{0}_{N_1\times N_2} & -\mathbf{w}_1\mathbf{w}_1^H\bar{\mathbf{h}}_{1k} \\ \mathbf{0}_{N_2\times N_1} & \vartheta_{1k}\mathbf{I}_{N_2} + \gamma_k\mathbf{W}_2 & \gamma_k\mathbf{W}_2\bar{\mathbf{h}}_{2k} \\ -\bar{\mathbf{h}}_{1k}^H\mathbf{w}_1\mathbf{w}_1^H & \gamma_k\bar{\mathbf{h}}_{2k}^H\mathbf{W}_2 & \big(-\vartheta_{1k}\varepsilon_k^2 - \bar{\mathbf{h}}_{1k}^H\mathbf{w}_1\mathbf{w}_1^H\bar{\mathbf{h}}_{1k} \\ & & +\gamma_k\bar{\mathbf{h}}_{2k}^H\mathbf{W}_2\bar{\mathbf{h}}_{2k} + \sigma_{ek}^2\gamma_k\big) \end{bmatrix} \succeq 0 \quad \text{for} \quad k \in \{1,..,K\}, \tag{5.26}$$

$$\begin{bmatrix} \vartheta_{2k}\mathbf{I}_{N_1} + \gamma_k\mathbf{w}_1\mathbf{w}_1^H & \mathbf{0}_{N_1\times N_2} & \gamma_k\mathbf{w}_1\mathbf{w}_1^H\bar{\mathbf{h}}_{1k} \\ \mathbf{0}_{N_2\times N_1} & \vartheta_{2k}\mathbf{I}_{N_1} - \mathbf{W}_2 & -\mathbf{W}_2\bar{\mathbf{h}}_{2k} \\ \gamma_k\bar{\mathbf{h}}_{1k}^H\mathbf{w}_1\mathbf{w}_1^H & -\bar{\mathbf{h}}_{2k}^H\mathbf{W}_2 & \big(-\vartheta_{2k}\varepsilon_k^2 + \gamma_k\bar{\mathbf{h}}_{1k}^H\mathbf{w}_1\mathbf{w}_1^H\bar{\mathbf{h}}_{1k} \\ & & -\bar{\mathbf{h}}_{2k}^H\mathbf{W}_2\bar{\mathbf{h}}_{2k} + \sigma_{ek}^2\gamma_k\big) \end{bmatrix} \succeq 0 \quad \text{for} \quad k \in \{1,..,K\}, \tag{5.27}$$

Since the problem is convex, we use a SDP solver to find the solution. The optimum beamforming vector satisfies the $\mathbf{W}_2 = \mathbf{w}_2\mathbf{w}_2^H$ as in the sub-problem II. Finally, all sub-problems are iteratively solved till the final MSE value is converged. The final algorithm to obtain beamforming vectors is provided as

Algorithm 5.1. Modern wireless devices have higher processing powers, and hence the algorithm can be used at the user nodes. The $\mathbf{w}_r$ is sent to the relay node prior data transmission.

Algorithm 5.1 Secure robust beamforming design for ellipsoidal uncertainty model

Information about $K, \mathrm{P}_{\max}, \gamma_k, \sigma^2, \sigma_r^2, \sigma_{ek}^2, N_i, \varepsilon_k, \mathbf{H}_{ir}, \bar{\mathbf{h}}_{ik} (\forall i \ \& \ \forall k)$ is available.

1: **initialize** : Beamforming vectors $\mathbf{w}_i = \sqrt{\frac{\mathrm{P}_{\max}}{N_i}}\mathbf{1}$.
2: **repeat**
3: **for** $m = 1 : M$ **do**
4: Fix $\mathbf{w}_1$ and $\mathbf{w}_2$ obtained from step 6 (Or step 1 at $m = 1$). Find optimum $\mathbf{w}_r$ from (5.13).
5: Fix $\mathbf{w}_2$ and $\mathbf{w}_r$ obtained from step 4. Solve problem (5.18)-(5.22) to find optimum $\mathbf{w}_1$.
6: Fix $\mathbf{w}_1$ and $\mathbf{w}_r$ obtained from step 5. Solve problem (5.23)-(5.27) to find optimum $\mathbf{w}_2$.
7: **end for**
8: **until** MSE_r converge.

5.3.2 Perfect CSI on the user-to-eavesdropper channel

When $\varepsilon_k = 0$, the optimization problem (5.7) can be solved only with two sub-problems. The first sub-problem is similar to (5.13) and the second one gives as

$$\begin{aligned} \min_{\mathbf{W},\mathbf{w}} \quad & \mathrm{Tr}(\mathbf{A}\mathbf{W}) - 2\Re(\mathbf{b}^H\mathbf{w}) + \sigma_r^2\mathbf{w}_r^H\mathbf{w}_r + 2 \\ \text{sub. to} \quad & \mathrm{Tr}(\mathbf{P}_i\mathbf{W}) - \mathrm{P}_{\max} \le 0, \qquad i \in \{1,2\}, \\ & \begin{bmatrix} \mathbf{W} & \mathbf{w} \\ \mathbf{w}^H & 1 \end{bmatrix} \succeq 0 \\ & \mathrm{Tr}(\mathbf{Q}_{ik}\mathbf{W}) - \sigma_{ek}^2\gamma_k \le 0 \qquad i \in \{1,2\} \ \& \ k \in \{1,..,K\}, \end{aligned} \tag{5.28}$$

where $\mathbf{w} = [\mathbf{w}_1; \mathbf{w}_2] \in \mathbb{C}^{N_1+N_2}$, $\mathbf{A} = [\mathbf{A}_1 \quad \mathbf{0}_{N_1\times N_2}; \mathbf{0}_{N_2\times N_1} \quad \mathbf{A}_2]$, $\mathbf{b} = [\mathbf{b}_1; \mathbf{b}_2]$, $\mathbf{P}_1 = [\mathbf{I}_{N_1} \quad \mathbf{0}_{N_2\times N_1}; \mathbf{0}_{N_1\times N_2} \quad \mathbf{0}_{N_2\times N_2}]$, $\mathbf{P}_2 = [\mathbf{0}_{N_1\times N_1} \quad \mathbf{0}_{N_2\times N_1}; \mathbf{0}_{N_1\times N_2} \quad \mathbf{I}_{N_2}]$,

$\mathbf{Q}_{1k} = [\mathbf{h}_{1k}\mathbf{h}_{1k}^H \quad \mathbf{0}_{N_2\times N_1}\ ;\ \mathbf{0}_{N_1\times N_2} \quad -\gamma_k\mathbf{h}_{2k}\mathbf{h}_{2k}^H]$, and $\mathbf{Q}_{2k} = [-\gamma_k\mathbf{h}_{1k}\mathbf{h}_{1k}^H$ $\mathbf{0}_{N_2\times N_1}; \mathbf{0}_{N_1\times N_2} \quad \mathbf{h}_{2k}\mathbf{h}_{2k}^H]$. This is also a SDP relaxation and can be solved with a SDP solver.

During the MA stage, the proposed design ensures that SINR at eavesdroppers stay below the threshold limit. Therefore, eavesdroppers can not decode at least one symbol from s_1 and s_2. During the BC stage, the relay broadcasts the XOR of the symbols, which is now an encrypted symbol for eavesdroppers. Therefore, the BC stage is not illustrated for the ellipsoidal uncertainty model. We verify this in the numerical results.

5.3.3 Numerical results

In this section, we first analyze the convergence of the proposed Algorithm 5.1. Next, Monte Carlo simulations are used with the proposed algorithm to illustrate the error performance of the TWR communication. Moreover, these simulations are applied to investigate the SINR distributions at a given eavesdropper. We consider a basic TWR system with a single eavesdropper, where all nodes are equipped with two antennas. All channels (including the estimated channel between the U_i and eavesdropper) are assumed to undergo Rayleigh fading with entries $\sim \mathcal{CN}(0,1)$. The error component is generated using truncated Gaussian distributions with entries $\sim \mathcal{CN}(0,1)$. The variance of the noise is considered equal at all nodes, i.e., $\sigma_r^2 = \sigma_{ek}^2 = \sigma^2$. Algorithm 5.1 is used to find beamforming vectors for each channel realization. Furthermore, the user symbols are created with BPSK modulation with unit power. The relay node performs ML estimation to find the XOR of transmitted messages. The numerical examples are performed for 10000 channel realizations.

In Fig.5.2, the convergence of the AMSE is illustrated with the number of iterations. Since we consider single eavesdropper, ε_k and γ_k are denoted as ε and γ. Different ε^2 and γ/σ^2 values are considered when $\mathrm{P}_{\max}/\sigma^2 = 10$ dB. The algorithm converges with a few number of iterations for all cases. The AMSE decreases with γ/σ^2. For fixed $\mathrm{P}_{\max}/\sigma^2$ and γ/σ^2, the AMSE decreases with ε^2. When ε^2 is high, the users are uncertain about the eavesdropper channel. Then, the users reduce their transmit powers to prevent eavesdropping. In such cases, the received signal power at the relay also reduces, which degrades its performance.

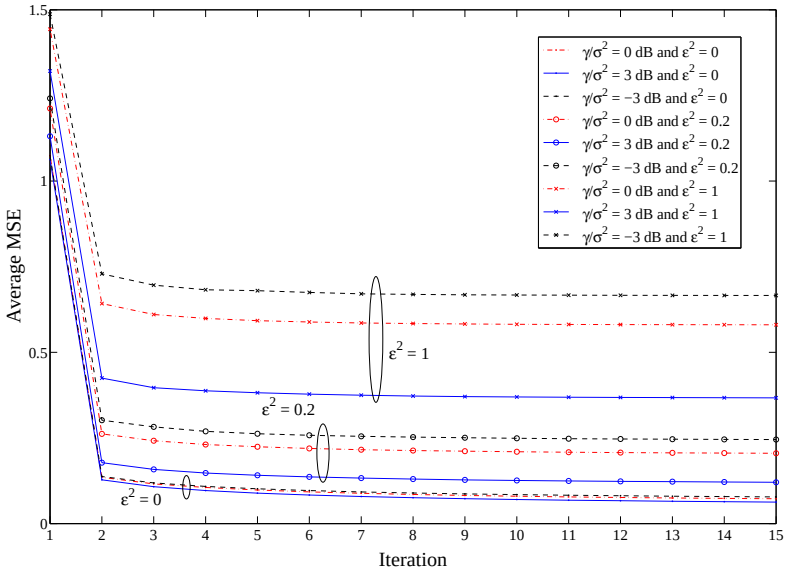

Fig 5.2. Convergence of the Algorithm 5.1. $K = 1$ **and** $\mathrm{P}_{\max}/\sigma^2 = 10$ **dB, [128] © 2014, IEEE.**

Fig.5.3 shows the average BER at the relay verses $\mathrm{P}_{\max}/\sigma^2$. The BER represents the PNC mapping error at the relay node. Two sub-optimal beamforming schemes are compared with the proposed secure beamforming scheme. The first sub-optimal scheme uses ZF precoding at the user nodes. The precoder at the U_i is obtained as pseudo-inverse of the U_i-to-relay channel, i.e. $\sqrt{\frac{\mathrm{P}_{\max}}{Tr(\mathbf{H}_{ir}\mathbf{H}_{ir}^H)^{-1}}}\mathbf{H}_{ir}^H(\mathbf{H}_{ir}\mathbf{H}_{ir}^H)^{-1}$. The second scheme is the unsecured optimal beamforming scheme, where the problem (5.7) is solved without the SINR constraints. The problem becomes QCQP of the $\mathbf{w}_1$ and $\mathbf{w}_2$ variables. Both are unsecured schemes since they do not prevent the eavesdropping of user information. Fig.5.3 shows that the ABER improves with the $\mathrm{P}_{\max}/\sigma^2$ for all these schemes. The unsecured optimal beamforming design provides the best BER performance to the TWR system. The unsecured ZF provides a lower performance than the rest during the low SNR region. There is a maximum error performance level that the secured optimal beamforming designs can achieve. Therefore, we expect ZF to provide better performance in the high SNR region than the proposed beamforming scheme. The eavesdropper SINR threshold γ/σ^2 is varied from 0 to 3 dB in the secured beamforming scheme, where the performance is

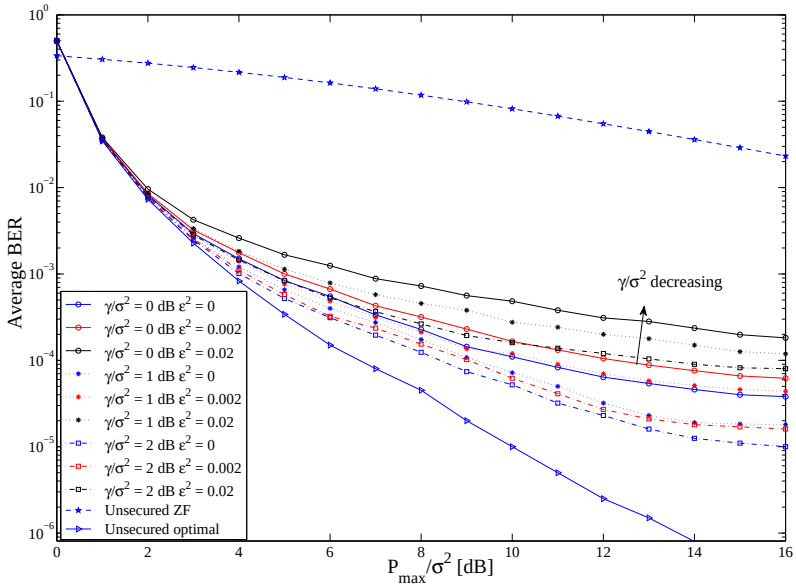

Fig 5.3. Average BER versus $\mathrm{P}_{\max}/\sigma^2$ for different ε and γ/σ^2, [128] © 2014, IEEE.

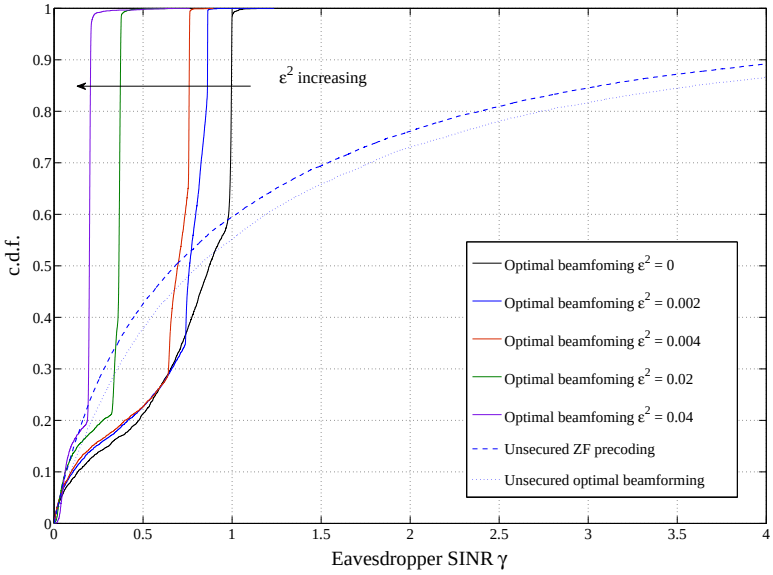

Fig 5.4. c.d.f. of the received SINR of s_1 at the eavesdropper. $\gamma/\sigma^2 = 0$ dB and $\mathrm{P}_{\max}/\sigma^2 = 10$ dB, [128] © 2014, IEEE.

improved with γ/σ^2. However, when the ε^2 is higher, the BER performance degrades. These observations are similar to the Fig.5.2.

Finally, Fig.5.4 shows the c.d.f. of the received SINR of s_1 at the eavesdropper. We assume $\mathrm{P}_{\max}/\sigma^2 = 10$ dB and $\gamma/\sigma^2 = 0$ dB. In the perfect CSI scenario, the maximum received SINR at the eavesdropper is limited at the desired level (0 dB in this simulation). However, when ε^2 is higher, the maximum received SINR at the eavesdropper is lower than the desired level (for interception). This reflects that the beamforming design provides higher security even with the imperfect CSI. In the sub-optimal scenarios, it is clear that the SINR is not limited at the eavesdropper. This allows eavesdropper to intercept information.

5.4 Robust beamforming under Gaussian Markov Uncertainty model

When the CSI error follows GMU model, the robust beamforming design is different from the previous section. Both MA and BC stages are considered in the beamforming design.

5.4.1 Beamforming for MA Stage

We assume GMU model [147] for the U_i-to-E_k channel as

$$\mathbf{H}_{ik} = \sqrt{1-\beta_{ik}^2}\bar{\mathbf{H}}_{ik} + \beta_{ik}\mathbf{E}_{ik}, \tag{5.29}$$

where $\bar{\mathbf{H}}_{ik} \in \mathbb{C}^{N_k \times N_i}$ is the estimated channel component with entries are assumed to be $\sim \mathcal{CN}(0, \sigma^2)$, $\mathbf{E}_{ik} \in \mathbb{C}^{N_k \times N_i}$ is the error component with entries are assumed to be $\sim \mathcal{CN}(0, \sigma^2)$, and $\beta_{ik} \in [0, 1]$ controls the amount of uncertainty in the CSI. We rewrite this by including the reciever beamfoming vector at the E_k, and obtain $\mathbf{h}_{ik} = \sqrt{1-\beta_{ik}^2}\bar{\mathbf{h}}_{ik} + \beta_{ik}\mathbf{e}_{ik}$, where all random entries are $\sim \mathcal{CN}(0, \sigma^2)$.

Now, the SINR constraints of the optimization problem (5.7) consist of error components. These error components have a known Gaussian distribution, therefore, a robust beamforming design can be considered by taking expectation in terms of error variables. After some algebraic manipulations on (5.7), the

robust optimization problem is reformulated as in (5.30)-(5.32).

$$\min_{\mathbf{w}_1,\mathbf{w}_2,\mathbf{w}_r} \quad \sum_{i=1}^{2} \left(\mathbf{w}_r^H \mathbf{H}_{ir}\mathbf{w}_i\mathbf{w}_i^H\mathbf{H}_{ir}^H\mathbf{w}_r - 2\Re(\mathbf{w}_r^H\mathbf{H}_{ir}\mathbf{w}_i)\right) + \sigma_r^2\mathbf{w}_r^H\mathbf{w}_r + 2 \quad (5.30)$$

$$\text{sub. to} \quad \mathbf{w}_i^H\mathbf{w}_i \leq \mathrm{P}_{\max} \qquad i \in \{1,2\} \quad (5.31)$$

$$(1-\beta_{ik}^2)\mathbf{w}_i^H\bar{\mathbf{h}}_{ik}\bar{\mathbf{h}}_{ik}^H\mathbf{w}_i + \beta_{ik}^2\sigma^2\mathbf{w}_i^H\mathbf{w}_i - \gamma_k(1-\beta_{jk}^2)\mathbf{w}_j^H\bar{\mathbf{h}}_{jk}\bar{\mathbf{h}}_{jk}^H\mathbf{w}_j$$
$$-\gamma_k\beta_{jk}^2\sigma^2\mathbf{w}_j^H\mathbf{w}_j \leq \gamma_k\sigma_{ek}^2 \qquad (i,j) \in \{i \neq j|1,2\} \;\&\; \forall k. \quad (5.32)$$

This is a non-convex optimization problem and we use an iterative method to solve this. The problem is divided into following two sub-problems.

Sub-problem I

Here, the transmit beamforming vectors $\mathbf{w}_1$ and $\mathbf{w}_2$ are considered fixed. The optimal $\mathbf{w}_r$ is given by the 5.13.

Sub-problem II

When $\mathbf{w}_r$ is fixed, the problem (5.30)-(5.32) can be reformulated by taking $\mathbf{w} = [\mathbf{w}_1;\mathbf{w}_2] \in \mathbb{C}^{N_1+N_2}$. Then, the problem becomes a quadratic optimization problem as

$$\begin{aligned} \min_{\mathbf{w}} \quad & \mathbf{w}^H\mathbf{A}\mathbf{w} - 2\Re(\mathbf{b}^H\mathbf{w}) + \sigma_r^2\mathbf{w}_r^H\mathbf{w}_r + 2 \\ \text{sub. to} \quad & \mathbf{w}^H\mathbf{P}_i\mathbf{w} - \mathrm{P}_{\max} \leq 0 \qquad \forall\, i \\ & \mathbf{w}^H\mathbf{A}_{ik}\mathbf{w} - \gamma_k\sigma_{ek}^2 \leq 0 \quad \forall\, i \;\&\; \forall\, k, \end{aligned} \quad (5.33)$$

where

$$\mathbf{A}_{1k} = \begin{bmatrix} (1-\beta_{1k}^2)\bar{\mathbf{h}}_{1k}\bar{\mathbf{h}}_{1k}^H + \beta_{1k}^2\sigma^2\mathbf{I}_{N_1} & \mathbf{0}_{N_1\times N_2} \\ \mathbf{0}_{N_2\times N_1} & -\gamma_k\left((1-\beta_{2k}^2)\bar{\mathbf{h}}_{2k}\bar{\mathbf{h}}_{2k}^H + \beta_{2k}^2\sigma^2\mathbf{I}_{N_2}\right) \end{bmatrix},$$

and

$$\mathbf{A}_{2k} = \begin{bmatrix} -\gamma_k\left((1-\beta_{1k}^2)\bar{\mathbf{h}}_{1k}\bar{\mathbf{h}}_{1k}^H + \beta_{1k}^2\sigma^2\mathbf{I}_{N_1}\right) & \mathbf{0}_{N_2\times N_1} \\ \mathbf{0}_{N_1\times N_2} & (1-\beta_{2k}^2)\bar{\mathbf{h}}_{2k}\bar{\mathbf{h}}_{2k}^H + \beta_{2k}^2\sigma^2\mathbf{I}_{N_2} \end{bmatrix}.$$

This is not a convex optimization problem. However, according to [142, p.654, Ap. B.1], this can be solved by reformulating it into a SDP. The SDP relaxation

can be obtained as in (5.34).

$$\begin{aligned} \min \quad & \mathrm{Tr}(\mathbf{AW}) - 2\Re(\mathbf{b}^H\mathbf{w}) + \sigma_r^2\mathbf{w}_r^H\mathbf{w}_r + 2 \\ \text{sub. to} \quad & \mathrm{Tr}(\mathbf{P}_i\mathbf{W}) - \mathrm{P}_{\max} \leq 0 \qquad \forall i \\ & \mathrm{Tr}(\mathbf{A}_{ik}\mathbf{W}) - \gamma_k\sigma_{ek}^2 \leq 0 \quad \forall i \ \& \ \forall k \\ & \begin{bmatrix} \mathbf{W} & \mathbf{w} \\ \mathbf{w}^H & 1 \end{bmatrix} \succeq 0. \end{aligned} \tag{5.34}$$

Now, the problem (5.34) is convex, and can be solved with the interior point method. In general, rank-one solution of $\mathbf{W}$ is required to find the optimal $\mathbf{w}$ of the original problem. The procedure to obtain the rank-one solution are described in [148, 149]. Both sub-problems are iteratively solved till the final MSE_r is converged. The final algorithm to obtain beamforming vectors is provided as Algorithm 5.2.

Algorithm 5.2 Secure beamforming design for MA stage

Information about $K, \mathrm{P}_{\max}, \gamma_k, \sigma^2, \sigma_{ek}^2, \sigma_r^2, N_i, \beta_{ik}, \mathbf{H}_{ir}, \mathbf{h}_{ik}(\forall i, \forall k)$ is available.

1: **initialize** : Beamforming vectors $\mathbf{w}_i = \sqrt{\frac{\mathrm{P}_{\max}}{N_i}}\mathbf{1}$.
2: **repeat**
3: **for** $m = 1 : M$ **do**
4: Fix $\mathbf{w}_1$ and $\mathbf{w}_2$ obtained from step 5 (Or step 1 at $m = 1$). Find optimum $\mathbf{w}_r$ from (5.13).
5: Fix $\mathbf{w}_r$ obtained from step 4. Solve problem (5.34) to find optimum $\mathbf{W}$. Obtain optimal rank-one solution of $\mathbf{W}$ to find $\mathbf{w}_1$ and $\mathbf{w}_2$.
6: **end for**
7: **until** MSE_r converge.
8: Update $\mathbf{w}_r$ at the relay.

5.4.2 Beamforming for BC Stage

The CSI of $\mathbf{H}_{rk}$ $(\forall k)$ at the relay node is assumed to follow GMU model. Considering post-processing at the E_k, we have $\mathbf{h}_{rk} = \sqrt{1-\beta_{rk}^2}\bar{\mathbf{h}}_{rk} + \beta_{rk}\mathbf{e}_{rk}$, where all entries of $\bar{\mathbf{h}}_{rk}$ and $\mathbf{e}_{rk}$ are $\sim \mathcal{CN}(0, \sigma^2)$. $\beta_{rk} \in [0, 1]$ controls the amount of uncertainty in the CSI.

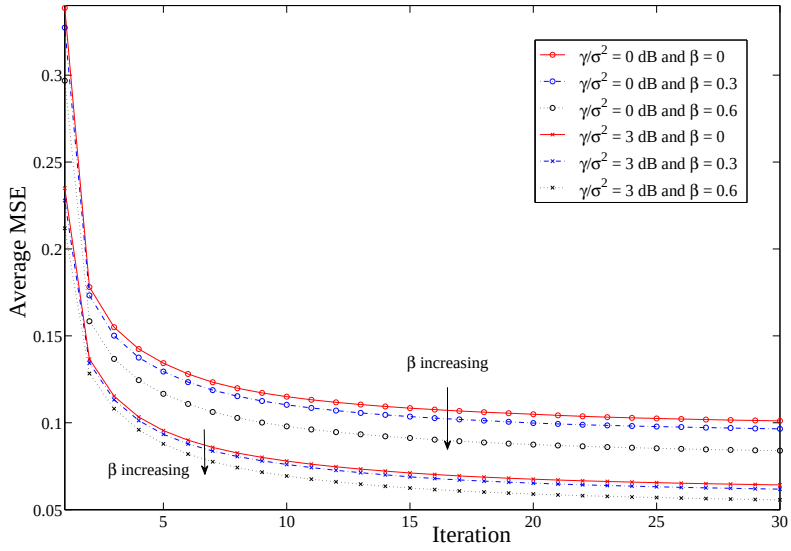

Fig 5.5. Convergence of the Algorithm 5.2. $K = 4$**, and** $\mathrm{P}_{\max}/\sigma^2 = 10$ **dB.**

The problem (5.9) is considered with this CSI model. Similar to the previous stage, the robust beamforming design is considered by taking expectation in terms of error variables, where the reformulated robust optimization problem is obtained as

$$\begin{aligned} \min_{\mathbf{v}_1,\mathbf{v}_2,\mathbf{v}_r} \quad & \sum_{i=1}^{2} 0.5\big(\rho \mathbf{v}_i^H \mathbf{H}_{ir}^T \mathbf{v}_r \mathbf{v}_r^H \mathbf{H}_{ir}^* \mathbf{v}_i - 2\rho \Re(\mathbf{v}_i^H \mathbf{H}_{ir}^T \mathbf{v}_r) + \sigma_i^2 \mathbf{v}_i^H \mathbf{v}_i + 2\rho\big) \\ \text{sub. to} \quad & \mathbf{v}_r^H \mathbf{v}_r \leq \mathrm{P}_{\max}/\rho \\ & (1-\beta_{rk}^2)\mathbf{v}_r^H \bar{\mathbf{h}}_{rk} \bar{\mathbf{h}}_{rk}^H \mathbf{v}_r + \beta_{rk}^2 \sigma^2 \mathbf{v}_r^H \mathbf{v}_r \leq \hat{\gamma}_k \sigma_{ek}^2/\rho \quad \forall k. \end{aligned} \tag{5.35}$$

This is also a non-convex optimization problem, and the problem is divided into sub-problems and solved iteratively. First, the transmit beamforming vector $\mathbf{v}_r$ at the relay is considered fixed, the solution of $\mathbf{v}_i$ is obtained as,

$$\mathbf{v}_i = \left(\mathbf{H}_{ir}^T \mathbf{v}_r \mathbf{v}_r^H \mathbf{H}_{ir}^* + \sigma_i^2 \mathbf{I}_{N_i}\right)^{-1} \mathbf{H}_{ir}^T \mathbf{v}_r \quad i = 1, 2. \tag{5.36}$$

Next, the receiver beamforming vectors $\mathbf{v}_1$ and $\mathbf{v}_2$ are considered fixed. Then, the modified problem (5.35) becomes convex QCQP of the variable $\mathbf{v}_r$. This can be easily solved with the interior point method. Finally, the iterative method is used in the BC stage as similar to the Algorithm 5.2.

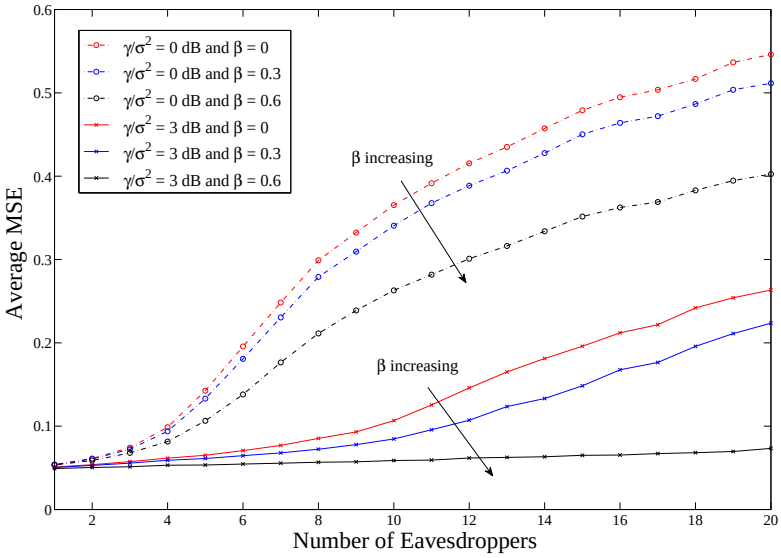

Fig 5.6. Average MSE versus number of eavesdroppers. $\mathrm{P}_{\max}/\sigma^2 = 10$ **dB.**

5.4.3 Numerical results

A similar Monte Carlo simulation set-up is considered as in the section 5.3.3 except for the parameters β_{ik} and β_{rk} which control the amount of uncertainty in the CSI. All are assumed to be β to simplify the discussion. Moreover, the SINR threshold levels at eavesdroppers are equal to γ. In Fig.5.5, the convergence of the Algorithm 5.2 is illustrated with the number of iterations. Different β and γ/σ^2 values are considered when $\mathrm{P}_{\max}/\sigma^2 = 10$ dB. For all cases, the algorithm converges with a small number of iterations. The AMSE decreases with γ/σ^2 and uncertainty parameter β. Since the convergence of the algorithm is fast, this is suitable to consider in practical deployments. The iterative scheme used in the BC stage has a similar convergence pattern. Therefore, it is not illustrated.

Fig.5.6 shows the AMSE at the relay versus the number of eavesdroppers. The AMSE increases with the number of eavesdroppers K. When K is high, the optimization problem has more constraints. Then the feasibility set becomes smaller. Therefore, the AMSE increases with K. However, when β increases the AMSE degrades. This is possible as the robust optimization problem is formulated by taking the expectation of SINR constraints.

The SINR distributions at E_1 during both MA and BC stages are illustrated

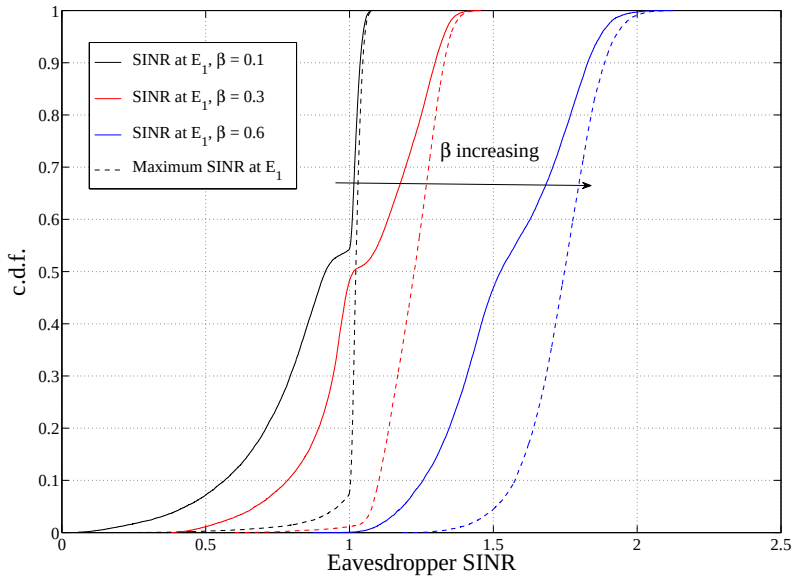

Fig 5.7. c.d.f. of the received SINR at E_1. $K = 4$, and $\mathrm{P}_{\max}/\sigma^2 = 10$ dB.

in Fig.5.7 and Fig.5.8. During the MA stage, the c.d.f. of the SINR of symbol s_1 and maximum SINR of symbols s_1 and s_2 are shown in Fig.5.7. There we assume four eavesdroppers, $\mathrm{P}_{\max}/\sigma^2 = 10$ dB, and $\gamma/\sigma^2 = 0$ dB. The maximum SINR always has a certain gap with the SINR of s_1. In a near perfect CSI scenario, i.e., $\beta = 0.1$, the maximum SINR at E_1 is almost limited at the desired level (0 dB in this simulation). When β is higher, the maximum SINR at the eavesdropper exceeds the desired level. Eavesdroppers can intercept user information in such scenarios. This can be avoided by reducing γ in the optimization problem.

Fig.5.8 shows the c.d.f. of the received SINR of symbol s_r at E_1 during the BC stage. We assume the same simulation parameters except for $\rho = 1$. For all β values, the received SNR at the eavesdropper is almost limited at the desired level. Therefore, the eavesdropper is prevented from decoding s_r. Even though the eavesdropper succeeds in decoding one symbol during the MA stage, it can not decode the other symbol during the BC stage.

Finally, Fig.5.9 shows the ABER for bi-directional communication. Bit errors at both users are considered, and plotted with $\mathrm{P}_{\max}/\sigma^2$. Similar simulation parameters are used as with the Fig.5.7 and Fig.5.8. There is a maximum error performance level that the secured optimal beamforming designs can achieve.

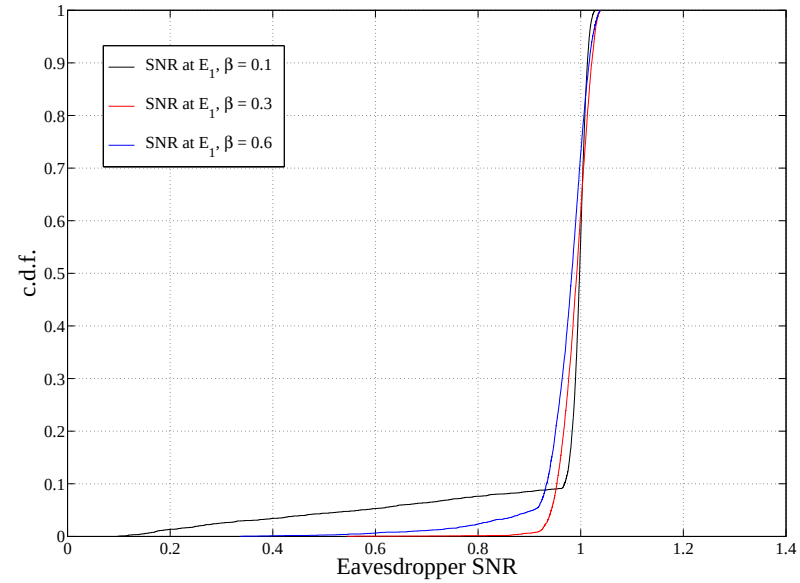

Fig 5.8. c.d.f. of the received SNR of s_r at E_1. $K = 4$, and $\mathrm{P}_{\max}/\sigma^2 = 10$ dB.

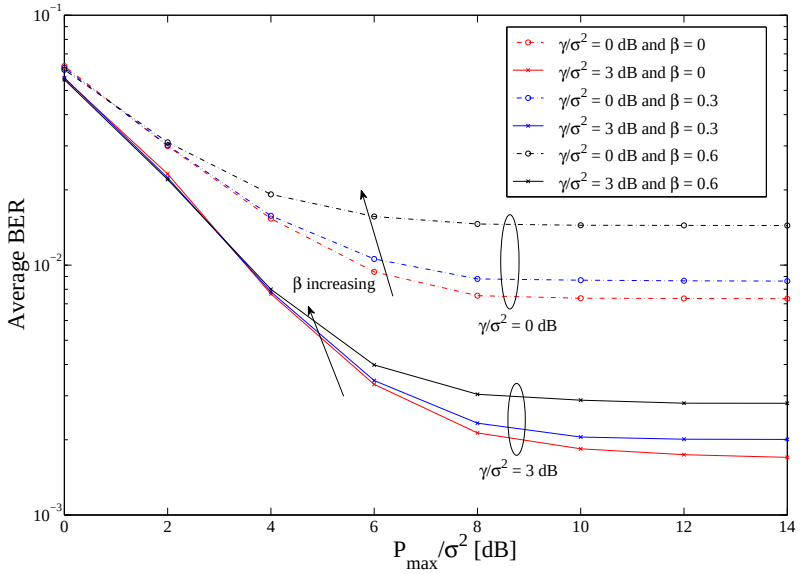

Fig 5.9. Average BER versus $\mathrm{P}_{\max}/\sigma^2$ for different β and γ/σ^2.

The SINR constraints which are adopted to prevent eavesdropping produce such behavior. Error performance is better when the γ/σ^2 is high. Thus, we can expect better error performance in a secure environment. The error performance degrades when β increases. Considering bi-directional communication, this reflects that uncertainty of CSI has an unfavorable effect on the TWR performance.

5.5 Summary and discussion

In this chapter, we discussed robust secure beamforming schemes to prevent eavesdropping on the MIMO TWR system. The relay node was considered to perform PNC mapping which provided an added security by transmitting XOR of two received information. Multiple eavesdroppers were considered with multiple antennas at each eavesdropper. The performance of the user communication was improved by minimizing MSE at both MA and BC stages, where we used SINR policy for eavesdroppers to prevent intercepting user information. Therefore, the proposed secure beamforming designs were based on minimizing MSE, subject to the power and SINR threshold constraints. Particularly, the CSI of user-eavesdroppers channels was imperfect at the user nodes. Thus, two different channel uncertainty models were used to solve the optimization problems.

First, the ellipsoidal uncertainty model was considered to characterize CSI error at the user nodes. The optimization problem became non-convex, and iterative method was adopted to find optimal solutions. The sub-problems were reformulated as SDP relaxations and solved with convex optimization tools. Numerical results suggested that the proposed algorithm converged fast and provided higher security. With this model, the c.d.f. of received SINR at a given eavesdropper was numerically investigated for different error bounds. The robust beamforming design perfectly limited the received SINR at the eavesdropper during the MA stage. Therefore, the beamforming design during the BC stage was not mandatory. At least one message should be decoded during the MA stage to recover the other one during the BC stage.

Next, we considered GMU model for the CSI of user-eavesdropper and relay-eavesdropper channels. The optimization problems were solved with iterative approach in both MA and BC stages. Proposed algorithms were used to analyze the performance of the TWR and investigate the SINR distribution at a given eavesdropper. Numerical results suggested that the algorithm converged fast and

provided higher security. Unlike in the earlier model, this required beamforming during both stages to provide higher secrecy for the TWR communication. This occurred mainly due to the SINR constraint, which was considered by taking the expectation over Gaussian error variable.

6 Conclusions and future directions

In this chapter, we summarize the most notable contributions and main results obtained in this thesis, and we highlight some future research directions.

6.1 Conclusions

This thesis has investigated MIMO relaying scenarios in wireless communication systems. A greater emphasis was placed on to analyze relevant practical situations on MIMO dual-hop relaying and MIMO TWR systems. The first chapter was used to present the motivation for the research and related prior studies. Chapters 2-5 mainly concentrated on studying AF MIMO relaying over asymmetric fading channels, joint precoder-decoder designs on MIMO TWR systems, MIMO TWR based underlay D2D communication, and secure beamforming of MIMO TWR systems. In particular for MIMO TWR systems, more stress was placed on to facilitate PNC mapping at the relay.

In Chapter 2, a complete analysis on non-coherent AF MIMO dual-hop relaying over Rayleigh-Rician fading environment was considered to find the benefits of the relay deployments in the presence of a LoS path to the destination. Several AF MIMO dual-hop cases were considered with OSTBC, optimal single stream beamforming, and multiple relays. The main attention was given to study OSTBC based AF MIMO dual-hop system, where CSI was not required at the source and relay nodes. The statistical parameters of the received SNR at the destination were derived using finite-dimensional random matrix theory. In particular, the expressions for the m.g.f., moments, and probability distributions were obtained for the received SNR. Initially, the relay-destination channel was assumed to undergo non-i.i.d. Rician fading, and then other scenarios of Rician fading such as correlated Rician, i.i.d. Rician and Rayleigh were considered separately. The statistical results were used to analyze the performance of the system in terms of BER, AoF, outage probability, and diversity order and array gains.

For a fixed channel gain, the results indicated that the Rician factor had a significant influence on the performance of AF MIMO dual-hop system. The

usual understanding is that having a good LoS component provides a better performance, which was not found to be true according to the study. In fact, it was the case only when the relay or destination was equipped with a single antenna. When all nodes have multiple antennas, the performance degraded with a higher Rician factor. This is possible as the MIMO is benefited by having good scattering environment which enhances the diversity gain. Nevertheless, it is possible to argue that the channel gain can be higher in LoS relay deployment. In such cases, the performance improves due to the higher channel gain. The studies on other transmission techniques also suggested a similar behavior. Furthermore, the optimal single stream beamforming based AF MIMO relaying provided better performance than the OSTBC based scheme, where it utilized CSI knowledge to find beamforming vectors.

The focus of Chapter 3 was given to study MIMO TWR systems with PNC mapping at the relay node. The complexity of the PNC mapping was treated by incorporating precoders and decoders at the nodes, which provided independent streams at the relay node. The ZF criterion was used at the nodes when the perfect CSI was available at the nodes. The power allocation was determined to maximize the bi-directional sum-rate, where KKT conditions were used to obtain the optimal solution. When CSI was imperfect at the nodes, we proposed robust joint precoder-decoder scheme based on minimizing WMSE. The error components were quantified by utilizing an orthogonal training sequence. During both MA and BC stages of TWR, optimization problems were formulated considering CSI error, antenna correlations, and transmit power constraints. These problems became non-convex and were solved by using iterative algorithms. The proposed algorithms provided the global optimal solutions. The impact of antenna correlation, and CSI error on the TWR performance were numerically investigated with several other schemes. With these precoder-decoders designs, the study revealed that we can simplify the complexity of MIMO PNC mapping and improve overall performance of TWR.

In Chapter 4, the MIMO D2D communication undelaying cellular communication was investigated considering two D2D modes, namely PNC based D2D and direct D2D. With the PNC based D2D communication, devices that were far apart used a relay station to assist their bi-directional communication. Joint precoder-decoder schemes were proposed to improve the performance and mitigate the interference of BS-MS and D2D communications. This was also used

to simplify PNC mapping at the relay node.

For PNC based D2D mode, distributed and centralized optimization approaches were used in the joint design. Particularly, both D2D and BS-MS communications minimized their MSE, subjected to the transmit power and interference threshold constraints. The greedy optimization method was used in the distributed approach, where a given distributed problem was solved in a globally optimal manner using an iterative approach. Then, the precoder variables were exchanged between the RS and BS. As verified by the numerical results, this improved the final solution. The problem became a multi-criterion optimization problem in the centralized approach, and we solved it to find Pareto optimal points. The centralized method was utilized to show that the distributed approach also gives near Pareto optimal solutions. Numerical results also showed that the use of the interference threshold limit in each communication improved the average error performances of both D2D and BS-MS communications.

For the direct D2D mode, a given distributed problem was solved analytically using the KKT conditions. Then the final solutions were improved by adopting the same distributed approach as PNC based D2D mode. The numerical analysis showed several significant improvements of D2D communication. Dynamic mode selection scheme with proposed D2D modes gave a higher performance in the system. All other compared modes were inferior to the dynamic mode selection. The PNC based D2D mode expanded the coverage area for D2D communication. When the devices are very close to each other, the direct D2D mode was the preferred mode. When they are far apart, and a relay node is available to assist, the PNC based D2D mode was the desired option.

Finally, secure beamforming schemes for MIMO TWR in an unsecured environment were proposed in Chapter 5. Two users communicated over the trusted relay node with PNC mapping at the relay, where multiple eavesdroppers were interested in decoding the information. The proposed secure beamforming designs were based on minimizing MSE, subject to the power and SNR policy for eavesdroppers to prevent intercepting user information. Both MA and BC stages were considered in the design. The PNC mapping provided additional security by transmitting XOR of two received information during the BC stage. Two different channel uncertainty models were used as the CSI of user-eavesdropper channels was imperfect at nodes. In the ellipsoidal uncertainty model, the problems became non-convex, and iterative methods were adopted to find optimal

solutions. The sub-problems were reformulated as SDP relaxations and solved with convex optimization tools. In the GMU model, the optimization problems were solved with the same method as used in both MA and BC stages. For the ellipsoidal uncertainty model, the robust beamforming design perfectly limited the received SINR at the eavesdropper during the MA stage. Therefore, secure beamforming design for the BC stage was not mandatory. At least one message should be decoded during the MA stage to recover the other one during BC stage. However, beamforming for both stages were required in the GMU model to provide higher secrecy for the TWR communication. More importantly, the PNC based TWR system can be identified as a secure method compared to other relaying schemes to cope with possible security issues.

6.2 Future directions

It is possible to distinguish several other related MIMO relaying scenarios which are important for future wireless systems. One important direction of interest is information and energy transmissions employing relay nodes. Energy efficient system designs, with performance levels comparable to and exceeding the presently available techniques, will play a major role for future wireless communication. We are currently working on such a scenario, where the relay acts as an energy harvesting node. The received signal is split at the relay, where part of the energy of the received signal energy is stored, and another part is transmitted to the destination. Optimal beamforming at nodes can be used to improve the overall performance, and are useful to analyze the achievable trade-off between energy and information rate. Such energy harvesting relaying can be further studied with many other cases, e.g. assuming multiple energy harvesting receivers, considering traffic aware information relaying and energy harvesting, and utilizing movement patterns of the devices to schedule information relaying and harvesting energy.

For MIMO dual-hop relaying, analytical performance study of Rician-Rayleigh fading scenario is also essential to understand the consequences of such a situation. Our effort in finding analytical derivations of the statistical parameters for instantaneous SNR at the destination is not successful. However, potential studies will provide valuable insight to understanding asymmetric fading scenarios. Additionally, it is possible to identify many other MIMO dual-hop relaying

schemes which can be useful for future wireless systems.

Many studies on MIMO TWR have considered that relay supports only pair of users for the bi-directional communication. However, PNC mapping at the relay can be complex in multi-user TWR schemes. Thus, the relay node requires new techniques to handle multi-user PNC mapping. In this thesis, MIMO PNC mapping is investigated for the cases where perfect and imperfect CSI is available at the source nodes. CSI knowledge allowed us to mitigate multi-stream interference at the relay node. When the CSI is not available at the source, new methods are required to facilitate PNC mapping at the relay. Transmission methods, which are similar to space-time coding can play a significant role in such studies.

Recent studies on massive MIMO have indicated various benefits for wireless systems. These systems use a large number of antennas at the nodes, and PNC mapping in such a scenario can be challenging as estimating XOR of transmitted messages is a complicated task. In particular, the required processing capability can be significantly higher to implement ML estimation techniques. New methods are needed to handle such issues of massive MIMO PNC coding. Since many studies on massive MIMO now focus on ZF precoding schemes, it is worth to investigate such designs with PNC.

There are still many unsolved, but interesting problems in the context of MIMO relay assisted D2D communication. For example, D2D is considered in single operator environment in most cases. In a multi-operator environment, the devices that belong to different operators can also communicate using D2D mode. This is more spectrally efficient as devices can utilize much wider spectrum. Multi-operator spectrum sharing is now an important area of research, where operators are allowed to share the spectrum. Further investigation on D2D communication in such scenarios is required to realize the benefits of the wider spectrum. Furthermore, novel device discovery algorithms are needed to facilitate multi-operator D2D communication.

In the context of secure MIMO TWR systems, the beamforming designs assume that the eavesdroppers do not cooperate in the decoding of the user information. However, the chances of possible interceptions are high when eavesdroppers collectively decode the user information. The problem discussed in the thesis should be altered to provide secure transmission over such scenarios. In particular, this can be done by making some changes in the constraints of

the problem. Moreover, there can be other methods to avoid such corporate eavesdropping. Since TWR system has three legitimate nodes, the eavesdropper coordinations (if the coordination happens via wireless links) can be tracked at the legitimate nodes, which can be used to locate eavesdropper locations.

References

1. Index CVN (2013) Global mobile data traffic forecast update, 2012–2017. http://www-test. cisco. com/c/en/US/solutions/collateral/service-provider/visual-networking-index-vni/white_paper_c11-520862.pdf .
2. Hasna MO & Alouini MS (2004) End-to-end performance of transmission systems with relays over rayleigh-fading channels. IEEE Trans. Wireless Commun. 2(6): 1126–1131.
3. Bletsas A, Khisti A, Reed D & Lippman A (2006) A simple cooperative diversity method based on network path selection. IEEE J. Sel. Areas Commun., 24(3): 659–672.
4. Karagiannidis GK, Tsiftsis TA & Mallik RK (2006) Bounds for multihop relayed communications in Nakagami-m fading. IEEE Trans. Commun. 54(1): 18–22.
5. Foschini G & Gans M (1998) On limits of wireless communications in a fading environment when using multiple antennas. Wireless Per. Commun. 6(3): 311–335.
6. Telatar IE (1999) Capacity of multi-antenna Gaussian channels. Euro. Trans. Telecommun 10(6): 585–596.
7. Winters JH, Salz J & Gitlin RD (1994) The impact of antenna diversity on the capacity of wireless communication systems. IEEE Trans. Commun. 42(2): 1740–1751.
8. Winters JH (1987) On the capacity of radio communication systems with diversity in a Rayleigh fading environment. IEEE J. Sel. Areas Commun. 5(5): 871–878.
9. Sendonaris A, Erkip E & Aazhang B (2003) User cooperation diversity. Part I. System description. IEEE Trans. Commun. 51(11): 1927–1938.
10. Sendonaris A, Erkip E & Aazhang B (2003) User cooperation diversity. Part II. Implementation aspects and performance analysis. IEEE Trans. Commun. 51(11): 1939–1948.
11. Laneman JN, Tse DNC & Wornell GW (2004) Cooperative diversity in wireless networks: Efficient protocols and outage behavior. IEEE Trans. Inform. theory 50(12): 3062–3080.
12. Hasna M & Alouini M (2004) A performance study of dual-hop transmissions with fixed gain relays. IEEE Trans. Wireless Commun. 3(6): 1963–1968.
13. Nosratinia A, Hunter TE & Hedayat A (2004) Cooperative communication in wireless networks. IEEE Commun. Mag. 42(10): 74–80.
14. Laneman JN & Wornell GW (2000) Energy-efficient antenna sharing and relaying for wireless networks. In: IEEE Wireless Commun. and Networ. Confe. (WCNC), volume 1. Chicago, USA.
15. Yang Y, Hu H, Xu J & Mao G (2009) Relay technologies for WiMAX and LTE-advanced mobile systems. IEEE Commun. Mag. 47(10): 100–105.
16. Hoymann C, Chen W, Montojo J, Golitschek A, Koutsimanis C & Shen X (2012) Relaying operation in 3GPP LTE: challenges and solutions. IEEE Commun. Mag. 50(2): 156–162.
17. Loa K, Wu CC, Sheu ST, Yuan Y, Chion M, Huo D & Xu L (2010) IMT-advanced

relay standards [WiMAX/LTE update]. IEEE Commun. Mag. 48(8): 40–48.
18. Bradford GJ & Laneman JN (2010) A survey of implementation efforts and experimental design for cooperative communications. In: Proc. IEEE Int. Conf. Acoustics, Speech, and Signal Processing (ICASSP), pp. 5602–5605. Texas, USA.
19. Murphy P, Sabharwal A & Aazhang B (2009) On building a cooperative communication system: Testbed implementation and first results. EURASIP J. Wireless Commun. Netw. 2009: 1–9.
20. Zetterberg P, Mavrokefalidis C, Lalos AS & Matigakis E (2009) Experimental investigation of cooperative schemes on a real-time DSP-based testbed. EURASIP J. Wireless Commun. Netw. 2009: 15.
21. Jing Y & Jafarkhani H (2009) Single and multiple relay selection schemes and their achievable diversity orders. IEEE Trans. Wireless Commun., 8(3): 1414–1423.
22. Lee IH & Kim D (2008) End-to-end BER analysis for dual-hop OSTBC transmissions over Rayleigh fading channels. IEEE Trans. Commun. 56(3): 347–351.
23. Fan Y & Thompson J (2007) Mimo configurations for relay channels: theory and practice. IEEE Trans. Wireless Commun. 6(5): 1774–1786.
24. Peters SW & Heath RW (2008) Nonregenerative MIMO relaying with optimal transmit antenna selection. IEEE Signal Processing Letters 15: 421–424.
25. Bölcskei H, Nabar RU, Oyman O & Paulraj AJ (2006) Capacity scaling laws in MIMO relay networks. IEEE Trans. Wire. Commun. 5(6): 1433–1444.
26. Yeh S & Leveque O (2007) Asymptotic capacity of multi-level amplify-and-forward relay networks. In: Proc. IEEE Int. Symp. on Infor. Theo. (ISIT), pp. 1436–1440. Nice, France.
27. Morgenshtern VI & Bölcskei H (2007) Crystallization in large wireless networks. IEEE Trans. Inform. Theory 53(10): 3319–3349.
28. Morgenshtern VI & Bölcskei H (2006) Random matrix analysis of large relay networks. In: Proc. 44th Allerton Ann. Conf. Commun., Control, and Computing, pp. 106–112.
29. Wagner J, Rankov B & Wittneben A (2008) Large n analysis of amplify-and-forward MIMO relay channels with correlated Rayleigh fading. IEEE Trans. Inform. Theory 54(12): 5735–5746.
30. Chen S, Wang W, Zhang X & Sun Z (2010) Performance analysis of OSTBC transmission in amplify-and-forward cooperative relay networks. IEEE Trans. Veh. Technol. 59(1): 105–113.
31. Kang M & Alouini MS (2003) Largest eigenvalue of complex Wishart matrices and performance analysis of MIMO MRC systems. IEEE J. Sel. Areas Commun. 21(3): 418–426.
32. Song S & Letaief K (2012) System Design, DMT Analysis, and Penalty for Non-Coherent Relaying. IEEE Trans. Commun. 60(9): 2489–2498.
33. Dhaka K, Mallik RK & Schober R (2013) Optimisation of power allocation for asymmetric relay placement in multi-hop relay systems. Communications, IET 7(2): 128–136.
34. Yang N, Elkashlan M, Yuan J & Shen T (2010) On the SER of fixed gain amplify-and-forward relaying with beamforming in Nakagami-m fading. IEEE Commun. Lett. 14(10): 942–944.

35. Jin S, McKay MR, Zhong C & Wong KK (2010) Ergodic capacity analysis of amplify-and-forward MIMO dual-hop systems. IEEE Trans. Inform. Theory 56(5): 2204–2224.
36. Dharmawansa P, McKay MR & Mallik RK (2010) Analytical performance of amplify-and-forward MIMO relaying with orthogonal space-time block codes. IEEE Trans. Commun. 58(7): 2147–2158.
37. Song Y, Shin H & Hong EK (2009) MIMO cooperative diversity with scalar-gain amplify-and-forward relaying. IEEE Trans. Commun. 57(7): 1932–1938.
38. Louie R, Li Y, Suraweera H & Vucetic B (2009) Performance analysis of beamforming in two hop amplify and forward relay networks with antenna correlation. IEEE Trans. Wireless Commun., 8(6): 3132–3141.
39. da Costa D & Aïssa S (2009) Cooperative dual-hop relaying systems with beamforming over Nakagami-m fading channels. IEEE Trans. Wireless Commun. 8(8): 3950–3954.
40. Min H, Lee S, Kwak K & Hong D (2009) Effect of multiple antennas at the source on outage probability for amplify-and-forward relaying systems. IEEE Trans. Wireless Commun., 8(2): 633–637.
41. Zhong C, Ratnarajah T, Jin S & Wong K (2012) Performance analysis of optimal single stream beamforming in MIMO dual-hop AF systems. IEEE J. Sel. Areas Commun. 30(8): 1415–1427.
42. Alamouti SM (1998) A simple transmit diversity technique for wireless communications. IEEE J. Sel. Areas in Commun. 16(8): 1451–1458.
43. Tarokh V, Jafarkhani H & Calderbank AR (1999) Space-time block codes from orthogonal designs. IEEE Trans. Inf. Theory 45(5): 1456–1467.
44. Tarokh V, Jafarkhani H & Calderbank AR (1999) Space-time block coding for wireless communications: performance results. IEEE Jour. Sele. Are. Commun. 17(3): 451–460.
45. Chalise BK & Vandendorpe L (2008) Outage probability analysis of a MIMO relay channel with orthogonal space-time block codes. IEEE Commun. Lett. 12(4): 280–282.
46. Yang Q, Zhong Y & Kwak KS (2009) Symbol error rate of cooperative transmission using OSTBC. IEICE Trans. Commun. 92(1): 338–341.
47. Suraweera HA, Karagiannidis GK & Smith PJ (2009) Performance analysis of the dual-hop asymmetric fading channel. IEEE Trans. Wireless Commun. 8(6): 2783–2788.
48. Adinoyi A & Yanikomeroglu H (2006) On the performance of cooperative wireless fixed relays in asymmetric channels. In: Proc. IEEE GLOBECOM, pp. 1–5. San Francisco, CA.
49. Yacoub M, Fraidenraich G & Santos Filho J (2005) Nakagami-m phase-envelope joint distribution. IET Electronics Letters 41(5): 259–261.
50. Mallik RK (2010) A new statistical model of the complex Nakagami-m fading gain. IEEE Trans. Commun. 58(9): 2611–2620.
51. Jayasinghe LKS, Rajatheva N, Dharmawansa P & Latva-aho M (2013) Noncoherent amplify-and-forward MIMO relaying with OSTBC over Rayleigh-Rician fading channels. IEEE Trans. Vehi. Tech. 62(4): 1610–1622.
52. Jayasinghe LKS, Rajatheva N, Dharmawansa P & Latva-aho M (2011) Dual hop

MIMO OSTBC communication over rayleigh-rician channel. In: Proc. IEEE 73rd Vehi. Tech. Conf. (VTC Spring), pp. 1–5. Budapest, Hungary.
53. Jayasinghe P, Jayasinghe LKS, Juntti M & Latva-aho M (2014) Performance analysis of optimal beamforming in fixed-gain AF MIMO relaying over asymmetric fading channels. IEEE Trans. Commun. 62(4): 1201–1217.
54. Jayasinghe P, Jayasinghe LKS, Juntti M & Latva-aho M (2013) Performance analysis of optimal beamforming in AF MIMO relaying over asymmetric fading channels. In: Proc. IEEE 24th Int. Symp. Per. Ind. and Mob. Rad. Comm. (PIMRC), pp. 708–712. London, UK.
55. Jayasinghe P, Jayasinghe LKS, Juntti M & Latva-aho M (2014) Relay selection on dual hop af MIMO with osbtc over asymmetric fading channels. In: Proc. IEEE Wire. Commun. Netw. Conf. (WCNC). Istanbul, Turkey. to appear.
56. Jayasinghe P, Jayasinghe LKS, Juntti M & Latva-aho M (2014) Effect of cci and feedback delay on the multi-antenna af relaying over asymmetric fading channels. In: Proc. IEEE Wire. Commun. Netw. Conf. (WCNC). Istanbul, Turkey. to appear.
57. Munoz O, Agustin A & Vidal J (2004) Cellular capacity gains of cooperative MIMO transmission in the downlink. In: Proc. Int. Zurich Seminar on Communications (IZS), pp. 22–26. Zurich, Switzerland.
58. Scutari G, Barbarossa S & Ludovici D (2003) Cooperation diversity in multihop wireless networks using opportunistic driven multiple access. In: Proc. IEEE SPAWC 2003, pp. 170–174. Rome, Italy.
59. Larsson P, Johansson N & Sunell KE (2006) Coded bi-directional relaying. In: Proc.IEEE 63rd Veh. Technol. Conference, 2006 (VTC), volume 2, pp. 851–855. Melbourne, Australia.
60. Rankov B & Wittneben A (2007) Spectral efficient protocols for half-duplex fading relay channels. IEEE J. Sel. Areas Commun. 25(2): 379–389.
61. Rankov B & Wittneben A (2005) Spectral efficient signaling for half-duplex relay channels. In: Proc. Asilomar Conf. Signals, Syst. and Comput., pp. 1066–1071. Pacific Grove, CA.
62. Zhang S, Liew SC & Lam PP (2006) Hot topic: physical-layer network coding. In: Proc. Mobicomm 2006, p. 365. LA, CA.
63. Popovski P & Yomo H (2006) Bi-directional amplification of throughput in a wireless multi-hop network. In: Proc. IEEE 63rd Vehi. Tech. Conf. (VTC), volume 2. Melbourne, Australia.
64. Zhang S, Liew S & Lu L (2008) Physical layer network coding schemes over finite and infinite fields. In: Proc. IEEE Global Telecommunications Conference (GLOBECOM), pp. 1–6. New Orleans, LA.
65. Nazer B & Gastpar M (2011) Compute-and-forward: Harnessing interference through structured codes. IEEE Tran. Info. Theo. 57(10): 6463–6486.
66. Nam W, Chung SY & Lee YH (2010) Capacity of the gaussian two-way relay channel to within bit. IEEE Tran. Info. Theo. 56(11): 5488–5494.
67. Katti S, Gollakota S & Katabi D (2007) Embracing wireless interference: analog network coding. In: ACM SIGCOMM Comp. Commun. Rev., volume 37, pp. 397–408.
68. Koike-Akino T, Popovski P & Tarokh V (2009) Optimized constellations for two-

way wireless relaying with physical network coding. IEEE J. Sel. Are. Commun. 27(5): 773–787.
69. Cui T & Kliewer J (2008) Memoryless relay strategies for two-way relay channels: performance analysis and optimization. In: Proc. IEEE Int. Conf. Commun. (ICC), pp. 1139–1143. Beijing, China.
70. Wilson M, Narayanan K, Pfister H & Sprintson A (2010) Joint physical layer coding and network coding for bidirectional relaying. IEEE Trans. Infor. Theo. 56(11): 5641–5654.
71. Nazer B & Gastpar M (2011) Reliable physical layer network coding. Proc. IEEE 99(3): 438–460.
72. Liew SC, Zhang S & Lu L (2013) Physical-layer network coding: Tutorial, survey, and beyond. Physical Communication 6: 4–42.
73. Kim S & Chun J (2008) Network coding with linear MIMO pre-equalizer using modulo in two-way channel. In: Proc. IEEE Wire. Commun. Netw. Conf. (WCNC), pp. 517–521. Las Vegas, US.
74. Yang H, Lee K & Chun J (2007) Zero-forcing based two-phase relaying. In: Proc. IEEE International Conference on Coomunications (ICC), 2007, pp. 5224–5228. Glasgow, Scotland.
75. Zhang S & Liew SC (2010) Physical layer network coding with multiple antennas. In: Proc. IEEE Wire. Commun. Netw. Conf. (WCNC), pp. 1–6. Sydney, Australia.
76. Koike-Akino T (2010) Adaptive network coding in two-way relaying MIMO systems. In: Proc. IEEE Glo. Tele. Conf. (GLOBECOM), pp. 1–6. Miami, US.
77. Yang T, Yuan X, Ping L, Collings IB & Yuan J (2013) A new physical-layer network coding scheme with eigen-direction alignment precoding for MIMO two-way relaying. IEEE Tran. commun. 61(3): 973–986.
78. Zhou QF, Li Y, Lau FCM & Vucetic B (2010) Decode-and-forward two-way relaying with network coding and opportunistic relay selection. IEEE Tran. commun. 58(11): 3070–3076.
79. Ding Z, Krikidis I, Thompson J & Leung KK (2011) Physical layer network coding and precoding for the two-way relay channel in cellular systems. IEEE Tran. Sig. Proce. 59(2): 696–712.
80. Jayasinghe LKS, Rajatheva N & Latva-aho M (2012) Energy efficient MIMO two-way relay system with physical layer network coding. In: Proc. IEEE Wire. Commun. Netw. Conf. (WCNC), pp. 1–5. Paris, France.
81. Jayasinghe LKS, Rajatheva N & Latva-aho M (2012) Joint pre-coder and decoder design for physical layer network coding based MIMO two-way relay system. In: Proc. IEEE Int. Conf. Commun. (ICC), pp. 5645–5649. Ottawa, Canada.
82. Yang J & Roy S (1994) On joint transmitter and receiver optimization for multiple-input-multiple-output (MIMO) transmission systems. IEEE Trans. Commun. 42(12): 3221–3231.
83. Sampath H, Stoica P & Paulraj A (2001) Generalized linear precoder and decoder design for MIMO channels using the weighted MMSE criterion. IEEE Trans. Commun. 49(12): 2198–2206.
84. Guan W & Luo H (2008) Joint MMSE Transceiver Design in Non-regenerative MIMO Relay systems. IEEE Comm. Letters 12(7): 517–519.

85. Lee KJ, Lee KW, Sung H & Lee I (2009) Sum-rate maximization for two-way MIMO amplify-and-forward relaying systems. In: IEEE 69th VTC Spring 2009., pp. 1–5. IEEE.
86. Xu S & Hua Y (2011) Optimal design of spatial source-and-relay matrices for a non-regenerative two-way MIMO relay system. IEEE Trans. Wire. Commun. 10(5): 1645–1655.
87. Wang R & Tao M (2012) Joint source and relay precoding designs for MIMO two-way relaying based on MSE criterion. Tran. on Sign. Proc. 60(3): 1352–1365.
88. Xing C, Ma S & Wu Y (2010) Robust joint design of linear relay precoder and destination equalizer for dual-hop amplify-and-forward mimo relay systems. IEEE Trans. Sig. Proc. 58(4): 2273–2283.
89. Ding Z & Leung KK (2011) Impact of imperfect channel state information on bi-directional communications with relay selection. IEEE Trans. Sig. Proc. 59(11): 5657–5662.
90. Jayasinghe LKS, Rajatheva N & Latva-aho M (2013) Robust precoder-decoder design for physical layer network coding-based MIMO two-way relaying system. EURASIP J. Wire. Commun. and Net. 2013(1): 1–16.
91. Jayasinghe LKS, Rajatheva N & Latva-aho M (2013) Robust joint precoder-decoder design for PNC based MIMO two-way relaying system. In: Proc. IEEE 78th Vehi. Tech. Conf. (VTC Fall), pp. 1–5. Las Vegas, USA.
92. Hassibi B & Hochwald B (2003) How much training is needed in multiple-antenna wireless links? IEEE Trans. Infor. Theo. 49(4): 951–963.
93. Xing C, Fei Z, Wu Y, Ma S & Kuang J (2011) Robust transceiver design for af mimo relay systems with column correlations. In: Proc. IEEE ICSPCC 2011, pp. 1–6. Xi'an,China.
94. Ding M & Blostein S (2009) Mimo minimum total mse transceiver design with imperfect csi at both ends. IEEE Trans. Sig. Proc. 57(3): 1141–1150.
95. Thoen S, Van der Perre L, Gyselinckx B & Engels M (2001) Performance analysis of combined transmit-sc/receive-mrc. IEEE Trans. Commun. 49(1): 5–8.
96. Suraweera HA, Tsiftsis TA, Karagiannidis GK & Faulkner M (2009) Effect of feedback delay on downlink amplify-and-forward relaying with beamforming. In: Proc. IEEE GLOBECOM, pp. 1–6. Hawaii, USA.
97. Amarasuriya G, Tellambura C & Ardakani M (2010) Feedback delay effect on dual-hop MIMO AF relaying with antenna selection. In: Proc. IEEE GLOBECOM, pp. 1–5. Miami, Florida, USA.
98. Dahlman E, Parkvall S & Skold J (2011) 4G: LTE/LTE-Advanced for Mobile Broadband. Academic Press.
99. Pekka J, Chia-Hao Y, Klaus D, Cassio R, Carl W, Klaus H, Olav T & Visa K (2009) Device-to-device communication underlaying cellular communications systems. Int'l J. Commun. Netw. and Sys. Sci. pp. 169–178.
100. Doppler K, Rinne M, Wijting C, Ribeiro C & Hugl K (2009) Device-to-device communication as an underlay to LTE-advanced networks. IEEE Commun. Mag. 47(12): 42–49.
101. Haykin S (2005) Cognitive radio: brain-empowered wireless communications. IEEE Journal on Selected Areas in Communications 23(2): 201–220.
102. Jayasinghe L & Rajatheva N (2010) Optimal power allocation for relay assisted

cognitive radio networks. In: Proc. IEEE 72nd Vehi. Tech. Conf. Fall (VTC 2010-Fall), pp. 1–5. Ottawa, Canada.
103. Huang K, Lau V & Chen Y (2009) Spectrum sharing between cellular and mobile ad hoc networks: transmission-capacity trade-off. IEEE J. Sel. Areas Commun. 27(7): 1256–1267.
104. Fodor G, Dahlman E, Mildh G, Parkvall S, Reider N, Miklós G & Turányi Z (2012) Design aspects of network assisted device-to-device communications. IEEE Commun. Mag. 50(3): 170–177.
105. Osseiran A, Doppler K, Ribeiro C, Xiao M, Skoglund M & Manssour J (2009) Advances in device-to-device communications and network coding for IMT-advanced. ICT Mobile Summit .
106. Belleschi M, Fodor G & Abrardo A (2011) Performance analysis of a distributed resource allocation scheme for d2d communications. In: IEEE GLOBECOM Workshops, pp. 358–362. Houston, Texas, USA.
107. Zulhasnine M, Huang C & Srinivasan A (2010) Efficient resource allocation for device-to-device communication underlaying LTE network. In: Proc. IEEE Int. Conf. on Wireless and Mobi. Comput., Networ. and Commun. (WiMob), pp. 368–375. IEEE.
108. Yu CH, Doppler K, Ribeiro C & Tirkkonen O (2011) Resource sharing optimization for device-to-device communication underlaying cellular networks. IEEE Trans. Wireless Commun. 10(8): 2752–2763.
109. Hakola S, Chen T, Lehtomaki J & Koskela T (2010) Device-to-device (D2D) communication in cellular network-performance analysis of optimum and practical communication mode selection. In: Proc. IEEE Wire. Commun. Netw. Conf. (WCNC), pp. 1–6. Sydney, Australia.
110. Lei L, Zhong Z, Lin C & Shen X (2012) Operator controlled device-to-device communications in LTE-advanced networks. IEEE Wire. Commun. 19(3): 96–104.
111. Corson MS, Laroia R, Li J, Park V, Richardson T & Tsirtsis G (2010) Toward proximity-aware internetworking. IEEE Wire. Commun. Lett. 17(6): 26–33.
112. Asadi A, Wang Q & Mancuso V (2014) A survey on device-to-device communication in cellular networks. IEEE Commun. Surv. Tutor. pp. 1–1.
113. Jayasinghe LKS, Jayasinghe P, Rajatheva N & Latva-aho M (2015) Linear precoder-decoder design of MIMO device-to-device communication underlaying cellular communication. IEEE Trans. Commun. 62(12): 4304–4319.
114. Jayasinghe LKS, Jayasinghe P, Rajatheva N & Latva-aho M (2013) MIMO physical layer network coding based underlay device-to-device communication. In: Proc. IEEE 24th Int. Symp. Per. Ind. and Mob. Rad. Comm. (PIMRC), pp. 89–94. London, UK.
115. Wyner AD (1975) The wire-tap channel. Bell System Technical Journal, The 54(8): 1355–1387.
116. Khisti A & Wornell GW (2010) Secure transmission with multiple antennas i: The MISOME wiretap channel. IEEE Tran. Info. Theo. 56(7): 3088–3104.
117. Oggier F & Hassibi B (2011) The secrecy capacity of the MIMO wiretap channel. IEEE Tran. Info. Theo. 57(8): 4961–4972.
118. Goel S & Negi R (2008) Guaranteeing secrecy using artificial noise. IEEE Trans.

Wire. Commun. 7(6): 2180–2189.
119. Park K, Wang T & Alouini M (2013) On the jamming power allocation for secure amplify-and-forward relaying via cooperative jamming. IEEE J. on Sel. Are. in Commun. 31(9): 1741–1750.
120. Dong L, Han Z, Petropulu A & Poor H (2010) Improving wireless physical layer security via cooperating relays. IEEE Trans. Sig. Proc. 58(3): 1875–1888.
121. Ding Z, Xu M, Lu J & Liu F (2012) Improving wireless security for bidirectional communication scenarios. IEEE Trans. Vehicu. Techn. 61(6): 2842–2848.
122. Tekin E & Yener A (2008) The general gaussian multiple-access and two-way wiretap channels: Achievable rates and cooperative jamming. IEEE Trans. Inf. Theo. 54(6): 2735–2751.
123. Liao W, Chang T, Ma W & Chi C (2011) Qos-based transmit beamforming in the presence of eavesdroppers: An optimized artificial-noise-aided approach. IEEE Trans. Sig. Proc. 59(3): 1202–1216.
124. Li Q & Ma W (2011) Optimal and robust transmit designs for miso channel secrecy by semidefinite programming. IEEE Trans. Sig. Proc. 59(8): 3799–3812.
125. Gerbracht S, Scheunert C & Jorswieck EA (2012) Secrecy outage in MISO systems with partial channel information. IEEE Trans. Info. Fore. and Secu. 7(2): 704–716.
126. Mukherjee A & Swindlehurst AL (2011) Robust beamforming for security in MIMO wiretap channels with imperfect csi. IEEE Trans. Sign. Proce. 59(1): 351–361.
127. Wang X, Wang K & Zhang X (2013) Secure relay beamforming with imperfect channel side information. IEEE Tran. Vehi. Techn. 62(5): 2140–2155.
128. Jayasinghe LKS, Jayasinghe P, Rajatheva N & Latva-aho M (2014) Secure beamforming design for physical layer network coding based MIMO two-way relaying. IEEE Comm. Lett. 18(7): 1270–1273.
129. Jayasinghe LKS, Jayasinghe P, Rajatheva N & Latva-aho M (Submitted) Robust d2d communication in the presence of multiple eavesdroppers. In: Proc. IEEE Int. Conf. Commun. (ICC). London, UK.
130. Jayasinghe LKS, Rajatheva N & Latva-aho M (2011) Optimal power allocation for PNC relay based communications in cognitive radio. In: Proc. IEEE Int. Conf. Commun. (ICC), pp. 1–5. Kyoto, Japan.
131. Jayasinghe LKS, Jayasinghe P, Rajatheva N & Latva-aho M (Submitted) Optimal beamforming for energy and information transmission over energy harvesting relay. IEEE Comm. Lett. .
132. Shin H & Lee JH (2004) Performance analysis of space-time block codes over keyhole Nakagami-m fading channels. IEEE Trans. Veh. Technol. 53(2): 351–362.
133. Jafarkhani H (2005) Space-Time Coding: Theory and Practice. Cambridge Univ. Press.
134. Gradshteyn IS & Ryzhik IM (1994) Table of Integrals, Series and Products .
135. Bölcskei H, Borgmann M & Paulraj AJ (2003) Impact of the propagation environment on the performance of space-frequency coded MIMO-OFDM. IEEE Selec. Area Commun. 21(3): 427–439.
136. Simon MK & Alouini MS (2000) Digital Communication over Fading Channels.

Wiley, New York, 2nd edition.
137. Kang M & Alouini MS (2006) Capacity of MIMO Rician channels. IEEE Trans. Wireless Commun 5(1): 112–122.
138. Wang Z & Giannakis GB (2003) A simple and general parameterization quantifying performance in fading channels. IEEE Trans. Commun. 51(8): 1389–1398.
139. Charash U (1979) Reception through nakagami fading multipath channels with random delays. IEEE Trans. Commun. 27(4): 657–670.
140. Holter B & ien GE (2005) On the amount of fading in MIMO diversity systems. IEEE Trans. Wire. Commun. 4(5): 2498–2507.
141. Wilson MP, Narayanan K, Pfister HD & Sprintson A (2010) Joint physical layer coding and network coding for bidirectional relaying. IEEE Tran. Info. Theo. 56(11): 5641–5654.
142. Boyd S & Vandenberghe L (2004) Convex Optimization. Cambridge University Press, UK.
143. Jose J, Ashikhmin A, Whiting P & Vishwanath S (2011) Channel estimation and linear precoding in multiuser multiple-antenna TDD systems. IEEE Trans. Vehi. Tech. 60(5): 2102–2116.
144. Hjorungnes A & Gesbert D (2007) Complex-valued matrix differentiation: Techniques and key results. IEEE Trans. Sign. Proces. 55(6): 2740–2746.
145. Grant M, Boyd S & Ye Y (2012) CVX: Matlab software for disciplined convex programming, version 2.0 beta. Recent Advances in Learning and Control pp. 95–110.
146. Grant M & Boyd S (2008) Graph implementations for nonsmooth convex programs. In: Blondel V, Boyd S & Kimura H (eds.) Recent Advances in Learning and Control, pp. 95–110. Springer-Verlag Limited.
147. Nosrat-Makouei B, Andrews JG & Heath RW (2011) MIMO interference alignment over correlated channels with imperfect CSI. IEEE Trans. Sig. Proc. 59(6): 2783–2794.
148. Sidiropoulos N, Davidson T & Luo Z (2006) Transmit beamforming for physical-layer multicasting. IEEE Trans. Sig. Proc. 54(6): 2239–2251.
149. Tseng P (2003) Further results on approximating nonconvex quadratic optimization by semidefinite programming relaxation. SIAM J. Optim. 14(1): 268–283.
150. Chiani M, Win MZ & Zanella A (2003) On the capacity of spatially correlated MIMO Rayleigh-fading channels. IEEE Trans. Inform. Theory 49(10): 2363–2371.
151. Abramowitz M & Stegun IA (1972) Handbook of mathematical functions: with formulas, graphs, and mathematical tables. 55. Courier Dover Publications.
152. Bertsekas DP (1999) Nonlinear programming. Athena Scientific.

Appendix 1 : Proof of Theorem 2.1

We consider the definition of the m.g.f. to derive the expression (2.16).

$$M_\gamma(s) = \mathcal{E}_\gamma\{e^{-s\gamma}\}. \tag{1.0.1}$$

Substituting the instantaneous SNR (2.15) into (1.0.1) gives,

$$\begin{aligned} M_\gamma(s) &= \mathcal{E}_{\mathbf{H}_1,\mathbf{H}_2}\left\{\exp(-s\alpha\overline{\gamma}a^2\mathrm{Tr}(\mathbf{H}_1^H\mathbf{H}_2^H\mathbf{K}^{-1}\mathbf{H}_2\mathbf{H}_1))\right\} \\ &= \mathcal{E}_{\mathbf{H}_2}\{M_{\gamma|\mathbf{H}_2}(s)\}. \end{aligned} \tag{1.0.2}$$

Source-relay channel $\mathbf{H}_1$ has a matrix-variate complex Gaussian distribution. Therefore, we can write $M_{\gamma|\mathbf{H}_2}(s)$ as [136]

$$M_{\gamma|\mathbf{H}_2}(s) = \frac{1}{\det(\mathbf{I}_{N_R} + s\alpha\overline{\gamma}a^2\mathbf{H}_2^H\mathbf{K}^{-1}\mathbf{H}_2)^{N_S}}. \tag{1.0.3}$$

We use singular value decomposition (SVD) on $\mathbf{H}_2$ and obtain following expression for $M_{\gamma|\mathbf{\Phi}}(s)$using [36, Eq.30]

$$M_{\gamma|\mathbf{\Phi}}(s) = \prod_{k=1}^{q}\left(\frac{1}{1+\frac{s\alpha\overline{\gamma}a^2\sigma^2\phi_k}{1+a^2\sigma^2\phi_k}}\right)^{N_S}, \tag{1.0.4}$$

where $\phi_1, \phi_2, ..., \phi_q$ are nonzero ordered eigenvalues ($0 < \phi_1 < \phi_2 < ... < \phi_q < \infty$) of $\frac{1}{\sigma^2}\mathbf{H}_2\mathbf{H}_2^H$ and $\mathbf{\Phi} = \mathrm{diag}(\phi_1, \phi_2, ..., \phi_q)$. Moreover, the joint eigenvalue distribution of $\frac{1}{\sigma^2}\mathbf{H}_2\mathbf{H}_2^H$ is given by [31]

$$f_{\phi_1,..,\phi_q}(\phi_1, .., \phi_q) = \frac{c}{\det(\mathbf{V})}\ \det(\ {}_0F_1(t; \phi_i\lambda_j))\det(\mathbf{W})\prod_{k=1}^{q}\phi_k^{p-q}e^{-\phi_k} \tag{1.0.5}$$

where $0 < \phi_1 < \phi_2 < ... < \phi_q < \infty$, ${}_0F_1(\cdot;\cdot)$ is the generalized hypergeometric function defined in [134],

$$c = \frac{e^{-\mathrm{Tr}(\mathbf{\Lambda})}}{(\Gamma(t))^q}, \tag{1.0.6}$$

and $\mathbf{W}$ is $q \times q$ vandermonde matrix with its determinant given by

$$\det(\mathbf{W}) = \det(\phi_i^{q-j}) = \prod_{l<k}^{q}(\phi_l - \phi_k). \tag{1.0.7}$$

The unconditional m.g.f. can now be obtained by averaging (1.0.4) with respect to (1.0.5) to yield

$$M_\gamma(s) = \frac{c}{\det(\mathbf{V})} \int \cdots \int_{\mathcal{D}} \prod_{k=1}^{q} \left(\frac{1}{1 + \frac{s\alpha\overline{\gamma}a^2\sigma^2\phi_k}{1+a^2\sigma^2\phi_k}} \right)^{N_S} \det(\mathbf{W}) \times \det({}_0F_1(t; \phi_i\lambda_j)) \prod_{k=1}^{q} \phi_k^{p-q} e^{-\phi_k} \, d\phi_1 ... d\phi_q \tag{1.0.8}$$

where $\mathcal{D} = \{0 < \phi_1 < \phi_2 < ... < \phi_q < \infty\}$. This multiple integral can be solved using [150, Corollary 2] to obtain

$$M_\gamma(s) = \frac{c}{\det(\mathbf{V})} \det\left(\int_0^\infty \frac{y^{p-i} \, e^{-y} \, (1 + a^2\sigma^2 y)^{N_S}}{(1 + a^2(1 + \alpha\overline{\gamma}s)\sigma^2 y)^{N_S}} \, {}_0F_1(t; y\lambda_j) \, dy \right). \tag{1.0.9}$$

Here we introduce $\mathbf{I}(s)$ as a $q \times q$ matrix with $(i,j)^{th}$ element given by,

$$(\mathbf{I}(s))_{i,j} = \int_0^\infty \frac{y^{p-i} e^{-y} (1 + a^2\sigma^2 y)^{N_S} \, {}_0F_1(t; y\lambda_j)}{(1 + a^2(1 + \alpha\overline{\gamma}s)\sigma^2 y)^{N_S}} \, dy. \tag{1.0.10}$$

We use the infinite series expansion of the ${}_0F_1(t; y\lambda_j)$ [134] and the binomial expansion to simplify (1.0.10) as

$$(\mathbf{I}(s))_{i,j} = \sum_{k=0}^{N_S} \sum_{l=0}^{\infty} \binom{N_S}{k} \frac{(a^2\sigma^2)^k \lambda_j^l}{(t)_l \Gamma(l+1)} \int_0^\infty \frac{y^{p+k+l-i} \, e^{-y}}{(1 + a^2(1 + \alpha\overline{\gamma}s)\sigma^2 y)^{N_S}} \, dy. \tag{1.0.11}$$

Finally, the m.g.f. (2.17) is obtained using [134, Eq. 3.383.5].

Appendix 2 : Proof of Corollary 2.1 and 2.2

Here, we present derivation of the m.g.f. of the SNR for the scenarios where relay-destination channel undergoes correlated Rician, and i.i.d. Rician fading.

In the correlated Rician fading scenario, $\overline{\mathbf{H}}_2$ is not a full rank matrix. Therefore, we consider $\frac{\eta^2}{\sigma^2}\overline{\mathbf{H}}_2\overline{\mathbf{H}}_2{}^H$ to have m positive eigenvalues, where $0 < m < q$. We denote $0 < \lambda_{q-m+1} < \lambda_{q-m+2} < .. < \lambda_q < \infty$ as non-zero ordered eigenvalues of $\frac{\eta^2}{\sigma^2}\overline{\mathbf{H}}_2\overline{\mathbf{H}}_2{}^H$. All other eigenvalues $\lambda_1, \lambda_2, .., \lambda_{q-m}$ are considered as zero. Thus taking the limit of m.g.f. in non-i.i.d. Rician we have,

$$M_\gamma(s)_{\text{cor}} = \lim_{\lambda_1,\lambda_2,..,\lambda_{q-m}\to 0} M_\gamma(s). \tag{2.0.1}$$

We use m.g.f. given in (1.0.9) and it gives 0/0 for the limit. Therefore we use l'H$\widehat{o}$pital rule to evaluate it. We take $(j-1)^{th}$ derivative with respect to λ_j for elements in jth column/ row of $\mathbf{I}(s)$ and $\mathbf{V}$ as in [31]. Then we evaluate limit of λ_j as it goes to zero for $j = 1, .., q-m$. This gives

$$\begin{aligned}\lim_{\lambda_j\to 0}\frac{d^{j-1}}{d\lambda_j^{j-1}}(\mathbf{I}(s))_{i,j} &= \frac{\Gamma(t)}{\Gamma(p-q+j)}\lim_{\lambda_j\to 0}\int_0^\infty {}_0F_1(p-q+j; y\lambda_j)\\ &\quad\times\frac{y^{p-i+j-1}\ e^{-y}(1+a^2\sigma^2y)^{N_S}}{(1+a^2(1+\alpha\overline{\gamma}s)\sigma^2y)^{N_S}}\ dy\\ &= \frac{\Gamma(t)}{\Gamma(p-q+j)}\int_0^\infty y^{p-i+j-1}\ e^{-y}\\ &\quad\times\frac{(1+a^2\sigma^2y)^{N_S}}{(1+a^2(1+\alpha\overline{\gamma}s)\sigma^2y)^{N_S}}\ dy.\end{aligned} \tag{2.0.2}$$

After differentiation and taking the limit as above $\det(\mathbf{V})$ becomes

$$\det(\mathbf{V}) = (-1)^{q(q-1)/2}(\lambda_{q+1-m}\lambda_{q+2-m}...\lambda_q)^{q-m}\prod_{i=m}^{q-1}\Gamma(q-i)\det(\mathbf{V}_m), \tag{2.0.3}$$

where $\mathbf{V}_m$ is $m\times m$ vandermonde matrix with its determinant given by

$$\det(\mathbf{V}_m) = \prod_{q-m<l<k}^{q}(\lambda_k-\lambda_l). \tag{2.0.4}$$

Now, we interchange the i^{th} row with the $(q-i+1)^{th}$ row for $i = 1, 2, ..., \lfloor q/2\rfloor$ in above modified determinant of $\mathbf{I}(s)$, where $\lfloor q/2\rfloor$ refers to the largest integer less

than or equal to $q/2$. This cancels $(-1)^{q(q-1)/2}$ term coming from the $\det(\mathbf{V})$. After some algebraic manipulations, we can simplify (2.0.1) as

$$M_{\gamma}(s)_{\text{cor}} = \frac{c\,\Gamma(t)^{q-m}\det(\mathbf{I}_{\text{cor}}(s))}{(\lambda_{q+1-m}\lambda_{q+2-m}...\lambda_q)^{q-m}} \times \frac{1}{\prod_{z=1}^{q-m}\Gamma(p-q+z)\prod_{r=m}^{q-1}\Gamma(q-r)}. \tag{2.0.5}$$

Here, we consider resultant determinant as $\det(\mathbf{I}_{\text{cor}}(s))$. Entries of 1^{st} to $(q-m)^{th}$ columns are given by the following expression;

$$(\mathbf{I}_{\text{cor}}(s))_{i,j} = \int_0^{\infty} \frac{y^{p-q+i+j}\ e^{-y}\ (1+a^2\sigma^2 y)^{N_S}}{(1+a^2(1+\alpha\overline{\gamma}s)\sigma^2 y)^{N_S}} dy. \tag{2.0.6}$$

Entries of $(q-m+1)^{th}$ to q^{th} columns are given by

$$(\mathbf{I}_{\text{cor}}(s))_{i,j} = \int_0^{\infty} \frac{y^{p-q+i-1}e^{-y}(1+a^2\sigma^2 y)^{N_S}\ {}_0F_1(t;y\lambda_j)}{(1+a^2(1+\alpha\overline{\gamma}s)\sigma^2 y)^{N_S}} dy. \tag{2.0.7}$$

These can be further simplified to give (2.20).

In the i.i.d. Rician scenario, entries of $\overline{\mathbf{H}}_2$ are identical. Therefore, only one eigenvalue is non-zero in $\frac{\eta^2}{\sigma^2}\overline{\mathbf{H}}_2\overline{\mathbf{H}}_2{}^H$. We consider λ_q as the non-zero eigenvalue. Thus taking the limit of m.g.f. in non-i.i.d. Rician we have,

$$M_{\gamma}(s)_{\text{iid}} = \lim_{\lambda_1,\lambda_2,..,\lambda_{q-1}\to 0} M_{\gamma}(s). \tag{2.0.8}$$

We use a similar method as in the previous derivation. Here, $m=1$ and after differentiation and taking the limit as above $\det(\mathbf{V})$ becomes

$$\det(\mathbf{V}) = (-1)^{q(q-1)/2}\lambda_q^{q-1}\prod_{i=1}^{q-1}\Gamma(q-i). \tag{2.0.9}$$

After some algebraic manipulations and interchanging rows as in the previous proof, we can simplify (2.0.8) as

$$M_{\gamma}(s)_{\text{iid}} = \frac{c\,\Gamma(t)^{q-1}\det(\mathbf{I}_{\text{iid}}(s))}{\lambda_q^{q-1}\prod_{m=1}^{q-1}\Gamma(p-q+m)\Gamma(q-m)}. \tag{2.0.10}$$

Here, we consider resultant determinant as $\det(\mathbf{I}_{\text{iid}}(s))$. The column entries of $\det(\mathbf{I}_{\text{iid}}(s))$ are the same as the entries of the $\det(\mathbf{I}_{\text{cor}}(s))$ with $m=1$. This can be further simplified to give (2.21). A similar procedure is valid for Rayleigh scenario.

Appendix 3 : Proof of Theorem 2.2

Since we have the expression for m.g.f., the following relationship for the moments of the SNR γ can be used,

$$m_n = \mathcal{E}\{\gamma^n\} = (-1)^n \frac{d^n}{ds^n}(M_\gamma(s)) \mid_{s=o} . \tag{3.0.1}$$

Prior to taking the derivative of the m.g.f., we consider a property of the determinant differentiation as follows. Let $\mathbf{\Omega}$ be a matrix that has entries with variable x. We denote the determinant of $\mathbf{\Omega}$ as

$$\det(\mathbf{\Omega}) = d(\boldsymbol{\omega}_1, \boldsymbol{\omega}_2, ..., \boldsymbol{\omega}_n). \tag{3.0.2}$$

where $\boldsymbol{\omega}_j$ can be either jth column or row. The first differentiations give n number of determinants as shown below

$$\frac{d}{dx}\det(\mathbf{\Omega}) = d(\boldsymbol{\omega}_1', \boldsymbol{\omega}_2, ..., \boldsymbol{\omega}_n) + d(\boldsymbol{\omega}_1, \boldsymbol{\omega}_2', ..., \boldsymbol{\omega}_n) + .. + d(\boldsymbol{\omega}_1, \boldsymbol{\omega}_2, ..., \boldsymbol{\omega}_n'), \tag{3.0.3}$$

where $\boldsymbol{\omega}_j'$ denotes the jth row/column differentiated with respect to x. Therefore, the first derivative of a determinant results in a sum of determinants. When all columns are variables of x, this provides n number of determinants. For the second derivative the same principle is valid and we can have a summation with maximum of n^2 determinants. We use this property to prove the following. First moment of the SNR is

$$\begin{aligned} m_1 &= -\frac{d}{ds}(M_\gamma(s))|_{s=o} \\ &= \frac{-\ e^{-\mathrm{tr}(\mathbf{\Lambda})}}{(\Gamma(t))^q}\frac{d}{ds}\det\left(\int_0^\infty \frac{y^{p-i}\ e^{-y}\ (1+a^2\sigma^2 y)^{N_S}}{(1+a^2(1+\alpha\overline{\gamma}s)\sigma^2 y)^{N_S}}\ {}_0F_1(t; y\lambda_j)\ \ dy\right)|_{s=o}\ \ . \end{aligned}$$

This can be expanded with the sum of determinants $\mathbf{I}(k)$ where k represents the kth column subjected to the differentiation. In $\mathbf{I}(k)$, k^{th} column entries can be found as below

$$\begin{aligned} &\frac{d}{ds}\int_0^\infty \frac{y^{p-i}\ e^{-y}\ (1+a^2\sigma^2 y)^{N_S}}{(1+a^2(1+\alpha\overline{\gamma}s)\sigma^2 y)^{N_S}}\ {}_0F_1(t; y\lambda_k)\ dy \\ &= \int_0^\infty \frac{-N_S a^2\sigma^2\alpha\ \overline{\gamma} y^{p-i+1}e^{-y}}{(1+a^2(1+\alpha\overline{\gamma}s)\sigma^2 y)^{N_S+1}}(1+a^2\sigma^2 y)^{N_S}\ {}_0F_1(t; y\lambda_k)dy\ . \end{aligned} \tag{3.0.4}$$

Applying $s = 0$ reduces above expression into

$$\int_0^{\infty} \frac{-N_S a^2\sigma^2\alpha\overline{\gamma} y^{p-i+1} e^{-y}\ {}_0F_1(t; y\lambda_k)}{(1+a^2\sigma^2 y)}\, dy$$
$$= -N_S a^2\sigma^2\alpha\overline{\gamma} \sum_{l=0}^{\infty} \frac{\lambda_k^l\ \Gamma(p+l-i+2)}{(t)_l\ l!\ (a^2\sigma^2)^{p+l-i+2}} U\big(p+l-i+2; p+l-i+2; \frac{1}{a^2\sigma^2}\big). \tag{3.0.5}$$

All other column entries ($j = 1, 2, 3, ..q : j \neq k$) are obtained by putting $s = 0$ to (1.0.10)

$$\int_0^{\infty} y^{p-i} e^{-y}\ {}_0F_1(t; y\lambda_j)\, dy = \Gamma(p-i+1)\ {}_1F_1(p-i+1; t; \lambda_j).$$

Therefore, $\det(\mathbf{I}(k))$ entries satisfy (2.22). We can obtain the second moment of the SNR given in (2.23) using the second derivative and proceed with the similar steps.

Appendix 4 : Proof of Theorem 2.4 and 2.5

4.1 Probability density function

Exact probability density of the SNR γ is derived by inverse Laplace transformation. We start by inverting (1.0.4) to obtain the conditional p.d.f. as

$$f_{\gamma|\mathbf{\Phi}}(\gamma) = \mathcal{L}^{-1}\left\{M_{\gamma|\mathbf{\Phi}}(s)\right\} = \mathcal{L}^{-1}\left\{\left(1+\frac{s\alpha\overline{\gamma}a^2\sigma^2\phi}{1+a^2\sigma^2\phi}\right)^{-N_S}\right\} \tag{4.1.1}$$

where $\mathcal{L}^{-1}$ denotes the inverse Laplace transform operator. We can evaluate this inverse transform as

$$\mathcal{L}^{-1}\left\{M_{\gamma|\mathbf{\Phi}}(s)\right\} = \frac{\gamma^{N_S-1}e^{-\frac{\gamma}{\alpha\overline{\gamma}}}(1+a^2\sigma^2\phi)^{N_S}e^{\frac{-\gamma}{\alpha a^2\sigma^2\phi\overline{\gamma}}}}{\Gamma(N_S)(\alpha\overline{\gamma}\sigma^2a^2)^{N_S}\phi^{N_S}}. \tag{4.1.2}$$

We use density of ϕ to evaluate the $f_\gamma(\gamma)$ from $f_{\gamma|\mathbf{\Phi}}(\gamma)$. The p.d.f. of ϕ from (1.0.5) is given as

$$h_\phi(\phi) = \frac{e^{-\lambda}}{\Gamma(p)}\ {}_0F_1(p;\phi\lambda)\ \phi^{p-1}e^{-\phi} \tag{4.1.3}$$

By integrating with the p.d.f. of ϕ

$$\begin{aligned} f_\gamma(\gamma) =& \frac{e^{-\lambda}\gamma^{N_S-1}e^{-\frac{\gamma}{\alpha\overline{\gamma}}}}{\Gamma(p)\Gamma(N_S)(\alpha\overline{\gamma}\sigma^2a^2)^{N_S}}\int_0^\infty \frac{y^{p-1}e^{-y}}{y^{N_S}} \\ & \times\ {}_0F_1(p;y\lambda)\ (1+a^2\sigma^2y)^{N_S}e^{\frac{-\gamma}{\alpha a^2\sigma^2y\overline{\gamma}}}\ dy. \end{aligned} \tag{4.1.4}$$

Next, we expand $(1+a^2\sigma^2y)^{N_S}$ using the binomial theorem to yield

$$\begin{aligned} f_\gamma(\gamma) =& \frac{e^{-\lambda}\gamma^{N_S-1}e^{-\frac{\gamma}{\alpha\overline{\gamma}}}}{\Gamma(p)\Gamma(N_S)(\alpha\overline{\gamma}\sigma^2a^2)^{N_S}}\sum_{j=0}^{N_S}(a^2\sigma^2)^j \\ & \times\int_0^\infty y^{p-1-N_S+j}e^{\left(-y-\frac{\gamma}{\alpha a^2\sigma^2y\overline{\gamma}}\right)}\ {}_0F_1(p;y\lambda)dy. \end{aligned} \tag{4.1.5}$$

Now we can write the integral with the infinite series expansion of ${}_0F_1(p;y\lambda)$ as

$$\begin{aligned} f_\gamma(\gamma) =& \frac{e^{-\lambda}\gamma^{N_S-1}e^{-\frac{\gamma}{\alpha\overline{\gamma}}}}{\Gamma(p)\Gamma(N_S)(\alpha\overline{\gamma}\sigma^2a^2)^{N_S}}\sum_{j=0}^{N_S}(a^2\sigma^2)^j\int_0^\infty y^{p-1-N_S+j} \\ & \times e^{\left(-y-\frac{\gamma}{\alpha a^2\sigma^2y\overline{\gamma}}\right)}\sum_{l=0}^{\infty}\frac{y^l\lambda^l}{(p)_l\Gamma(l+1)}\ dy\ . \end{aligned} \tag{4.1.6}$$

After taking out the infinite summation from the integral and taking $r = p + l + j - N_S$ gives

$$f_\gamma(\gamma) = \frac{e^{-\lambda}\gamma^{N_S-1}e^{-\frac{\gamma}{\alpha\overline{\gamma}}}}{\Gamma(p)\Gamma(N_S)(\alpha\overline{\gamma}\sigma^2a^2)^{N_S}}\sum_{j=0}^{N_S}(a^2\sigma^2)^j \times \sum_{l=0}^{\infty}\frac{\lambda^l}{(p)_l\Gamma(l+1)}\int_0^\infty y^{r-1}e^{\left(-y-\frac{\gamma}{\alpha a^2\sigma^2 y\overline{\gamma}}\right)}\,dy. \tag{4.1.7}$$

This integral can be solved using [134, Eq. 3.478.4] to obtain (2.24).

4.2 Cumulative distributive function

From the definition,

$$F(\gamma) = \int_0^\gamma f_\gamma(x)dx = \int_{\mathbf{\Phi}} f_{\mathbf{\Phi}}(\mathbf{\Phi})\int_0^\gamma f_{\gamma|\mathbf{\Phi}}(x)\,dxd\mathbf{\Phi}. \tag{4.2.1}$$

This can be rewritten with the conditional m.g.f. as

$$F(\gamma) = \int_{\mathbf{\Phi}} f_{\mathbf{\Phi}}(\mathbf{\Phi})\mathcal{L}^{-1}\left\{\frac{M_{\gamma|\mathbf{\Phi}}(s)}{s}\right\}\,d\mathbf{\Phi}. \tag{4.2.2}$$

We consider the case $q = 1$ and have

$$\begin{aligned}\mathcal{L}^{-1}\left\{\frac{M_{\gamma|\mathbf{\Phi}}(s)}{s}\right\} &= \mathcal{L}^{-1}\left\{\frac{1}{s\left(1+\frac{\alpha a^2\sigma^2\overline{\gamma}\phi}{1+a^2\sigma^2\phi}\right)^{N_S}}\right\} \\ &= 1 - e^{-\frac{\gamma}{\alpha\overline{\gamma}}\left(1+\frac{1}{1+a^2\sigma^2\phi}\right)}\sum_{k=0}^{N_S-1}\frac{\gamma^k}{k!\alpha^k\overline{\gamma}^k} \\ &\quad\times\left(1+\frac{1}{1+a^2\sigma^2\phi}\right)^k\end{aligned} \tag{4.2.3}$$

We use density of ϕ (4.1.3) and (4.2.3) to simplify (4.2.2). After some algebraic manipulations (4.2.2) gives

$$F(\gamma) = 1 - \frac{e^{-\left(\lambda+\frac{\gamma}{\alpha\overline{\gamma}}\right)}}{\Gamma(p)}\sum_{k=0}^{N_S-1}\sum_{i=0}^{k}\frac{\binom{k}{i}\gamma^k}{k!\alpha^k\overline{\gamma}^k a^{2i}\sigma^{2i}}\int_0^\infty \phi^{p-i-1} \times e^{\left(-\phi-\frac{\gamma}{\alpha a^2\sigma^2\overline{\gamma}\phi}\right)}\,{}_0F_1(p;\phi\lambda)\;\;d\phi. \tag{4.2.4}$$

Finally, with more algebraic manipulations as used in p.d.f case, we obtain (2.26).

Appendix 5 : Proof of Theorem 2.6

As described in Section 2.3.2, the asymptotic expression of the m.g.f. of y, where $y = \alpha\tilde{a}^2 \mathrm{Tr}(\mathbf{H}_1^H \mathbf{H}_2^H \tilde{\mathbf{K}}^{-1} \mathbf{H}_2 \mathbf{H}_1)$, is used to find diversity order and array gain.

5.1 Derivation for $q = 1$

The m.g.f. of y can be obtained following similar steps as in Appendix 1. For $q = 1$, the m.g.f. is given by,

$$\begin{aligned} M_y(s) =& \frac{e^{-\lambda}}{\Gamma(p)} \sum_{k=0}^{N_S} \sum_{l=0}^{\infty} \frac{\binom{N_S}{k} a^{2k} \sigma^{2k} \lambda^l \ \Gamma(p+k+l)}{(p)_l \ l! \ (a^2\sigma^2(1+\alpha s))^{p+k+l}} \\ & \times U\left(p+k+l; p+k+l+1-N_S; \frac{1/a^2\sigma^2}{1+\alpha s}\right). \end{aligned} \tag{5.1.1}$$

By applying asymptotic properties of confluent hypergeometric function of the second kind [151], we have

$$U\left(p+k+l; p+k+l+1-N_S; \frac{1/a^2\sigma^2}{1+\alpha s}\right) \approx$$

$$\begin{cases} \frac{\Gamma(p+k+l-N_S)}{\Gamma(p+k+l)} \left(\frac{1}{a^2\sigma^2(1+\alpha s)}\right)^{1-(p+k+l-N_S)} & \text{if } \ p+k+l \geq N_S+1 \\ \frac{-1}{\Gamma(p+k+l)} \left(\ln\left(\frac{1}{a^2\sigma^2(1+\alpha s)}\right) + \psi(p+k+l)\right) & \text{if } \ p+k+l = N_S \\ \frac{\Gamma(-(p+k+l-N_S))}{\Gamma(N_S)} & \text{if } \ p+k+l \leq N_S-1, \end{cases} \tag{5.1.2}$$

where $\psi(\cdot)$ is the digamma function.
First, we consider the case $p > N_S$, the expression (5.1.1) becomes

$$M_y(s) = \frac{e^{-\lambda}}{\Gamma(p)} \sum_{k=0}^{N_S} \sum_{l=0}^{\infty} \frac{\binom{N_S}{k} (a^2\sigma^2)^k \lambda^l \ \Gamma(p+k+l-N_S)}{(p)_l \ l! \ (a^2\sigma^2)^{N_S} (1+\alpha s)^{N_S}}. \tag{5.1.3}$$

When $s \to \infty$, we use the approximation $(1+\alpha s))^{N_S} \approx \alpha^{N_S} s^{N_S}$. Therefore, the asymptotic expansion of the m.g.f. of y is obtained as

$$M_y(s) = \frac{e^{-\lambda}}{\Gamma(p)} \sum_{k=0}^{N_S} \sum_{l=0}^{\infty} \frac{\binom{N_S}{k} (a^2\sigma^2)^k \lambda^l \ \Gamma(p+k+l-N_S)}{(p)_l \ l! \ (a^2\sigma^2)^{N_S} \alpha^{N_S} s^{N_S}}. \tag{5.1.4}$$

Next, we consider $p < N_S$. By expanding the summation (5.1.1) over k and l, we can see that the lowest exponent of $\frac{1}{s}$ is given for the term $k = 0$ and $l = 0$. Therefore, the asymptotic expansion of the m.g.f. for $p < N_S$ is obtained as

$$M_y(s) \approx \frac{e^{-\lambda}\Gamma(N_S - p)}{p\Gamma(N_S)(a^2\sigma^2)^p\alpha^p s^p}. \tag{5.1.5}$$

The expressions (5.1.4) and (5.1.5) satisfies the expressions (2.35)-(2.37)

5.2 Derivation for $q = 2$

For $q = 2$ the m.g.f. of y is given by

$$\begin{aligned} M_\gamma(s) =& \frac{e^{-(\lambda_1+\lambda_2)}}{(\Gamma(p-1))^2(\lambda_1+\lambda_2)} \sum_{k=0}^{N_S}\sum_{l=0}^{\infty}\sum_{m=0}^{N_S}\sum_{n=0}^{\infty} \frac{\binom{N_S}{k}\binom{N_S}{m}(a^2\sigma^2)^{k+m}\Gamma(p+k+l)}{(p-1)_l(p-1)_n l!n!} \\ &\times \frac{\Gamma(p+m+n-1)U\left(p+k+l; p+k+l+1-N_S; \frac{1/a^2\sigma^2}{1+\alpha s}\right)}{(a^2\sigma^2(1+\alpha s))^{2p+k+m+n+l-1}} \\ &\times U\left(p+m+n-1; p+m+n-N_S; \frac{1/a^2\sigma^2}{1+\alpha s}\right)(\lambda_1^l\lambda_2^n - \lambda_2^l\lambda_1^n) \end{aligned} \tag{5.2.1}$$

As in the earlier scenario, we use asymptotic properties of confluent hypergeometric function of the second kind to discuss cases for $p < N_S - 1$, $p = N_S$, and $p > N_S + 1$. The procedure to find asymptotic m.g.f. follows the similar steps and is therefore omitted.

Appendix 6 : Existence of a global solution of PNC based joint design

The optimization problem $\mathcal{A}$ is given as

$$\begin{aligned} \min_{\mathbf{F}_1,\mathbf{F}_2,\mathbf{G}} \quad & \mathcal{E}_{\mathbf{E}}\{\mathrm{WMSE}_m[\mathbf{F}_1,\mathbf{F}_2,\mathbf{G}]\} \\ \text{subject to} \quad & \mathrm{Tr}(\mathbf{F}_1\mathbf{F}_1^H+\mathbf{F}_2\mathbf{F}_2^H)\leq \mathrm{P_T}. \end{aligned} \tag{6.0.1}$$

An optimization problem with several variables can always be minimized by first minimizing over some of the variables, and then minimizing over the remaining ones [142, p.133, Sec. 4.1.3]. Therefore, (6.0.1) can be reformulated as follows,

$$\min_{\mathbf{F}_1,\mathbf{F}_2\in\ \mathfrak{F}} \quad \min_{\mathbf{G}=f(\mathbf{F}_1,\mathbf{F}_2)} \quad \mathcal{E}_{\mathbf{E}}\{\mathrm{WMSE}_m\big[\mathbf{F}_1,\mathbf{F}_2,\mathbf{G}\big]\}, \tag{6.0.2}$$

where $\mathbf{G}=f(\mathbf{F}_1,\mathbf{F}_2)$ is a function of $\mathbf{F}_1$ and $\mathbf{F}_2$, and $\mathfrak{F}=\{(\mathbf{F}_1,\mathbf{F}_2)\mid \mathrm{Tr}(\mathbf{F}_1\mathbf{F}_1^H+\mathbf{F}_2\mathbf{F}_2^H)\leq \mathrm{P_T}\}$. The inner optimization in problem (6.0.2) has no constraints and the solution for $f(\mathbf{F}_1,\mathbf{F}_2)$ can be obtained as

$$\begin{aligned} f(\mathbf{F}_1,\mathbf{F}_2)=&(\mathbf{F}_1^H\bar{\mathbf{H}}_{m1}^H+\mathbf{F}_2^H\bar{\mathbf{H}}_{m2}^H)(\bar{\mathbf{H}}_{m1}\mathbf{F}_1\mathbf{F}_1^H\bar{\mathbf{H}}_{m1}^H+\bar{\mathbf{H}}_{m2}\mathbf{F}_2\mathbf{F}_2^H\bar{\mathbf{H}}_{m2}^H \\ &+\mathrm{Tr}(\sigma_1^2\mathbf{Q}_1+\sigma_2^2\mathbf{Q}_2)\mathbf{R}_r+\sigma^2\mathbf{I}_N)^{-1}. \end{aligned} \tag{6.0.3}$$

Then, we can replace $\mathbf{G}$ with this and the final objective function has variables $\mathbf{F}_1$ and $\mathbf{F}_2$,

$$\min_{\mathbf{F}_1,\mathbf{F}_2\in\ \mathfrak{F}} \mathcal{E}_{\mathbf{E}}\{\mathrm{WMSE}_m[\mathbf{F}_1,\mathbf{F}_2]\}, \tag{6.0.4}$$

where

$$\begin{aligned} \mathcal{E}_{\mathbf{E}}\{\mathrm{WMSE}_m\}=&\sum_{i=1}^{2}\Big(\mathrm{Tr}\big(\mathbf{W}f(\mathbf{F}_1,\mathbf{F}_2)\bar{\mathbf{H}}_{mi}\mathbf{F}_i\mathbf{F}_i^H\bar{\mathbf{H}}_{mi}^H f(\mathbf{F}_1,\mathbf{F}_2)^H \\ &-\mathbf{W}f(\mathbf{F}_1,\mathbf{F}_2)\bar{\mathbf{H}}_{mi}\mathbf{F}_i-\mathbf{W}\mathbf{F}_i^H\bar{\mathbf{H}}_{mi}^H f(\mathbf{F}_1,\mathbf{F}_2)^H\big) \\ &+\mathrm{Tr}(\mathbf{Q}_i)\mathrm{Tr}(\mathbf{P}_i)\Big)+\mathrm{Tr}(2\mathbf{W}+\sigma^2\mathbf{W}f(\mathbf{F}_1,\mathbf{F}_2)f(\mathbf{F}_1,\mathbf{F}_2)^H) \end{aligned} \tag{6.0.5}$$

It can be find that the feasible set ($\mathfrak{F}$) of the optimization problem (6.0.4) is closed and bounded as in [142, p.30, Sec. 2.2.3]. From [152, p.653, A.6 (g)],

we can argue that the feasible set is compact. The objective function (6.0.5) is continuous at all points of the feasible set. From all these facts, and according to the theorem [152, p.654, A.8], there exists a global minimum for the problem (6.0.4).

Finally, according to [142, p.130, Sec. 4.1.3], the original problem (6.0.1) has a global minimum. It can be proved that if $(\mathbf{F}_1; \mathbf{F}_2; \mathbf{G})$ provides optimum precoders and decoder, so is $(\mathbf{F}_1\mathbf{U}; \mathbf{F}_2\mathbf{U}; \mathbf{U}^H\mathbf{G})$, where $\mathbf{U}$ is a unitary matrix. Therefore, the solution presented here is only up to a unitary matrix. However, the global minimum is the same for all these unitary transforms, and do not have an impact on the performance of the system.

A similar procedure is valid to show the existence of global minimum for the modified problems $\mathcal{B}$.

Appendix 7 : Algorithm to find optimum $\mathbf{F}$ and $\mathbf{G}$

Here, we consider an algorithm to solve modified problem (4.38), when $\mathbf{F}_I$ is fixed. This is non-convex in $(\mathbf{F};\mathbf{G})$. However, as we showed in the Appendix 6, this also has a global minimum.

Objective function and constraints are continuously differentiable functions, and by [152, Proposition 3.3.1], optimal solutions should satisfy Karush-Kuhn-Tucker (KKT) necessary conditions for optimality. Therefore, we write the Lagrangian for the optimization problem as

$$\begin{aligned}\Lambda(\mathbf{F},\mathbf{G},\mu_1,\mu_2) = \mathrm{Tr}\Big((\mathbf{GHF}-\mathbf{I}_N)(\mathbf{GHF}-\mathbf{I}_N)^H + (\mathbf{GH}_{ic}\mathbf{F}_I)(\mathbf{GH}_{ic}\mathbf{F}_I)^H \\ + \sigma^2\mathbf{GG}^H\Big) + \mu_1\big(\mathrm{Tr}(\mathbf{H}_{og}\mathbf{FF}^H\mathbf{H}_{og}^H) - \mathrm{I_{th}}\big) \\ + \mu_2\big(\mathrm{Tr}(\mathbf{FF}^H) - \mathrm{P_{max}}\big),\end{aligned} \tag{7.0.1}$$

where, μ_1 and μ_2 are dual variables associated with inequalities. Since KKT conditions are necessary and sufficient to solve this optimally, these can be obtained as

$$\mathbf{HF} = \mathbf{HFF}^H\mathbf{H}^H\mathbf{G}^H + \mathbf{H}_{ic}\mathbf{F}_i\mathbf{F}_i^H\mathbf{H}_{ic}^H\mathbf{G}^H + \sigma^2\mathbf{G}^H, \tag{7.0.2}$$

$$\mathbf{GH} = \mathbf{F}^H\mathbf{H}^H\mathbf{G}^H\mathbf{GH} + \mu_1\mathbf{F}^H\mathbf{H}_{og}^H\mathbf{H}_{og} + \mu_2\mathbf{F}^H, \tag{7.0.3}$$

$$\mu_1 \geq 0 \quad , \ \mu_1\big(\mathrm{Tr}(\mathbf{H}_{og}\mathbf{FF}^H\mathbf{H}_{og}^H) - \mathrm{I_{th}}\big) = 0, \tag{7.0.4}$$

$$\mu_2 \geq 0 \quad , \ \mu_2\big(\mathrm{Tr}(\mathbf{FF}^H) - \mathrm{P_{max}}\big) = 0. \tag{7.0.5}$$

Both $\mathbf{G}$ and $\mathbf{F}$ equal to zero satisfies these conditions. However, our intention is to find non-zero solutions for optimum $\mathbf{G}$ and $\mathbf{F}$. We can identify following cases for μ_1 and μ_2 to solve these KKT conditions.

Case 1 : $\mu_1 = 0$ *and* $\mu_2 > 0$

Non-zero solution of $\mathbf{G}$ can be obtained from (7.0.2) as

$$\mathbf{G} = \mathbf{F}^H\mathbf{H}^H\big(\mathbf{HFF}^H\mathbf{H}^H + \mathbf{R}\big)^{-1}, \tag{7.0.6}$$

where $\mathbf{R} = \mathbf{H}_{ic}\mathbf{F}_I\mathbf{F}_I^H\mathbf{H}_{ic}^H + \sigma^2\mathbf{I}_N$. We assume all matrices to be non-singular, therefore, inverses exist. Then, (7.0.3) can be reformulated by substituting

(7.0.6) as

$$\mathbf{F}^H(\mathbf{F}\mathbf{F}^H + \mathbf{H}^H\mathbf{R}^{-1}\mathbf{H})^{-1} = \mathbf{F}^H(\mathbf{F}\mathbf{F}^H + \mathbf{H}^H\mathbf{R}^{-1}\mathbf{H})^{-1}\mathbf{F}\mathbf{F}^H(\mathbf{F}\mathbf{F}^H + \mathbf{H}^H\mathbf{R}^{-1}\mathbf{H})^{-1} + \mu_2\mathbf{F}^H. \tag{7.0.7}$$

Next, by taking the eigenvalue decomposition $\mathbf{H}^H\mathbf{R}^{-1}\mathbf{H} = \mathbf{V}_1\mathbf{\Lambda}_1\mathbf{V}_1^H$, where $\mathbf{V}_1 \in \mathbb{C}^{N\times N}$ is a unitary matrix, and $\mathbf{\Lambda}_1$ is a $N \times N$ diagonal matrix $\mathbf{\Lambda}_1 = \text{diag}\{\lambda_{11}, .., \lambda_{1N}\}$. We further simplify (7.0.7) into

$$\mathbf{V}_1\mathbf{\Lambda}_1^{-1}\mathbf{V}_1^H = \mu_2(\mathbf{F}\mathbf{F}^H + \mathbf{V}_1\mathbf{\Lambda}^{-1}\mathbf{V}_1^H)(\mathbf{F}\mathbf{F}^H + \mathbf{V}_1\mathbf{\Lambda}_1^{-1}\mathbf{V}_1^H). \tag{7.0.8}$$

Further simplification gives $\mathbf{\Lambda}_1^{-1} = \mu_2(\mathbf{V}_1^H\mathbf{F}\mathbf{F}^H\mathbf{V}_1 + \mathbf{\Lambda}_1^{-1})^2$. Here, it can be seen that the $\mathbf{V}_1^H\mathbf{F}\mathbf{F}^H\mathbf{V}_1 + \mathbf{\Lambda}_1^{-1}$ should be diagonal. We can also argue that the unitary transformation of $\mathbf{F}$ also satisfies this relationship, i.e., $\mathbf{V}_1^H\mathbf{F}\mathbf{U}\mathbf{U}^H\mathbf{F}^H\mathbf{V}_1 + \mathbf{\Lambda}_1^{-1}$ will also be diagonal. Therefore, without loss of generality we consider $\mathbf{V}^H\mathbf{F}$ as diagonal, and the optimum solution of $\mathbf{F}$ is given by

$$\mathbf{F} = \mathbf{V}_1(\mu_2^{-\frac{1}{2}}\mathbf{\Lambda}_1^{-\frac{1}{2}} - \mathbf{\Lambda}_1^{-1})^{\frac{1}{2}}. \tag{7.0.9}$$

To find optimum $\mathbf{G}$, we substitute (7.0.9) in (7.0.6),

$$\mathbf{G} = \mu_2^{\frac{1}{2}}\mathbf{\Lambda}_1^{\frac{1}{2}}(\mu_2^{-\frac{1}{2}}\mathbf{\Lambda}_1^{-\frac{1}{2}} - \mathbf{\Lambda}_1^{-1})^{\frac{1}{2}}\mathbf{\Lambda}_1^{-1}\mathbf{V}_1^H\mathbf{H}^H\mathbf{R}^{-1}. \tag{7.0.10}$$

Optimum μ_2 can be found by substituting optimum $\mathbf{F}$ (7.0.9) into (7.0.5),

$$\mu_2 = \left(\frac{\text{Tr}(\mathbf{\Lambda}_1^{-\frac{1}{2}})}{\text{P}_{\max} + \text{Tr}(\mathbf{\Lambda}_1^{-1})}\right)^2. \tag{7.0.11}$$

Case 2 : $\mu_1 > 0$ ***and*** $\mu_2 = 0$

We can simplify (7.0.3) by substituting (7.0.6), which gives

$$\mathbf{H}_{og}^{-H}\mathbf{H}^H(\mathbf{H}\mathbf{F}\mathbf{F}^H\mathbf{H}^H + \mathbf{R})^{-1}\mathbf{H}\mathbf{H}_{og}^{-1} = \mathbf{H}_{og}^{-H}\mathbf{H}^H(\mathbf{H}\mathbf{F}\mathbf{F}^H\mathbf{H}^H + \mathbf{R})^{-1}\mathbf{H}\mathbf{F}\mathbf{F}^H\mathbf{H}^H(\mathbf{H}\mathbf{F}\mathbf{F}^H + \mathbf{R})^{-1}\mathbf{H}\mathbf{H}_{og}^{-1} + \mu_1\mathbf{I}_N. \tag{7.0.12}$$

Next, we consider eigenvalue decomposition $\mathbf{H}_{og}^{-H}\mathbf{H}^H\mathbf{R}^{-1}\mathbf{H}\mathbf{H}_{og}^{-1} = \mathbf{V}_2\mathbf{\Lambda}_2\mathbf{V}_2^H$, where $\mathbf{V}_2 \in \mathbb{C}^{N\times N}$ is a unitary matrix, and $\mathbf{\Lambda}_2$ is a $N \times N$ diagonal matrix

$\mathbf{\Lambda}_2 = \text{diag}\{\lambda_{21}, .., \lambda_{2N}\}$. The simplified expression is given by

$$\mathbf{V}_2\mathbf{\Lambda}_2^{-1}\mathbf{V}_2^H = \mu_1(\mathbf{H}_{og}\mathbf{F}\mathbf{F}^H\mathbf{H}_{og}^H + \mathbf{V}_2\mathbf{\Lambda}_2\mathbf{V}_2^H)(\mathbf{H}_{og}\mathbf{F}\mathbf{F}^H\mathbf{H}_{og}^H + \mathbf{V}_2\mathbf{\Lambda}_2\mathbf{V}_2^H). \tag{7.0.13}$$

Further simplification gives $\mathbf{\Lambda}_2^{-1} = \mu_1(\mathbf{V}_2^H\mathbf{H}_{og}\mathbf{F}\mathbf{F}^H\mathbf{H}_{og}^H\mathbf{V}_2 + \mathbf{\Lambda}_2^{-1})^2$. We can see that the $\mathbf{V}_2^H\mathbf{H}_{og}\mathbf{F}\mathbf{F}^H\mathbf{H}_{og}^H\mathbf{V}_2 + \mathbf{\Lambda}_2^{-1}$ should be diagonal. As with the previous case, without loss of generality we consider $\mathbf{V}_2^H\mathbf{H}_{og}\mathbf{F}$ as diagonal, and the optimum solution of $\mathbf{F}$ is given by

$$\mathbf{F} = \mathbf{H}_{og}^{-1}\mathbf{V}_2(\mu_1^{-\frac{1}{2}}\mathbf{\Lambda}_2^{-\frac{1}{2}} - \mathbf{\Lambda}_2^{-1})^{\frac{1}{2}}. \tag{7.0.14}$$

To find optimum $\mathbf{G}$, we substitute (7.0.14) in (7.0.6)

$$\mathbf{G} = \mu_1^{\frac{1}{2}}(\mu_1^{-\frac{1}{2}}\mathbf{\Lambda}_2^{-\frac{1}{2}} - \mathbf{\Lambda}_2^{-1})^{\frac{1}{2}}\mathbf{V}_2^H\mathbf{H}_{og}^{-1}\mathbf{\Lambda}_2^{\frac{1}{2}}\mathbf{H}_{og}\mathbf{H}^{-1}. \tag{7.0.15}$$

Optimum μ_1 is obtained by substituting optimum $\mathbf{F}$ (7.0.14) into (7.0.4).

$$\mu_1 = \left(\frac{\text{Tr}(\mathbf{\Lambda}_2^{-\frac{1}{2}})}{\text{I}_{\text{th}} + \text{Tr}(\mathbf{\Lambda}_2^{-1})}\right)^2 \tag{7.0.16}$$

Algorithm 7.0.1 Optimum joint design for $\mathbf{F}$ and $\mathbf{G}$

Channel state information is available. Information about N, $\text{P}_{\max}$, I_{th}, and σ^2 is available.

1: **initialize/ update** : Initialize $\mathbf{L}_k = \sqrt{(\text{P}_{\max}/N)}\mathbf{I}_N$, $\mathbf{M}_k = \mathbf{I}_N$, $(k = 1, 2)$. Update precoder $\mathbf{F}_I$.
2: Perform eigenvalue decomposition of $\mathbf{H}^H\mathbf{R}^{-1}\mathbf{H}$, and obtain μ_2 by (7.0.11).
3: $\mathbf{L}_1$ obtain from (7.0.9), and $\mathbf{M}_1$ obtain from (7.0.10). Find $\text{MSE}_1^{\text{dir}}[\mathbf{L}_1, \mathbf{M}_1]$ from (4.39).
4: Perform eigenvalue decomposition of $\mathbf{H}_{og}^{-H}\mathbf{H}^H\mathbf{R}^{-1}\mathbf{H}\mathbf{H}_{og}^{-1}$, and obtain μ_1 by (7.0.16).
5: $\mathbf{L}_2$ is obtained by (7.0.14), and $\mathbf{M}_2$ is obtained by (7.0.15). Find $\text{MSE}_2^{\text{dir}}[\mathbf{L}_2, \mathbf{M}_2]$ from (4.39).
6: $k^* = \text{Arg}_k \min(\text{MSE}_1^{\text{dir}}, \text{MSE}_2^{\text{dir}})$.
7: Update $\mathbf{F} = \mathbf{L}_{k^*}$ and $\mathbf{G} = \mathbf{M}_{k^*}$.

Case 3 : $\mu_1 \neq 0$ ***and*** $\mu_2 \neq 0$

Here, both inequality constraints need to be satisfied with equality in a given channel instance. This happens only when $\mathbf{H}_{og} = \mathbf{I}_N$, which is not practical. Therefore, both μ_1 and μ_2 cannot be greater than zero, and at least one dual variable has to be zero in a given time.

Case 4 : $\mu_1 = 0$ ***and*** $\mu_2 = 0$

This provides $\mathbf{F} = 0$ and $\mathbf{G} = 0$ as the only optimum solution. Our focus was to find non-zero solutions, therefore, case 4 does not exist.

With these observations, one dual variable should be equal to zero, and other one should be non-zero in a given channel instance. Algorithm 7.0.1 can be used to find the optimum $\mathbf{F}$ and $\mathbf{G}$ considering all scenarios.

Book orders:
Granum: Virtual book store
http://granum.uta.fi/granum/

UNIVERSITY OF OULU P.O. Box 8000 FI-90014 UNIVERSITY OF OULU FINLAND

ACTA UNIVERSITATIS OULUENSIS

SERIES EDITORS

A
SCIENTIAE RERUM NATURALIUM
Professor Esa Hohtola

B
HUMANIORA
University Lecturer Santeri Palviainen

C
TECHNICA
Postdoctoral research fellow Sanna Taskila

D
MEDICA
Professor Olli Vuolteenaho

E
SCIENTIAE RERUM SOCIALIUM
University Lecturer Veli-Matti Ulvinen

F
SCRIPTA ACADEMICA
Director Sinikka Eskelinen

G
OECONOMICA
Professor Jari Juga

H
ARCHITECTONICA
University Lecturer Anu Soikkeli

EDITOR IN CHIEF
Professor Olli Vuolteenaho

PUBLICATIONS EDITOR
Publications Editor Kirsti Nurkkala

UNIVERSITY of OULU
OULUN YLIOPISTO

ISBN 978-952-62-0738-4 (Paperback)
ISBN 978-952-62-0739-1 (PDF)
ISSN 0355-3213 (Print)
ISSN 1796-2226 (Online)